

Catalyst – generally catalyst particles are nearly spherical shaped bodies that do not polish well and are found incorporated into the carbon matrix (Plate IIIC & IIID, **Figure 5**).

Using this classification, a point count analysis of the volume percentage distribution of carbon textures was performed at 625X magnification in oil immersion by traversing the sample based upon a 0.6 x 0.4 mm grid perpendicular to the particle gradient and identifying the textural element under a crosshair held in a microscope eyepiece. A total of 500 counts were accumulated from each of two polished surfaces for a total of 1000 counts and the results reported as a volume percentage in **Table 6**.

RESULTS AND DISCUSSION

The DOs were characterized by proximate/ultimate analyses, SIMDIS GC, and ^1H and ^{13}C NMR. Marfork and W. Kentucky #6 coals were characterized by proximate/ultimate analyses and a Geisler plastometer. Solvent extraction reactions with Marfork coal/EI-107 DO and W. Kentucky #6/CP-DO were completed. Coker runs were completed using W. Kentucky #6/CP-DO.

Characterization of the Feed Materials

The feed materials have been characterized by proximate and ultimate analyses as well as SIMDIS GC. The results for the DOs are shown in **Tables 1, 3, and 4**. **Table 2** contains the characterization data for Marfork coal and W. Kentucky #6 coal.

Of the four DOs tested, Valero and EI-107 were more aromatic, were denser, had a lower H/C ratio, and had ~3 wt% sulfur. Conversely, BP-DO and CP-DO were more aliphatic, were less dense, had a higher H/C ratio, and < 1 wt% sulfur. The boiling point cut point distributions for all of the decant oils were very similar, although CP-DO was slightly heavier with more material boiling in the fuel oil range. CP-DO was chosen as the extraction solvent for reaction with W. Kentucky #6 because of the high quantity of material, and low sulfur content; however, CP-DO had a high H/C ratio (and therefore, was most likely more aliphatic than some DOs), and may have affected solvent extraction yields.

W. Kentucky #6 was chosen because it was used as a liquefaction coal previously and the coal that showed the highest extraction yield in anthracene oil at UKCAER. [5] W. Kentucky #6 has similar fluidity to Marfork coal, and also has a slightly higher H/C ratio.

Solvent Extraction Data in 1 L Stirred Autoclave

Table 7 shows the conversion of the coal using the DO EI-107/Marfork coal and CP-DO/W. Kentucky #6 coal. All solvent extraction experiments were done for 1 h. The conversion ranged from 43-53 wt% for DO EI-107/Marfork coal, and 27-62 % for CP-DO/W. Kentucky #6 coal.

Table 7: Solvent extraction experiments, coal conversion and yield data, data from previous and current research

Rxn No.	Coal	Solvent/Coal ^a	Reactor Type	Temp (°C)	Press (psig) ^b	Total Mass (g) ^c	Coal Conv ^d
	Marfork	EI-107 ^e 10:1	1 L SA (10 μ) ^f	360	600	220	40.0
	Marfork	EI-107 10:1	1 L SA (1 μ) ^f	360	475	220	41.7
	Marfork	EI-107 10:1	1 L SA (10 μ) ^f	390	560	220	58.9
	Marfork	EI-107 10:1	1 L SA (10 μ)	400	630	220	59.7
	Marfork	EI-107 7:1	1 L SA (10 μ)	390	600	160	44.0
	Marfork	EI-107 7:1	1 L SA (10 μ)	400	600	160	51.0
	Marfork	EI-107 9:1	1 L SA (10 μ)	390	630	200	53.0
	W. Kent #6	CP-DO ^g 9:1	1 L SA (10 μ)	390	760	200	52.5
	W. Kent #6	CP-DO 7:1	1 L SA (10 μ)	390	600	160	62.5
	W. Kent #6	CP-DO 5:1	1 L SA (10 μ)	390	650	120	57.5
	W. Kent #6	CP-DO 5:1	1 L SA (10 μ)	390	810	300	48.0
	W. Kent #6	CP-DO 5:1	1 L SA (10 μ)	390	810	300	53.0
	W. Kent #6	CP-DO 5:1	1 L SA (10 μ)	390	810	324	40.7
	W. Kent #6	CP-DO 5:1	1 L SA (10 μ)	390	600	300	44.0
	W. Kent #6	CP-DO 5:1	1 L SA (10 μ)	390	700	300	36.0
36	W. Kent #6	CP-DO 10:1	1 L SA (10 μ)	390	350	222	60
37	W. Kent #6	CP-DO 10:1	1 L SA (10 μ)	390	500	330	37.8
38	W. Kent #6	CP-DO 10:1	1 L SA (10 μ)	390	500	330	39.5
39	W. Kent #6	CP-DO 10:1	1 L SA (10 μ)	390	750	330	42.4
40	W. Kent #6	CP-DO 10:1	1 L SA (10 μ)	390	750	330	33.7
42	W. Kent #6	CP-DO 10:1	1 L SA (10 μ)	390	750	330	27.3
44	W. Kent #6	CP-DO 10:1	1 L SA (10 μ)	390	500	330	62.1
45	W. Kent #6	CP-DO 10:1	1 L SA (10 μ)	390	500	330	46.9
46	W. Kent #6	CP-DO 10:1	1 L SA (10 μ)	390	500	330	54.0
47	W. Kent #6	CP-DO 10:1	1 L SA (10 μ)	390	500	330	46.8
48	W. Kent #6	CP-DO 10:1	1 L SA (10 μ)	390	500	330	44.3

^a solvent to coal ratio, Decant Oil (DO)

^b Pressure at temperature

^c Total mass = total mass fed to reactor, solvent+coal

^d coal conversion, wt%

^e EI-107 = Decant oil EI-107 from United Refining

^f 1 L stirred autoclave, hot filtration using Pope Scientific filter, 10 μ and 1 μ filters

^g CP-DO = ConocoPhillips decant oil

Under the conditions at 360°C for 1 h (~41%), the conversion using DO was lower than when using LCO. However, in previous research [5], the optimal conditions for reactions of DO and West Kentucky #6 coal was at 390-410°C. Reactions of Marfork coal with EI-107 DO were carried out at higher temperature and a lower solvent-to-coal ratio. The optimal conditions for

DO-107 and Marfork coal were at 390-400°C (58.9-59.7 wt% conversion). A few experiments were tried at 5:1, 7:1, and 9:1 to determine if mechanical problems or lower conversions would preclude running at these ratios. At 5:1, the filter plugged completely, so the reactions with ratios of 7:1 and 9:1 were completed. At both 7:1 and 9:1, the conversions ranged from 44-53.0 wt% and extract yield was 10-43%, with the optimum temperature at 390°C.

The same conditions were used on CP-DO and W. Kentucky #6 coal. Reaction conditions were tested at solvent:coal ratios of 7:1 and 5:1 (conversion 57.5-62.5 wt%, extract yield 32-70%). However, when adding a greater amount of coal+solvent slurry in the reactor (from 220 g to 330 g), at a 5:1 ratio, the pressure was higher in the reactor at temperature and the conversion went down slightly (conversion ~50-55 wt%, extract yield 17-32.5 wt%). While conversion appeared to be reproducible, extract yield was not as reproducible. Towards the end of the extraction runs, most were done with a solvent-to-coal ratio of 10:1 to keep the filter from plugging. There was a wide range of conversions for CP-DO/W. Kentucky #6 coal. For runs #36-44, there are some relatively high conversions at ~60% and some very low conversions at ~27%. Two runs were not included (#41 and #43) because the reactor plugged and no data were obtained.

Coker Runs with Solvent Extracted Coal

Coker runs were done with 1500-3000 g of feed material; solvent extraction feed was lower than typical coker feeds, mainly because there was a limited amount of the coal extraction feed available. Results are shown in **Table 8**. Some problems were encountered in the coker. Apparently CP-DO has a high amount of waxy (heavy aliphatics) material as part of its composition. This explains why the H/C ratio is higher for CP-DO than other DOs tested. The waxy material built up in the overhead lines and almost plugged the baseline reaction. The overhead lines were wrapped with heat tape to prevent plugging in subsequent runs. It also explains why the extract yield is lower than what has been published by UKCAER; a highly aliphatic content decant oil would most likely extract less coal than a highly aromatic decant oil. However, CP-DO was chosen as the extraction medium primarily because it had a low sulfur content, an important factor for production of carbon anodes.

Overall, since the pressure was at ~40 psig, the coke yield was higher and the liquid yield was lower compared to previous PSU research where the pressure was 25 psig. For DO alone (#142), the coke yield was 24.6% and the liquid yield was 61.1 %, while for the coal-extracted feed (#143), the coke yield was higher, 32.9%, and the liquid yield lower, 48.4 %. When adding the catalyst to the coal extract (#144) coker run, the coke yield was 26.9 % and the liquid yield was 50.8 %, in between the yields for CP-DO alone and the coal extract run, an indication that the catalyst influenced the coke and liquid yield. However, further coke and liquid characterization is necessary to see how the coal extract and adding catalyst influenced the chemical nature of the products.

Table 8. Conditions and product distributions for coking

Run #	142	143	144*
Decant oil (%)	CP-DO (100%)	Coal Extract (100%)	Coal Extract Catalyst
Conditions			
Feedstock, hours	3 h 30 min.	2 h 50 min	1 h 50 min.
Reactor Pressure (psig)	36.8	39.7	38.2
Hold at 500 °C, hrs	24	24	24
Feed rate, g/min	16.9	17.6	20.2
Preheater inlet, °C	123	128	129
Preheater outlet, °C	445	446	448
Coke drum inlet, °C	465	470	467
Coke drum lower/middle, °C	456	457	458
Coke drum top, °C	442	436	441
Material Fed to Reactor (g)	3553	2840	1845
Product			
Liquid/coke	2.48	1.47	1.87
% Coke	24.6	32.9	26.9
% Liquid	61.1	48.4	50.8
% Gas	14.3	18.7	22.2

*Run 144 ended early due to plugging of catalyst injector

Characterization of Products

Coke Characterization

Bulk Chemical Properties of Cokes

Results from proximate and ultimate analyses for the three cokes given in **Table 5** show a relatively uniform low-ash and moisture content coke of high carbon and uniform hydrogen and nitrogen. The minor differences observed in ash, volatile matter and sulfur yields can be explained by the blend components employed. Higher ash for coke derived from run #144 can be explained by the addition of inorganic catalyst particles, while the higher volatile matter and sulfur content in cokes from run #143 and #144 can be explained by the addition of coal extract containing the higher sulfur content of W. Kentucky #6 coal (2.6 %) compared to the straight run of CP-DO used in run #142. However, understanding why volatile matter would be higher in the cokes using coal extract is difficult to explain when there was only a minor increase in hydrogen and a decrease in oxygen by difference.

Petrographic Properties of Cokes

Microscope characterization of the three cokes shows that there are more similarities than differences. The photomicrographs seen in Plate I (**Figure 3**) define about 80% of the textural elements found in each of the three delayed cokes regardless of the blend proportions or run conditions. What is more, they are typical of most petroleum coke derived from relatively low sulfur decant oil. So the small domain, domain, mosaic and flow domain textures define these cokes as shown in **Table 6**. Point count analysis of these cokes, in general, revealed that as coal extract and/or catalyst were added to the CP-DO and delayed coker, there was a decrease in the larger more elongated optical textures (i.e., domain and flow domain) and an increase in the small domain carbon. However, there are some fine details, some minor differences that have been observed, as discussed in the following paragraphs.

As seen in **Figure 3** (Plate I, run #142) and **Figure 4** (Plate II, run #143), micrographs show some finely textured, elongated inclusions within the petroleum coke. These have been observed in other circumstances as wall-scale derived from the deposition of pyrolytic carbon, i.e., gas-phase carbon deposition. Particles of wall-scale observed fully included within petroleum coke textures may have spalled and fallen into the forming coke as suggested by Plates ID and IIA, whereas those particles found at the edge may have still been in contact with the reactor wall upon removal from the coker (Plate IIB). Wall scale particles were found in all coke samples, but less so in #142 using 100% CP-DO.

Another textural component that appeared in coke specimens made with coal extract (runs #143 and #144) resembled the mosaic texture derived from the enhancement of vitrinite during coal/decant oil coking experiments, i.e., groupings of irregular-shaped isochromatic units dispersed in larger and more rounded isochromatic regions derived from the decant oil as seen in Plate IIC for run #143. Photomicrographs in **Figure 6** show different areas of this texture and Plates IVA and IVB represent the same particle viewed under oblique polarized light with minimal retardation to show that these areas are associated with micron size metallic particles as

well as coal inertinite. The metallic particles, although very small, do not appear to be sulfide minerals. However, all such regions inspected had this dispersed metallic phase.

Another textural component observed only in cokes having been made with coal extract can be observed in Plate IID for run #143 (**Figure 4**) and in Plates III A and IIIB (**Figure 5**) for run #144. At first glance the carbon in each of these micrographs has a mottled appearance that on closer inspection reveals the formation or deposition of a secondary phase within a fairly stable or even solid matrix. Some particles appear to have been formed by the infilling of randomly distributed pores of fairly uniform size with isotropic pitch or by pyrolytic carbon deposited from the vapor phase or the development of a mesophase. Particles showing incompletely filled pores were observed. At this point the significance of these observations is unknown, but during point count analysis 3.8% and 4.0% of the particles encountered in coke from runs #143 and #144 exhibited this texture, respectively.

Finally, Al₂O₃ catalyst was employed in run #144. Rounded particles of the catalyst were observed individually (Plate IIIC) or in clusters (Plate IIID) (**Figure 5**) in that coke; they exhibited no signs of alteration and appeared to have little local influence on coke textures.

Liquid Characterization

Simulated distillation GC data are shown in **Table 9**, and vacuum distillation data are shown in **Table 10**. Based on the SIMDIS GC data, the coal extract in CP-DO is heavier than the CP-DO. The overhead liquids from all the coking runs are lighter than the feeds, as expected. The overhead liquids from the CP-DO (run #142) are definitely lighter, with more gasoline, jet fuel, and diesel fractions and less fuel oil. The trend is similar for the coal extract overhead liquids (#143) compared to the feed extract, but compared to run #142, run #143 has slightly less fuel oil and more diesel and jet fuel. When adding the catalyst to the reaction (run #144 overhead liquids), there is more fuel oil and less diesel fuel compared to the overhead liquids of run #143. A similar trend is observed in the vacuum distillation cuts, but the lighter fractions compose much less of the samples than was observed in the SIMDIS GC.

Table 9: Simulated distillation cut point table for CP-DO, coal extract, and overhead liquids from three runs.

Test #	CP-DO	Extract	142	143	144
IBP-180 °C Gasoline	0.04	0.27	4.62	3.18	2.66
180-270 °C Jet Fuel	1.44	3.73	7.83	8.84	9.01
270-322°C Diesel	4.05	5.94	12.67	17.18	14.69
332 °C-FBP Fuel Oil	93.48	89.11	73.93	69.84	72.68

Table 10: Vacuum distillation cut point table for CP-DO, coal extract, and overhead liquids from three runs.

Test #	CP-DO	Extract	142	143	144
IBP-180 °C Gasoline	0.0	0.1	1.0	0.4	0.4
180-270 °C Jet Fuel	0.7	0.4	3.0	3.0	1.4
270-322 °C Diesel	1.3	1.8	1.0	2.0	2.9
332 °C-FBP Fuel Oil	96.9	97.7	92.0	95.0	95.4

GC/MS data of vacuum distilled fractions are shown in **Tables 11 and 12**. When comparing the GC/MS of each fraction of the two feed materials, the extract includes heavier aromatics compared to the original CP-DO. However, once the CP-DO (run #142) and the extract (run #143) were coked, the liquid products, while also lighter, were also more paraffinic; the overhead liquids from run #143 are even more paraffinic than the overhead liquids in the CP-DO (run #142), so much of the coal-based material in the extract is probably incorporated in the coke. However, when adding the catalyst (run #144), the overhead liquids from the extract become more aromatic. It appears the catalyst is able to facilitate the cracking of smaller aromatic compounds into the liquid product.

CONCLUSIONS

The DOs and coal were characterized. The decant oil chosen for reaction with W. Kentucky #6 was from ConocoPhillips, CP-DO; it had a low sulfur content, had the highest H/C ratio, and had the most material available for reaction. W. Kentucky #6 had similar fluidity to Marfork coal, and also had a slightly higher H/C ratio. Coal extraction conversion with Marfork coal and EI-107 DO, at 360°C and 1 h, was ~40%, with liquid yields ~38%. The conversions at 390-400°C and a 10:1 solvent to coal ratio increased to ~60%. Lowering the solvent to coal ratio to 9:1 and 7:1 reduced conversion to ~44-53 % and extract yield to 10-43%, and could not be done at all at 5:1 due to plugging of the filter. When reacting with W. Kentucky #6 coal and CP-DO, conversion at 390°C and 7:1 solvent to coal ratio was about 63%; however, when increasing the amount of slurry in the reactor (from 220 g to 330 g), conversion was reduced to <55 wt%. In the most recent reactions completed, a 10:1 solvent to coal ratio was used in order to keep the filter operating consistently. Conversions were a little lower (~45-55%). Enough feed was produced to conduct short delayed coker runs in our large lab scale coker. Three coker runs were completed. CP-DO produced the lowest amount of coke and highest amount of liquid, while extracted coal liquids had the highest coke yield and lowest liquid yield. Adding catalyst to the extracted coal liquids (#144) decreased the coke yield and increased the liquid yield relative to the extracted liquids (#143). The overhead liquids from all the coking runs are lighter than the feed materials before reaction, as expected. The overhead liquids from the CP-DO (#142) are definitely lighter, with more gasoline, jet fuel, and diesel fractions and less fuel oil. The trend is

Table 11. Composition of vacuum fractions for whole samples based on GC/MS^a results (wt%)

Classification	Gasoline		Jet fuel		Diesel		Fuel Oil	
	CP-DO	Extract	CP-DO	Extract	CP-DO	Extract	CP-DO	Extract
Paraffins	n/a	20.9	4.9	18.0	6.9	12.4	8.5	7.6
Cycloparaffins	n/a	4.3	5.2	2.0	1.5	0.0	2.8	8.1
Benzenes	n/a	2.2	62.3	13.7	3.6	2.3	27.8	25.2
Indanes	n/a	22.9	16.0	17.2	7.0	1.8	1.0	0.0
Naphthalenes	n/a	30.1	11.6	49.1	80.9	74.0	4.0	0.0
Tri-ring +	n/a	0.0	0.0	0.0	0.0	4.2	55.9	59.1
Other	n/a	0.0	0.0	0.0	0.0	5.2	0.0	0.0

^a Percent distributions belong to the ratio of GC-MS peak areas.

Table 12. Composition of vacuum fractions for overhead liquids based on GC/MS^a results (wt%)

Classification	Gasoline			Jet fuel			Diesel			Fuel Oil		
	142	143	144	142	143	144	142	143	144	142	143	144
Paraffins	88.0	94.7	57.4	77.0	82.6	49.9	59.6	51.5	37.1	9.5	5.7	5.1
Cycloparaffins	0.12	5.3	2.6	6.9	12.1	1.8	7.1	7.8	1.0	2.8	1.2	1.6
Benzenes	0.0	0.0	31.1	16.1	5.3	26.7	25.3	7.0	4.3	22.8	27.4	27.1
Indanes	0.0	0.0	4.6	0.0	0.0	11.0	3.5	28.4	8.0	0.4	0.1	1.3
Naphthalenes	0.0	0.0	3.3	0.0	0.0	6.6	0.9	4.8	49.7	8.7	8.0	35.0
Tri-ring +	0.0	0.0	0.0	0.0	0.0	0.0	0.0	0.0	0.0	55.7	57.2	61.7
Other	0.0	0.0	1.0	0.0	0.0	2.1	3.47	0.4	0.0	0.0	0.0	0.9

^a Percent distributions belong to the ratio of GC-MS peak areas.

similar for the coal extract overhead liquids (#143) compared to the feed extract, but compared to #142, #143 has slightly less fuel oil and more diesel and jet fuel. When adding the catalyst to the reaction (#144 overhead liquids), there is more fuel oil and less diesel fuel compared to the overhead liquids of #143. When comparing the GC/MS of each fraction of the two feed materials, the extract includes heavier aromatics compared to the original CP-DO. However, once the CP-DO and the extract were coked, the liquid products, while also lighter, were also more paraffinic; the overhead liquids from #143 are even more paraffinic than the overhead liquids from CP-DO (#142), so much of the coal-based material in the extract is probably incorporated in the coke. However, when adding the catalyst (#144), the overhead liquids from the extract become more aromatic. It appears the catalyst is able to facilitate the cracking of smaller aromatic compounds into the liquid product, which also affected the product distribution with lower coke yield and higher liquid yield.

Generally, there were few differences observed in the bulk properties of coke made from the CP-DO, coal extract and/or catalyst reactions. Minor differences include a slight but significant increase in the volatile matter yield, ash and sulfur content as well as a decrease in the larger and more elongated optical textures for the coke generated from coal extracts relative to the coke generated from CP-DO alone. There appeared to be a minor amount of carbon that could be linked with coal and as blend proportion became more severe (i.e., 100% CP-DO, CP-DO /coal extract, CP-DO /coal extract/catalyst); more pyrolytic carbon wall scale was observed in the coke.

REFERENCES

- [1] Sawarkar, A.N., Pandit, A.B., Samant, S.D., Joshi, J.B., 'Petroleum residue upgrading via delayed coking: A review,' *Can. J. Chem. Engr.* **2007**, 85, 1-24..
- [2] E. N. Givens, M. A. Collura, R. W. Skinner and E. J. Greskovich, *Hydrocarbon Processing* **1978**, 195-2002.
- [3] N. Okuyama, N. Komatsu, T. Shigehisa, T. Kaneko and S. Tsuruya, *Fuel Processing Technology* **2004**, 85, 947-967.
- [4] T. Yoshida, T. Takanohashi, K. Sakanishi, I. Saito, M. Fujita and K. Mashimo, *Fuel* **2002**, 81, 1463-1469.
- [5] R. Andrews, D. Jacques, T. Rantell and J. Hower, **2006**, 'Mild coal extraction for production of anode coke,' in *An industrial-based consortium to develop premium carbon products from coal*, Ed. Bruce Miller, DOE No. FC26-03NT41874, OSTI ID: 898973, in *Information Bridge: DOE Scientific and Technical Information*, Sept. 29, 2006, <http://www.osti.gov/bridge>.
- [6] C. E. Clifford Burgess, A. Boehman, B. Miller, G. Mitchell, L. Rudnick, C. Song and H. Schobert, *Proceedings of the 31st International Technical Conference on Coal Utilization & Fuel Systems* **2006**.

- [7] C. E. Clifford Burgess, Ö. Gül, J. M. Griffith, P. Aksoy, G. Mitchell, M. Escallon, U. Suriapraphadilok and H. Schobert, *Preprints of ACS Division Fuel Chemistry* **2007**, *52*, 408-410.
- [8] S. Butnark, M. Badger and H. Schobert, *Preprints of ACS Division Petroleum Chemistry* **2000**, *45*, 493-495.
- [9] S. Butnark, M. Badger, H. Schobert and G. Wilson, *Preprints of ACS Division Petroleum Chemistry* **2002**, *47*, 201-203.
- [10] J. M. Griffith, C. E. Clifford Burgess, L. R. Rudnick and H. H. Schobert, *Preprints of ACS Division Fuel Chemistry* **2004**, *49*, 627-629.
- [11] J. M. Griffith, L. R. Rudnick and H. H. Schobert, *Preprints of ACS Division Petroleum Chemistry* **2006**, *51 (1)*, 231-237.
- [12] J. M. Griffith, C. E. Burgess Clifford, L. R. Rudnick and H. H. Schobert, *Preprints of ACS Division Petroleum Chemistry* **2006**, *51 (2)*, 600-601.
- [13] J. M. Griffith, C. E. Burgess Clifford, L. Rudnick and H. Schobert, *Energy & Fuels* **2009**, *23 (9)*, 4553-4561.
- [14] Ö. Gül, L. Rudnick and H. Schobert, *Energy & Fuels* **2006**, *20*, 1647-1655.
- [15] C.E. Burgess Clifford, Principal Investigator, A. Boehman, B.G. Miller, G. Mitchell, C. Song, H.H. Schobert, co-PIs, "Refinery Integration of By-Products from Coal-Derived Jet Fuels", Final Report, Grant DE-FC26-03NT41828, September 18, 2003 – March 31, 2008, Date Issued: July 25, 2008.

Anthracite Fines for Foundries: Coke and Graphite Substitution

CPCPC Final Report

Reporting Period Start Date: March 01 2008
Reporting Period End Date: Aug 31 2009

Principal Author(s) from Penn State: Fred Cannon
He Huang
John Fox
Yujue Wang
Robert Voigt
Adam Redding
Weifang Chen

Report Issued September 2009

DOE Prime Award number: DE-FC26-03NT41874
Subcontract number: 3554-TPSU-DOE-1874

Principal Investigator: Fred S. Cannon, Professor
Department of Civil and Environmental Engineering
The Pennsylvania State University
225 Sackett Engineering Building
University Park, PA, 16802
Tel: 814-863-8754
Email: fcannon@psu.edu

DISCLAIMER

This report was prepared as an account of work sponsored by an agency of the United States Government. Neither the United States Government nor any agency thereof, nor any of their employees, makes any warranty, express or implied, or assumes any legal liability or responsibility for the accuracy, completeness, or usefulness of any information, apparatus, product, or process disclosed, or represents that its use would not infringe privately owned rights. Reference, herein to any specific commercial product, process, or service by trade name, trademark, manufacturer or otherwise does not necessarily constitute or imply its endorsement, recommendation, or favoring by the United States Government or any agency thereof. The view and opinions of authors expressed therein do not necessarily state or reflect those of the United States Government or any agency thereof.

ABSTRACT

Various protocols were developed to bind anthracite fines by a renewable bio-source binder as a coke replacement in iron foundries. The amount of coke replaced was targeted at different levels. The mechanical properties of anthracite pellets were tested at both room temperature and extremely high temperature (the melting temperature of iron). Mechanical strengths at room temperature are important for the low level coke replacement. For high level coke replacement, both room temperature and high temperature strengths are crucial to the cupola furnace operation. Renewable organic binder and additives rendered outstanding mechanical properties for the anthracite pellets at room temperature. However, organic materials lost their strengths at high temperature. With the addition of silicon powders, the anthracite pellets developed very high compressive strength at high temperature. Because silicon is also a necessary additive to the foundry cupola furnace, anthracite pellets with silicon powders will neither deteriorate the chemistry in the cupola furnace nor add additional cost to the metal casting process.

TABLE OF CONTENTS

DISCLAIMER	2
ABSTRACT	3
TABLE OF CONTENTS.....	4
List of Figures	5
List of Tables	6
1. BACKGROUND AND OBJECTIVES	7
2. EXECUTIVE SUMMARY	8
3. EXPERIMENTAL PROCEDURE	9
3.1 UV treatment.....	9
3.2 Raw materials.....	10
3.3 Binded anthracite pellet preparation	10
3.4 Mechanical property tests	11
3.4.1 Drop shatter test (DST).....	11
3.4.2 Unconfined compressive strength test	11
3.5 High temperature pyrolysis.....	11
4. RESULTS AND DISCUSSION	12
4.1 Effect of ultraviolet on the binding strength of collagen-based binder	12
4.2 Effect of pre-heat on the binding strength of collagen-based binder.....	12
4.3 Effect of sugar additives on the properties of anthracite pellets.....	13
4.4 Effect of adding ceramic additives on high temperature binding strengths.....	18
5. CONCLUSIONS	26
REFERENCES	26

List of Figures

Figure 1. Increase of temperature in front of Xenon UV system (cm distance from lamp)	9
Figure 2. The setup for the drop shatter test	11
Figure 3. SEM images of anthracite particles bound by 1% collagen-based binders at room temperature (1) and at 70 °C (2)	13
Figure 4. The anti-breakage strength of anthracite pellets with different sugar contents	14
Figure 5. Intensive drop shatter test of pellets with different binder and sugar contents	15
Figure 6. SEM images of anthracite particles bound by 1% collagen-based binders and 1.5% fructose.....	16
Figure 7. Crosslinking between sugar and a peptide chain.....	16
Figure 8. The effect of adding sodium silicate on room temperature anti-breakage strength of the anthracite pellet	19
Figure 9. SEM images of anthracite pellets with 18% sodium silicate before and after being pyrolyzed at 1400 °C.....	21
Figure 10. SEM images of anthracite pellets with 10% ferrosilicon mixture before and after being pyrolyzed at 1400 °C.....	22
Figure 11. SEM images of anthracite pellets with 10% silicon powder before and after being pyrolyzed at 1400 °C.....	23
Figure 12. SEM images of anthracite pellets with 10% kaolinite before and after being pyrolyzed at 1400 °C.....	24
Figure 13. The XRD patterns of several anthracite pellets before and after being pyrolyzed at 1400 °C under nitrogen environment	25

List of Tables

Table 1. Ultimate analysis of anthracite fines and foundry coke (% , dry base)	10
Table 2. The heat content of the anthracite fines and foundry coke used in this study (Btu/lb)	10
Table 3. Mechanical strengths of anthracite pellets bound at different temperatures	12
Table 4. The compressive strength and strain of different anthracite pellets	13
Table 5. Weight change of sugar and collagen binder mixtures due to crosslink	17
Table 6. Mechanical strengths at different temperatures of pellets with different ceramic additives	18

1. BACKGROUND AND OBJECTIVES

The price of energy sources and raw material has increased dramatically in recent years due to the uncontrolled development of the world economy and speculations. For iron foundries using cupolas, the price of its fuel, coke, increased 450% (from \$100/ton to \$550/ton) between 2002 and 2007. Unfortunately, nowadays coke is the sole fuel source for foundry cupolas. Therefore the foundries suffered a tremendous increase in operation costs without other options. On the other hand, anthracite, once a widely used fuel source is now seldom used. This is especially true for the smaller sized anthracite fines which are rejected by most industries and left in the valleys of the Pennsylvania coal region. With a heat value about 24.7 million Btu/ton, which is close to the heat value of normal coke (28 million Btu/ton), anthracite has the potential to replace at least part of the coke as cupola fuel. However, there are drawbacks in using anthracite as cupola fuel as compared to coke.

First the combustion rate of coke is much faster than that of anthracite chunks. During the coke production, cellulosic structure is formed on the coking coal. This cellulosic structure significantly increases the surface area of the coke and promotes the reaction of coke with oxygen. For big sized anthracites, there is no cellulosic structure and the combustion rate of anthracite chunks is slow. In fact before the discovery of coke, anthracite was used to melt iron in a cupola. When anthracite pieces as big as a normal adult male can lift were used, 5 tons of iron can be melted per ton of anthracite, which is much smaller than that of coke (10 to 11 tons of iron per ton of coke).[1] In this way 1 ton of coke is equal to more than two tons of anthracite. However, the iron melting number of anthracite can be increased by decreasing the anthracite size. When anthracite of adult fist size was used the iron melting number increased to 7.5 to 8.[1] Therefore, it is logical to hypothesize that by using anthracite fines, the iron melting number can be further increased to close to that of coke. However using anthracite fines in cupola will raise another problem.

Normally in a cupola, air is blown into the bottom of the cupola and travels upwards at a high flow rate to provide oxygen for combustion. Small anthracite particles added from the charging door have little chance to reach the firing zone of the cupola. Some foundries tried to add anthracite fines with iron charges. Most of the anthracite fines were collected in the baghouse without being burned. This problem can be solved by binding the anthracite fines into bigger size bricks. These bricks can not be blown away by the gas flow and will pass through the heating zone to reach the fire zone. In the fire zone, these bound bricks will have a much higher combustion rate than anthracite chunks. In this way a small part of the coke used in a cupola can be replaced by the bound anthracite bricks. However, it is known that coke also maintains certain mechanical strength in the melting zone of a cupola. This property is important for a fuel bed to accumulate at the bottom of the cupola.[2] If a large part of coke was replaced by the bound anthracite bricks, and these bricks could not maintain enough mechanical strength in the melting zone before being burned out, the fuel bed will not exit. Therefore, in order to replace a substantial amount of coke in the cupola, the mechanical strength of the bound brick at high temperature is also important.

In this study, a renewable non-toxic binder produced from pig collagen will be used to bind anthracite fines. Other techniques (such as UV[3-6], and heat treatment) and organic additives [7-17] have the ability to increase the binding strength of this collagen-based binder at room temperature. The high temperature strength in these pellets was proposed to be achieved by the addition of ceramic materials a pressureless sinter process[18-23].

2. EXECUTIVE SUMMARY

Pre-heat treatment was tested as the first protocol to increase the binding strength of the collagen-based binder. When heated at temperature higher than 61 °C, the triple helix structure of collagen will be opened and the collagen-water mixture will become a solution. When the temperature drops to room temperature, gelatin of the collagen solution will occur. This sol-gel process improved the performance of the binders. During the mixing process, because the binders were in the same phase as the water, they could be much easily and evenly distributed over the surface of the anthracite particles. And interconnected strings of binders were formed once the gelatin process took place. Also this gelatin process increased the curing speed of the bound anthracite pellets. When compared to pellets bonded with unheated binders, the pellets made by pre-heated binders achieved about a 10 times increase in compressive strength (increased from 20 psi to 200 psi). The surface of the pellets made by the pre-heated binder started to pick up strength after 10 minutes, which is much faster than the un-heated one.

Ultraviolet irradiation starts curing the pellet from its surface due the nature of the ultraviolet light. Under ultraviolet treatment, the surface of the pellet adsorbs the energy of ultraviolet first and then transfers the energy inwards. After 1.5 minutes of irradiation about 1-2 mm under the pellet surface was cured and became hard. Twelve minutes of irradiation on the rotating pellet generated a hard shell of 4-5 mm thickness. However, the ultraviolet treatment didn't significantly increase the strength of the anthracite pellets.

Glucose and fructose were added into the anthracite pellets to increase their mechanical strengths at room temperature. Glycation occurs when a sugar molecule bonds with protein structure. This reaction provides more cross-links between the collagen binders. Therefore it will likely increase the binding strength of the collagen binder. With very low binder dosage (0.2%), the existence of 1 gram monosaccharide dramatically increased the compressive strength of the anthracite pellets by about 700 to 900%. While with 0.5% and 1% binder, adding up to 1 gram monosaccharide didn't increase the compressive strength of the anthracite pellets. In contrast with increasing monosaccharide amount, the compressive strength of the anthracite pellet decreased. To the extreme, when 5 gram sugar was added, the pellets became very soft and durable. During the compressive strength test, the pellets never experienced failure during the test. Although they were deformed significantly, they were still a whole piece. Also with monosaccharide, the pellets became more elastic than the pellets without monosaccharide. Within certain deformation range, the pellets with monosaccharide can return to their original shape when the force is removed. Increase in elasticity benefited the anti-breakage strength of these pellets. Without any sugar additives, the anthracite pellets with 0.5% of 1% collagen-based binders had lower anti-breakage strength than the foundry coke did. With increasing sugar amount, the anti-breakage strength of the anthracite

pellets increased. With 1% collagen, 1% fructose or 1.5% glucose, the anti-breakage strength became higher than that of the foundry coke tested in this study. Also, the compressive strengths of the pellets were still as high as the pellets with only 1% collagen-based binder.

In order to increase the mechanical strength of the pellets at extremely high temperature several inorganic additives were tested. It was found that pellets with sodium silicate or ferrosilicon can hold strength at high temperature. When 10 grams silicon powders were used, the remained compressive strength of the pellet was about 120 psi. In addition, ferrosilicon is currently used as a cupola furnace additive in the iron foundries to provide silicon. Anthracite fines bound with silicon powders will not alternate the chemistry in the cupola and will add little cost to the system.

3. EXPERIMENTAL PROCEDURE

3.1 UV treatment

A RC-500B pulsed UV curing system was obtained from Xenon Corporation. The power input of this UV system is 600 watts. When the UV lamp is turned on, the temperature in front of the UV lamp will also increase. The temperature change profile 3 cm and 1 cm away from the lamp is shown in Figure 1.

For UV treatment, the anthracite pellets were placed 3 cm away from the front of the UV lamp. Then the pellets were exposed to the UV light for a range of times, from zero to 12 minutes.

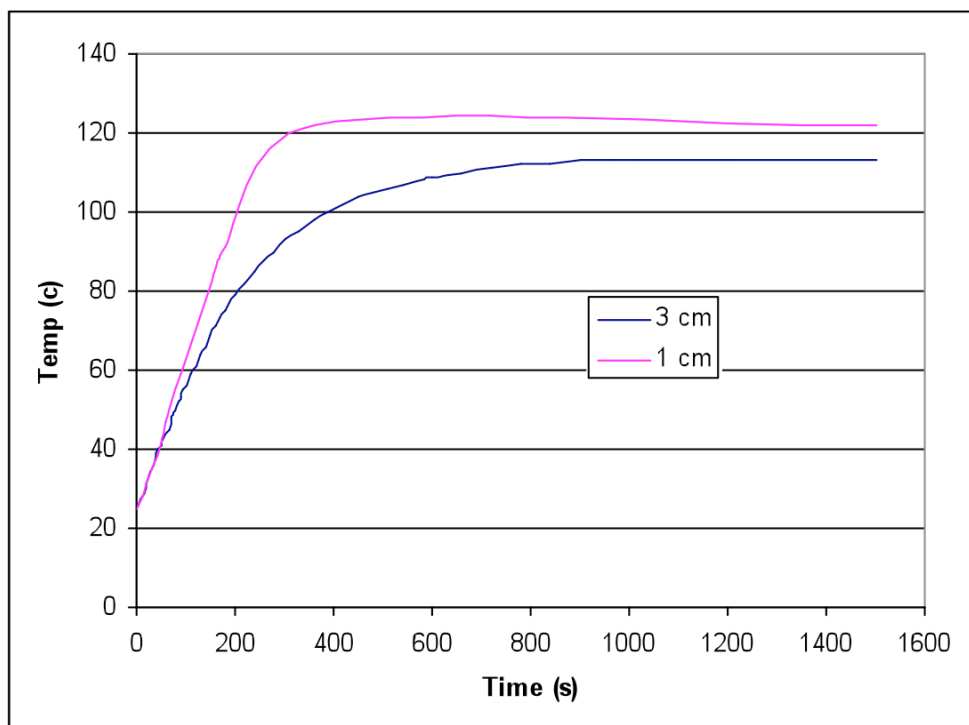


Figure 1. Increase of temperature in front of Xenon UV system (cm distance from lamp)

3.2 Raw materials

Anthracite fines used in this research were obtained from Jeddo Coal Company (Wilkes-Barre, PA) as #5 anthracite fines with particle size less than 3/64 inches. The approximate analysis of the anthracite fines is list in Table 1. The heat content of these anthracite fines are compared with a foundry coke used in some foundries in Table 2. Collagen-based binder was produced by Hormel Foods Company (Austin, MN) and received in lab as dry and small granular form. Glucose and Fructose were obtained from VWR. Sodium silicate was provided by J.B. DeVenne Inc. (Berea, OH). Ferrosilicon was provided by Miller and Company LLC (Rosemont, IL).

Table 1. Ultimate analysis of anthracite fines and foundry coke (% , dry base)

	C	H	N	S	O	Ash
Anthracite fines	85.30	1.81	1.12	0.55	1.84	9.39
Foundry coke	88.44	0.69	1.48	0.63	0.87	7.89

Table 2. The heat content of the anthracite fines and foundry coke used in this study (Btu/lb)

Sample	Heat content as received	Heat content dried
Anthracite fines	12680	13335
Foundry coke	12953	13194

3.3 Binded anthracite pellet preparation

All anthracite fines were dried at 105 °C overnight to remove the moisture before pellet making. Binder, other additives (if added), water and anthracite fines were mixed directly at room temperature (25 °C). The mixture was stirred thoroughly and then packed into a smooth brass cylindrical mold (2.86 cm (1.125”) in diameter and 5 cm (2”) in length). About 275 KPa (40 psi) pressure was applied to each side of the mold to compress the pellet. Finally the pellet was extruded from the mold and weighed. This protocol is designated as “room temperature binding” in this report.

Also the binder was mixed with water and preheated in a water bath at different temperatures (50 °C, 70 °C, and 90 °C). This preheating procedure allowed the denaturalization of the binder structure; and it formed a gelatin solution. This process took about 2 minutes. Then anthracite fines were poured in and mixed with the gelatin solution. Finally the mixture was processed through the same packing and extrusion procedures as the “room temperature binding”. This protocol is designated as “preheated binding” in this report.

The curing process of pellets made from “room temperature binding” took more than 24 hours under ambient conditions. In contrast, the curing process of pellets made from “preheated binding” took less than 2 hours for all the three temperatures tested. However those pellets were still left under ambient conditions for about 12 hours. All cured pellets were stored in a chamber at room temperature with 30-40% humidity until testing, unless noted otherwise. No further drying of the anthracite pellets were performed before the other testing protocols herein were conducted.

3.4 Mechanical property tests

Mechanical strengths of bound anthracite fines at room temperature were tested by methods recommended in the literature. For lab-scale experiments, compressive strength test and drop shatter test are the two most popular tests. Most of the pellets were measured by these two tests. Abrasive tests were conducted on selected samples.

3.4.1 Drop shatter test (DST)

The drop shatter test is a standard for foundry coke to test its strength against breakage (anti-breakage strength). The drop shatter test in this study was designed to compare the differences between various binding systems and the setup for this test is shown in Figure 2.

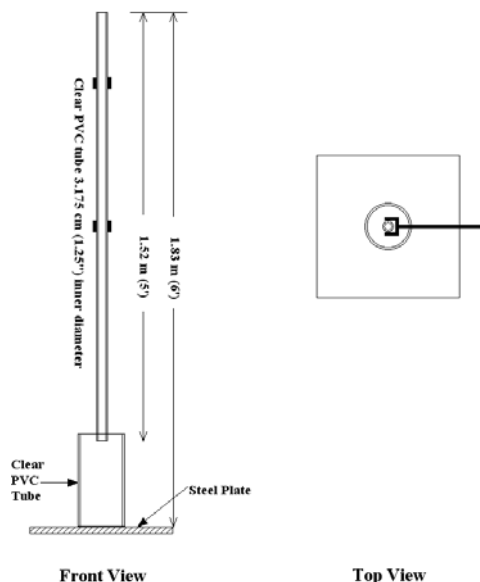


Figure 2. The setup for the drop shatter test

The anthracite pellets were dropped from the top of the long PVC tube with one flat end down, and then dropped again with the other end down. This step was repeated five times. The pellets were dropped for a total of 10 times. Also if no major piece (>50% of the original weight) of the pellet remained after a drop, the test was stopped and 0% was recorded for the test. Before every drop, the impact point on the steel plate was cleaned of debris. Then the weight of the major remaining piece was obtained.

3.4.2 Unconfined compressive strength test

The unconfined compressive strength of anthracite pellets were determined by a Simpson-Gerosa electronic universal sand strength machine. A horizontally moving arm applies pressure on a pellet until failure. Final compressive force is calculated based on the diameter of the original pellet sample.

3.5 High temperature pyrolysis

The anthracite pellets were pyrolyzed in an environmentally controlled tube furnace. Nitrogen gas was passed through the tube at a very low flowrate. The temperature of the oven was increased from room temperature to 1400 °C at the rate 3 °C/min. Then the

temperature was kept at 1400 °C for 2 hours. After that, the temperature was decreased to room temperature at 3 °C/min. Finally, the pyrolyzed pellets were tested for their compressive strengths following the same procedure as the un-pyrolyzed pellets.

4. RESULTS AND DISCUSSION

4.1 Effect of ultraviolet on the binding strength of collagen-based binder

The pellets made from “room temperature binding” were very soft and could be easily broken even after 2 hours under ambient condition, because the non-preheated collagen can not be sufficiently cured by the ambient air. As mentioned in Section 3.3, it took days for the pellets made from “room temperature binding” to be cured. In contrast, UV irradiation hardened one surface of a pellet made from “room temperature binding” in 90 seconds. When a rotating motor was used to rotate the pellet at a low speed during UV irradiation, it took 10 minutes to harden all the surfaces of the pellet. UV has a limit in penetration. After this treatment the pellet actually obtained a hard shell with the thickness of 1 to 5 mm depending on the treatment time.

4.2 Effect of pre-heat on the binding strength of collagen-based binder

Table 3 compares the compressive strength and drop shatter test results of pellets with 1% collagen-based binder at different temperatures. Only the binding materials (binder, additives, and water) were preheated. The anthracite fines were added at room temperature.

Table 2. Mechanical strengths of anthracite pellets bound at different temperatures

Binding temperature	UCS (psi)	ABS (% retained after 10 drops)
90 °C	192	85
70 °C	179	76
50 °C	115	67
25 °C	20	0

UCS- Unconfined Compressive Strength; ABS- Anti-breakage Strength

It is clear that the collagen-based binder prepared at room temperature didn't produce anthracite pellets with strong mechanical properties. The pellets were broken into small pieces during the DST and usually it took only 1 or 2 drops. Also, the pellets bound at room could only support a compressive stress of 20 psi. The mechanical strength of anthracite pellets kept increasing with increasing preparation temperature. The biggest difference was between 25 °C and 50 °C. The anti-breakage strength of the pellets increased from 0 to 67% and the compressive strength increased by about 500%. In order to pursue the balance between better binder performance and easy-control procedure, most of the pellets tested in following experiments were made with collagen-based binder and additives solution pre-heated at 70 °C.

SEM images revealed the difference between the anthracite pellets bound with binders at room temperature and preheated at 70 °C (Figure 3). If the binders were added at room

temperature, they bound the anthracite particles only at the places where the particles contacted with each other. On the contrast, in addition to binding anthracite particles at their contacting points the preheated binders also formed strings that bind particles together. The strings attached on the surface of one anthracite particle and stretched to link with the binding materials that attach the neighboring anthracite particles. These extra binding strings provided additional strength for the anthracite pellets. This difference may be contributed by the heat denaturalization of the collagen binders in water. At room temperature, individual collagen binder particle adsorbs water and increases in size. However they don't dissolve in water easily. As temperature increases, the mixture of water and collagen binders became a viscose solution. When it was cooled again, the solution became a whole piece of gel. This sol-gel process improved the performance of the binders. During the mixing process, because the binders were in the same phase as the water, they were easily and evenly distributed over the surface of the anthracite particles. Interconnected strings of binders were formed once the gelatin process took place.

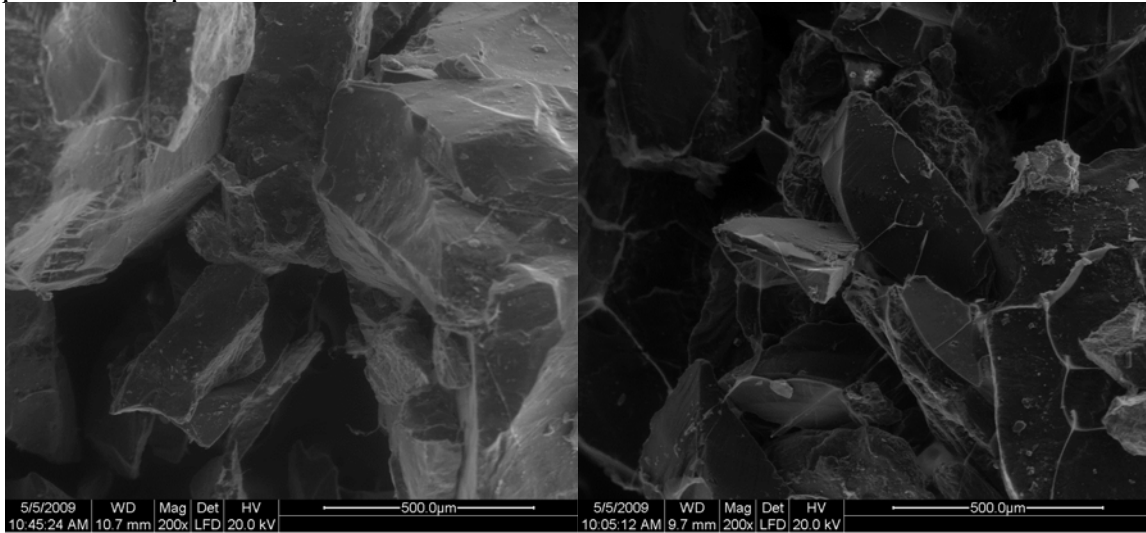


Figure 3. SEM images of anthracite particles bound by 1% collagen-based binders at room temperature (1) and at 70 °C (2)

4.3 Effect of sugar additives on the properties of anthracite pellets

Table 4 lists the compressive strength and maximum strain of different pellets before they were crushed in the compressive strength tester.

Table 3. The compressive strength and strain of different anthracite pellets

Binding components			Maximum stress (psi)	Maximum Strain (mil)
Binder (g)	Glucose /or Fructose (g)	Anthracite (g)		
0.2	0	100	8.89	53.4
0.2	G1	100	52.69	116.3
0.2	F1	100	78.48	62.47
0.5	0	100	125.4	72
0.5	G0.5	100	92.4	122.3
0.5	G1.5	100	77.3	230.8
0.5	G2.5	100	85.5	293

0.5	F0.5	100	135.69	140.4
0.5	F1.5	100	58.06	317.7
0.5	F2.5	100	35.58	410.63
1	0	100	179	110.8
1	G1	100	123	191
1	G5	100	86.5	700 ^a
1	F1	100	159	319.57
1	F5	100	29.40	700 ^a

With very low binder dosage (0.2%), the existence of 1 gram monosaccharide dramatically increased the compressive strength of the anthracite pellets by about 700 to 900%. Whereas with 0.5% and 1% binder, adding up to 1 gram monosaccharide didn't increase the compressive strength of the anthracite pellets. In contrast with increasing monosaccharide content, the compressive strength of the anthracite pellet decreased. For examples, when 5 gram sugar was added, the pellets became very soft and durable. During the compressive strength test, the pellets never experienced failure during the test. Although they were deformed significantly, they were still a whole piece. Also with monosaccharide, the pellets became more elastic than the pellets without monosaccharide. Within a certain deformation range, the pellets with monosaccharide can return to their original shape when the force is removed. The increase in elasticity benefited the anti-breakage strength of these pellets as shown in Figure 4.

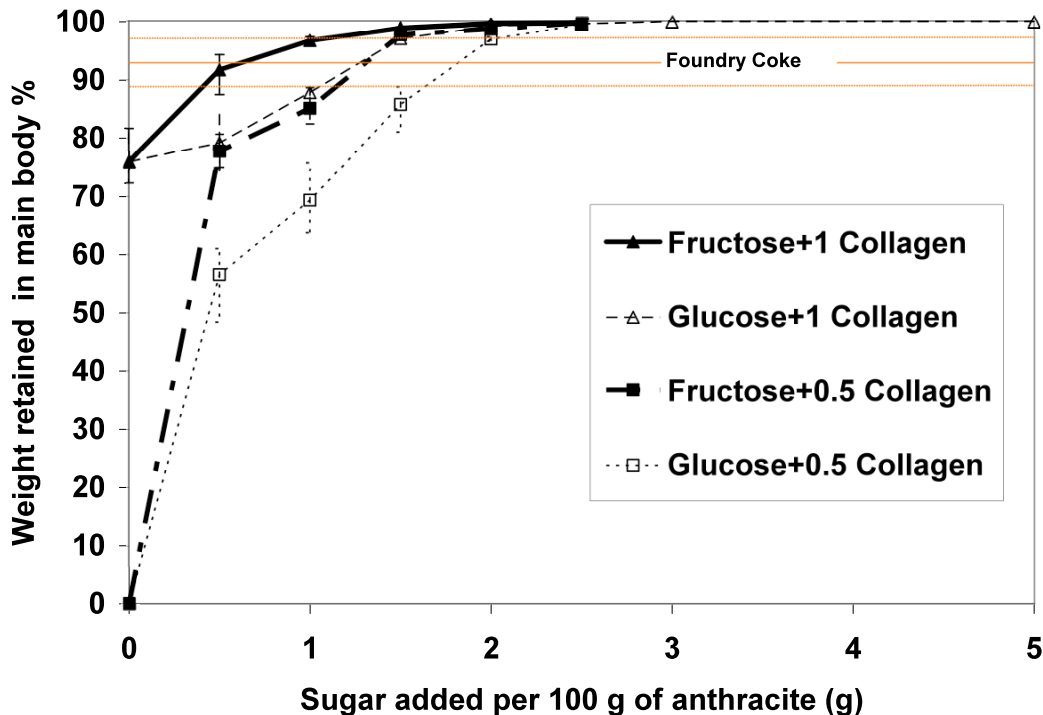


Figure 4. The anti-breakage strength of anthracite pellets with different sugar contents

Without any sugar additives, the anthracite pellets with 0.5% or 1% collagen-based binders had lower anti-breakage strength than the foundry coke did. With increasing

sugar content, the anti-breakage strength of the anthracite pellets increased. With 1% collagen, 1% fructose or 1.5% glucose, the anti-breakage strength became higher than that of the foundry coke tested in this study. Also, the compressive strengths of the pellets were still as high as the pellets with only 1% collagen-based binder. Even with 0.5% collagen binder, the anti-breakage strength can be increased to a level higher than the foundry coke if enough sugar was added. However, as shown in Table 4, too much sugar addition will greatly decrease the compressive strength of the pellets. Also with only 0.5% binder, some cracks appeared on some of the pellets after the drop shatter test. Figure 5 shows although some pellets with 0.5% collagen-based binder had better anti-breakage strength than the coke in the normal drop shatter test, they were weaker in the intensive drop test. Figure 4 also shows the difference between fructose and glucose in increasing the anti-breakage strength of the anthracite pellets. For both 0.5% and 1% collagen dosages, when a small amount of sugar was added, the pellets with fructose had much higher anti-breakage strength than the pellets with glucose. As the sugar content increased, the difference in anti-breakage strength between these two types of pellets decreased. When more than 2.5g of sugar was added, the drop shatter test used in this study can not tell the difference between the two sugars.

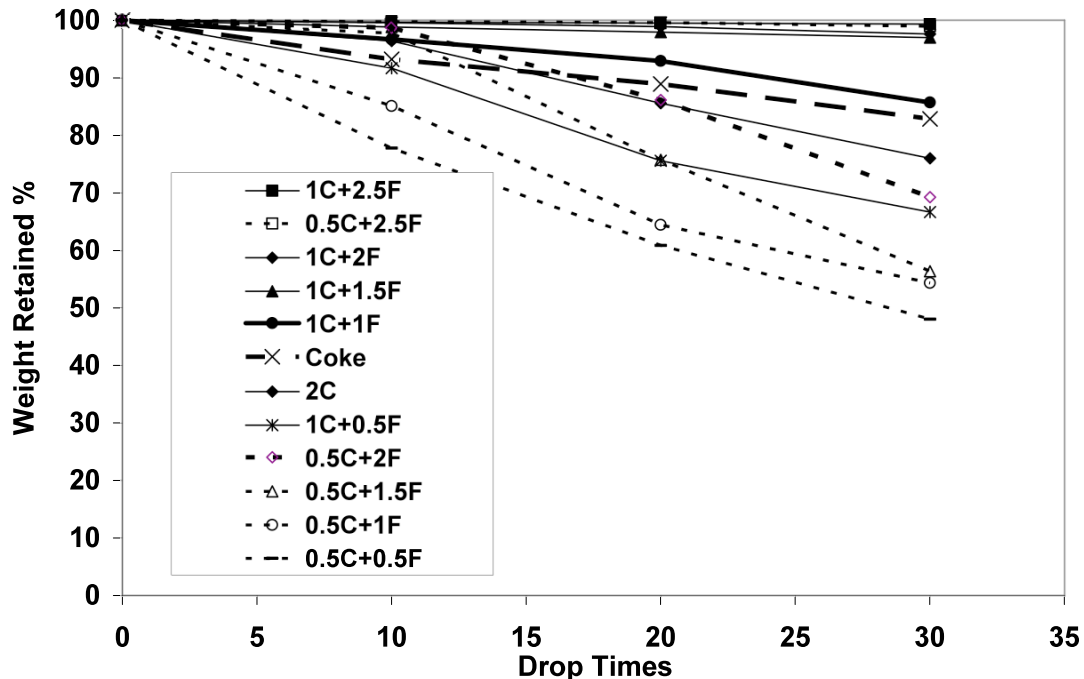


Figure 5. Intensive drop shatter test of pellets with different binder and sugar contents

Adding monosaccharide affects the strength of the collagen-based binder by several potential mechanisms. First, it is obvious that with the extra amount of fructose or glucose, the volume of hydrocarbon materials increased in the anthracite pellets. This increase in volume helped the distribution of collagen binders when they were mixed with the anthracite particles. The SEM photos of anthracite particles bound with 1% collagen binder and 1.5% fructose (Figure 6) revealed that more strings were formed on the surface of the anthracite particles than those bound with 1% collagen binder only (see Figure 3). This affected the strength of the anthracite pellets significantly when a very

small dosage (0.2%) of collagen-based binder was used as shown in Table 4. Monosaccharide is a cost-effective replacement for collagen-based binders for a simple increase in binder dosage.

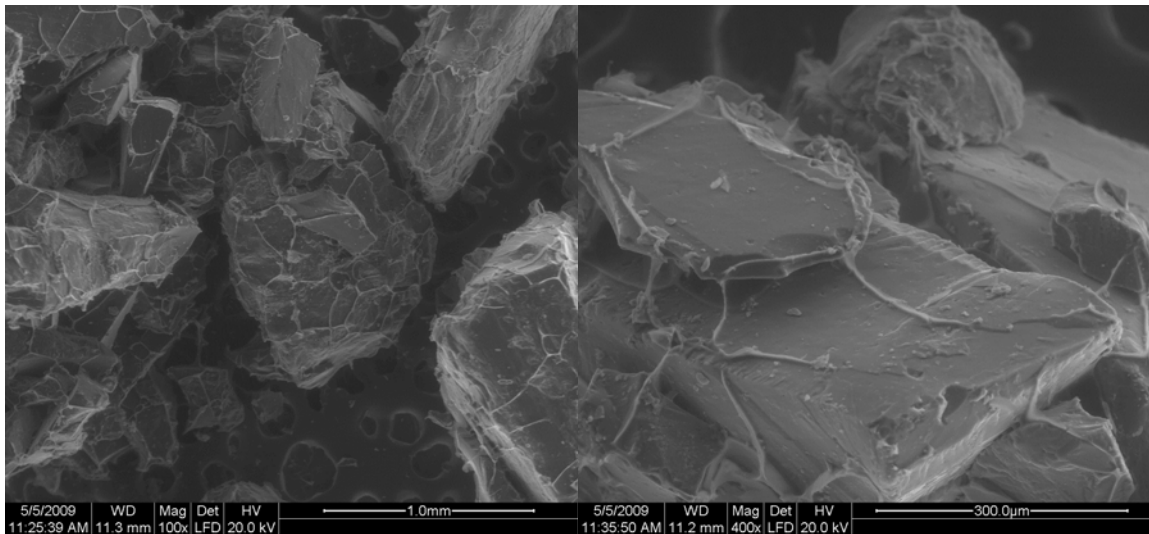


Figure 6. SEM images of anthracite particles bound by 1% collagen-based binders and 1.5% fructose

Second, it is known that monosaccharide (such as fructose and glucose) can react with protein, especially collagen to cause crosslinking of collagen. This reaction is initiated between the aldehyde group of the sugar and an additional amino group on the peptide chain. Some amino acids, such as lysine, have more than one amino group. Figure 7 shows the reaction between glucose and lysine.

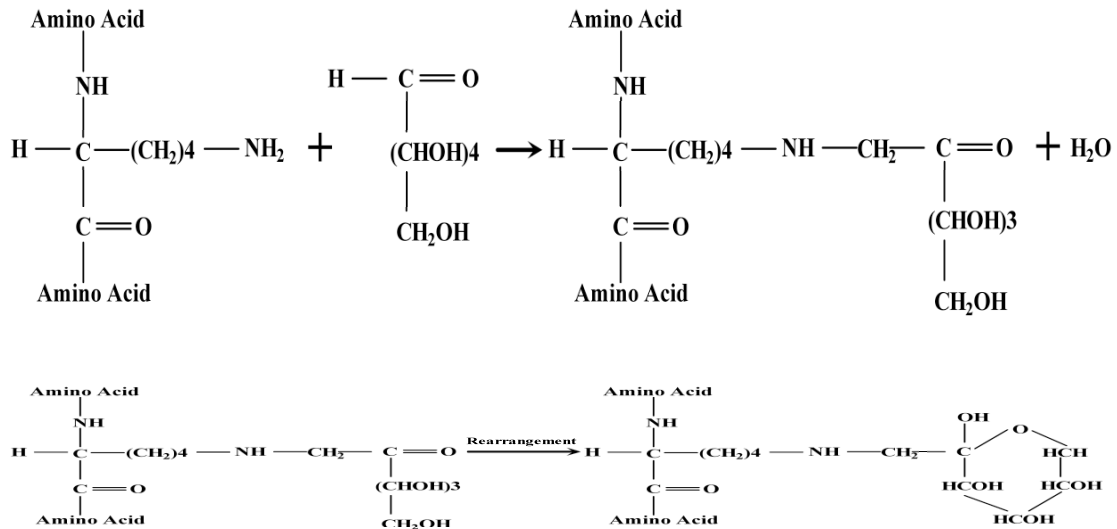


Figure 7. Crosslinking between sugar and a peptide chain

The reaction between monosaccharide and collagen binder can be verified by experimental data as listed in Table 5. Samples containing 5 grams collagen-based binder and 5 grams sugar were mixed in a water solution. The mixture was then dried at 70 °C for more than 1 week. Samples with 5 grams sugar only and samples with 5 grams collagen-based binder only also went through the same procedure as blanks. Because water generated during the crosslink reaction evaporated from the system, the final mass of the system is less than the summation of the original weights of sugar and binder. This crosslinking may also affect the binding strength of the collagen-based binder. Furthermore, this crosslink reaction requires that the monosaccharide molecule is in its chain formation. It is known that fructose exists more in its chain molecular form than glucose does. This may explain why fructose performed better than glucose in increasing the binding strength.

Table 4. Weight change of sugar and collagen binder mixtures due to crosslink

	O.M. (g)	F.M. (g)	M. L. (g)	H ₂ O(g) ^a
C	5	4.635	0.37	-
G	5	5	0	-
F	5	5	0	-
G+C	5+5	8.193	1.807	1.437
F+C	5+5	8.275	1.725	1.355

a: water generated from the crosslink

O.M.-original mass, F.M.-final mass after dried at 70 °C, M.L.-mass loss, C-collagen binder, G-glucose, F-fructose

Finally, another well known affect is that monosaccharide will also make the collagen-based binder softer. With a certain amount of monosaccharide in the collagen-based binder, the mixture becomes more elastic. It certainly contributed to the increase in the anti-breakage strength of the anthracite pellets. However, if too much sugar is added, the pellets become too soft to support heavy loads. As shown in Table 4, when more than 1.5 grams of fructose were added the compressive strength of the pellet decreased dramatically.

Because of their benignities, relative low costs and combustibility, fructose or glucose are feasible as additives to the collagen-based binder. Adding fructose or glucose will increase the anti-breakage and anti-abrasive strength. These properties are important for the anthracite pellets both in the transportation process and in the dropping zone of the cupola furnace. However, as an organic material monosaccharide inherits the same shortcoming as the collagen-based binder and will be destroyed at high temperature. Therefore with sugar additives only, the pellets still can not maintain enough strength in the cupola melting zone to form the fuel bed. Bound with collagen-based binder and sugar only, the anthracite fines may replace a small part of the coke usage; however there will still be a substantial amount of coke required to maintain the fuel bed in the copula furnace. Therefore a significant amount of coke with the appropriate strength at high temperature is necessary.

4.4 Effect of adding ceramic additives on high temperature binding strengths

When ceramic materials are added, it is also important that the ceramic additives should not deteriorate the mechanical strength of bound anthracite fines at room temperature.

The compressive strength and anti-breakage strength of anthracite pellets with different silicate contents are listed in Table 6.

Table 5. Mechanical strengths at different temperatures of pellets with different ceramic additives

Binder contents (grams based on per 100 grams anthracite fines)								CS room (psi)	ABS (%)	CS high (psi)
C	F	N	M	K	B	FeSi	Si			
1	0	0	0	0	0	0	0	179	76	0
1	1.5	0	0	0	0	0	0	159	99	0
1	0	0	0	0	1	0	0	20	0	N/D
1	0	0	1	0	0	0	0	20	0	N/D
1	0	3	0	0	0	0	0	N/D	90.12	0
1	1.5	3	0	0	0	0	0	N/D	90.32	0
1	0	6	0	0	0	0	0	356	98.73	0
1	1.5	6	0	0	0	0	0	N/D	98.5	0
1	5	6	0	0	0	0	0	360	98.5	0
1	1.5	9	0	0	0	0	0	340	97.82	4
1	1.5	18	0	0	0	0	0	N/D	N/D	20
1	0	0	0	1	0	0	0	N/D	91	0
1	1.5	0	0	1	0	0	0	273	95.73	0
1	1.5	0	0	5	0	0	0	275	95.86	0
1	0	0	0	10	0	0	0	N/D	N/D	1
1	0	0	0	0	0	5	0	N/D	79.86	2
1	0	0	0	0	0	10	0	N/D	87.57	10
1	0	0	0	0	0	0	10	N/D	91.16	124

C- Collagen binder; F- Fructose; N- Sodium silicate; M- Montmorillonite; K- Kaolinite; B-Bentonite clay; FeSi- Ferrosilicon; CS- Compressive Strength; ABS-Anti-breakage Strength; N/D- not determined

It was found that the mechanical strength of the anthracite pellets decreased greatly when bentonite clay was added. Other silicates did not deteriorate the binding strength of the collagen binder. With kaolinite added, the pellets with 1% collagen and 1.5% fructose experienced a significant increase in compressive strength and the anti-breakage strength remained above 95%. Adding sodium silicate will also increase the strength of the anthracite pellets. As shown in Figure 8, with 3% sodium silicate added, the anti-breakage strength of the anthracite pellets increased from 76% to 90%. It further increased to 98% with 6% sodium silicate and remained at the same level when 9% sodium silicate was added. Also, pellets with additional 1.5% fructose showed similar anti-breakage strength as the pellets with the same amount of collagen-based binder and sodium silicate (except 0%).

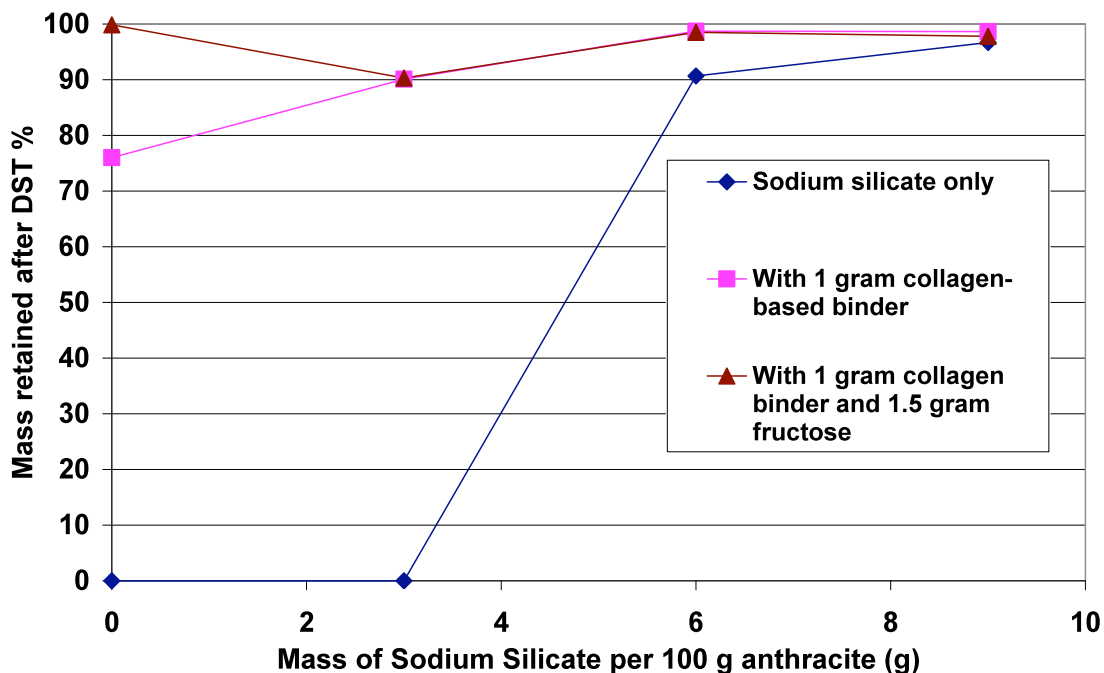


Figure 8. The effect of adding sodium silicate on room temperature anti-breakage strength of the anthracite pellet

The hypothesis of adding ceramic materials such as sodium silicate is that these ceramic materials will sinter and form a porous ceramic structure at high temperature. This ceramic structure is supposed to be the mechanism that holds the anthracite particles together at high temperature. However, it is also important that the ceramic materials should not significantly deteriorate the mechanical properties of the anthracite pellets at room temperature. The results indicate that bentonite clay (montmorillonite with some impurities) and montmorillonite are not suitable as ceramic additives. Montmorillonite increases in volume dramatically when mixed with water. This property likely contributes to the deterioration of the collagen binding strength. On the contrast, kaolinite, ferrosilicon, and sodium silicate were introduced into the anthracite pellets without damaging their strength. In deed, a dramatic increase in mechanical strength was observed when sodium silicate was added with collagen-based binder, and a slight increase was observed when kaolinite or ferrosilicon was added. The enhancement from adding sodium silicate is obvious, because sodium silicate itself can be used as a binder also. However, it is also known that collagen will crosslink with silicates[9]. Sodium silicate solution cross-linked with the collagen solution intensively. Precipitations were observed in the collagen solution right after the addition of sodium silicate solution. Results from both drop shatter tests and abrasive tests indicate that when sodium silicate was added sugars had little effect on the mechanical properties of the anthracite pellets. It is most likely that the fast crosslink between sodium silicate and collagen-based binder also eliminated the chance for sugars to crosslink with the collagen binder, because the reaction between sugar and collagen is much slower. Kaolinite and ferrosilicon didn't show thus intensive crosslink reaction with the collagen solution.

Pellets with addition of kaolinite, sodium silicate, ferrosilicon, and silicon were tested for their compressive strength after being pyrolyzed at 1400 °C. The results are also listed in Table 6. It is clear that the amount of ceramic material has to reach a certain level for the pellet to retain some strength after pyrolysis. Also different materials had different effects on the retained compressive strength. Silicon powder is the most effective ceramic material in term of retained compressive strength.

SEM images in Figures 9-12 show the difference between different anthracite pellets before and after pyrolysis. For pellets with sodium silicate, the sodium silicate experienced shrinkage during the high temperature sintering process. Finally silicate strings were formed between anthracite particles to bind the anthracite fines together. Different scenarios took place in the pellets with ferrosilicon powders. During pyrolysis, nano-fibers were formed from ferrosilicon powders. These nano-fibers coated on the surfaces of anthracite particles and bound the anthracite particles together. The pellet with silicon powder formed much more nano-fibers than that with ferrosilicon and cement mixture did. As a result, the pellet with silicon powder retained 124 psi compressive strength after being pyrolyzed at 1400 °C. The intensive amount of nano-fibers at the surfaces of the anthracite fines also turned the color of anthracite fines into blue-white. The small spheres in pyrolyzed kaolinite added pellets (Figure 12) provide evidence that the kaolinite powders melted during the pyrolysis. When there are too many adjacent kaolinite particles, they melted together into small pieces and bound neighboring anthracite particles as bridges. However, the strength of these bridges is much weaker than those with nano-fibers.

In addition to the much bigger retained compressive strength after pyrolysis, silicon also holds other advantages in this application as compared to sodium silicate. First, silicon is a necessary addition in the cupola meting process and normally silicon is added into the cupola at 3% of the fuel on a weight base. Adding 10% silicon into the anthracite briquettes and replacing up to 50% of the foundry coke by anthracite briquettes will have little effect on the chemistry in the cupola. Second, for the same reason, no additional cost will be added by silicon additives because silicon will be added in the cupola anyway. Finally, since ferrosilicon was added in the anthracite fines as powder or granular form, it will not block the combustion of anthracite fines as much as the sodium silicate solution did.

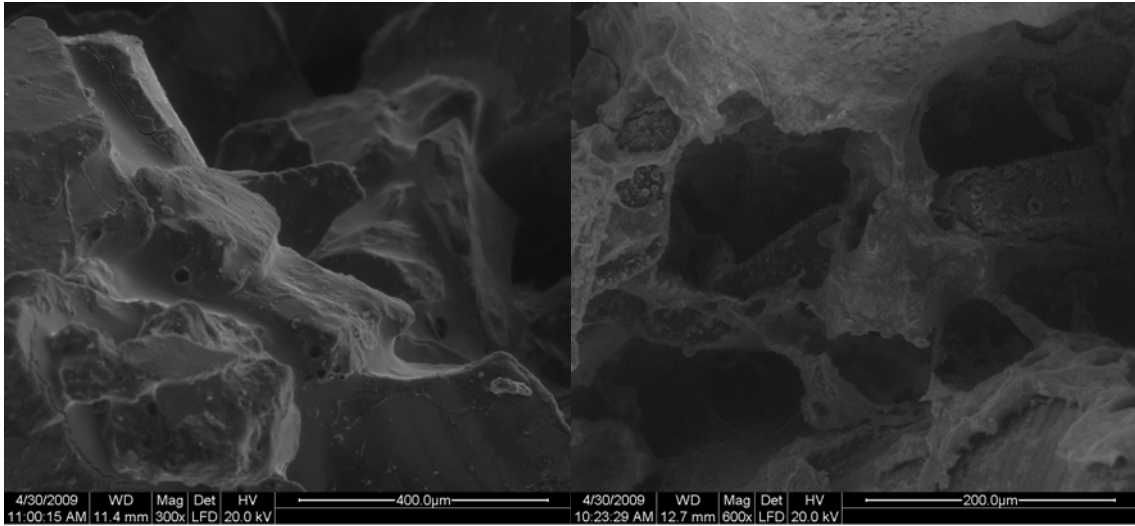


Figure 9. SEM images of anthracite pellets with 18% sodium silicate before and after being pyrolyzed at 1400 °C

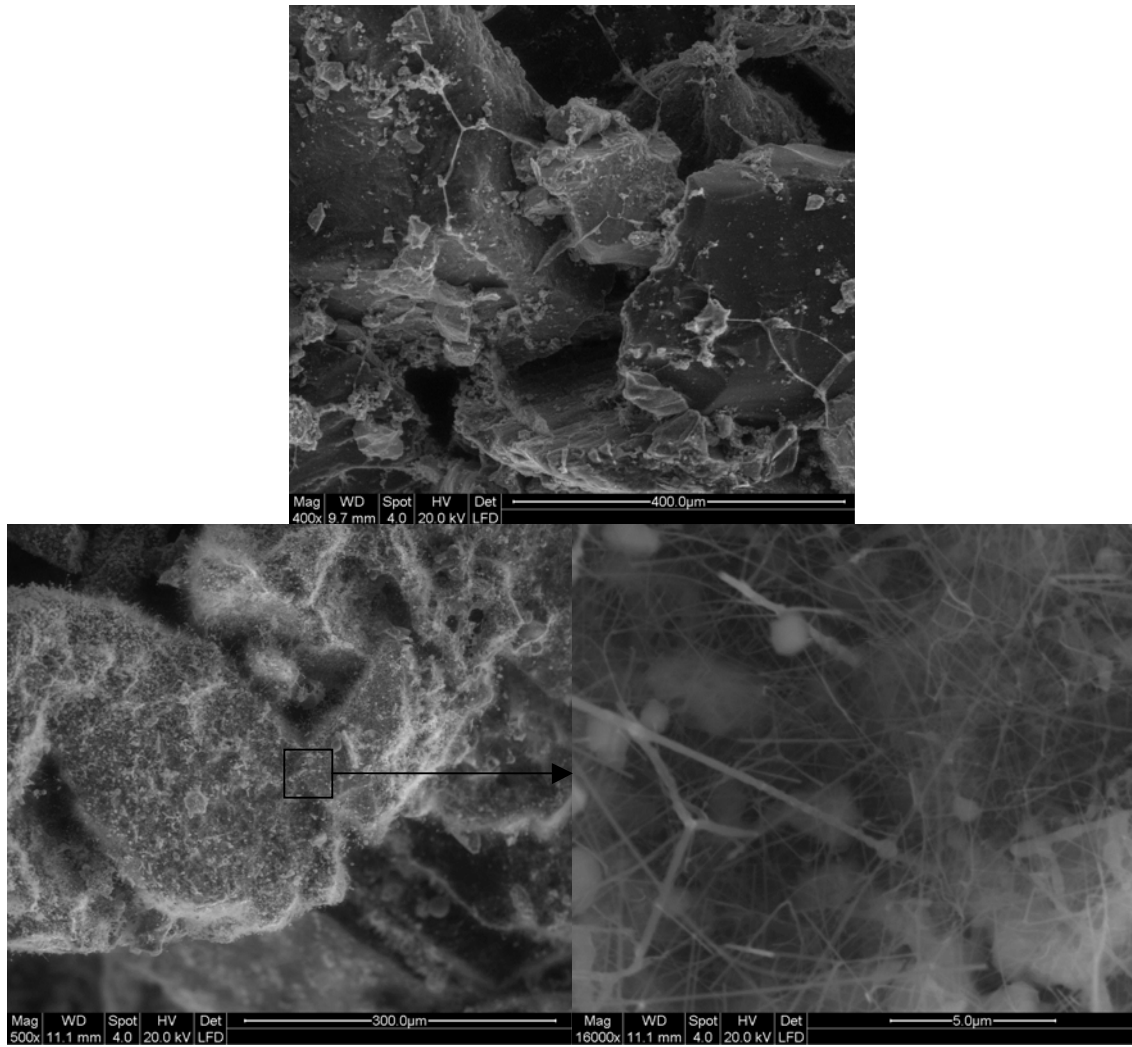


Figure 10. SEM images of anthracite pellets with 10% ferrosilicon mixture before and after being pyrolyzed at 1400 °C

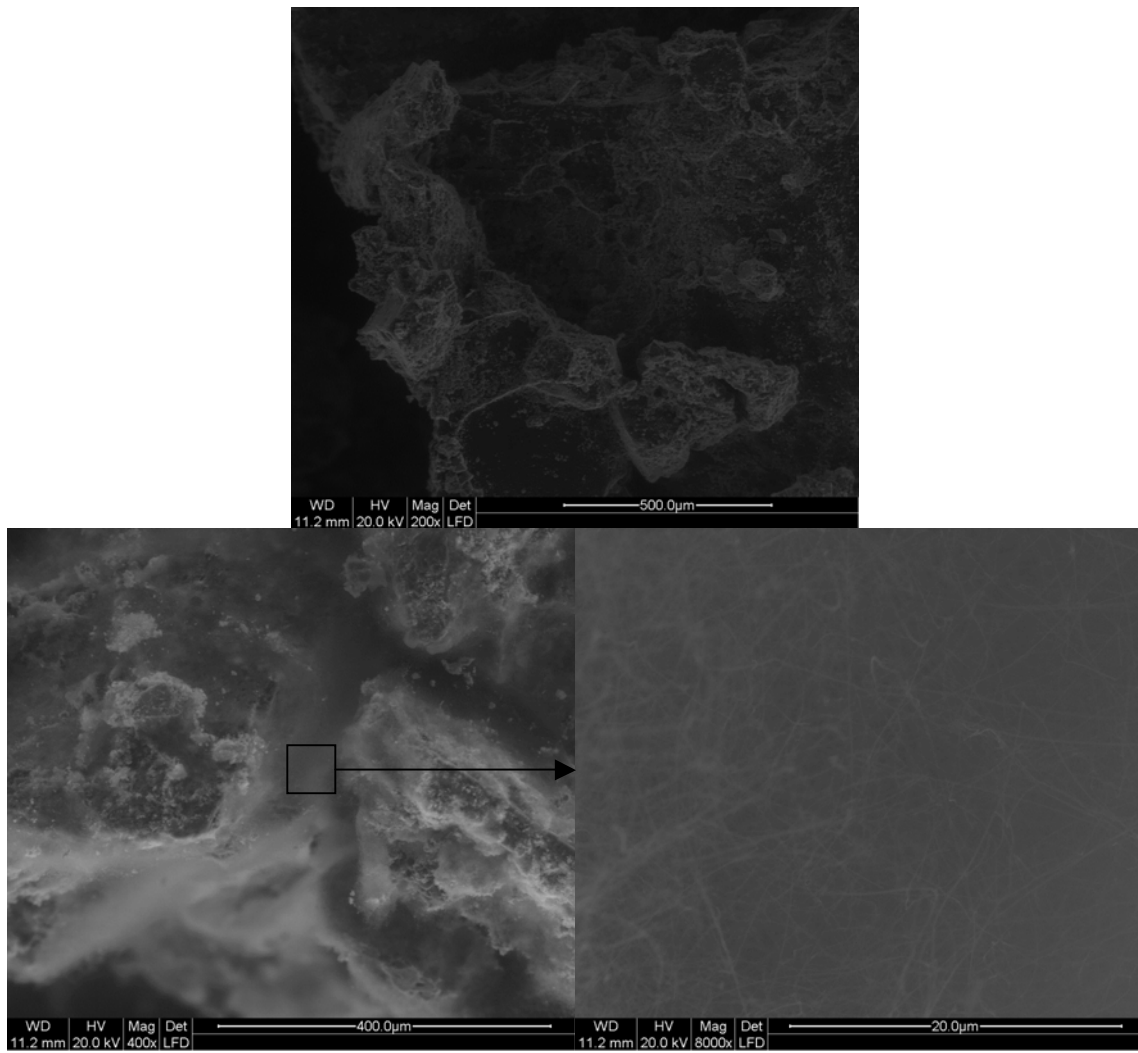


Figure 11. SEM images of anthracite pellets with 10% silicon powder before and after being pyrolyzed at 1400 °C

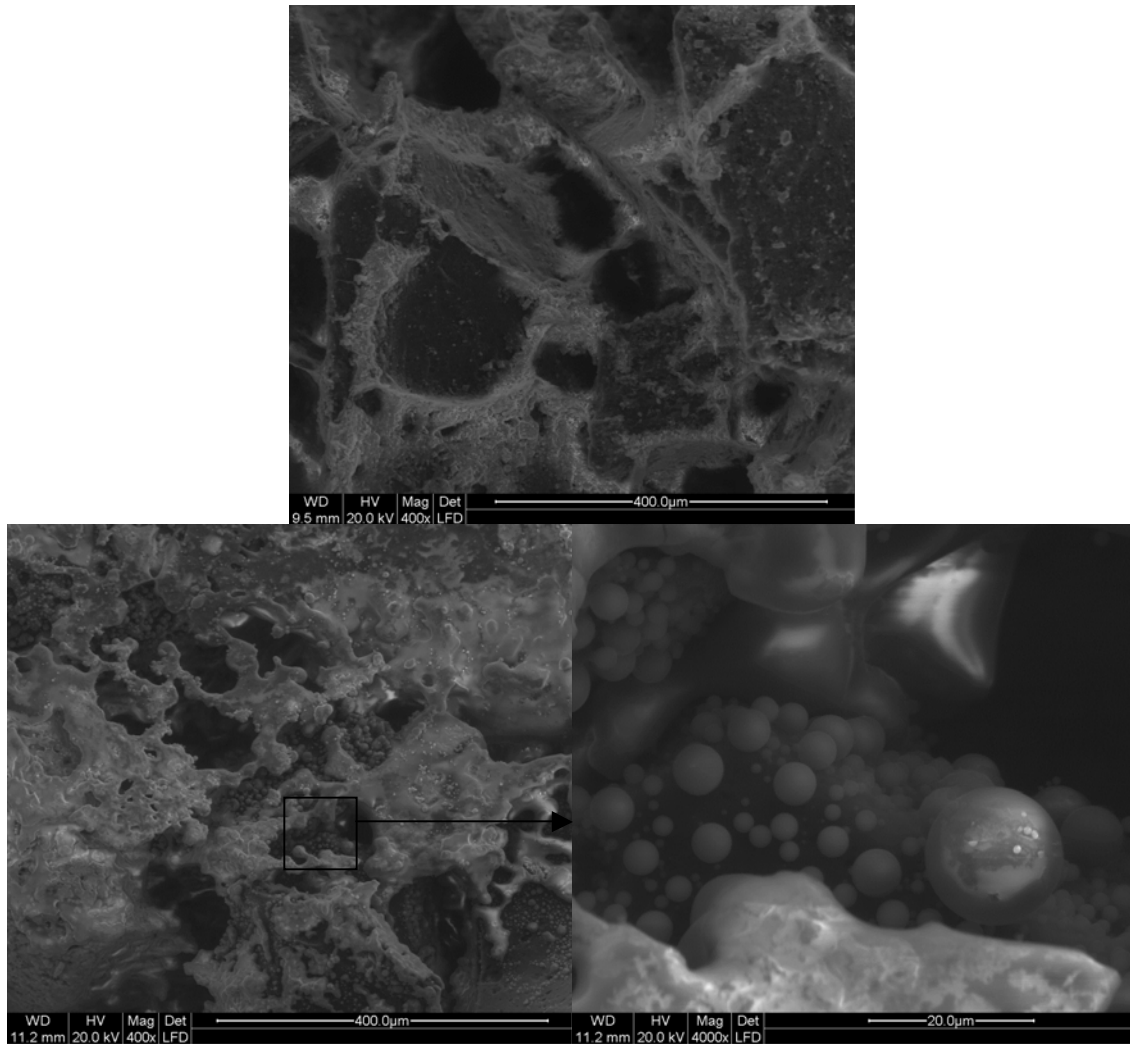


Figure 12. SEM images of anthracite pellets with 10% kaolinite before and after being pyrolyzed at 1400 °C

XRD patterns provided some information in crystal structure change and chemical reactions during the pyrolysis (Figure 13). The XRD pattern of raw anthracite indicates the existences of muscovite, kaolinite and SiO_2 with the semi-crystallized graphite. When an additive was added, the XRD patterns before pyrolysis showed the combination of crystals in the mixtures except for sodium silicate. The XRD pattern for the mixture of sodium silicate and anthracite was still similar to that of raw anthracite. The pyrolysis process enhanced the crystallization of the graphite and eliminated all other pre-existing crystals in the anthracite. In addition to the same changes, the pyrolysis process produced cristobalite and moissanite when silicon was added with anthracite. Pellets with sodium silicate had a similar pattern with pellets with ferrosilicon after the pyrolysis, except the peaks for cristobalite and moissanite are much smaller. In the pellet with kaolinite, the kaolinite disappeared after the pyrolysis, while mullite was detected in the pyrolysis product.

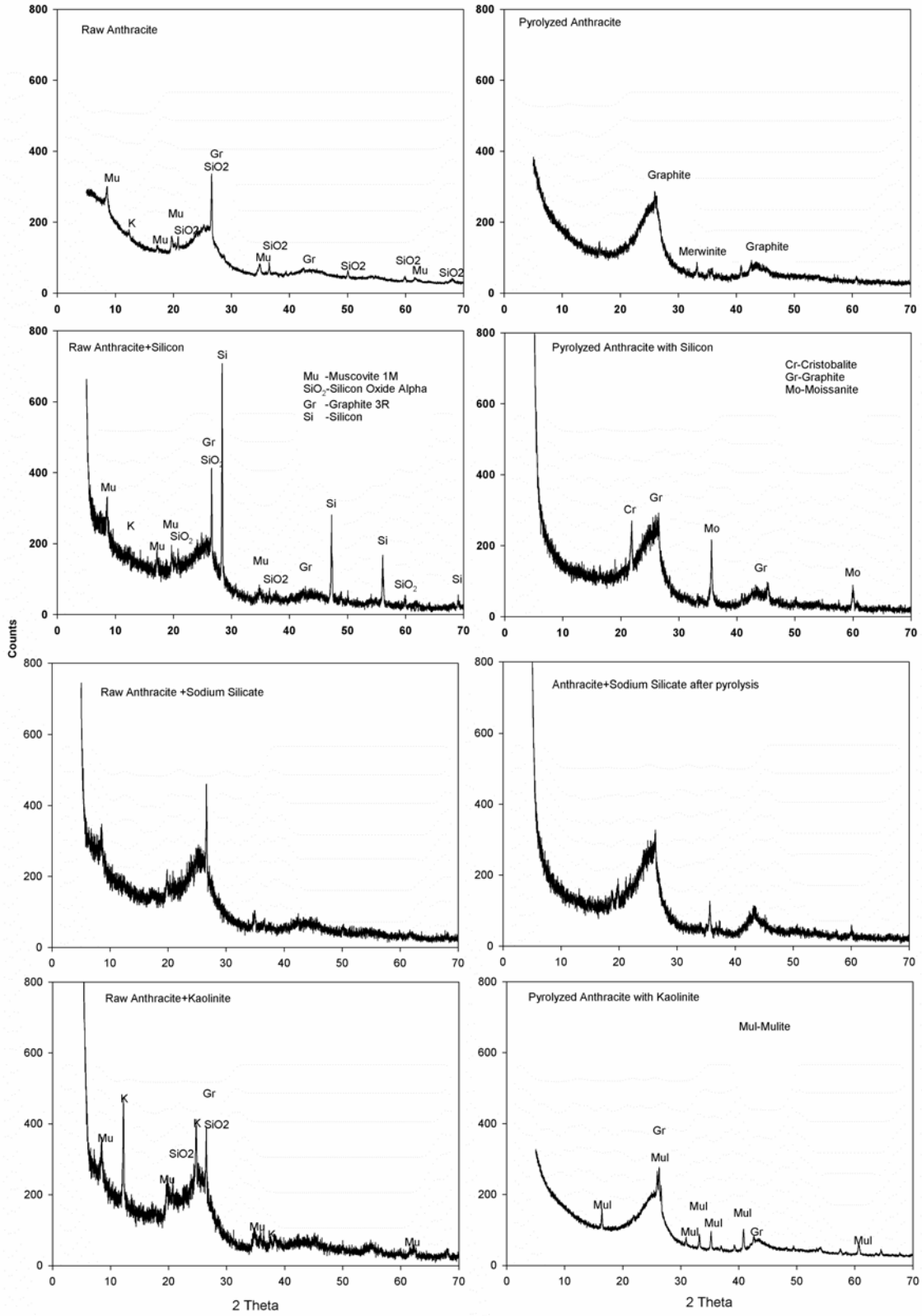


Figure 13. The XRD patterns of several anthracite pellets before and after being pyrolyzed at 1400 °C under nitrogen environment

5. CONCLUSIONS

Lab test results have confirmed that the replacement of foundry coke by bound anthracite fines is promising.

First, anthracite fines have similar chemical properties as the foundry coke does. Caloric analysis showed that anthracite fines have similar heat content as the foundry coke. Elemental analysis suggested that the anthracite fines contain less sulfur than the foundry coke.

Second, different binder combinations can bind the anthracite fines together to satisfy the mechanical strength requirements of coke replacement at different levels. By using renewable and cost effective organic materials only, anthracite fines can be bound into pellets with very good room temperature mechanical strength (better than the foundry coke in term of anti-breakage strength). These bound anthracite fines are good enough to replace foundry coke in the cupola furnace at very low level. The bound anthracite fines must maintain enough strength at very high temperature in order to replace more foundry coke in the cupola. Inorganic materials were introduced with the collagen-based binder to increase the strength of the bound anthracite fines at high temperature. Various inorganic materials were tested for this proposal and ferrosilicon is the best additive. It has the biggest retained compressive strength; will not add extra cost; and will not change the chemistry in the copula.

Currently, two different recipes are suggested for binding anthracite pellets together to replace foundry coke at pilot-scale test. For lower level coke replacement (up to 10%), 1 g collagen-based binder plus 1.5 g fructose should be added with per 100 g anthracite fines because high temperature strength is not concerned. For high level coke replacement (more than 30%), 10 g silicon powders should be added in addition to the organics. Pilot-scale tests of coke replacement by anthracite briquettes in a real cupola have been scheduled for fall 2009 at a foundry in Pennsylvania and will provide direct information regarding the effect of coke replacement on the whole melting process.

REFERENCES

1. Kirk, E., *The Cupola Furnace*. 1903, Philadelphia: Henry Carey Baird & Co.
2. Moldenke, R., *The Principles of Iron Foundry*. 1917, New York: McGraw-Hill Book Company Inc.
3. Chan, B.P. and K.F. So, *Photochemical crosslinking improves the physicochemical properties of collagen scaffolds*. Journal of Biomedical Materials Research Part A, 2005. **75A**(3): p. 689-701.
4. Ohan, M.P., K.S. Weadock, and M.G. Dunn, *Synergistic effects of glucose and ultraviolet irradiation on the physical properties of collagen*. Journal of Biomedical Materials Research, 2002. **60**(3): p. 384-391.
5. Raiskup-Wolf, F., et al., *Collagen crosslinking with riboflavin and ultraviolet-A light in keratoconus: Long-term results*. Journal Of Cataract And Refractive Surgery, 2008. **34**(5): p. 796-801.
6. Bailey, A.J. and D.N. Rhodes, *Irradiation-induced Crosslinking of Collagen*. Radiation Research, 1964. **22**: p. 606-621.

7. Chang, M.C., et al., *Preparation of a porous hydroxyapatite/collagen nanocomposite using glutaraldehyde as a crosslinkage agent*. Journal of Materials Science Letters, 2001. **20**(13): p. 1199-1201.
8. Charulatha, V. and A. Rajaram, *Crosslinking density and resorption of dimethyl suberimidate-treated collagen*. Journal of Biomedical Materials Research Part A, 1996: p. 478-486.
9. Coradin, T., O. Durupthy, and J. Livage, *Interactions of amino-containing peptides with sodium silicate and colloidal silica: A biomimetic approach of silicification*. Langmuir, 2002. **18**(6): p. 2331-2336.
10. Duan, X. and H. Sheardown, *Crosslinking of collagen with dendrimers*. Journal of Biomedical Materials Research Part A, 2005. **75A**(3): p. 510-518.
11. Eyre, D.R. and J.J. Wu, *Collagen Cross-links*. Top Curr Chem, 2005. **247**: p. 207-229.
12. Fujimoto, D. and K. Horiuchi, *Acceleration of glucose-mediated crosslinking of collagen by free lysine*. Experientia, 1986. **42**: p. 405.
13. Harriger, M.D., et al., *Glutaraldehyde crosslinking of collagen substrates inhibits degradation in skin substitutes grafted to athymic mice*. Journal of Biomedical Materials Research, 1997. **35**(2): p. 137-145.
14. Verzijl, N., et al., *Crosslinking by advanced glycation end products increases the stiffness of the collagen network in human articular cartilage - A possible mechanism through which age is a risk factor for osteoarthritis*. Arthritis And Rheumatism, 2002. **46**(1): p. 114-123.
15. Tanzer, M.L., *Cross-Linking of Collagen*. Science, 1973. **180**(4086): p. 561-566.
16. Sell, D.R., et al., *Glucosepane is a major protein cross-link of the senescent human extracellular matrix - Relationship with diabetes*. Journal Of Biological Chemistry, 2005. **280**(13): p. 12310-12315.
17. Sajithlal, G.B., P. Chithra, and G. Chandrakasan, *Advanced glycation end products induce crosslinking of collagen in vitro*. Biochimica Et Biophysica Acta-Molecular Basis Of Disease, 1998. **1407**(3): p. 215-224.
18. Baharvandi, H.R. and A.M. Hadian, *Pressureless Sintering of TiB₂-B₄C Ceramic Matrix Composite*. Journal Of Materials Engineering And Performance, 2008. **17**(6): p. 838-841.
19. Carter, C.B. and M.G. Norton, *Ceramic Material: Science and Engineering*. 2007, New York: Springer.
20. Liu, C.X., et al., *Pressureless sintering of large-scale fine structural alumina matrix ceramic guideway materials*. Materials Science And Engineering A-Structural Materials Properties Microstructure And Processing, 2007. **444**(1-2): p. 58-63.
21. Sciti, D., S. Guicciardi, and A. Bellosi, *Properties of a pressureless-sintered ZrB₂-MoSi₂ ceramic composite*. Journal of American Ceramic Society, 2006. **89**(7): p. 2320-2322.
22. Upadhyaya, G.S., *Sintered Metallic and Ceramic Materials*. 1999, Chichester: John Wiley & Sons, LTD.
23. Yang, F.Y., et al., *Mechanical properties of short carbon fiber reinforced ZrB₂-SiC ceramic matrix composites*. Materials Letters, 2008. **62**(17-18): p. 2925-2927.

**COAL-DERIVED ACTIVATED CARBON FOR THE ADSORPTIVE REMOVAL
OF NITROGEN FROM NEEDLE COKE FEEDSTOCK**

FINAL REPORT

Reporting Period
March 1, 2008 to October 31, 2009

Report Prepared by

Peter G. Stansberry & John C. Chang
GrafTech International Holdings, Inc.
12900 Snow Road
Parma, OH 44103

Report Issued
November 2009

DOE Prime Award Number DE-FC26-03NT41874
Subaward Number 3555-GTI-DOE-1874

Contributors

John W. Zondlo
Department of Chemical Engineering
College of Engineering and Mineral Resources
P. O. Box 6102
West Virginia University
Morgantown, WV 26506-6102

&

James R. Pagnotti
Jeddo Coal Company
46 Public Square, Suite 600
Wilkes-Barre, PA 18701

DISCLAIMER

This report was prepared as an account of work sponsored by an agency of the United States Government. Neither the United States Government nor any agency thereof, nor any of their employees, makes any warranty, express or implied, or assumes any legal liability or responsibility for the accuracy, completeness, or usefulness of any information, apparatus, product, or process disclosed, or represents that its use would not infringe privately owned rights. Reference herein to any specific commercial product, process, or service by trade name, trademark, manufacturer, or otherwise does not necessarily constitute or imply its endorsement, recommendation, or favoring by the United States Government or any agency thereof. The views and opinions of authors expressed herein do not necessarily state or reflect those of the United States Government or any agency thereof.

Abstract

Two anthracite coal samples were activated in a fluidized-bed reactor using carbon dioxide at elevated temperature. Anthracite A and anthracite B were activated at 900°C, 925°C, and 950°C up to about 80 wt% conversions (burn-off) with the resultant activated carbons characterized by surface area determinations. The surface area developed for anthracite A was 788 m²/g after reacting at 900°C for 10 hr. The surface area developed for anthracite B was 1388 m²/g after reacting at 900°C for 20 hr. It was observed that lower activation temperatures result in carbons with higher total surface areas. The surface of a commercial activated carbon Nuchar SA 20 was modified by oxidation with nitric acid or air in an effort to introduce oxygen functional groups. The extent of oxygen incorporation was measured indirectly using a pH procedure where it was found that all of the oxidized carbons were more effective in nitrogen removal from Koppers heavy coal-tar distillate (CTD) than the un-oxidized carbon. Contacting Nuchar SA 20 using toluene as a diluent precipitated nitrogen-containing components from the CTD, which resulted in spurious nitrogen determinations. A new solvent system and procedure were explored whereby carbon disulfide was found superior to toluene in terms of boiling point and solvency. Batch-adsorption experiments consisting of 10 g of CTD and 40 g of carbon disulfide with 7 g of the air-oxidized Nuchar SA 20 were conducted in nine series for a total of 57 adsorption experiments. The material from each batch experiment was combined to give approximately 400 g of total product. Control samples, which were mixtures of CTD and carbon disulfide without the activated carbon, as well as the feed CTD, were also analyzed for nitrogen content in parallel with each series. The average nitrogen content for the control samples and treated samples was 0.869 wt% and 0.578 wt%, respectively. The net result for the batch experiments shows that the nitrogen content was reduced by 33.4 %. The denitrogenated CTD was carbonized in a batch coker under 50 psi nitrogen pressure at 475°C for 20 hours. The yield of green coke was 42.2 wt%. The green coke was calcined to 1,420°C with a calcined coke yield of 79 wt%. The calcined coke was fashioned into a 19-mm diameter graphite test rod along with a sample consisting of a petroleum-based coke for use as a control for determination of coefficient of thermal expansion (CTE), density, and specific resistivity. The CTE for the treated CTD and control graphite test rods were 0.209 and 0.107 ppm/°C, respectively.

Table of Contents

Disclaimer	ii
Abstract	iii
Table of Contents	iv
List of Tables	v
List of Figures	vi
1.0 Introduction	1
2.0 Executive Summary	2
3.0 Experimental	3
3.1 Nitrogen Determination	3
3.2 Activation of Anthracite Coals	4
3.3 Activated Carbon Surface Modification	5
3.3.1 Modification by Nitric Acid	5
3.3.2 Modification by Air	6
3.3.3 Determination of Surface pH	6
3.4 Solvent Selection and Adsorption Procedure	6
3.4.1 Procedure with Toluene	6
3.4.2 Procedure with Carbon Disulfide	6
3.4.3 Procedure Using Air-Oxidized Nuchar SA 20 and CS ₂ Diluent	7
3.5 Carbonization of CTD and Fabrication of Graphite Specimens ..	8
4.0 Results and Discussion	8
4.1 Activation of Anthracite Coals	8
4.1.1 Activation of Anthracite A	8
4.1.2 Activation of Anthracite B	13
4.2 Nitrogen Removal from CTD	16
4.2.1 Results of Initial Adsorption Experiments	16
4.2.2 Nitrogen Removal from CTD Using Un-Oxidized Nuchar SA 20	18
4.2.3 Nitrogen Removal from CTD Using Oxidized Nuchar SA 20	20
4.2.4 Effects of Activated Anthracite B on Nitrogen Removal	22
4.2.5 Preparation of Denitrogenated CTD for Carbonization	23
4.3 Fabrication and Results of Graphite Test Specimens	26
5.0 Conclusions	27
6.0 References	28

List of Tables

Table I Boiling points of various solvents	7
Table II Results of activation of anthracite A	9
Table III Activation of anthracite B	13
Table IV Elemental composition of heavy coal-tar distillate and decanted oil	17
Table V Reduction in nitrogen content by Nuchar SA 20	17
Table VI Nitrogen in the treated CTD along with the nitrogen removed vs. amount of carbon added to 50 cc of 4:1 CS ₂ : CTD solution	18
Table VII pH values of unoxidized and oxidized carbons	20
Table VIII Nitrogen distribution between solution and added carbon	21
Table IX Results of denitrogenation of CTD	24
Table X Statistical results on treating CTD with oxidized Nuchar SA 20	25
Table XI Product yield from batch coking of denitrogenated Koppers CTD ..	26
Table XII Properties of graphite test specimens	27

List of Figures

Figure 1 Schematic diagram of the elemental analyzer set up for nitrogen analysis	4
Figure 2 Percentage of anthracite A reacted at 900°C vs. time	9
Figure 3 Total surface area and mesopore surface area for anthracite A reacted at 900°C	10
Figure 4 Percentage of anthracite A reacted at 925°C vs. time	10
Figure 5 Total surface area and mesopore surface area for anthracite A reacted at 925°C	11
Figure 6 Percentage of anthracite A reacted at 950°C vs. time	12
Figure 7 Total surface area and mesopore surface area for anthracite A reacted at 950°C	12
Figure 8 Percentage of anthracite B reacted at 900°C vs. time	14
Figure 9 Total surface area and mesopore surface area for anthracite B reacted at 900°C	14
Figure 10 Percentage of anthracite A reacted at 925°C vs. time	15
Figure 11 Total surface area and mesopore surface area for anthracite B reacted at 925°C	15
Figure 12 Percentage of anthracite B reacted at 950°C vs. time	16
Figure 13 Total surface area and mesopore surface area for anthracite A reacted at 950°C	16
Figure 14 Plot of nitrogen removed vs. amount of carbon with CS ₂ as the solvent	19
Figure 15 Plot of nitrogen removed vs. amount of carbon in two-step adsorption process	20
Figure 16 Plot of nitrogen removed vs. amount of oxidized carbons	21
Figure 17 Plot of nitrogen removed vs. amount of carbon with THF as the solvent	22
Figure 18 Effect of activated anthracite B on nitrogen removal vs. time	23
Figure 19 Effect of oxidation of anthracite B on nitrogen removal	23
Figure 20 Temperature profile during batch coking of treated CTD	26

1.0 Introduction

Needle coke is the most important industrial raw material for making graphite electrodes as used in the electric arc furnace (EAF) for making steel from scrap metals. The EAF method is more energy efficient than that of conventional steel making from iron ore in the blast furnace. There is an annual demand for one million metric tons of high-quality needle coke worldwide. From the total demand less than 15 % of the needle coke is derived from coal-based raw materials. In the United States, there are no producers of needle coke from coal. Needle coke produced domestically are based on petroleum sources, such as that made by Conoco-Phillips and Seadrift.

Coal-based feedstocks have inherent advantages over petroleum counterparts because of molecular structure. High-temperature coal tars, coal extracts, and other similar materials are, in general, more aromatic and contain less side chains. If treated properly, the coefficient of thermal expansion (CTE, a major indicator of coke quality) for coal-based needle coke could be superior to that of petroleum-based needle coke (1). However, as demonstrated from our previous CPCPC sponsored project, the needle coke thus derived had a high puffing behavior during the graphitization process, probably due to high nitrogen content (2). Thus nitrogen compounds need to be eliminated prior to coking and graphitization.

In the current project, activated carbons produced from anthracite coal were tested as a possible means in selectively removing nitrogen-containing compounds from coal-based distillates. The parameters of the activation were varied so as to manipulate the resultant surface area, pore-size distribution, and surface chemistry. Select activated carbons were tested for their effectiveness at removing nitrogen compounds from a coal-based distillate that is free of quinoline-insoluble matter. A commercial activated carbon, Nuchar SA 20, was also examined for nitrogen removal ability. After adsorption, the treated distillate was carbonized and converted into needle coke. The nature of the needle coke along with its nitrogen content was assessed.

There is commercial interest in seeking alternate sources for needle coke since the current value of needle coke varies from \$1,000 to \$1,500 per metric ton, and is continually rising. The results of this study could lead to two value-added carbon products from coal, viz., activated carbon and coal-based coke precursor. The potential exists to blend the coal-tar distillate after denitrogenation with petroleum feedstocks to exploit the advantages of both raw materials for delayed coking facilities at US refineries.

2.0 Executive Summary

Samples of decanted oil (petroleum derived, Seadrift) and heavy coal-tar distillate (CTD, Koppers) were supplied by GrafTech. These raw materials are the same used in previous CPCPC projects as potential needle coke precursors. Thus, the results of the current project can be compared to the earlier results. A sample of commercial activated carbon (Nuchar SA-20, Westvaco) was chosen as a reference adsorbent. Jeddo Coal Company supplied two anthracite coals.

West Virginia University assembled a fluidized-bed activation reactor that can provide 100-gram quantities of activated anthracite per run. The anthracite coal samples were activated using carbon dioxide at elevated temperature. Both anthracites were cleaned to produce low-ash coals prior to activation. Anthracite A and anthracite B were activated at 900 °C, 925 °C, and 950 °C up to about 80 wt% conversions (burn-off) with the resultant activated carbons characterized by surface area determinations. The surface area developed for anthracite A was 788 m²/g after reacting at 900 °C for 10 hr. The surface area developed for anthracite B was 1388 m²/g after reacting at 900 °C for 20 hr. It was observed that for both coals lower activation temperatures result in carbons with higher total surface areas. The activation rate for anthracite B was slightly slower than anthracite A, with anthracite B producing higher surface areas. Moreover, anthracite B activated at 900 °C for 20 hr had mesopore surface area of about 420 m²/g, nearly more than four times that of anthracite A.

The surfaces of anthracite B (activated 900°C, 15 hours, surface area 1,400 m²/g) and Nuchar SA 20 were modified by oxidation with nitric acid or air in an effort to introduce oxygen functional groups. The extent of oxygen incorporation for the commercial activated carbon was measured indirectly using a pH procedure. The untreated Nuchar SA 20 produced a solution having a pH of 5.8. Air oxidized Nuchar SA 20, and nitric acid oxidized Nuchar SA 20 for 22 and 24 hr, generated solutions with pH values of 4.5, 3.3, and 3.1 respectively. It is apparent that oxidation of the commercial activated carbon incorporates acidic functionality. More importantly, it was found that all of the oxidized Nuchar SA 20 and activated anthracite B were more effective in nitrogen removal from CTD than the un-oxidized carbon.

A reliable analytical method was developed to detect nitrogen-containing compounds in the two “oils” used in this project. An elemental analyzer was retrofitted to detect nitrogen-containing compounds accurately at levels below 100 ppm.

Contacting Nuchar SA 20 using toluene as a diluent precipitated nitrogen-containing components from the CTD, which resulted in spurious nitrogen determinations. Therefore another solvent system was found. In addition to toluene, tetrahydrofuran and carbon disulfide were explored, whereby carbon disulfide was found superior to toluene and tetrahydrofuran in terms of boiling point, solvency, and adsorption capacity on the activated carbon. The nitrogen content in the treated CTD along with the nitrogen remaining on the carbon after adsorption was measured so that a nitrogen balance could be determined. The results of the nitrogen balance show that

despite the many operations in processing and the small amounts of nitrogen in the samples, the nitrogen balance closes on average to about 10%.

The supply of both anthracite coals was consumed during the course of the activation experiments, and replenishments with identical coals could not be found before the project could be completed. Thus the decision was made to continue with the project by using the commercial activated carbon Nuchar SA 20 in order to demonstrate nitrogen removal. Nuchar SA 20 that was oxidized in air for three hours at 300°C was used for batch-adsorption experiments. Each experiment consisted of 10 g of CTD and 40 g of carbon disulfide with 7 g of the oxidized Nuchar SA 20, which were conducted in nine series for a total of 57 adsorption experiments. The material from each batch experiment was combined to give approximately 400 g of total product. Control samples, which were mixtures of CTD and carbon disulfide without the activated carbon, as well as the feed CTD, were also analyzed for nitrogen content in parallel with each series. The average nitrogen content for the control samples and treated samples was 0.869 wt% and 0.578 wt%, respectively. The net result for the batch experiments shows that the nitrogen content was reduced by 33.3 %. The nitrogen content of the combined CTD was 0.59 wt%, or about one-third the amount of nitrogen in the feed CTD.

The denitrogenated CTD was converted into green coke using the pilot-scale coking facilities at the GrafTech Parma R&D center. Batch coking of the treated CTD was conducted in a stainless steel reactor system with dimensions 11.75 inches inside diameter by 57 inches inside length. The reactor was pressurized to 50 psi with nitrogen and held constant at 50 psi throughout the coking cycle by an automatic pressure control system. The yield of green coke was 42.2 wt%. The treated CTD was calcined to 1,420°C and fabricated into a 19-mm diameter test rod using a conventional coal-tar binder pitch, baked, and then graphitized. A petroleum-based needle coke was processed in parallel with the treated CTD coke as a control. The coefficient of thermal expansion for the treated CTD and control graphite test rods were 0.209 and 0.107 ppm/°C, respectively.

3.0 Experimental

3.1 Nitrogen Determination

The Koppers heavy coal-tar distillate and decanted oil were first analyzed for carbon, hydrogen, nitrogen, and sulfur composition using a Flash EA 1112 elemental analyzer. The instrument was then retrofitted to measure only organic nitrogen in order to improve detection at low concentrations. The change was made to improve sensitivity because it was anticipated that the nitrogen content could reach very low concentrations, especially after adsorption with activated carbon, in which the conventional multi-element-analysis method would not be sufficiently sensitive.

The following procedure was followed to analyze percentage of nitrogen. A schematic diagram of the nitrogen analysis system is shown in Figure 1. An autosampler

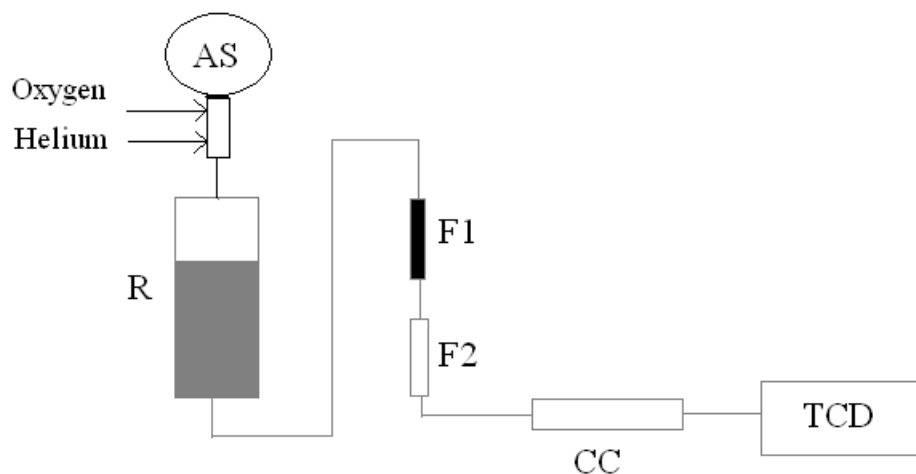


Figure 1. Schematic diagram of the elemental analyzer for nitrogen analysis.

(AS) was connected to a quartz combustion reactor (R) placed in a furnace at the temperature of 900 °C. The reactor outlet was connected to two traps (F1 and F2) in series. The second trap outlet was connected to an analytical gas chromatography column and the response to nitrogen was determined by a thermal conductivity detector (TCD).

The sample to be analyzed was weighed in a tin capsule before loading into the autosampler. Oxygen flowed into the combustion reactor for a preset time. After this time, the sample stored in the autosampler was dropped into the combustion reactor. When tin comes in contact with the oxidizing environment, a highly exothermic reaction was initiated. Temperature rose to approximately 1800 °C ensuring complete combustion of the entire sample. Following combustion, the gas flow was switched from oxygen to helium. The gas mixture (NO_x , CO_2 , H_2O) was passed near the exit portion of the combustion reactor where the oxidation of components was completed and then nitrogen oxides formed were reduced to molecular nitrogen by a catalytic reaction.

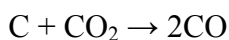
The gas mixture passed through the two traps: F1 was packed with magnesium perchlorate to retain water and F2 was packed with soda lime to remove carbon dioxide. The molecular nitrogen was then determined chromatographically and the peak integration conducted with dedicated computer and software. A standard lubricant oil (1.06 wt% N) was used for calibration of the gas chromatograph. Appropriate response factor was established following a conventional calibration procedure.

3.2 Activation of Anthracite Coals

Initially, a rotating quartz reactor was used for activation; however, it was found that, while the results from this reactor were reproducible, the quantity of activated carbon produced per batch was very small, on the order of a few grams. A new reactor system, which employed fluidized-bed technology, was constructed to supplant the rotating device. The fluidized-bed reactor is characterized by excellent gas-solid contact along with very efficient mixing and heat transfer. The use of such a reactor should result in

more uniform and consistent activation with better control over the surface properties of the resultant activated carbon. Moreover, the amount of carbon per batch can be increased tenfold.

Thus, a fluidized bed reactor system was designed and constructed by researchers in the Chemical Engineering Department at West Virginia University. It consists of a 4 cm internal diameter and 122 cm long quartz tube fitted with a porous quartz frit. The tube was loaded with approximately 50 grams of powdered anthracite coal and placed in a high-temperature tube furnace. The powdered anthracite coal was sieved to give a range of particle diameters between -40 and +70 mesh. The fluidizing/reacting carbon dioxide gas flowed into the bottom of the tube, through the fluidized anthracite particles, and out the top of the reactor to a fume hood. The activation of the coal occurs with carbon dioxide gas via the following reaction:



During heat up, the bed was purged with nitrogen which was then switched to carbon dioxide, once the desired temperature was achieved. The two anthracite coals were cleaned by the supplier to give low-ash values. One coal sample is referred to as anthracite A. The other coal sample is referred to as anthracite B. Both coals were reacted at temperatures of 900 °C, 925 °C, and 950 °C for varying reaction times dependent on the temperature. Reaction times up to 20 hours were tested, with the extent of the coal reacted, or burn-off, being measured gravimetrically as shown in the mathematical expression below. In the equation, *M* represents the percentage of the coal that was moisture, and *V* represents the percentage of the coal that was volatile matter. These values were determined by doing a proximate analysis.

$$\% \text{Conv.} = [(\text{Initial wt.} - (M+V) \times \text{Initial wt.}) - \text{Final wt.}] / [\text{Initial wt.} - (M+V) \times \text{Initial wt.}]$$

3.3 Activated Carbon Surface Modification

3.3.1 Modification by Nitric Acid

Analytical-grade 68 % nitric acid was used for oxidative modification of the Nuchar SA 20 activated carbon and anthracite B (activated 900°C, 15 hours, surface area 1,400 m²/g) under mild conditions. The oxidation process was conducted by adding 100 ml of the nitric acid to 10 g of the activated carbon placed in a glass conical flask with a magnetic stirrer. The mixtures were kept at 30 °C for 22 hrs for one sample and 24 hrs for the other sample. The mixtures were filtered to separate the carbon from the acid solution. The treated sample was further washed with distilled water until the filtrate became pH neutral. The filter cake (treated carbon) was dried at 150 °C in a vacuum oven for 1 hr.

3.3.2 Modification by Air

Oxygen functional groups were introduced onto the surface of the commercial activated carbon Nuchar SA 20 and activated anthracite B (activated 900°C, 15 hours, surface area 1,400 m²/g) by oxidation to improve adsorptive capacity for nitrogen compounds. Oxidized material was made by placing the activated carbon in a stainless steel pan as a thin layer and heating to 300°C in an oven for 3 hours in air. After oxidation, the stainless steel pan with the sample was removed from the oven and cooled to room temperature. This procedure was repeated in order to produce sufficient quantities of oxidized activated carbon for the adsorption experiments.

3.3.3 Determination of Surface pH

A procedure for determining the acidity of the surface of the Nuchar SA 20 activated carbon was followed (3). A 0.5 g sample of activated carbon was added to 25 ml of water. The suspension was stirred for 24 hrs to reach equilibrium. Then the sample was filtered and the pH of the resulting solution was measured by means of a pH meter. While this is an indirect measure of surface pH, the relative values allow comparison of the different oxidation treatments.

3.4 Solvent Selection and Adsorption Procedure

3.4.1 Procedure with Toluene

An experimental procedure for treating "oils" with the activated carbon was developed starting with the CTD. The heavy coal-tar distillate is a highly viscous substance at normal temperature and needs to be diluted to facilitate contacting with the activated carbon. For this purpose, toluene was used as a solvent to dilute the CTD. Different solutions of CTD and toluene were prepared with various weight ratios of toluene-to-CTD, and good fluidity was observed at 1:3 wt ratio to process easily with the activated carbon through centrifugation and filtration. The commercial activated carbon Nuchar SA 20 was used for nitrogen adsorption after first drying the carbon at elevated temperature in a vacuum oven. Nuchar was added to the liquid mixture in a 1:5 wt:wt ratio. The solutions were agitated in a shaker bath set to 160 rpm at 50°C for twenty four hours. Afterward, the mixtures were centrifuge to remove the activated carbon from the liquid. The supernatant liquid was placed on a warm hot plate to promote the evaporation of the toluene until 25 wt% of the mass (the amount of toluene added) was removed. Samples of the treated heavy coal-tar distillate were analyzed for nitrogen content.

3.4.2 Procedure with Carbon Disulfide

Three solvents were chosen to dissolve heavy coal-tar distillate based on their boiling points and solubility properties, Table I. A solvent with a low boiling point has an advantage of quick evaporation from solution leaving behind only CTD. Since constant weight of the sample is an important condition in the nitrogen analysis step, it is necessary to remove all of the solvent before nitrogen analysis can be conducted.

Table I. Boiling points of various solvents.

	Solvent	Boiling Point, °C
1	Toluene	110
2	Carbon disulfide(CS ₂)	46
3	Tetrahydrofuran(THF)	66

Each of the above solvents was mixed with CTD in different weight ratios and added to a 125 ml flask. The flasks were tightly closed with rubber stoppers and wrapped with parafilm and placed in the shaker bath at 30°C and 165 rpm for 1 hr without any activated carbon. The solutions were filtered using vacuum flasks for the determination of undissolved CTD and the filtrates are subjected to solvent evaporation in a heated water bath with gentle shaking at a temperature near the boiling point of the respective solvent.

It was observed that carbon disulfide (CS₂) and tetrahydrofuran (THF) at 4:1 solvent-to-CTD wt ratio performed better than toluene at 5:1 wt ratio. In these experiments, virtually all of the original weight of the starting CTD was recovered. Further experiments were then conducted with CS₂ and THF at the 4:1 wt ratio to see which of these solvents performed better in keeping the CTD from precipitating. Carbon disulfide was chosen for further studies because of its low-boiling point and ability to maintain the CTD in solution.

3.4.3 Procedure Using Air-Oxidized Nuchar SA 20 and CS₂ Diluent

A procedure was established for all the adsorption experiments in which the air-oxidized activated carbon and carbon disulfide were used for the adsorption of nitrogen compounds from heavy coal-tar distillate in preparation for carbonization. A 50-g solution of 4:1 wt ratio of CS₂-to-CTD was prepared by adding 40 g of solvent to 10 g of CTD. Five grams of air-oxidized Nuchar SA 20 was added to the solution and mixed well. Prior to the addition, the carbon was vacuum heated to remove surface moisture. Then the flask was tightly closed with a rubber stopper and was placed in a shaking water bath at 30°C. After two hours of contact with carbon, the solution is carefully separated from the carbon through filtration. The walls of the flask and filter cake were washed with an extra 40 g of solvent to recover CTD trapped on the filter cake. Then the solvent was evaporated from the filtrate in a water bath till constant weight was achieved.

In order to provide about 400 g of treated CTD required for carbonization, the batch-wise adsorption experiments were conducted in nine series totaling 57 adsorptions, in addition to adsorptions that did not contain oxidized Nuchar SA 20 for use as controls. It was decided to take a conservative approach in conducting the adsorption experiments in small batches rather than one or two larger batches to ensure that the results would be consistent with our earlier work and to eliminate variation because of scaling up.

3.5 Carbonization of CTD and Fabrication of Graphite Test Specimens

About 380 grams of the denitrogenated CTD (section 3.4.3) was converted into green coke using the pilot-scale coking facilities at the GrafTech Parma R&D center. Conversion into green coke was accomplished in a stainless steel reactor system with dimensions 11.75 inches inside diameter by 57 inches inside length. A known quantity of the treated CTD was placed into a tared stainless steel canister and loosely sealed with a lid. The canister was placed on top of a support platform inside of the reactor such that the CTD was maintained within the center region of the heated zone to assure uniform heating. The reactor cover was bolted securely and the system pressurized with nitrogen gas and checked for leakage. The reactor was then pressurized to 50 psi with nitrogen gas and held constant at 50 psi throughout the coking cycle by an automatic pressure control system. Temperature was controlled by a computerized processor, which was programmed to heat the reactor contents 50°C/hr to 475°C and held at this temperature for 20 hours. After the coking cycle the reactor was cooled to room temperature, vented, and opened to remove the coked material. The canister was weighed to determine green coke yield and the product removed for further processing.

The green coke was calcined under an inert atmosphere in a tube furnace at 1,420°C and held at this temperature 30 minutes to drive off volatile matter and to densify the coke. The calcined coke was milled, sized, and mixed with a conventional coal-tar binder pitch in preparation of a graphite test rod. The mix was extruded hot into a 19 mm diameter rod and then baked in a sagger to 850°C while under an inert atmosphere. A test rod using a petroleum-based needle coke was processed in parallel with the CTD coke for use as a control. After baking, both specimens were graphitized to 3000°C in a tube furnace under an inert atmosphere. After graphitization, the rods were machined for determination of coefficient of thermal expansion (CTE), specific resistivity, and bulk density using test methods developed by GrafTech. An attempt was made to determine the effects of nitrogen removal from the CTD by using a proprietary puffing characteristic test, but was unsuccessful.

4.0 Results and Discussion

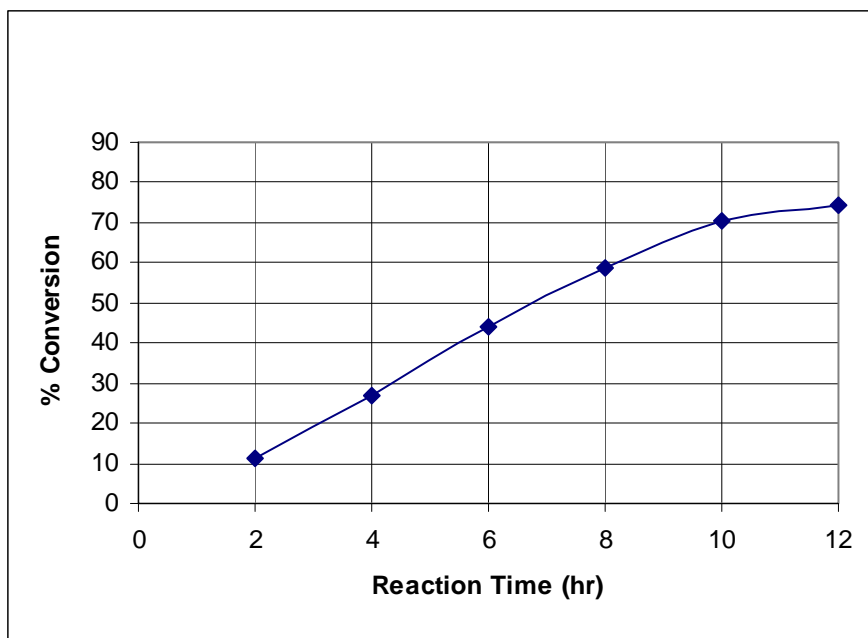
4.1 Activation of Anthracite Coals

4.1.1 Activation of Anthracite A

The results of activation of anthracite A for different temperatures are summarized in Table II. The results of activation at 900°C are provided graphically in Figures 2 and 3. It can be seen in Figure 2 that as the reaction time increased so does the percentage of coal that was reacted. At around 12 hours, the curve begins to level off meaning there is a maximum conversion of about 75 to 80 percent for these reaction conditions. In Figure 3, both the total surface area and mesopore surface area increase with conversion. Although the total surface area values are high (~800 m²/g), the mesopore surface area values do not exceed 100 m²/g, which is considered low.

Table II. Results of activation of anthracite A.

Temperature	Time (hr)	Conversion %	Total Surface Area (m ² /g)	Mesopore Surface Area (m ² /g)	Average Pore Size (nm)
900°C	2	11.1	128	0.3	1.87
	4	27.0	273	7.1	1.90
	6	43.9	431	17.7	1.93
	8	58.6	618	36.2	1.97
	10	70.3	788	78.9	2.07
	12	74.1	742	88.0	2.14
925°C	2	16.8	226	7.2	1.94
	4	39.8	398	20.5	1.96
	6	61.8	577	51.7	2.06
	7	60.0	585	58.5	2.12
	8	67.4	453	58.2	2.12
	10	77.7	651	117.2	2.37
950°C	1	14.1	153	4.6	1.94
	2	33.9	313	13.7	2.19
	3	53.6	363	41.9	2.20
	4	67.6	497	114.5	2.55
	5	75.4	441	69.8	2.36
	6	75.6	452	80.9	2.42

**Figure 2.** Percentage of anthracite A reacted at 900°C vs. time.

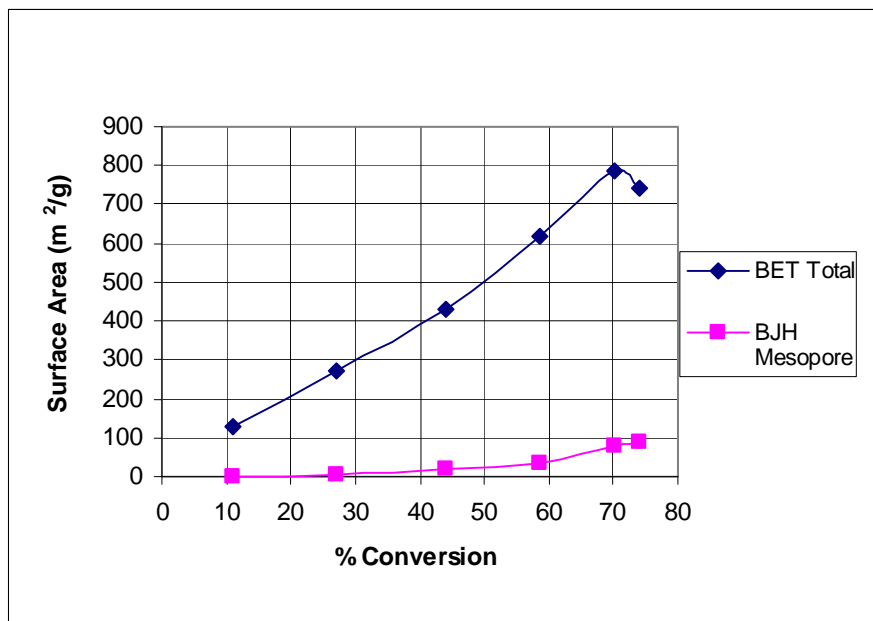


Figure 3. Total surface area and mesopore surface area for anthracite A reacted at 900°C.

The results for anthracite A when reacted at 925°C are shown in Figures 4 and 5. In general, conversion increases with reaction time while both total and mesopore surface area increase with conversion.

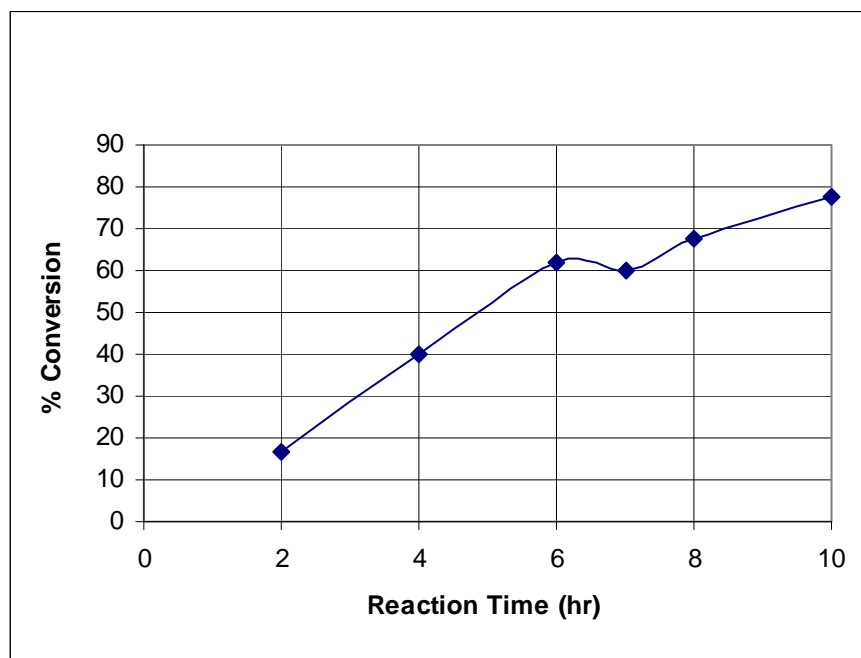


Figure 4. Percentage of anthracite A reacted at 925 °C vs. time.

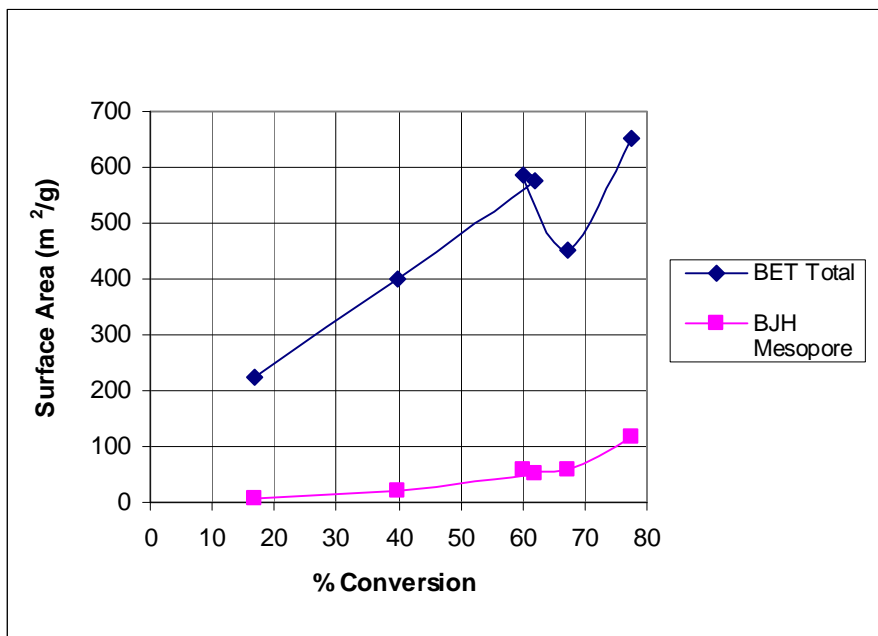


Figure 5. Total surface area and mesopore surface area for anthracite A reacted at 925°C.

The analysis of the anthracite A when reacted at 950°C is provided in Figures 6 and 7. For anthracite A reacted at 950°C, the conversion reaches a maximum at about 75%. From Figure 7, it appears that the maximum surface area can be obtained when the conversion is around 70%.

For anthracite A, greater total surface areas can be achieved when the coal is reacted at lower temperatures for longer times (higher conversion). Figures 3, 5, and 7 show that as the reaction temperature is increased, the total surface area drops considerably when comparing the same percent conversion. Thus it appears that slower reaction rates result in higher surface areas.

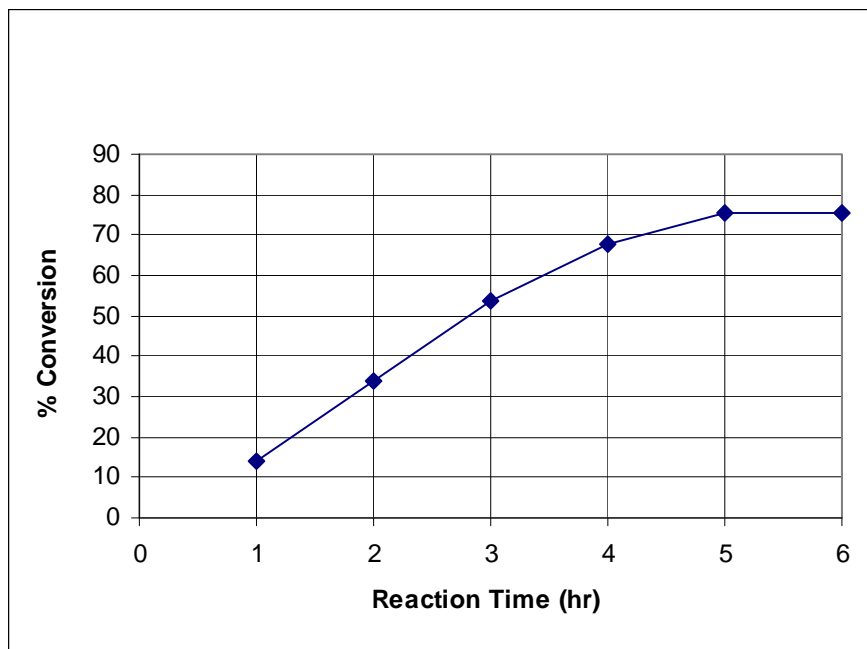


Figure 6. Percentage of anthracite A reacted at 950°C vs. time.

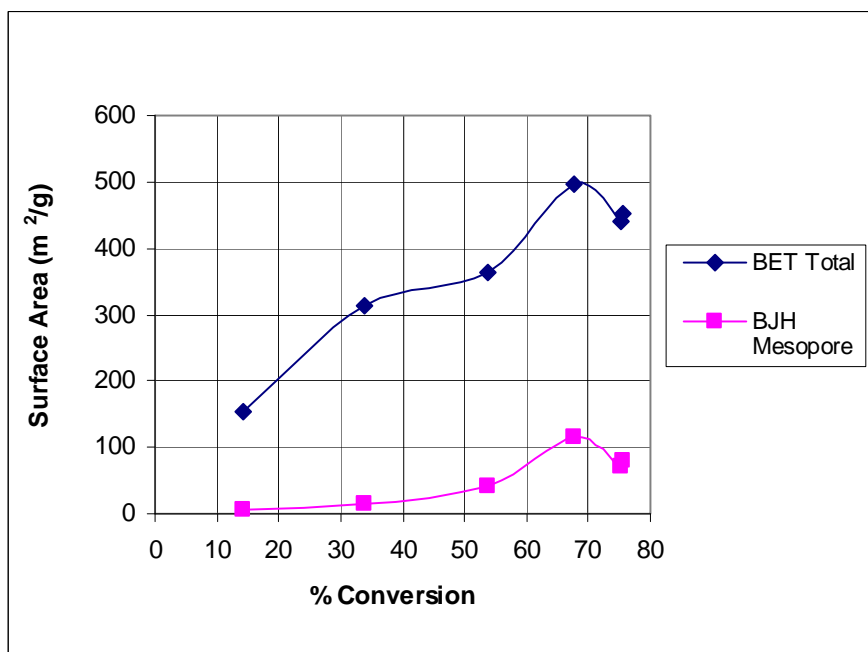


Figure 7. Total surface area and mesopore surface area for anthracite A reacted at 950°C.

4.1.2 Activation of Anthracite B

Anthracite B seems to follow the same activation trends as anthracite A; however, the reaction rate is slightly slower and anthracite B gives higher surface areas. The data for anthracite B are summarized in Table III.

Table III. Activation of anthracite B.

Temperature	Time (hr)	Conversion %	Total Surface Area (m ² /g)	Mesopore Surface Area (m ² /g)	Average Pore Size (nm)
900°C	4	13.0	218	0.0	1.76
	8	33.7	562	20.4	1.86
	12	59.0	-	-	-
	16	71.1	1103	223.7	2.11
	20	81.2	1388	419.9	2.29
925°C	3	8.4	-	-	-
	6	36.3	-	-	-
	9	62.2	873	182.9	2.12
	18	93.0	852	307.5	2.56
950°C	2.5	14.4	221	0.1	1.80
	5	34.2	437	46.5	1.95
	7.5	55.7	616	137.1	2.14
	10	70.7	686	204.8	2.34
	12.5	84.1	632	215.5	2.51
	15	84.6	713	258.1	2.55

The analyses of anthracite A reacted at 900°C are provided in Figures 8 and 9 where it can be seen from Figure 9 that very high surface areas were obtained. At a little over 80 % conversion, a total surface area of 1400 m²/g and a mesopore surface area over 400 m²/g were achieved.

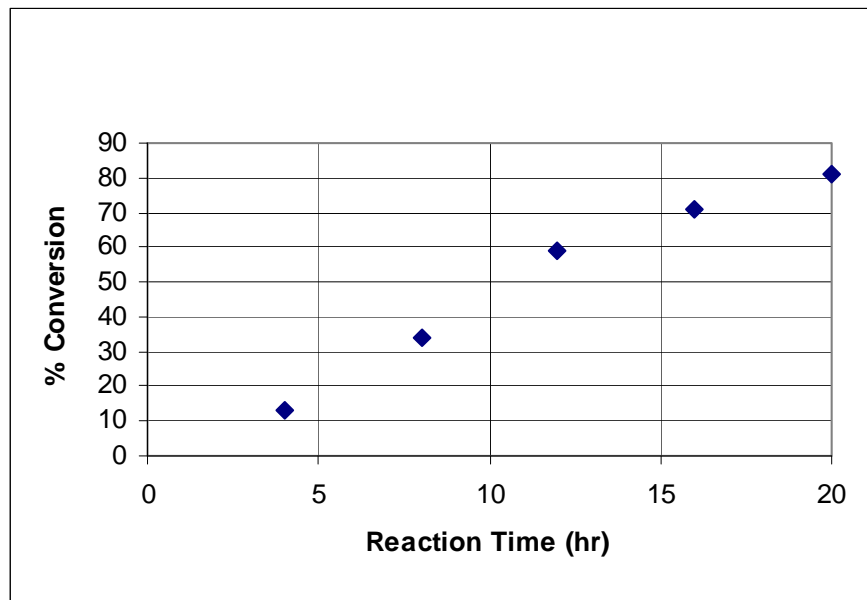


Figure 8. Percentage of anthracite B reacted at 900°C vs. time.

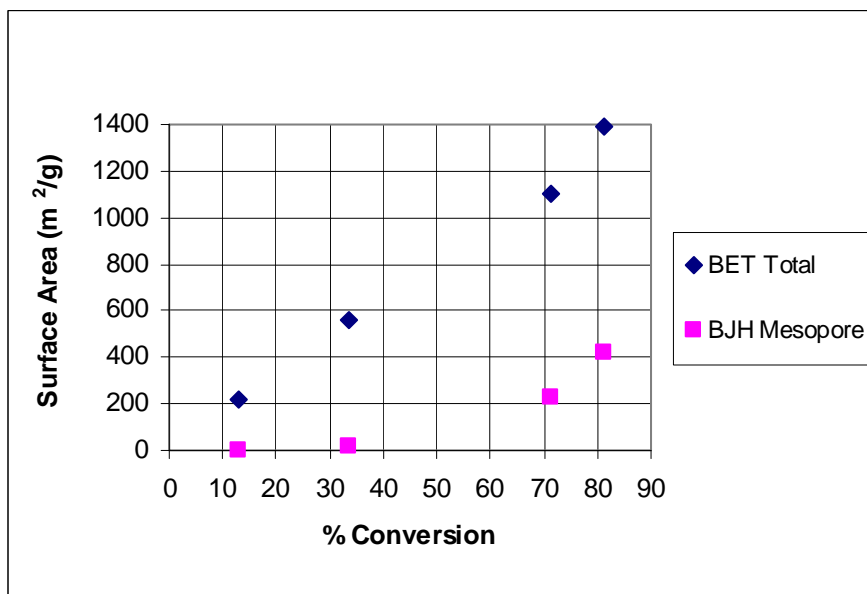


Figure 9. Total surface area and mesopore surface area for anthracite B reacted at 900°C.

Figures 10 and 11 illustrate the activation of anthracite B reacted at 925°C. Under these conditions it is unlikely that surface areas much greater than 1000 m²/g would be possible.

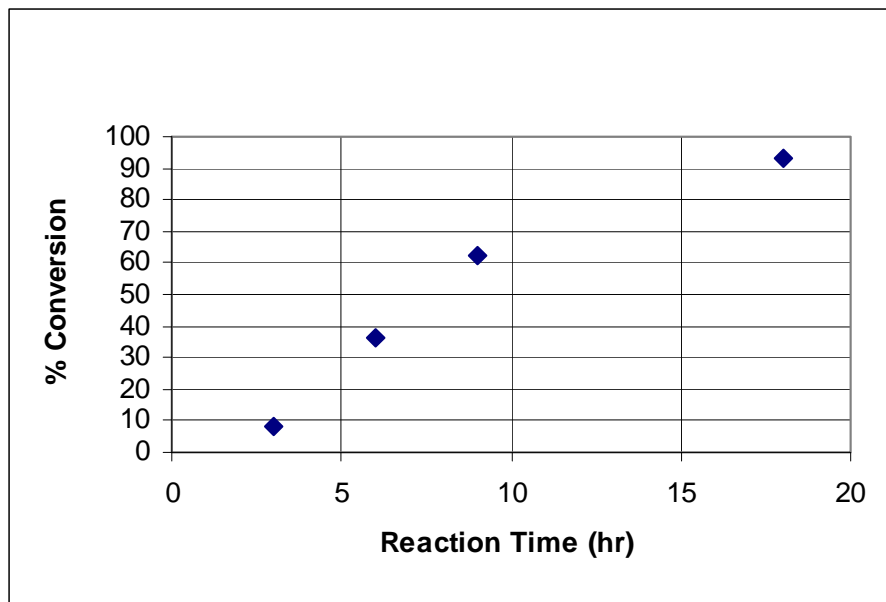


Figure 10. Percentage of anthracite B reacted at 925°C vs. time.

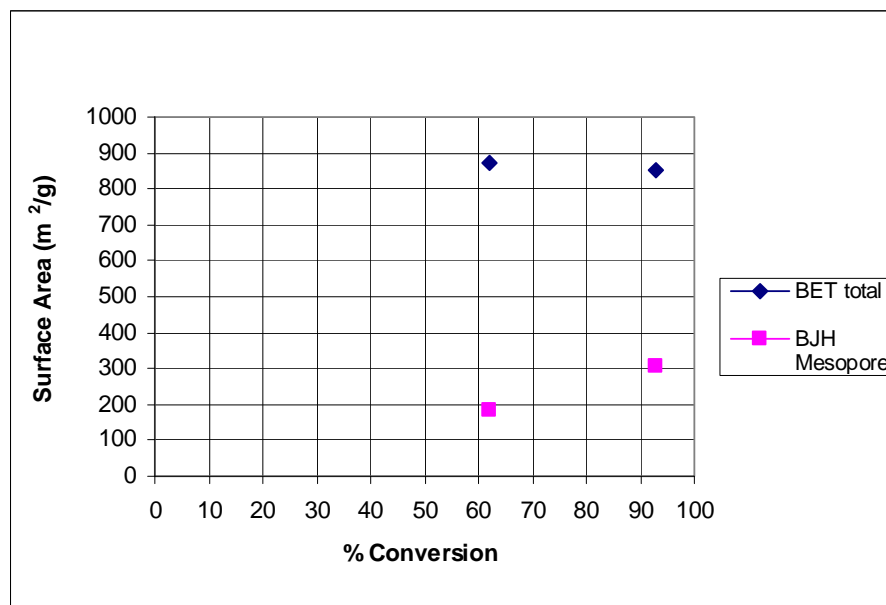


Figure 11. Total surface area and mesopore surface area for anthracite B reacted at 925°C.

The analyses of anthracite B reacted at 950°C are provided in Figures 12 and 13. From Figure 12 anthracite B can reach 85 % conversion when reacted at 950°C. This yields a total surface area of about 700 m²/g. Activation of anthracite B at the lower temperature, 900°C, generated an activated carbon with the highest total and mesopore surface areas.

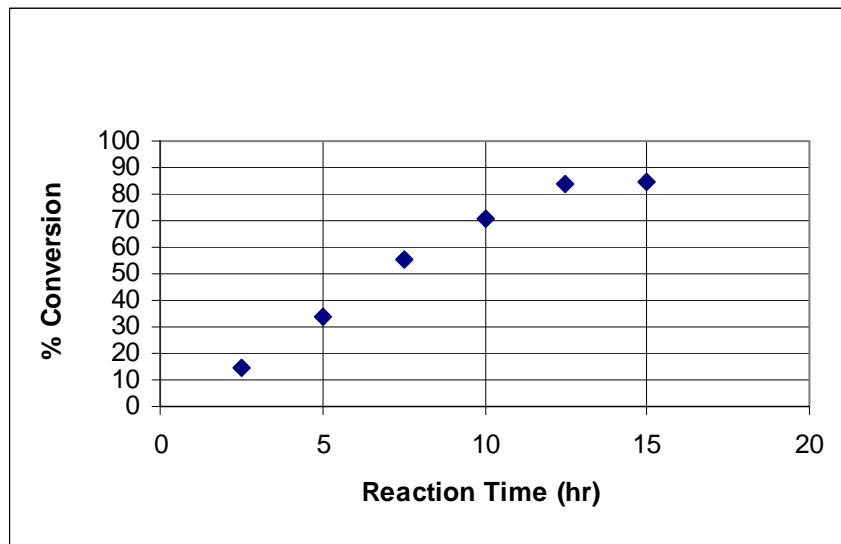


Figure 12. Percentage anthracite B reacted at 950°C vs. time.

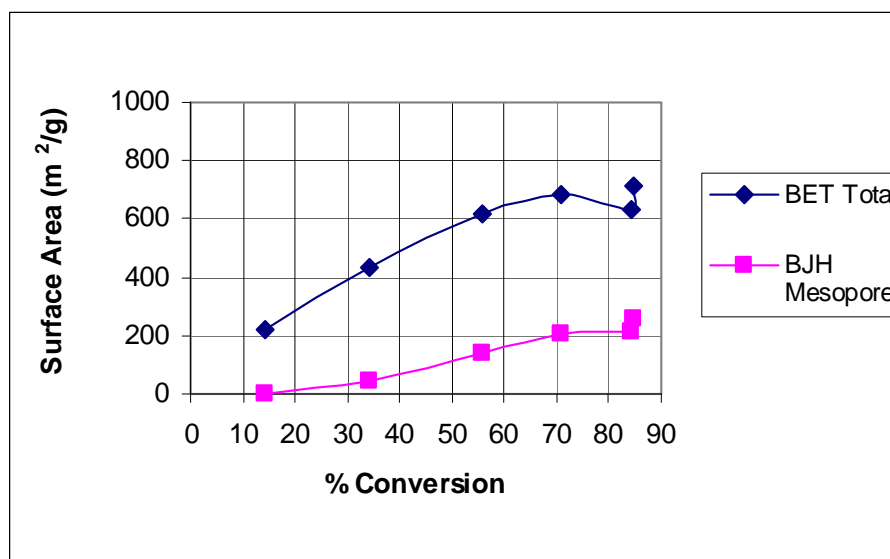


Figure 13. Total surface area and mesopore surface area for anthracite B reacted at 950°C.

4.2 Nitrogen Removal from CTD

4.2.1 Results of Initial Adsorption Experiments

The elemental composition of the feed “oils” before adsorption is provided in Table IV. As expected, both materials are aromatic because of their high carbon contents with the decanted oil being more aliphatic than the heavy coal-tar distillate. The heavy coal-tar distillate contains more than three times the nitrogen content as the decanted oil.

Table IV. Elemental composition of heavy coal-tar distilled and decanted oil.

Sample	Carbon (wt%)	Hydrogen (wt%)	Sulfur (wt%)	Nitrogen (wt%)
Heavy coal-tar distillate	92.34	5.95	0.37	1.22
Decanted oil	91.10	8.99	0.28	0.34

Table V shows the nitrogen content after treating the heavy coal-tar distillate with Nuchar SA 20 for 24 hours at 50 °C. The analyses were conducted in duplicate with four trails each. The results show that adsorption with the commercial activated carbon reduced the nitrogen content by about 38 %.

Table V. Reduction in nitrogen content by Nuchar SA 20.

	Sample 1 Nitrogen Content (wt%)	Sample 2 Nitrogen Content (wt%)
Trail 1	0.800	0.764
Trail 2	0.757	0.795
Trial 3	0.730	0.723
Trial 4	0.767	0.760
Average	0.764	0.760
Standard Deviation	0.029	0.030

There was concern that some of the nitrogen-containing species might be lost during the evaporation of toluene from the heavy coal-tar distillate. To test this the 75:25 wt:wt heavy coal-tar distillate and toluene solution was placed on a warm hot plate until 25 % of the mass was reduced, corresponding to the amount of toluene. A sample was tested for nitrogen content and found to be identical to the original, untreated feed material. Thus no nitrogen species were lost during evaporation.

However, we noted that following adsorption with activated carbon and subsequent workup and analysis, the nitrogen content was reduced by approximately the same extent no matter how the adsorption procedure was conducted. The observation that nitrogen content did not change suggested a shortcoming in the overall experimental procedure. Thus, an experiment without activated carbon was conducted in order to track the mass balance of heavy-coal tar distillate, and consequently nitrogen content, during the product workup. A 50-g sample of solution with 1:3 wt ratio of toluene-to-CTD was prepared in 125-ml flask and was placed in a shaker bath at 165 rpm and at a constant temperature of 30°C. After one hour the flask was taken out of the bath and centrifuged for 10 min at 2000 rpm. It was observed that some undissolved CTD had separated from the solution and had deposited at the bottom of centrifuge tubes. The undissolved CTD

was not visible in a freshly prepared solution nor was it detected after centrifugation after the activated carbon was added to the solution.

The undissolved CTD accounted for about 30% of the weight of the original CTD. The solution was filtered and the toluene evaporated from the filtrate. The resulting filtrate was then sent for nitrogen analysis. Compared to the feed CTD, the nitrogen content of the filtrate was reduced by 26% even without treating with carbon. Thus it was concluded that some nitrogen compounds were being removed in the form of undissolved solids.

4.2.2 Nitrogen Removal from CTD Using Un-Oxidized Nuchar SA 20

Experiments were carried out to test the efficiency of Nuchar SA 20 activated carbon to remove nitrogen species from coal tar distillate using CS₂ as diluent with different quantities of activated carbon. Undiluted CTD was treated along with solvent-diluted samples to confirm that no change in weight or nitrogen content was detected in the neat CTD. From the results of the nitrogen analysis, percent nitrogen removed from each sample was calculated and plotted, as shown in Table VI and Figure 14.

Table VI. Nitrogen in the treated CTD along with the nitrogen removed vs. amount of carbon added to 50 cc of 4:1 CS₂: CTD solution.

Amount of Carbon, g	%Nitrogen	% Nitrogen Removed
0	1.0160	0.00
1	0.7732	7.81
2	0.7928	22.32
3	0.6529	37.33
4	0.2998	55.74
5	0.4163	40.89
5	0.3717	47.22
5	0.5391	48.54
7	0.4817	54.18
7	0.1575	76.74
9	0.0509	92.00

As can be seen in Figure 14, the nitrogen removal is a strong function of the amount of carbon contacted with a fixed amount of CTD. While the results show scatter, better than 90% of the nitrogen-containing species was removed from the CTD for some runs. High levels of activated carbon results in a CTD with a nitrogen content of less than 0.1 wt% down from the original nitrogen content of about 1 wt% in the original CTD

feed. However, subsequent experiments could not achieve nitrogen removal levels above 40 % for reasons that are inexplicable.

A two-stage adsorption procedure was attempted in which CTD samples that were treated with 4 and 7 g of activated carbon respectively (Figure 15) in the first step, were treated further with 5 g of fresh carbon in a second step. The total nitrogen removed in the two-step process was 79 and 92 % for the two samples. Thus it appears that one step using 9 g of carbon (as shown in Figure 14) was as effective as two steps that use a total of 9 and 12 g of carbon.

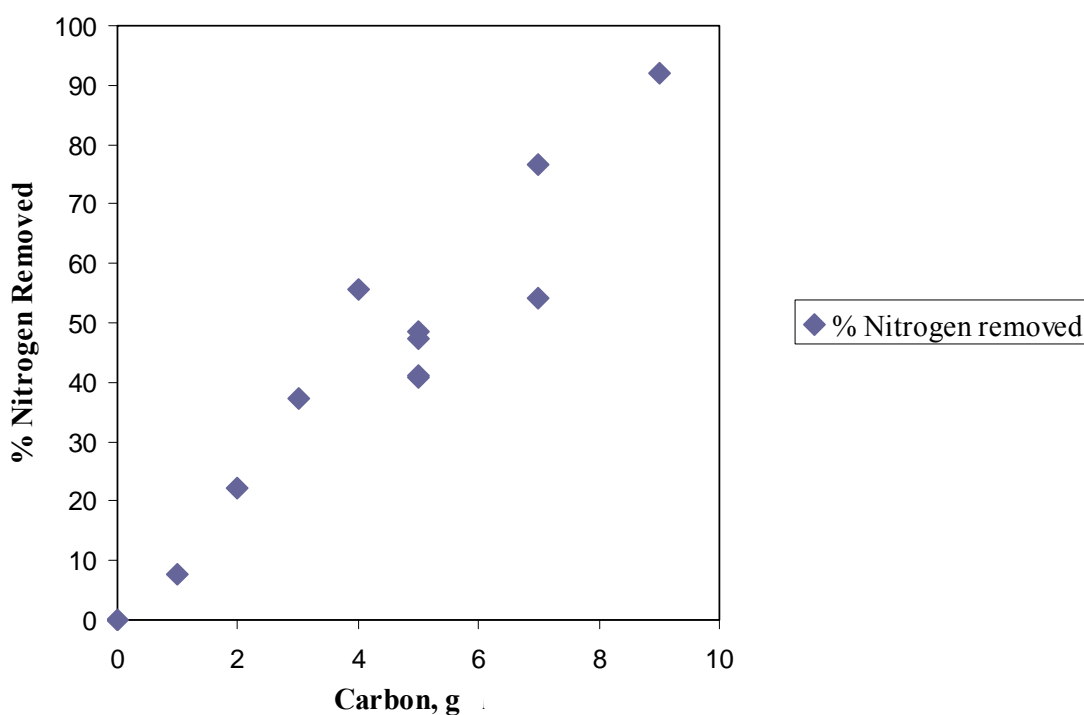


Figure 14. Plot of nitrogen removed vs. amount of carbon with CS₂ as the solvent.

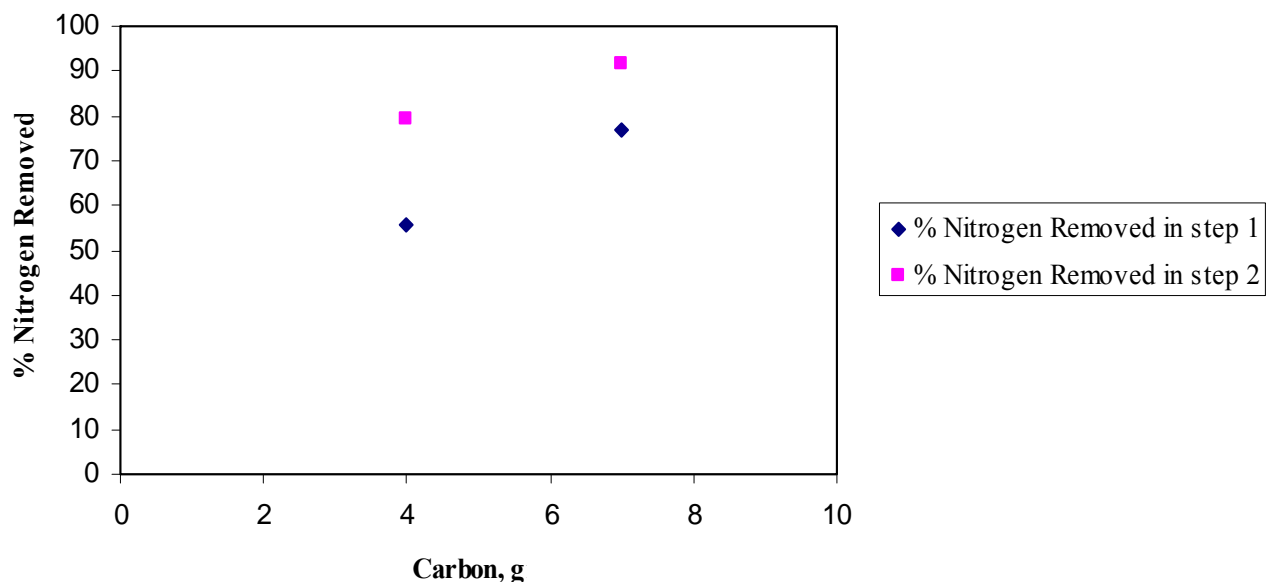


Figure 15. Plot of nitrogen removed vs. amount of carbon in two-step adsorption process.

4.2.3 Nitrogen Removal from CTD Using Oxidized Nuchar SA 20

The literature suggests that activated carbons with more acidic surface groups adsorbed more sulfur compounds from diesel fuel than the carbons with little or no acidic surface functionality. We inferred that nitrogen compounds in CTD might be affected similarly by surface functionality. Acidity of the oxidized Nuchar SA 20 samples was determined by the method described in reference 1, and the results are presented in Table VII.

Table VII. pH values of unoxidized and oxidized carbons.

	Sample	pH
1	Unoxidized Nuchar SA 20	5.8
2	1 hr air oxidized Nuchar SA 20	4.5
3	Nuchar SA 20 oxidized with nitric acid for 22 hrs	3.3
4	Nuchar SA 20 oxidized with nitric acid for 24 hrs	3.1

These oxidized carbons were then tested for adsorption of nitrogen compounds from CTD using 5 g of carbon and CS₂ as a diluent. The carbon oxidized with nitric acid for 24 hrs had the lowest surface pH and showed better nitrogen removal than any of the other carbons, as shown in Figure 16.

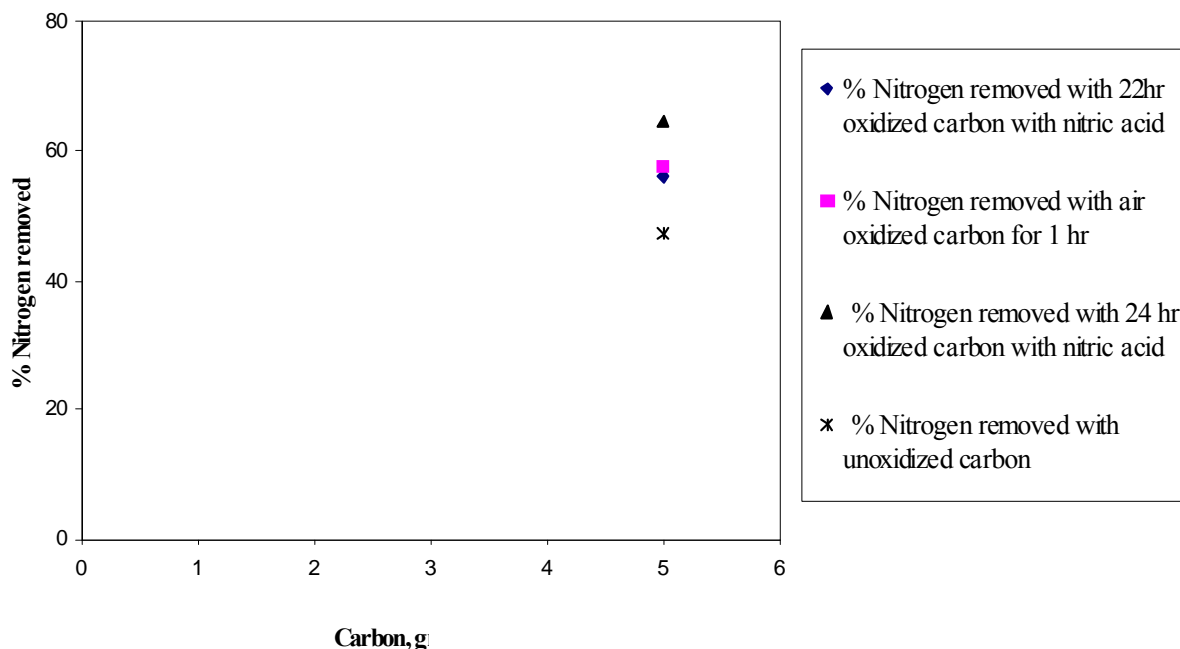


Figure 16. Plot of nitrogen removed vs. amount of different oxidized carbons.

While the improvement in nitrogen removal with the oxidized carbons was not dramatic (~30%), these results indicate that, as expected, the surface functionality of carbon does play a role in the nitrogen adsorption. Air oxidation appears to be a promising treatment since it requires a much shorter oxidation time and a much simpler reaction system. The percent nitrogen in the treated CTD along with the nitrogen remaining on the carbon after adsorption was determined so that a nitrogen balance could be obtained, Table VIII. The results of the nitrogen balance show that despite the many operations in processing and the small amounts of nitrogen in the samples, the nitrogen balance closes on average to about 10%. This gives some confidence that the procedure is working and the results are reasonably reliable.

Table VIII. Nitrogen distribution between solution and added carbon.

Carbon, g	Wt loss, g	Nitrogen starting solution, g	Nitrogen in liquid phase, g	Nitrogen in solid phase, g	Difference, g	% Difference
0	0.26	0.1016	0.1016	0	0	0
1	0.1	0.0865	0.0765	0.0062	0.0038	4.3931
2	0.53	0.1039	0.0769	0.0094	0.0176	16.9394
3	0.81	0.1070	0.0635	0.0423	0.0012	1.1215
4	1.00	0.0677	0.0269	0.0161	0.0247	36.4845
5	1.34	0.1036	0.0477	0.0422	0.0137	13.2239
7	1.68	0.1064	0.0423	0.0542	0.0099	9.3045
7	1.42	0.0677	0.0135	0.0510	0.0032	4.7267
9	2.57	0.0677	0.0037	0.0640	0	0

Figure 17 shows the results with THF as the solvent in a 4:1 solvent-to-CTD wt ratio. It can be seen that for similar ratios of CTD and activated carbon, the treatment with THF results in a much lower nitrogen removal when compared to the CS₂. Thus confirming that CS₂ was the preferred solvent.

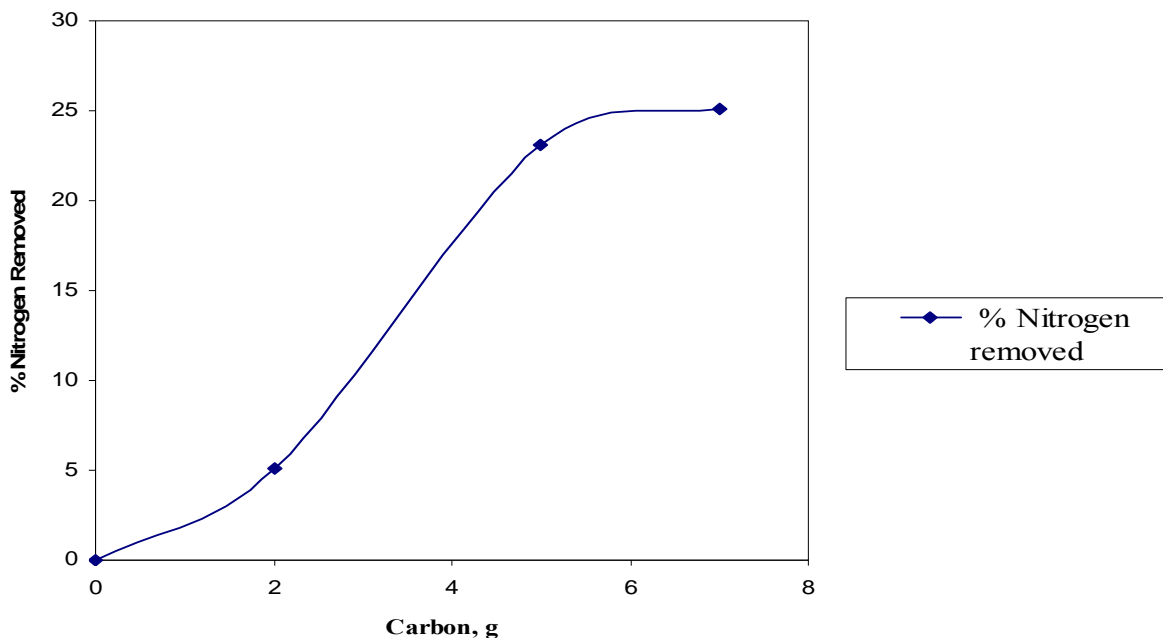


Figure 17. Plot of nitrogen removed vs. amount of carbon with THF as the solvent.

4.2.4 Effects of Activated Anthracite B on Nitrogen Removal

Anthracite B was activated at 900°C for 15 hours, which resulted in an activated carbon with a surface area of 1,400 m²/g. Samples of this material were oxidized with nitric acid and in air at 300°C using the methods described in sections 3.3.1 and 3.3.2, respectively. The procedure for contacting of the activated anthracite with CTD is described in section 3.4.3. Figure 18 shows the effect of nitrogen removal from the CTD as a function of time using un-oxidized activated anthracite up to six hours, where it can be seen that absorption is essentially complete within one hour with about 8 to 9 % of the nitrogen removed.

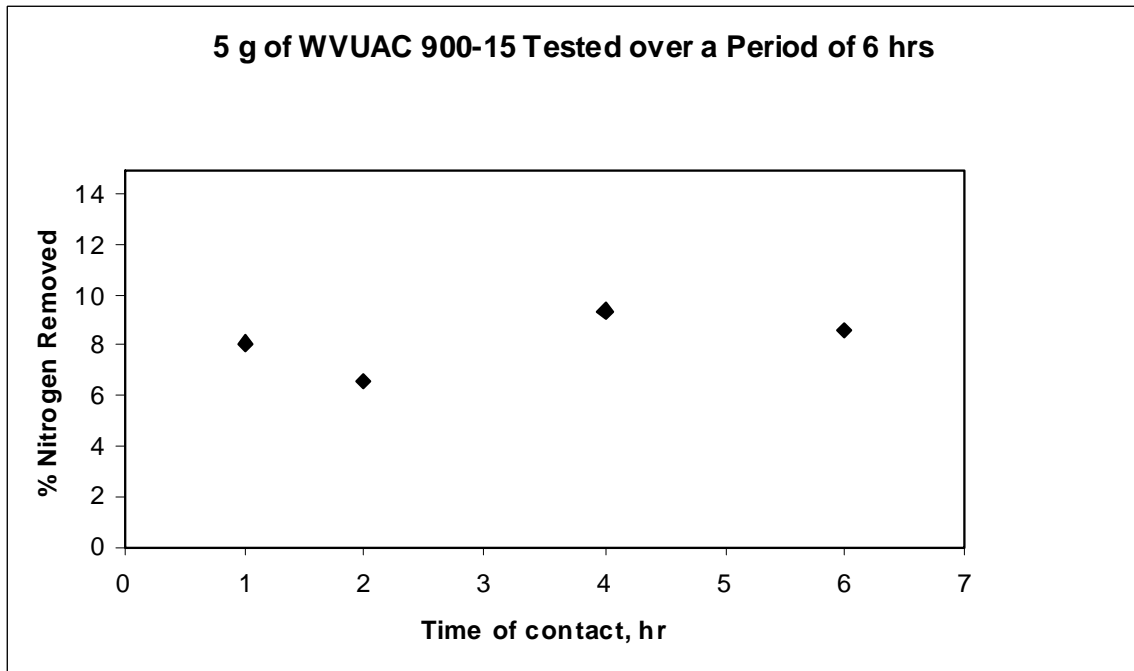


Figure 18. Effect of activated anthracite B on nitrogen removal vs. contact time.

Figure 19 shows the effect of oxidation of anthracite B with nitric acid or air on nitrogen removal. Oxidation with nitric acid increases nitrogen from about 9 % for the unoxidized activated coal to 14 %, while air oxidation increases nitrogen removal over 30 %.

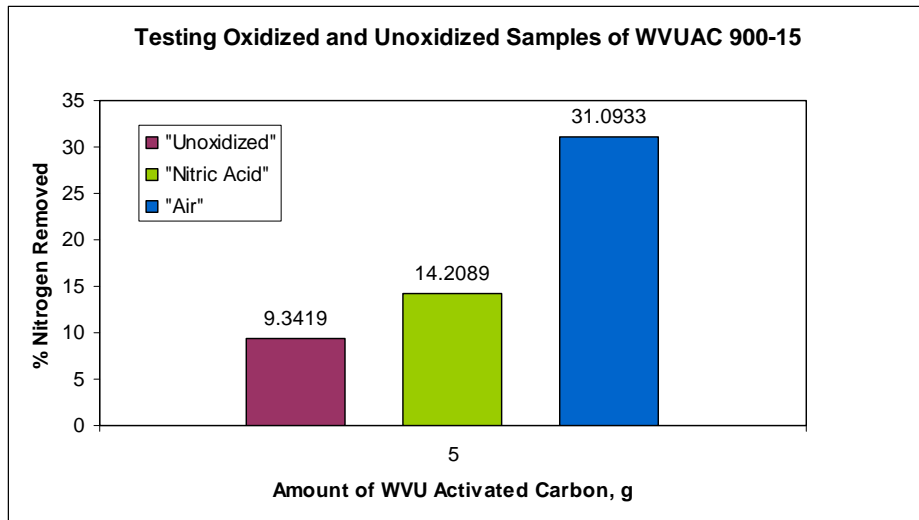


Figure 19. Effect of oxidation of anthracite B on nitrogen removal.

4.2.5 Preparation of Denitrogenated CTD for Carbonization

Although the experiments with oxidized activated anthracite B on nitrogen removal were promising, the supply of this coal was exhausted. Replenishment with an identical

anthracite coal was not possible and to activate and characterize another coal could not be accomplished before the end of this project. Thus, removal of nitrogen-containing compounds from Koppers heavy coal-tar distillate was conducted by first diluting 10 g of CTD with 40 g of carbon disulfide in a 125-mL Erlenmeyer flask. To the flask was added 7 g of air-oxidized Nuchar SA 20 activated carbon. The flask was sealed with a rubber stopper and parafilm then placed in a shaker bath at 30°C. After 2 hours in the shaker bath, the solution was removed from the activated carbon by filtration. The walls of the flask and filter cake were washed with an additional 40 g of carbon disulfide to recover remaining CTD. The carbon disulfide was removed from the filtrate by evaporation in a warm water bath until constant weight was obtained before sampling and determining nitrogen content.

In order to provide 400 g of treated CTD required for carbonization, the batch-wise adsorption experiments were conducted in nine series totaling 57 adsorptions, in addition to adsorptions that did not contain adsorbent for use as controls. It was decided to take a conservative approach in conducting the adsorption experiments in small batches rather than one or two larger batches to ensure that the results would be consistent with our earlier work and to eliminate variation because of scaling up.

The results for nitrogen removal are presented in Table IX and the average values and standard deviations are shown in Table X. The average nitrogen content for the control samples is slightly less than the nitrogen content for the feed material, but is within statistical error. Note that for Series IV it was assumed that the nitrogen content for the control sample was the same as nitrogen content for the feed in the calculation of nitrogen removal. Adsorption of the nitrogen compounds from the heavy coal-tar distillate by the air-oxidized Nuchar SA 20 was effective, resulting in a 33.4 percent reduction. The material from each batch was combined until approximately 400 g of total product was made. The nitrogen content for the combined product was 0.59 wt%, or about a one-third reduction in nitrogen compared to the feed CTD, consistent with the results of the batch experiments

Table IX. Results of denitrogenation of CTD.

Material	Series I		Series II		Series III	
	Nitrogen Content (wt%)	¹ Nitrogen Removed (%)	Nitrogen Content (wt%)	Nitrogen Removed (%)	Nitrogen Content (wt%)	Nitrogen Removed (%)
Feed	0.979	--	0.915	--	0.989	--
² Control	0.981	--	0.905	--	0.969	--
³ Treated	0.545	44.422	0.667	26.371	0.613	36.715
Treated	0.639	34.868	0.645	28.789	0.658	32.158
Treated	0.624	36.375	0.643	28.932	0.611	36.983
Treated	0.624	36.396	0.643	28.954	0.687	29.106
Treated	0.636	35.183	0.615	32.078	0.666	31.271
Treated	0.635	35.245	0.663	26.713	0.566	41.633
Treated	0.706	28.043	0.633	30.025	--	--

Table IX. (Continued)

Material	Series IV		Series V		Series VI	
	Nitrogen Content (wt%)	Nitrogen Removed (%)	Nitrogen Content (wt%)	Nitrogen Removed (%)	Nitrogen Content (wt%)	Nitrogen Removed (%)
Feed	0.809	--	0.878	--	0.785	--
Control	--	--	0.763	--	0.745	--
Treated	0.534	34.027	0.546	28.487	0.541	27.410
Treated	0.513	36.557	0.548	28.199	0.561	24.688
Treated	0.538	33.506	0.535	29.823	0.539	27.705
Treated	0.528	34.741	0.543	28.801	0.544	26.954
Treated	0.533	34.124	0.520	31.879	0.518	30.414
Treated	0.524	35.161	0.531	30.386	0.486	34.812
Treated	0.554	31.517	--	--	--	--

Material	Series VII		Series VIII		Series IX	
	Nitrogen Content (wt%)	Nitrogen Removed (%)	Nitrogen Content (wt%)	Nitrogen Removed (%)	Nitrogen Content (wt%)	Nitrogen Removed (%)
Feed	0.928	--	0.894	--	0.907	--
Control	0.908	--	0.912	--	0.826	--
Treated	0.555	38.854	0.579	36.497	0.561	32.070
Treated	0.542	40.231	0.574	37.045	0.567	31.296
Treated	0.555	38.821	0.605	33.691	0.492	40.433
Treated	0.586	35.451	0.568	37.735	0.541	34.466
Treated	0.615	32.213	0.605	33.592	0.532	35.56
Treated	0.577	36.398	0.524	42.503	0.523	36.596

¹ Nitrogen Removed (%) = [(N in Control) – (N in Treated)] / (N in Control) * 100 for each series.

² Control refers to the samples 10 g of heavy coal-tar distillate diluted with 40 g of carbon disulfide, no activated carbon added.

³ Treated refers to the samples 10 g of coal tar-distillate diluted with 40 g of carbon disulfide and with 7 g of oxidized Nuchar SA 20.

Table X. Statistical results on treating CTD with oxidized Nuchar SA 20.

	N in Feed (wt%)	N in Control (wt%)	N in Treated (wt%)	N Removal (%)
Average	0.898	0.869	0.578	33.4
Standard Deviation	0.068	0.086	0.053	4.4
Number of Samples	9	8	57	--

4.3 Fabrication and Results of Graphite Test Specimens

Figure 20 shows the temperature profile of the batch coker during the conversion of the CTD treated with the air-oxidized Nuchar SA 20 into green coke. The product thermocouples were located inside of the reactor with TC 2 near the bottom and TC 3 near the top of the canister. The shell thermocouple was used by the computer to control process temperature.

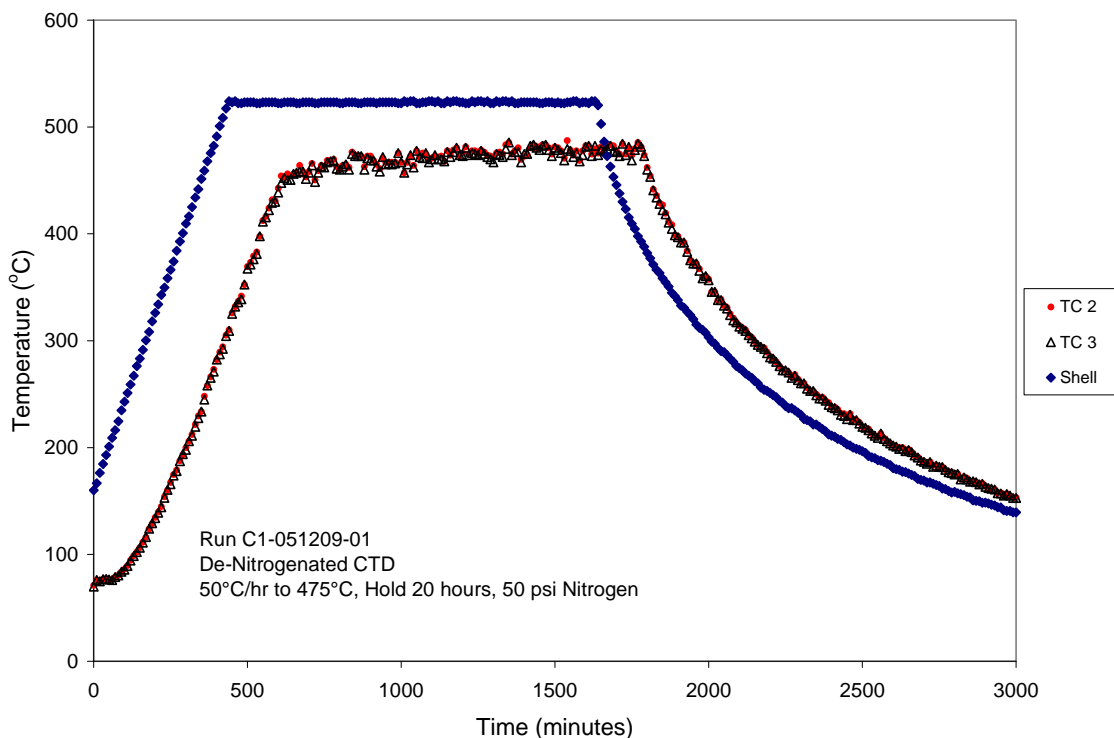


Figure 20. Temperature profile during batch coking of treated CTD.

Table XI shows the yield of green coke following pressure carbonization of the CTD. The yield of green coke under these conditions is consistent with the results of work reported elsewhere [1-2]. Note the absolute quantity of green coke is low because of the limited amount of treated CTD available. The yield of calcined coke after heat treating the green coke to 1,420°C was about 79%.

Table XI. Product yield from batch coking of denitrogenated Koppers CTD.

Weight Koppers CTD, grams	378.1
Weight green coke, grams	159.5
Yield of green coke, wt%	42.2

Attempts to measure the puffing character were unsuccessful because the test apparatus had mechanical failures that could not be repaired in time before the

completion of this project. However, Table XII shows the properties of the graphite test rods for the WVU and control coke. Also shown are the results for a test specimen of coke made from decanted oil. Although there are differences in bulk density and resistivity, the more important consideration is CTE. The CTE for the control is low compare to the other samples, probably since it was made from a premium needle coke. The CTE of the CTD coke is significantly lower than that for the decanted oil, confirming the coal-based feedstocks can make very good needle cokes for graphite products.

Table XII. Properties of graphite test specimens.

Sample No.	Feedstock	CTE ppm/°C	Bulk Density (g/cm ³)	Resistivity (μΩ-m)
1	CTD Coke	0.209	1.494	9.80
2	Control	0.107	1.472	9.04
3*	Decanted Oil	0.250	1.460	8.88

*From reference 2, Table XI.

5.0 Conclusions

Two anthracite coals (anthracite A and anthracite B) were converted into high-surface area carbons by activation in a fluidized-bed reactor using carbon dioxide as the reactant gas. The surface area developed for anthracite A was 788 m²/g after reacting at 900 °C for 10 hr. The surface area developed for anthracite B was 1388 m²/g after reacting at 900 °C for 20 hr. It was discovered that the higher surface areas were obtainable by activating the coals at lower temperatures but for longer periods of time. The apparent reactivity of the coals also affects the development of surface, i.e., the activation rate for anthracite B was slightly slower than anthracite A, with anthracite B producing higher surface areas. In addition, anthracite B activated at 900 °C for 20 hr had mesopore surface area of about 420 m²/g, nearly more than four times that of anthracite A.

The surfaces of the commercial activated carbon Nuchar SA 20 and activated anthracite B can be oxidized by nitric acid or heated air. The introduction of oxygen functional groups can be determined on a relative basis by using a pH procedure. The untreated Nuchar SA 20 produced a solution having a pH of 5.8. Air oxidized Nuchar SA 20, and nitric acid oxidized Nuchar SA 20 for 22 and 24 hr, generated solutions with pH values of 4.5, 3.3, and 3.1 respectively. All of the oxidized samples were more effective in removing nitrogen from a heavy coal-tar distillate than the un-oxidized activated carbon.

Contacting Nuchar SA 20 using toluene as a diluent precipitated nitrogen-containing components from the CTD, which resulted in spurious nitrogen determinations. Toluene, tetrahydrofuran, and carbon disulfide were tested as diluents for the adsorption procedure and it was found that carbon disulfide was superior to the other solvents in terms of boiling point, solvency, and adsorption capacity on the activated carbon. In some instances, up to 90 % of the original nitrogen in the CTD can

be removed by Nuchar SA 20 with carbon disulfide as the diluent. The results of the nitrogen balance show that despite the many operations in processing and the small amounts of nitrogen in the samples, the nitrogen balance closes on average to about 10%.

The heavy coal-tar distillate was treated with air-oxidized Nuchar SA 20 activated carbon resulting in a 33 % reduction in nitrogen content. This material was converted into green coke in a batch coker under 50 psi nitrogen pressure at 475°C for 20 hours. The yield of green coke was 42.2 wt%, based on the weight feed CTD. The green coke was calcined to 1,420°C with a calcined coke yield of 79 wt%. The treated CTD was fashioned into a 19 mm diameter graphite test rod along with a sample consisting of a petroleum-based coke for use as a control for determination of coefficient of thermal expansion (CTE), density, and specific resistivity. The CTE for the control sample is very low because it was made from a high-quality, highly crystalline needle coke. The CTE for the treated CTD and control graphite test rods were 0.209 and 0.107 ppm/°C, respectively. Although the CTE for the control sample is lower than the CTD sample, the CTE of the CTD coke is nevertheless significantly lower than that for the decanted oil, confirming the coal-based feedstocks can make very good needle cokes for graphite products.

6.0 References

- 1) “Needle Coke from Coal-Derived Feedstock ” Final Report by Doug J. Miller, John C. Chang, I.C. Lewis, R.T. Lewis, H. H. Schobert, M.M. Escallon, and L. Rudnick, CPCPC Contract Number 2867-GTIL-DOE-1874, June 30, 2006.
- 2) “Needle Coke from Nitrogen Removed and Coal-Derived Feedstock,” Final Report by Peter G. Stansberry and John C. Chang, CPCPC Contract Number 3332-GTI-DOE-1874, April 30, 2008.
- 3) “Effects of oxidative modification of carbon surface on the adsorption of sulfur compounds in diesel fuel,” Anning Zhou, Xiaoliang Ma, Chunshan Song; Manuscript accepted May 2008 for publication in *Applied Catalysis B: Environmental*.

Preparation and characterization of boron containing carbons derived from coal tar pitch

Final report

Report period starting date: 03/01/2008

Report period ending date: 01/31/2010

Report issue date: April 2010

Subcontract no: 3556-TPSU-DOE-1874

PI: Ramakrishnan Rajagopalan, Parvana Aksoy and Caroline Burgess Clifford

The Pennsylvania State University

University Park, PA 16802

DISCLAIMER

This report was prepared as an account of work sponsored by an agency of the United States Government. Neither the United States Government nor any agency thereof, nor any of their employees, makes any warranty, express or implied, or assumes any legal liability or responsibility for the accuracy, completeness, or usefulness of any information, apparatus, product, or process disclosed, or represents that its use would not infringe privately owned rights. Reference herein to any specific commercial product, process, or service by trade name, trademark, manufacturer, or otherwise does not necessarily constitute or imply its endorsement, recommendation, or favoring by the United States Government or any agency thereof. The views and opinions of authors expressed herein do not necessarily state or reflect those of the United States Government or any agency thereof.

Abstract

In our investigation, we report four different approaches to synthesize boron containing carbons derived from coal tar pitch precursor. Carbons with boron content as high as 25 wt% could be synthesized by pyrolysis of blends of polyborazylene/pitch precursors. The synthesized carbons were characterized using solid state B¹¹NMR and infrared spectroscopy. The incorporated boron was in trigonal or sp² hybridized state for all the four synthetic approaches suggesting that they were in the framework of the carbon. The electrochemical activity of the synthesized carbons was studied using cyclic voltammetry. Boron nitrogen carbons derived from polyborazylene/pitch showed strong electroadsorption of protons. The reversible electrochemical activity was helpful in fabricating an aqueous electrolyte based asymmetric capacitor with a cell voltage of 2.5 V and an energy density of 22 Wh/kg, which is almost four times greater than symmetric capacitors made using pitch derived carbons.

TABLE OF CONTENTS

1.	Executive Summary -----	5
2.	Experimental -----	6
	2.1 Synthesis of high surface area carbon derived from pitch -----	6
	2.2 Synthesis of boron doped carbons by direct mixing of pitch and tetraethylammonium borohydride (Approach 1)-----	6
	2.3 Synthesis of boron doped carbon using TEAB complex formation (Approach 2) -----	6
	2.4 Synthesis of BC _x (Approach 3) -----	7
	2.5 Synthesis of boron substituted carbon from polyborazylene (Approach 4)-----	7
	2.6 Synthesis of electrochemically active manganese dioxide -----	7
	2.7 Characterization of synthesized samples -----	8
	2.7.1 Solid state B-NMR spectroscopy-----	8
	2.7.2 Diffused reflectance infrared fourier transform spectroscopy (DRIFTS)-----	8
	2.8 Electrochemical Studies -----	9
	2.8.1 Electrochemical cell construction -----	10
	2.8.2 Electrode construction -----	10
	2.8.3 Three electrode cell setup -----	10
	2.8.4 Teflon press cell setup -----	11
	2.8.5 Mass balancing for asymmetric electrochemical capacitors -----	11
	2.8.6 Electrochemical testing -----	11
3.	Results and Discussion -----	12
	3.1. Solid state B-NMR studies -----	12
	3.2. DRIFTS studies on polyborazylene/pitch derived carbon (Approach 4) -----	15
	3.3. Electrochemical testing -----	17
	3.3.1. Optimization of electrochemical activity of electrodes -----	17
	3.3.2. Fabrication of asymmetric capacitor using synthesized carbons -----	20
4.	Conclusions -----	23
5.	References -----	24

1. Executive Summary

Our primary goal in this project was to incorporate substitutional boron in pitch derived carbon. Since boron is highly electronegative, incorporation of substitutional boron in carbon materials can lead to significant changes in the electronic character of the carbon. Substitutional boron in carbon would mean that the boron should be in sp^2 hybridized state and should be incorporated in the polyaromatic domains of carbon.

Three different approaches were used to incorporate boron in pitch derived carbons. 1-5 wt% of boron could be incorporated in the synthesized carbons by either pyrolysis of blends of pitch and boron containing precursors or impregnation of high surface area coal tar pitch derived carbons with boron complex. We were also successful in depositing BCx films synthesized by chemical vapor deposition method on pitch derived nanoporous carbons. The deposited BCx films contained almost 17 wt% boron. Solid State B^{11} NMR showed that the incorporated boron was all in trigonal or sp^2 hybridized state. Electrochemical studies did not show any significant activity as the surface area of the synthesized carbons was very low. A novel synthesis of boron nitrogen carbons was developed using pyrolysis of blends of polyborazylene/coal tar pitch precursors. Even though the synthesized carbons had very low surface area, they showed excellent electroactivity indicating strong electroadsorption of protons. The mechanism of electrochemical activity is not yet clear. However, we were encouraged to fabricate and test asymmetric capacitors using the synthesized boron containing carbons.

Asymmetric capacitors were fabricated using boron containing carbons synthesized using polyborazylene/pitch precursors and manganese dioxide as electrodes and aqueous 2M magnesium chloride as the electrolyte. The capacitor showed an energy density of 22 Wh/kg and was cyclable for more than 300 cycles with an operable cell voltage of 2.5V, which is significantly high for aqueous electrolytes. The capacitor showed almost four times improvement in energy densities as compared to symmetric capacitors fabricated using coal tar pitch derived carbons.

2. Experimental

2.1. *Synthesis of high surface area carbon derived from pitch*

Coal tar pitch was dissolved in tetrahydrofuran and the soluble (THFS) and insoluble fractions (THFI) of the pitch were extracted. THFS was mixed with sulfuric acid (1:1 by wt.) and allowed to polymerize for 24 hours. The resultant viscous solution was pyrolyzed at 800 C for 1 hour under argon atmosphere. The sample was then activated using CO₂ to increase the surface area [1,2]. The resultant sample was used for both the synthesis of boron doped carbons as well as fabrication of symmetric coin cell capacitors.

2.2. *Synthesis of boron doped carbons by direct mixing of pitch and tetraethylammonium borohydride (Approach 1)*

Coal tar pitch was dissolved in tetrahydrofuran and the soluble (THFS) and insoluble fractions (THFI) of the pitch were extracted. THFS was mixed with sulfuric acid (1:1 by wt.) and allowed to polymerize for 24 hours. The resultant viscous solution was mixed with tetraethylammonium borohydride (TEAB) (1:1 by wt.) and pyrolyzed at 800 C for 1 hour under argon atmosphere. In another experiment, THFS was directly mixed with TEAB and pyrolyzed under similar conditions. The resultant carbon was studied using solid state ¹¹B NMR.

2.3. *Synthesis of boron doped carbon using TEAB complex formation (Approach 2)*

0.1g of high surface area carbon derived from pitch was loaded in a flask and vacuumed for 3 hours. 0.5 gm of TEAB (dissolved in 5ml of methanol) was then added to the flask with the help of syringe keeping it under vacuum. The set-up was then heated at 100 degrees, in a sand bath, for 2-3 hrs until the methanol evaporates. Now 1gm of furfuryl alcohol (diluted with 5ml of

THF) were added to the flask with a syringe. The set up was heated continuously for 2-3 hrs until the THF evaporated and left behind a slurry or viscous residue. The residue was then pyrolyzed at 800 degrees and then allowed to cool down.

2.4. *Synthesis of BC_x (Approach 3)*

Boron trichloride and benzene were mixed slowly using helium as carrier gas. The resultant mixture was passed through a tube furnace which was heated at 900°C at a controlled flow rate of 20 ml/min. The deposited BC₃ was collected on a quartz glass placed inside the tube furnace. Detailed information on the synthesis conditions are reported elsewhere [3].

2.5. *Synthesis of boron substituted carbon from polyborazylene (Approach 4)*

Coal tar pitch was dissolved in tetrahydrofuran (THF) and the soluble fraction of the pitch was extracted. The soluble fraction was mixed with polyborazylene and dissolved in THF. This was followed by co-precipitation in pentane. The precipitate was then pyrolyzed under argon atmosphere at various temperatures (600°C, 700°C, 800°C, 900°C and 1000°C).

2.6. *Synthesis of electrochemically active manganese dioxide*

Aqueous solution of 0.5g of potassium permanganate was mixed with 0.05g of TritonX-100, 20 ml of Hexane and 5 ml of methanol, respectively. The mixture was then stirred for 10 minutes and ultrasonicated for 5 minutes. The solution turned brown in color indicating the formation of manganese dioxide. The solution was then filtered, washed and dried at 100 C to constant weight.

2.7. Characterization of synthesized samples

2.7.1. Solid state B-NMR spectroscopy

Solid state ^{11}B MAS NMR experiments were done using a Varian Inova spectrometer interfaced to a home-built 3.2 mm magic-angle spinning (MAS) probe operating at a magnetic field strength of 21.1 T (observation frequency of 288.9607362 MHz for ^{11}B). Boric acid was used as the reference. The bulk content of boron and the exact co-ordination of boron in the samples was determined.

2.7.2. Diffused reflectance infrared fourier transform spectroscopy (DRIFTS)

The infrared spectrum of powdered sample was collected using a Spectra Tech Collector II DRIFTS accessory using a Bruker IFS 66/S FTIR spectrometer. Powdered samples were filled in the DRIFTS cell and the spectra were collected and averaged over 600 scans.

2.8. Electrochemical Studies

2.8.1 Electrochemical cell construction

After the synthesis process was complete, the new material must be prepared and placed in electrochemical cell for testing. The first step in this process was to further refine the synthesized material by adding acetylene black to the material to enhance conductivity and by adding Teflon as a binder. After the material was mixed with the additives it was placed on a current collector made of either stainless steel mesh or woven carbon fiber. The electrodes were then soaked in an aqueous electrolyte, usually 2M KCl or 1M Sulfuric Acid. After being soaked the electrodes were placed in either a two or three electrode cell for testing. If a two electrode

cell was being used a polypropylene 5020 membrane was placed between the electrodes. Before being used in the electrochemical cell the polypropylene was cut to the size of the electrodes and soaked in the electrolyte.

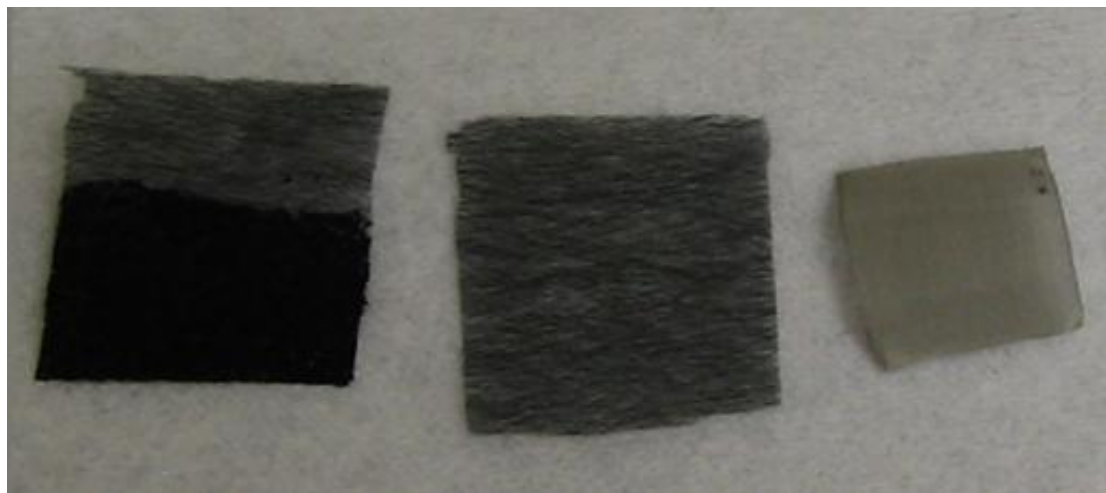


Figure 1. One carbon fiber current collector with electrode material (Left), one carbon fiber current collector without electrode material (Center) and one stainless steel mesh current collector (Right)

2.8.2 Electrode construction

In order for a synthesized material to be used in an electrochemical capacitor, it must be prepared by mixing in Teflon and acetylene black. The Teflon acts as a binder and holds the individual particles of manganese dioxide or activated carbon together and also holds the material on the current collector. Acetylene black increases the conductivity of the material. For the activated carbon electrodes, a mixture of 85 wt% carbon, 10 wt% Teflon and 5 wt% acetylene black was used. The manganese dioxide was a more resistive material, so more acetylene black was used for a mixture of 70 wt% manganese dioxide, 5 wt% Teflon and 25 wt% acetylene black. After the materials were mixed, THF was added to the mixture until a consistency of thin paint was achieved. This mixture was ultrasonicated for 30 minutes to insure even particle distribution

throughout the THF. Once the ultrasonication was completed, the material was painted onto a stainless steel or carbon mesh current collector with an ordinary paint brush and the THF was evaporated using a heat gun set to a moderate temperature. After the THF was evaporated, the electrode was ready to be used.

2.8.3 Three electrode cell setup

The three electrode cell setup was used to study an individual electrode. Once an electrode is prepared, it can be placed into a three electrode cell in order to determine its specific capacitance and voltage range. Besides the active electrode, the other two electrodes in the three electrode cell are the Pt counter electrode and the Ag/AgCl reference electrode. The Ag/AgCl reference electrode was stored in a saturated solution of KCl.

2.8.4 Teflon press cell setup



Figure 2. An electrochemical cell prepared in a Teflon press that is ready to be tested.

In this study, electrochemical capacitors were also created in a Teflon press. The first step in this method was to place two electrodes in a Teflon press with a polymer membrane placed between

them to prevent a short circuit from occurring. The press was then tightened to hold the electrodes in place. The press was then placed in a beaker, which is then filled with electrolyte. The whole setup was allowed to soak for four hours before testing.

2.8.5 Mass balancing for Asymmetric Electrochemical Capacitors

An electrochemical capacitor is essentially two capacitors in series, where each electrode and ion layer pair acts as a capacitor. In an asymmetric design, the mechanisms of charge storage in the positive and negative electrodes are different. Hence, electrochemical parameters such as specific capacitance and reversible charge/discharge potential range for the electrodes can also be different. In order to optimize the performance of both the electrodes, it is required to balance the charges on both the positive and negative electrodes. Using the values of specific capacitance and pseudocapacitance potential ranges determined by 3-electrode measurements, it is possible to estimate the mass ratio of both electrodes needed to balance the charges as shown below:

$$q_+ = q_- \Rightarrow m_+ C_+ \Delta E_+ = m_- C_- \Delta E_-$$

$$\frac{m_+}{m_-} = \frac{C_- \Delta E_-}{C_+ \Delta E_+}$$

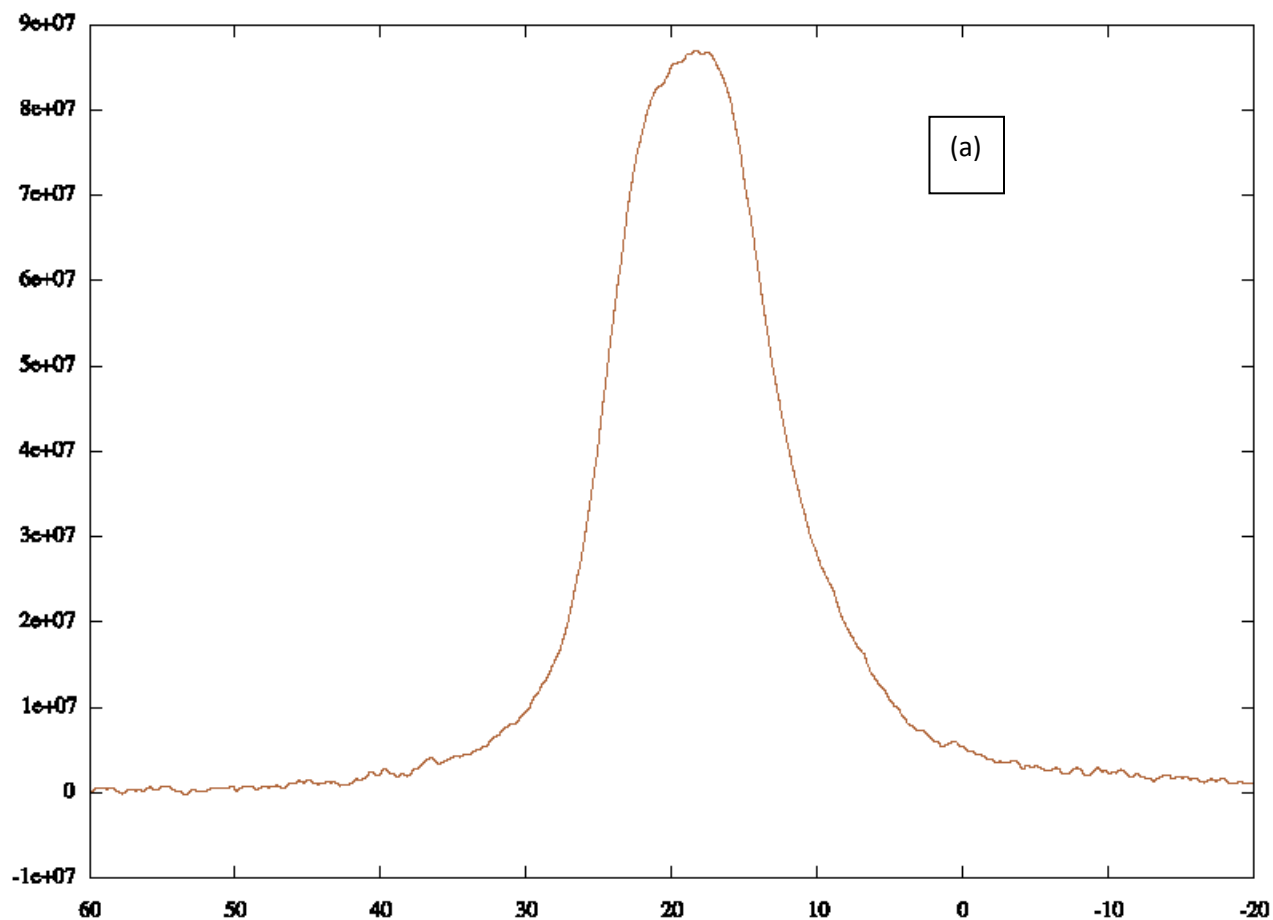
2.8.6 Electrochemical testing

Once a two or three electrode electrochemical cell was created, electrical tests were carried out to determine the materials properties. The cell to be tested was hooked up to a 5210 amplifier and 263A potentiostat. This hardware was operated via a computer running the Electrochemistry Power Suite program. This setup was used to perform the following tests: electrochemical impedance spectroscopy (EIS) tests, cyclic voltammetry (CV) tests, and constant current (CC) tests on the electrochemical cells.

3 Results and Discussion

3.1. Solid State B-NMR studies

The synthesized carbons were screened using solid state B-NMR to measure the amount of boron content and as well as the actual co-ordination of the incorporated boron in the sample. Figure 3 shows the ^{11}B NMR results of carbon derived from Approach 1.



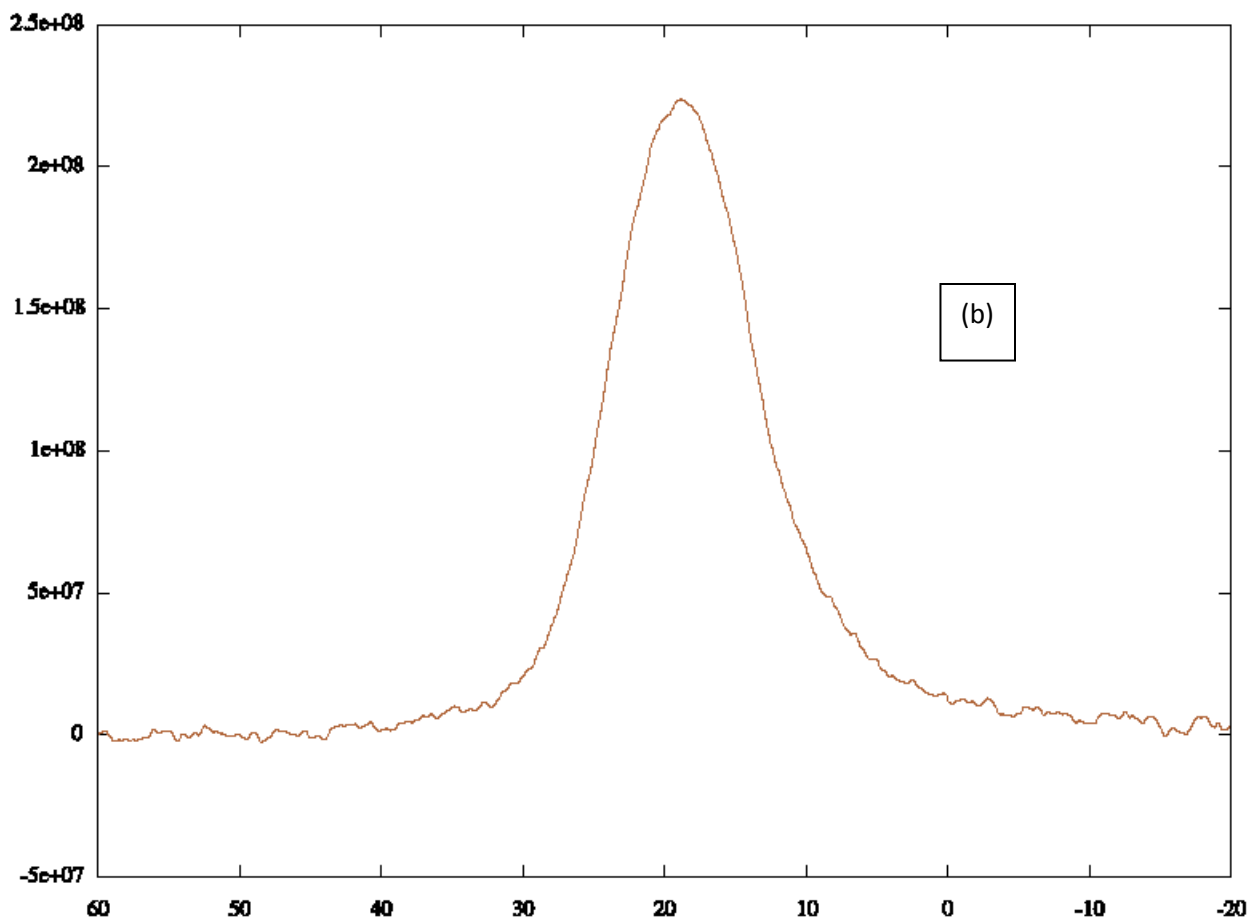


Figure 3 (a) ^{11}B NMR of carbon derived from THFS and TEAB, (b) ^{11}B NMR of carbon derived from THFS, sulfuric acid and TEAB (Approach 1)

Both the carbons show a single NMR peak shift at about 20ppm. This corresponds to trigonal sp^2 type boron. The results suggest that the boron is in the oxidized form. The amount of boron content in the sample was about 5 atomic%. Solid state B- NMR of high surface area carbon impregnated with complex formed with furfuryl alcohol and tetraethylammonium borohydride showed a similar downfield shifted peak at about 20 ppm (Approach 2). In addition to that peak, there was another peak below 10 ppm. These peaks suggests the presence of trigonal sp^2 boron in the sample and the presence of different co-ordination of boron. The small peak at 10 ppm may

be due to the presence of tetrahedral sp^3 boron sites. The amount of boron content in the sample was again limited to 3- 5 wt% by this method.

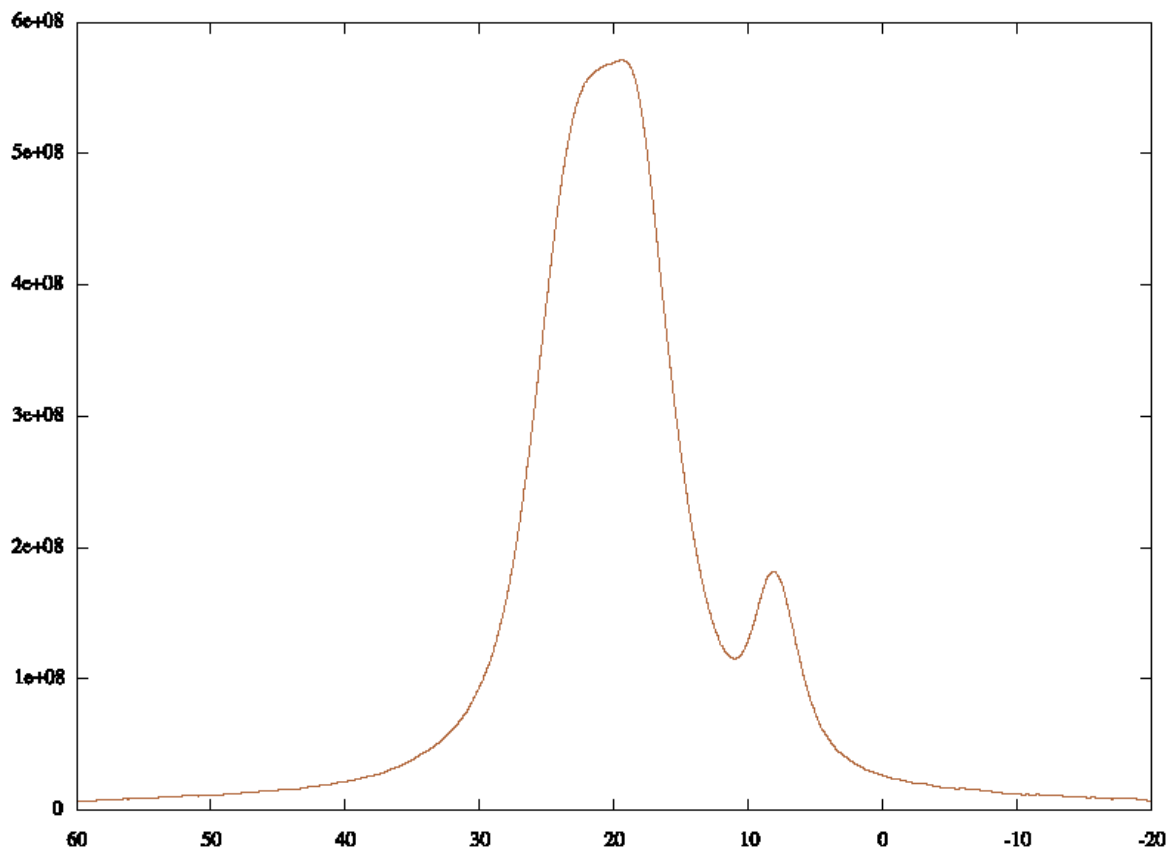


Figure 4. ^{11}B NMR of boron doped carbon made using boron complex of FA and TEAB (Approach 2)

In order to increase the boron content, we used a chemical vapor deposition approach (approach 3) to deposit a thin film of BC_x . Figure 5 shows the B-NMR spectrum of BC_x films. The amount of boron content was almost 15 wt% and almost all the boron incorporated in the carbon was in the sp^2 state. The challenge in this case was to conformally coat the layer onto a high surface area microporous carbon derived from pitch. The surface area of BC_x coated carbon dramatically decreased from 1500 m^2/g to 250 m^2/g indicating substantial clogging of micropores.

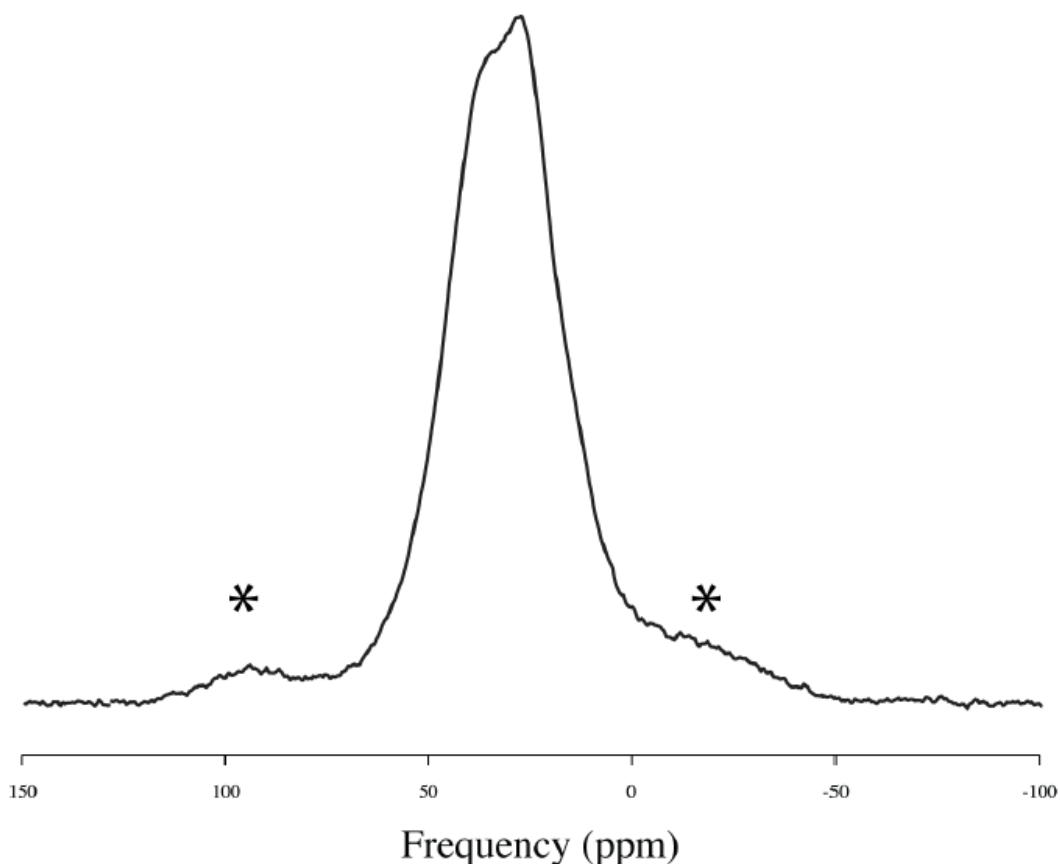


Figure 5. Solid State B-NMR spectrum showing a downfield shift centered at 32 ppm corresponding to trigonal sp^2 boron using Approach 3

3.2. DRIFTS studies on polyborazylene/pitch derived carbon (Approach 4)

Figure 6 shows the infrared spectra of boron containing carbons prepared using Approach 4. Three samples were synthesized at different pyrolysis temperatures ranging from 600 °C to 1000 °C. All the samples showed clear indications of the incorporation of boron/nitrogen bonds in the aromatic ring. The main characteristic peaks were seen at 3250 cm^{-1} , 1400 cm^{-1} , 1100 cm^{-1} , 900 cm^{-1} and 780 cm^{-1} corresponding to N-H str., B-N str., B-C str., C-H def. and B-N-B bending respectively [4]. The presence of these peaks even after pyrolysis at 1000 C shows that the boron, nitrogen and carbon are strongly bonded in the aromatic carbon framework. Elemental analysis using XPS showed that boron content in these materials can be as high as 25 at%.

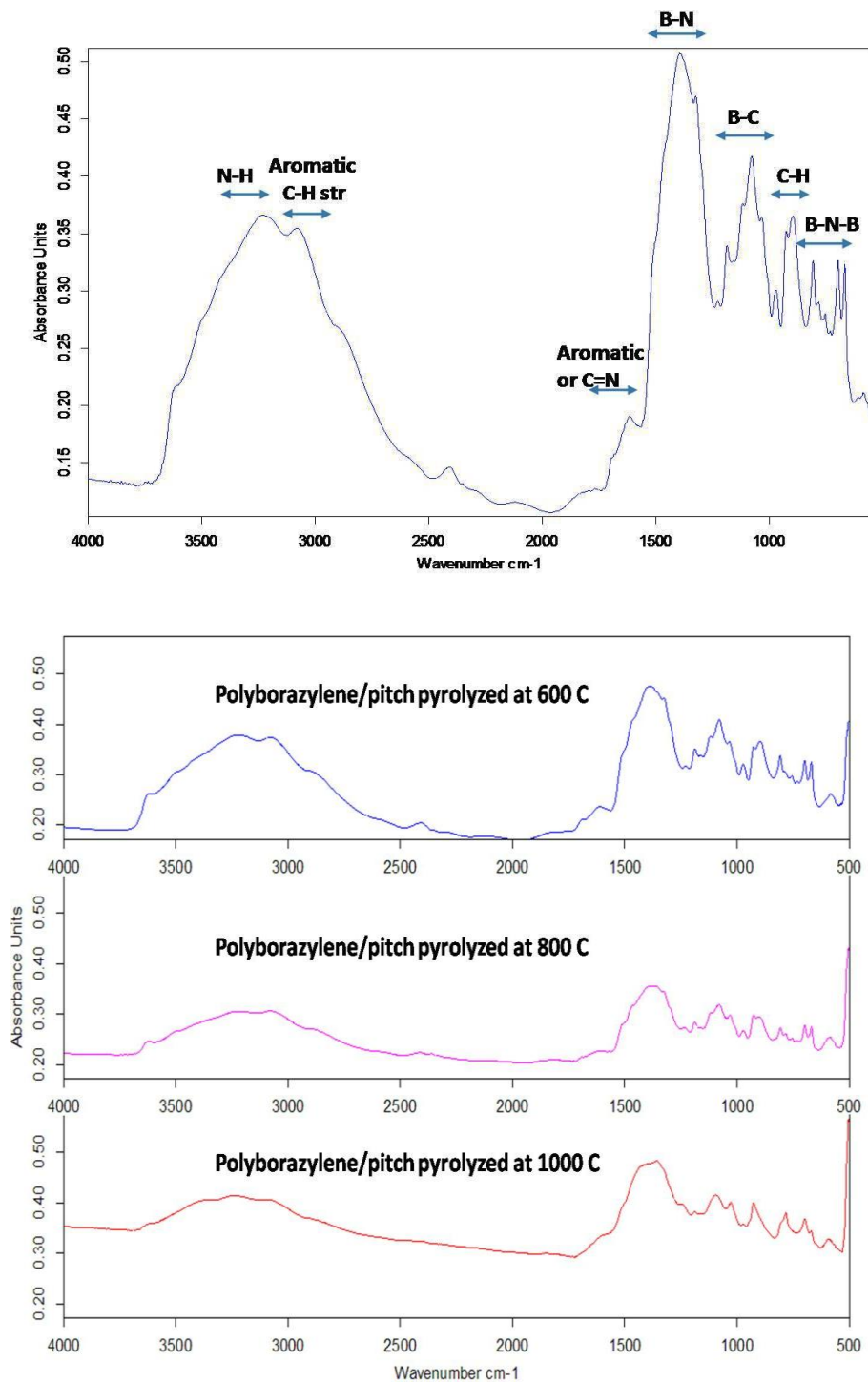


Figure 6. DRIFTS spectra of boron containing carbons derived from pyrolysis of pitch/polyborazylene blends

3.3. Electrochemical testing

3.3.1. Optimization of electrochemical activity of electrodes

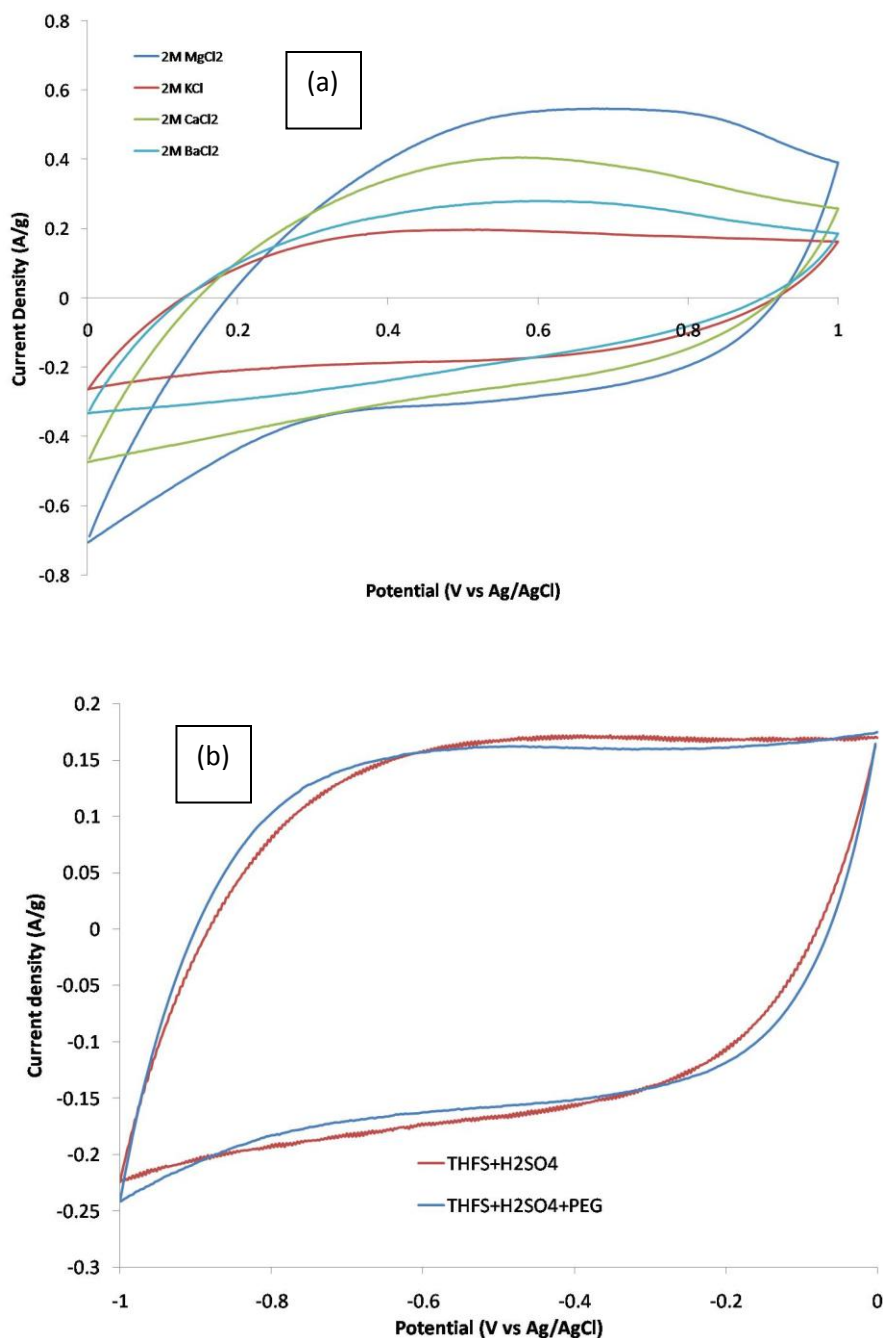


Fig 7 a. Electrochemical performance of Manganese dioxide electrode over a scan range of 0 to 1 V at 2 mV/s b. Electrochemical performance of activated carbon derived from pitch over a scan range of 0 to -1 V at 2 mV/s.

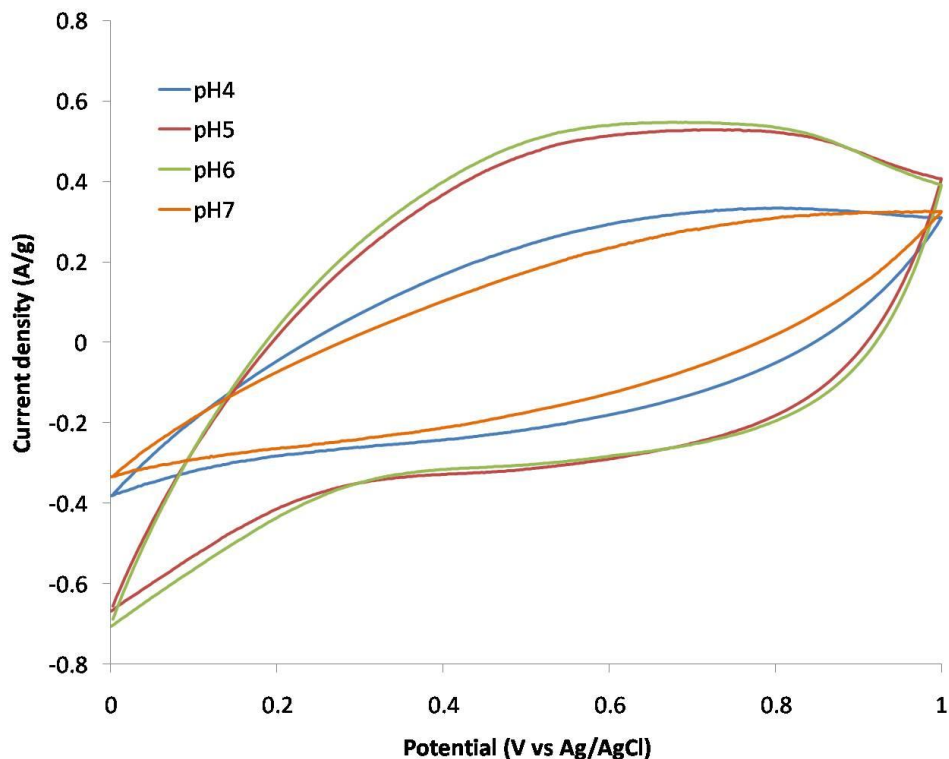


Figure 8. 3-electrode measurement of manganese dioxide as a function of pH of aqueous magnesium chloride solution

The electrochemical property of manganese dioxide was studied using four different electrolytes in a scan range of 0 to 1 V vs Ag/AgCl. It was shown that the specific capacitance of the electrode was dependent on the nature of the cations and was the highest, when we used magnesium chloride as the electrolyte ($Mg > Ca > Ba > K$) (as shown in Fig. 7a). Similarly, the electrochemical performance of the carbon was tested in a scan range of 0 to -1V vs Ag/AgCl using KCl as electrolyte (Fig 7b). The electrochemical performance of two different types of pitch carbon showed identical results. The presence of large amount of micropores aids in strong electrosorption of protons in the carbon resulting in a pseudocapacitive behavior. Capacitance as high as 100 F/g can be obtained from this phenomenon and the strong electrosorption of proton shifts the hydrogen evolution potential to almost -1.0 V vs Ag/AgCl. There also seems to be an

optimum pH at which the specific capacitance of Manganese dioxide is maximum. The specific capacitance was the highest when the pH of magnesium chloride was adjusted to 5 or 6 (Figure 8) and was close to 400 F/g.

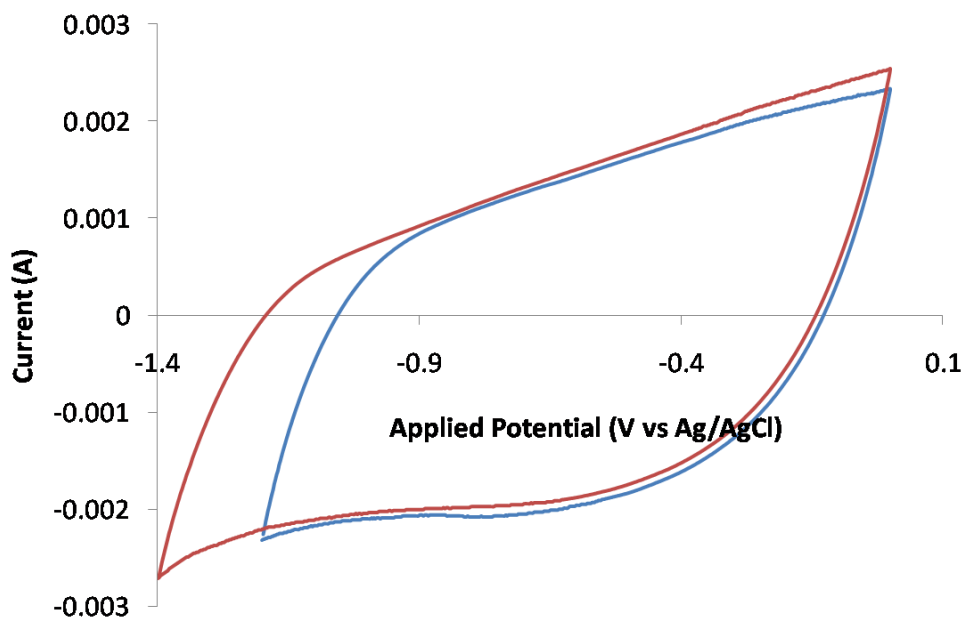


Figure 9. Evidence for strong electroadsorption of protons in carbon derived from polyborazylene/pitch derived carbons

The electroadsorption behavior of the carbon can be further enhanced when carbon derived from polyborazylene/pitch is used as a negative electrode as shown in Figure 9. The protons do not desorb almost until 1.4 V. The result was highly surprising and encouraging as the N_2 BET surface area of the electroactive material was only $50 \text{ m}^2/\text{g}$. This behavior can be used in designing an aqueous electrochemical asymmetric capacitor with increased cell voltage and high energy densities.

3.3.2. Fabrication of asymmetric capacitor using synthesized carbons

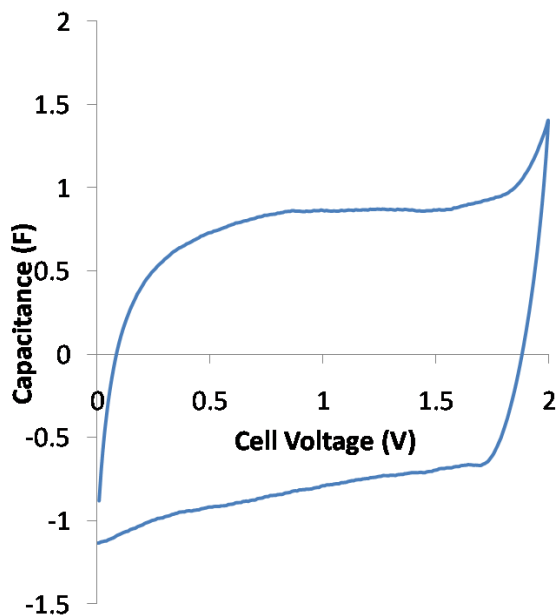


Figure 10. Cyclic voltammogram of asymmetric AC/MnO₂ two-electrode capacitor using aqueous magnesium chloride as the electrolyte tested using a scan rate of 10 mV/sec.

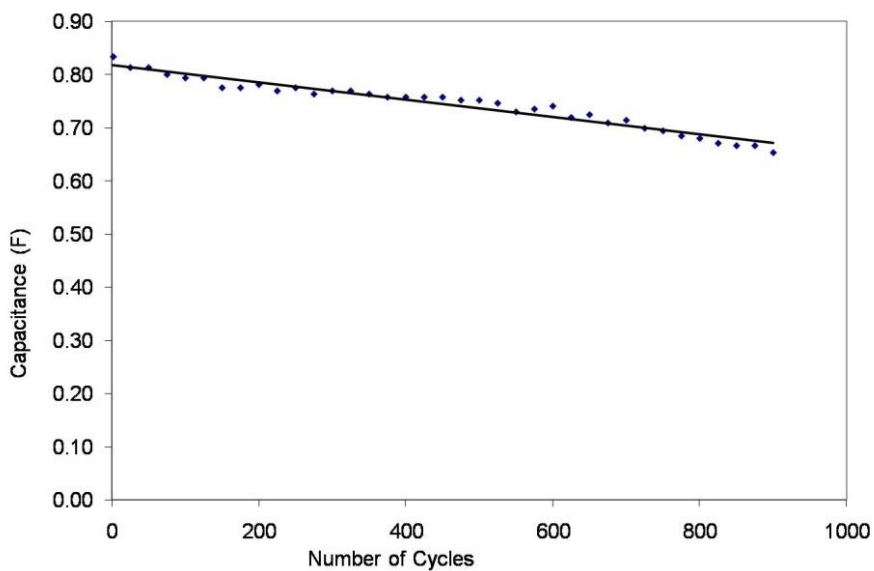


Figure 11. Performance of asymmetric electrochemical capacitor fabricated using AC derived from pitch/ Manganese dioxide using aqueous 2M MgCl₂ solution as electrolyte.

Asymmetric capacitor derived from pitch derived carbon/MnO₂ was constructed and a two electrode capacitor capable of operating at 2V in aqueous MgCl₂ solution was demonstrated as shown in Figure 10. The cell capacitance was about 0.8 F and the capacitor was cycled for 1000 cycles using galvanostatic charge/discharge method. Life cycle tests for over 1000 cycles showed capacitance fading of 20% (Figure 11). Careful analysis of both the half cell performance shows that the electroadsorption of protons in activated carbon deteriorates over a period of time.

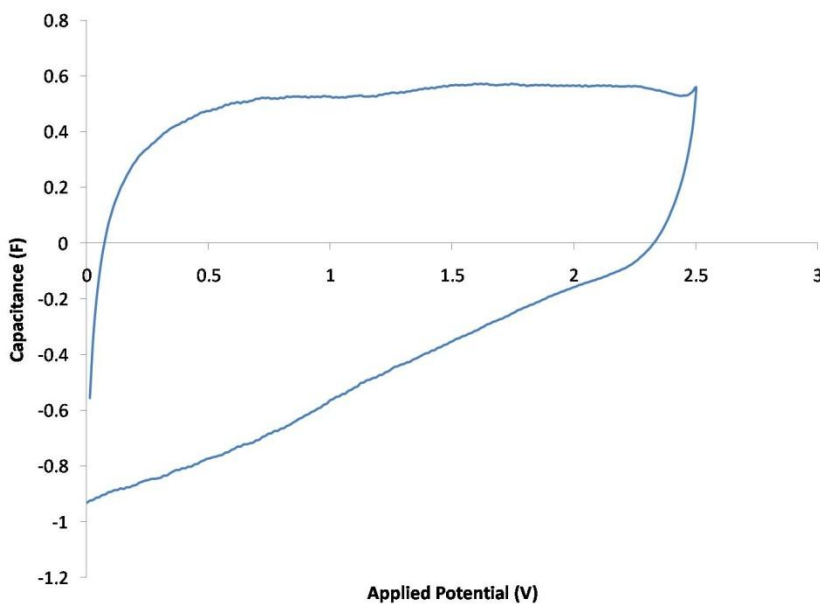


Figure 12. Cyclic voltammogram of asymmetric capacitor fabricated using boron doped pitch based carbons/ Manganese dioxide electrodes

An Asymmetric capacitor fabricated using polyborazylene /pitch blends has a cell capacitance of 0.6 F and cell voltage of 2.5 V (Figure 12), which is as high as organic electrolyte based capacitors. It was shown that energy densities as high as 22 Wh/kg can be obtained for this

sample and there is very little capacitance fading even after 300 cycles. The results looked very promising as we saw the energy densities improve by a factor of 4. However, due to the lack of availability of polyborazylene from the manufacturer, we could not pursue this systematic study further.

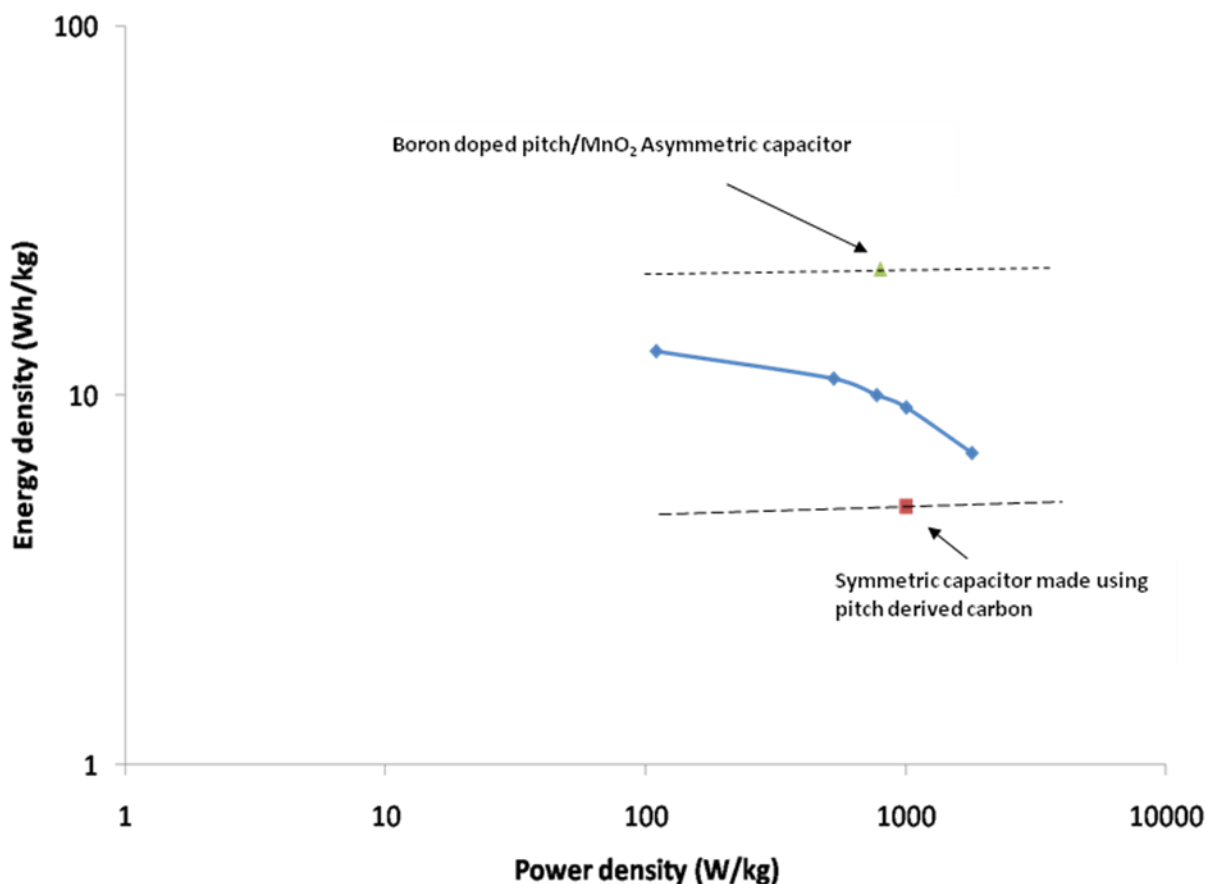


Figure 13. Ragone plot showing the comparison of the performance of symmetric and asymmetric capacitor derived using pitch derived carbon

Figure 13 shows the comparison of the performance of symmetric and asymmetric capacitors derived from coal tar pitch. The symmetric capacitors made of pitch derived activated carbon could store energy densities of 5 Wh/kg at 1 KW/kg. By designing an asymmetric capacitor using the strong electroadsorption of protons in these carbons and using manganese dioxide as a

pseudocapacitive electrode, the energy densities could be almost tripled to 13 Wh/kg for similar power densities. By designing a boron containing carbon, the electroadsorption of protons could be further enhanced and the energy densities could be increased by a factor of 4 to 22 Wh/kg for similar power densities. This was accomplished through a significant increase in the cell voltage of the capacitor due to an asymmetric design.

4. Conclusions

Boron containing pitch derived carbons were synthesized using four different approaches and the chemical state of boron in the carbons was analyzed using various techniques that include solid state B^{11} NMR and Infrared spectroscopy. The analysis showed that the incorporated boron is in trigonal state. Boron content in the synthesized carbons were as high as 15 atomic%. However, due to the lack of surface area, we did not see any significant electroactivity for these materials. To our surprise, boron nitrogen carbons synthesized using pyrolysis of polyborazylene/pitch precursor showed stronger electroadsorption of protons than the pitch derived high surface area nanoporous carbon. Asymmetric capacitors fabricated using these carbons and manganese dioxide had energy densities as high as 22 Wh/kg, which is almost two times higher than asymmetric pitch derived carbon/ MnO_2 capacitors and almost four times higher than symmetric pitch derived carbon capacitors. The cell voltage of these capacitors was extended upto 2.5V, as high as organic based electrolyte capacitors. However, since the designed capacitors are aqueous based electrolytes, the power densities are significantly higher than the organic electrolyte systems. The capacitors were cyclable upto 300 cycles and further study is warranted to predict the cycle life.

5. References

1. "Fabrication of electrochemical double layer capacitors using carbon derived from coal tar pitch/polyethylene glycol diacid blends" Proceedings of the International Technical Conference on Coal Utilization & Fuel Systems (2007) 32, 559 -562.
2. "Novel nanoporous carbon derived from coal tar pitch/polyethylene glycol diacid blends as electrodes for ultracapacitors" Materials Research Society Symposium Proceedings, 973E (2006).
3. "Synthesis and characterization of boron doped carbons" W. Cermignani, T.E. Paulson, C. Onneby and C.G. Pantano, Carbon, 33, 367 -374 (1995).
4. "Effects of nitrogen gas ratio on composition and microstructure of BCN films prepared by RF magnetron sputtering", Nakao S., Sonoda T., Tsugawa K., Choi J. and Kato T., Vacuum, 84, 642-647 (2010).

APPENDIX I: 2009 PROJECT FINAL REPORTS

The Production and Characterization of Metallurgical Coke Produced from Coal Using a Sulfur Dehydrogenation Process <i>Penn State University – Subcontract #3788-TPSU-DOE-1874.....</i>	<i>1577</i>
Development of Carbon-Based "Molecular Basket" Sorbent for CO₂ Capture from Flue Gas <i>Penn State University – Subcontract #3789-TPSU-DOE-1874.....</i>	<i>1620</i>
Relationship of Anthracite Structure to Isotropic Graphite <i>Penn State University – Subcontract #3808-TPSU-DOE-1874.....</i>	<i>1647</i>
Spectrally Selective Coal-derived Coatings for Solar Collectors <i>West Virginia University – Subcontract #3836-WVU-DOE-1874.....</i>	<i>1720</i>

The Production and Characterization of Metallurgical Coke Produced from Coal Using a Sulfur Dehydrogenation Process

Final Report

03/1/09 – 05/31/10

**Principle Authors: P.C. Painter, M. Sobkowiak, H. Schobert
August 16, 2010**

DOE Award Number: Subcontract # 3788-TPSU-DOE-1874 under DOE Prime DE-FC26-03NT41874

**The EMS Energy Institute
Penn State University
University Park, PA 16802**

Disclaimer

This report was prepared as an account of work sponsored by an agency of the United States Government. Neither the United States Government nor any agency thereof, nor any of their employees, makes any warranty, express or implied, or assumes any legal liability or responsibility for the accuracy, completeness, or usefulness of any information, apparatus, product, or process disclosed, or represents that its use would not infringe privately owned rights. Reference herein to any specific commercial product, process, or service by trade name, trademark, manufacturer or otherwise does not necessarily constitute or imply its endorsement, recommendation, or favoring by the United States Government or any agency thereof. The views and opinions of authors expressed herein do not necessarily state or reflect those of the United States Government or any agency thereof.

Abstract

The goal of this research was to develop methods for producing marketable forms of carbon from coals using a sulfur dehydrogenation process. If successful, this work would have considerable impact, allowing the development of a new, environmentally cleaner process for coke and carbon production, expanding the number of coals that can be used to make these products and allowing the development of a CO₂ free, carbon neutral, source of H₂.

This is a program of fundamental research to establish feasibility and an understanding of the relationships between processing conditions, coal structure, the mechanism of dehydrogenation, and the nature of the carbon being produced. One of the main goals of this research is to produce good quality carbon and/or coke at temperatures lower than those used in conventional methods.

There are three important factors in producing carbons from coal using sulfur dehydrogenation: the type of coal used, the time/temperature program and oven design. Based on previous work, it was postulated that coal required the appropriate time and conditions to form a mesophase before sulfur dehydrogenation commenced. This can be achieved using a two-oven system, so that the rate of heating of the coal and sulfur can be separately controlled and sulfur vapor introduced at a chosen point in the reaction. A series of temperature ramping experiments was devised and tested. These involved heating the coal to 550°C, holding at this temperature for different periods to allow mesophase development, then introducing sulfur vapor while raising the temperature to 700°C. In previous work the coal was usually held at this temperature for short times, usually 15 minutes.

Coke-like material with properties very close to those required for metallurgical coke have been produced, even though the maximum temperatures used were hundreds of degrees below those employed in conventional coke-making methods. The materials produced had high carbon values in the range 81% to 84.9% (by weight). The sulfur content was 0.7% or slightly less, but the volatile matter content was still too high – in the range 11.8% to 8.0%. For comparison, metallurgical coke has a fixed carbon value in the range 80% to 90% and volatile matter between 1% and 5%, with a sulfur content of about 0.5%.

Variations in the time/temperature program were explored in an attempt reduce the volatile matter content of the carbon products. In the modified temperature program, the holding time at 550°C was varied from 15 minutes to 120 minutes in order to allow additional time for the structural/chemical arrangements that are important for production of good quality coke and to reduce volatile matter.

Most of the research reported in this study and previous work utilized a mvb bituminous (coking) coal, DECS 30. An additional mvb bituminous (coking) DECS 13 coal, from West Virginia,⁶ was also examined. Carbons produced by sulfur dehydrogenation using this coal were the hardest coke-like material we have obtained. However, the volatile and sulfur content of these carbons makes them unsuitable for use as metallurgical coke.

Modifications to the design of the ovens were also made in order to intensify sulfur dehydrogenation. To achieve this, the diameter of the glass tube in which the coal or sulfur was loaded into the ovens was changed. Two experiments were performed. In the first experiment, the diameter of glass tube containing the coal was reduced to 2.5 cm. In previous work, both the tubes holding the coal and the sulfur had a diameter of 5 cm. During the second experiment, the glass tubes were reversed. The coal sample was loaded into the glass tube with a diameter of 5 cm, while in the second oven the sulfur was loaded into the glass tube with a diameter of 2.5 cm. Interesting carbons were produced, but not metallurgical coke.

An additional issue was also addressed. The supply of coking coals is limited and expensive. Good quality coke can be produced from a coal blend where primary coking coals are blended with a non-coking coal. Because coal fluidity is one of the most important factors influencing coke quality, a non-coking hvA coal, DECS 34, with a swelling index identical to the coking coal DECS 30 was chosen for study. However, under the condition used, a rather poor carbon in terms of mechanical properties was produced. A new addition to the PSU coal bank, DECS 36, was also tested. This coal is actually a blend of four hvA bituminous coals from West Virginia. This sample has exceptional fluidity and a high free swelling index. Good carbons, but not metallurgical coke, were produced.

Table of Contents

	Page
Abstract	3
Introduction	9
Executive Summary	10
Experimental	11
Results and Discussion	13
Conclusions	42
References	43

Graphical Materials

Figure 1: A picture of the carbon product obtained when coal DECS 13 alone was heated to 550°C and held at this temperature for 15 minutes. The temperature was then raised slowly to 700°C and held at this temperature for 1 hour.

Figure 2: SEM micrographs of the original coal DECS 13 (top) and the carbon product (bottom) pictured in figure 1.

Figure 3: SEM micrographs of the carbon product shown in figures 1 and 2.

Figure 4: SEM micrographs of the carbon product shown in figures 1-3.

Figure 5: A picture of the carbon product obtained when coal DECS 13 was heated to 550°C and held constant for 15 minutes. The temperature was then raised slowly to 700°C and held at this temperature for 1 hour. The sulfur vapor started to sweep through the coal bed after the 550°C ramp was over and continued until the reaction was complete.

Figure 6: SEM micrographs of the original coal DECS 13 (top) and the carbon product shown in figure 5.

Figure 7: SEM micrographs of the carbon product shown in figures 5 and 6.

Figure 8: A picture of the carbon product obtained when DECS 34 coal was heated to 550°C in the absence of sulfur and held at this temperature for 15 minutes. The temperature was then raised slowly to 700°C and held at this temperature for 1 hour.

Figure 9: SEM micrographs of the carbon product shown in figure 8.

Figure 10: SEM micrographs of the carbon product shown in figures 8 and 9.

Figure 11: SEM micrographs of the original DECS 30 (coking coal) coal (left) and the carbon product (right) produced under similar conditions to the material shown in figures 8-10..

Figure 12: A picture of the carbon product obtained when the DECS 34 coal alone was heated to 550°C and held at this temperature for 15 minutes. The temperature was then raised slowly to 700°C and held at this temperature for 1 hour. Sulfur dehydrogenation commenced at the start of this second heating ramp and continued until the reaction was complete.

Figure 13: SEM micrographs of the original DECS 34 coal (top) and the carbon product (middle and bottom) pictured in figure 12.

Figure 14: Additional SEM micrographs of the carbon product pictured in figure 12 and 13.

Figure 15: A picture of the carbon product obtained when the coal blend (5% DECS 34 and 95% DECS 30) was heated to 550°C and held at this temperature for 15 minutes. The temperature was then raised slowly to 700°C and held at this temperature for 1 hour.

Figure 16: SEM micrographs of the carbon product pictured in figure 15.

Figure 17: A picture of the carbon product obtained when the coal blend (5% DECS 34 and 95% DECS 30) was heated to 550°C and held at this temperature for 15 minutes. The temperature was then raised slowly to 700°C and held at this temperature for 1 hour. Sulfur dehydrogenation commenced at the start of this second heating ramp and continued until the reaction was completed.

Figure 18: SEM micrographs of the carbon product pictured in figure 17.

Figure 19: SEM micrographs of the carbon product pictured in figure 17 (bottom row) compared with those produced from DECS 34 (the middle row, right) and DECS 30 (top, right) under the same conditions.

Figure 20: A picture of the carbon product obtained when coal (5 % wt DECS 34 blend with 95% wt DECS 30) was heated to 550°C in the absence of sulfur and held at this temperature for 15 minutes. The temperature was then raised slowly to 700°C and held at this temperature for 6 hours. Sulfur dehydrogenation commenced at the start of this second heating ramp and continued until the reaction was complete.

Figure 21: SEM micrographs of the carbon product shown in figures 20.

Figure 22: SEM micrographs of the carbon product shown in figures 20 and 21.

Figure 23: The carbon product produced from coal DECS 30 under the same conditions as the carbon product from the blend pictured in figures 20-22.

Figure 24: A picture of the carbon product obtained when a coal blend (20% by wt DECS 34, 80% by wt DECS 30) was heated to 550°C in the absence of sulfur, and held at this temperature for 15 minutes. The temperature was then raised slowly to 700°C and held at this temperature for 1 hour. Sulfur dehydrogenation commenced at the start of this second heating ramp and continued until the reaction was complete.

Figure 25: A picture of the carbon product obtained when coal DECS 36 alone was heated to 550°C and held at this temperature for 15 minutes. The temperature was then raised slowly to 700°C and held at this temperature for 1 hour.

Figure 26: SEM micrographs of the carbon product shown in figures 25.

Figure 27: SEM micrographs of the carbon product shown in figures 25 and 26.

Figure 28: A picture of the carbon product obtained when coal DECS 36 was heated to 550°C in the absence of sulfur and held at this temperature for 15 minutes. The temperature was then raised slowly to 700°C and held at this temperature for 1 hour. The sulfur vapor started to sweep through the coal bed after the 550°C ramp was over and continued until the reaction was complete.

Figure 29: SEM micrographs of the original DECS 36 coal (top) and the carbon product (bottom) pictured in figure 28.

Figure 30: SEM micrographs of the carbon product pictured in figures 28 and 29.

Figure 31: SEM micrographs of the carbon product pictured in figures 28-30.

Figure 32: A picture of the carbon product obtained when coal DECS 30 was heated to 550°C in the absence of sulfur and held at this temperature for 120 minutes. The temperature was then raised slowly to 700°C and held at this temperature for 1 hour. The sulfur vapor started to sweep through the coal bed after 550°C ramp is over and continued until the reaction was complete.

Figure 33: SEM micrographs of the original coal DECS 30 (top) and the carbon product (bottom) pictured in figure 32.

Figure 34: SEM micrographs of the carbon product shown in figures 32 and 33.

Figure 35: A picture of the carbon product obtained when coal DECS 30 alone was heated to 550°C in the absence of sulfur and held at this temperature for 15 minutes. The temperature was then raised slowly to 700°C and held at this temperature for 1 hour. The sulfur vapor started to sweep through the coal bed after 550°C ramp is over and continued until the reaction was complete.

Figure 36: SEM micrographs of the carbon product shown in figure 35.

Figure 37: A picture of the carbon product obtained when the DECS 30 coal was loaded into the narrower 2.5 cm diameter glass tube and heated to 550°C in the absence of sulfur and held at this temperature for 15 minutes. The temperature was then raised slowly to 700°C and held at this temperature for 1 hour. The sulfur vapor started to sweep through the coal bed after the 550°C ramp was over and continued until the reaction was complete.

Figure 38: SEM micrographs of the original DECS 30 coal (top) and the carbon product (bottom) pictured in figure 37.

Figure 39: SEM micrographs of the carbon product shown in figures 37 and 38.

Figure 40: A picture of the carbon product obtained during the second experiment when coal DECS 30 was heated to 550°C in the absence of sulfur and held at this temperature for 15 minutes. The temperature was then raised slowly to 700°C and held at this temperature for 1 hour. The sulfur vapor started to sweep through the coal bed after the 550°C ramp was over and continued until the reaction was complete. The sulfur was loaded into the glass tube with a smaller (2.5 cm) diameter.

Figure 41: SEM micrographs of the original DECS 30 coal (top) and carbon product (bottom) pictured in figure 40.

Figure 42: Additional SEM micrographs of the carbon product shown in figures 40 and 41.

Introduction

The goal of this research was to develop a novel method for the production of premium carbon products from coal. The process has the potential for solving a number of problems. For example, only certain types of coal are suitable for metallurgical coke production and these are also becoming increasingly expensive. In addition, producing carbon products from coal is often a “dirty” business and there are a number of environmental challenges facing the industry. Clearly, a process that has the potential for producing premium carbon products from a broader range of coal types while mitigating a number of pollution concerns would be extremely valuable.

The immediate objective of the program of fundamental research was aimed at developing and extending the recent work of Jusino and Schobert.¹ In this research, vapor-phase sulfur was used to dehydrogenate a medium volatile bituminous coal through the formation of H₂S. Yields of 70–75% of the hydrogen in a medium volatile bituminous coal were obtained in this way. CO₂ was not produced in this process. Furthermore, the carbon so produced met or exceeded the specifications for fixed carbon, ash, low sulfur content and friability of conventional metallurgical coke, even though it was produced at lower temperatures than those used in typical by-product coke ovens.

In previous work, various aspects of the sulfur dehydrogenation process were studied.²⁻⁷ It was established that there are three important factors in the sulfur dehydrogenation process the type of coal used, the time/temperature program and oven design.

The importance of the time/temperature program follows from well-known aspects of coal carbonization. Between temperatures of 350°C and 450°C coal softens, melts, turns into a fluid, devolatilizes and vesiculates.⁸ Coking coals usually develop their maximum fluidity in this range. At higher temperatures (450°C–550°C), the coal begins to form coke. It is during this latter stage that the coal forms liquid crystals, which subsequently harden into the anisotropic domains that give coke its characteristic mosaic cell wall structure. In order to form such a mesophase prior to dehydrogenation, a two-oven system was developed,² so that the rate of heating the coal and sulfur can be separately controlled and sulfur vapor introduced at a chosen point in the reaction. A series of ramping experiments was devised where the coal was initially heated to a chosen “holding” temperature between 350°C to 550°C and kept there for a period that varied between 15 and 45 minutes. At the end of this period, sulfur vapor was allowed to sweep through the bed of coal while the temperature was raised to a final temperature of 600°C or 700°C and held at this final temperature for at least 1 hour. The material produced had fixed carbon values between 84 and 85.2 %, a sulfur content of 0.7% to 0.5%, and a volatile matter content between 9.1% and 11%. The volatile matter content is still too high, because standard metallurgical coke has values that range between 1% and 5%.

Building on this research, a modified time/temperature protocol was devised and the results are reported here. Previously, the coal was slowly heated to 550°C and held at this temperature for 15 minutes. At the end of this period, sulfur vapor was allowed to sweep through the coal bed, while the temperature was raised to 700°C and held there for at least 1 hour. In the modified temperature program, the holding time at 550°C was prolonged from 15 minutes to 120 minutes. The idea was to allow enough time for all structural/chemical arrangements that are important for the production of coke.

Modifications to the design of the ovens were also made in order to change the rate of sulfur dehydrogenation. The diameter of one or the other of the glass tubes where coal or sulfur

samples were loaded was reduced. Two experiments were performed. In the first, the coal sample was loaded into a glass tube with a diameter of 2.5 cm, while the second tube containing the sulfur was maintained at a diameter of 5 cm, as in previous work. In the second experiment the glass tubes were reversed. The sulfur was placed in a glass tube with narrow diameter (2.5 cm), while the coal sample was placed in a tube with a diameter of 5 cm. The carbon products obtained in these experiments were then characterized.

Most of the research reported previously utilized a mvb bituminous (coking) DECS 30 coal.^{2,4-6} In the work reported here a new mvb bituminous (coking) coal, DECS 13 from West Virginia,⁶ was also studied. This coal is a very high quality primary coking coal.

Another issue was also addressed. The supply of coking coals is limited and expensive. However, good quality coke can be produced from a coal blend where primary coking coals are blended with a non-coking coal. Accordingly, a non-coking hvb A bituminous coal, DECS 34, was studied. This coal has a swelling index identical to DECS 30 and a very good fluidity index, making it a good choice to be used in coal blends with DECS 30. Coal DECS 34 was carbonized alone and in blends with DECS 30 under the same conditions. Finally, DECS 36 was also studied. This is a new addition to our PSU coal sample bank and is actually a blend of four hvb A bituminous coals from West Virginia. This sample has an exceptionally high fluidity and a high free swelling index.

Executive Summary

The work reported here examines various protocols for dehydrogenating coal with sulfur to form carbons. Because the formation of metallurgical coke, the prime goal of this work, involves the formation of an intermediate mesophase, a two-oven system was previously developed, so that the rate of heating of the coal and sulfur can be separately controlled and sulfur vapor introduced at a chosen point in the reaction. Using this apparatus, various time/temperature programs were examined, with the goal of reducing the volatile matter in the carbons being produced. Carbons produced in previous work had volatile matter contents too high for use as metallurgical coke. In the modified temperature program, an initial holding time at 550°C was prolonged from 15 minutes to periods as long as 120 minutes. The idea was to allow enough time for all the structural and chemical arrangements that are crucial for the production of coke.

For the same reasons, modifications to the design of the ovens were made in order to change the rate of sulfur dehydrogenation. The diameter of one or the other of the glass tubes where coal or sulfur samples were loaded was reduced. Two experiments were performed. In the first, the coal sample was loaded into a glass tube with a diameter of 2.5 cm (previously 5 cm), while the second tube containing the sulfur was maintained at a diameter of 5 cm. In the second experiment the glass tubes were reversed: the sulfur was placed in a glass tube with a narrow diameter (2.5 cm), while the coal sample was placed in a tube with a diameter of 5 cm.

In addition to work on developing the dehydrogenation process, three new coals and coal blends were examined and compared. The carbon products obtained in all the experiments were then characterized. Although interesting carbons were produced, none had a low enough volatile matter content to be useful as metallurgical coke.

Experimental

The characteristics of the coals used in this work are summarized in Table 1.

Table 1: Elemental and proximate analysis of coals

Coal	C % daf	H % daf	N % daf	Total S % dry	Ash % dry	VM % dry	FC % dry	FSI Index
DECS 13	88.8	4.7	1.4	0.6	4.2	25.0	70.5	8.0
DECS 34	84.4	5.6	1.7	1.7	7.3	38.4	54.3	8.0
DECS 36	87.4	5.5	1.6	1.1	7.2	34.5	58.3	9.0
DECS 30	87.8	5.4	1.6	0.8	3.9	30.0	65.9	8.0

DECS 30 and DECS 13 are both mvb bituminous coking coals. DECS 30 was studied in previous work, but DECS 13 is a new coking coal that has very good thermoplastic properties. DECS 34 is a hvb A non-coking coal with a swelling index (FSI) identical to DECS 30. It was therefore deemed to be a good choice for used in blends with the coking coal DECS 30.

Coal DECS 36, classified as a high volatile A bituminous coal, is actually a blend of four hvA bituminous coals, all of Pennsylvania age. The sample has the following components:

1. River Fork Mine-Eagle seam
2. White Queen Mine- Upper Powellton (#2 Gas Seam)
3. Rivers Fork- Powellton seam
4. Marsh Fork (Slip Ridge) Mine- Lower Cedar Grove Seam

This sample has an exceptionally high fluidity and a high free swelling index.

A two-oven flow reactor was used in these experiments. One reactor contained the coal sample while the second contained sulfur. Each individual oven was similar in design to that described by Jusino and Schobert.¹ Essentially; each oven consists of a Pyrex glass tube (about 1 m long, initially 5 cm diameter), heated in an electric furnace. The ends of the reactor are closed with stoppers that have provisions for an inert gas sweep inlet tube and an exit tube. The inert gas sweeps the sulfur vapor, as it is held in a “boat” in the first oven, through a bed of coal in the second oven, and prevents the vapor from diffusing away from the coal. This procedure also allows the hydrogen sulfide produced to be swept out of the reactor into gas wash bottles that contain a solution of cadmium chloride. These solutions can be used to determine the amount of hydrogen sulfide generated.

Weighed quantities of coal or blends were placed in the first reactor and weighed quantities of sulfur were placed in a glass boat in the second oven. A typical heating program for the coal reactor was as follows: the coal was heated to 250°C at a rate of 5°C/min; from 250°C to 550°C the coal was heated at a rate of 3°C/min. The coal was then held constant at 550°C for 15 minutes. The temperature was then raised at a rate of 3°C/min to the final temperature of 700°C and held at this temperature for 1 hour. The sulfur vapor started to sweep through the coal bed after the 550°C ramp was over and continued until the reaction was complete. At the end of these reactions, nitrogen flow through the reactor was continued for several additional minutes. For

comparison purposes, the same experiments were performed with the coal alone (in the absence of sulfur) under the same conditions.

In some experiments a modified temperature program was used. In the modified temperature program, the holding time at 550°C was increased from 15 minutes to 120 minutes. The idea was to allow additional time for all the structural and chemical arrangements that are important for the production of good quality coke.

The design of the ovens was also modified in order to intensify dehydrogenation of coal by sulfur. To achieve this, the diameter of the glass tube in which the coal or sulfur was loaded into the ovens was changed. Two experiments were performed. First, the diameter of the glass tube containing the coal was reduced to 2.5 cm. During the second experiment, the glass tubes were reversed. The coal sample was loaded into the glass tube with a diameter of 5 cm, while in the second oven the sulfur was loaded into the glass tube with a diameter of 2.5 cm.

SEM micrographs of the carbon products were obtained using a Hitachi S-35000N scanning electron microscope (SEM). Proximate analysis of the carbon samples (volatile matter, VM; ash, and fixed carbon, FC) was performed using a LECO MAC-400 Proximate Analyzer. Sulfur content was determined using a LECO SC-32 analyzer.

Results and Discussion

Comparing coals.

DECS 30 coal was characterized extensively in previous work² and here we start by examining a different coking coal. Figure 1 shows a picture of the carbon product obtained when DECS 13 coal alone (in the absence of sulfur) was heated during the experiment described in the experimental section (holding time 15 minutes at 550°C, final temperature 700°C for 1 hour). Physically, it appeared to be a hard, shiny mass.



Figure 1: A picture of the carbon product obtained when coal DECS 13 alone was heated to 550°C and held at this temperature for 15 minutes. The temperature was then raised slowly to 700°C and held at this temperature for 1 hour.

SEM micrographs of the carbon product pictured in figure 1 and the original DECS 13 coal are compared in figure 2. It can be seen that the coal passed through a liquid stage and after consolidation, a swollen, hard, porous carbon product was produced. A closer examination of the carbon product (figures 3 and 4) shows that a majority of the pores are open and have a thick wall.

The proximate analysis of the carbon product obtained by heating this coal without sulfur (table 2) revealed a fixed carbon value of 80.1%, volatile matter of 11.8%, and total sulfur of 1.0%. For the original coal, these values were 70.5 %, 25% and 0.6 %, respectively.

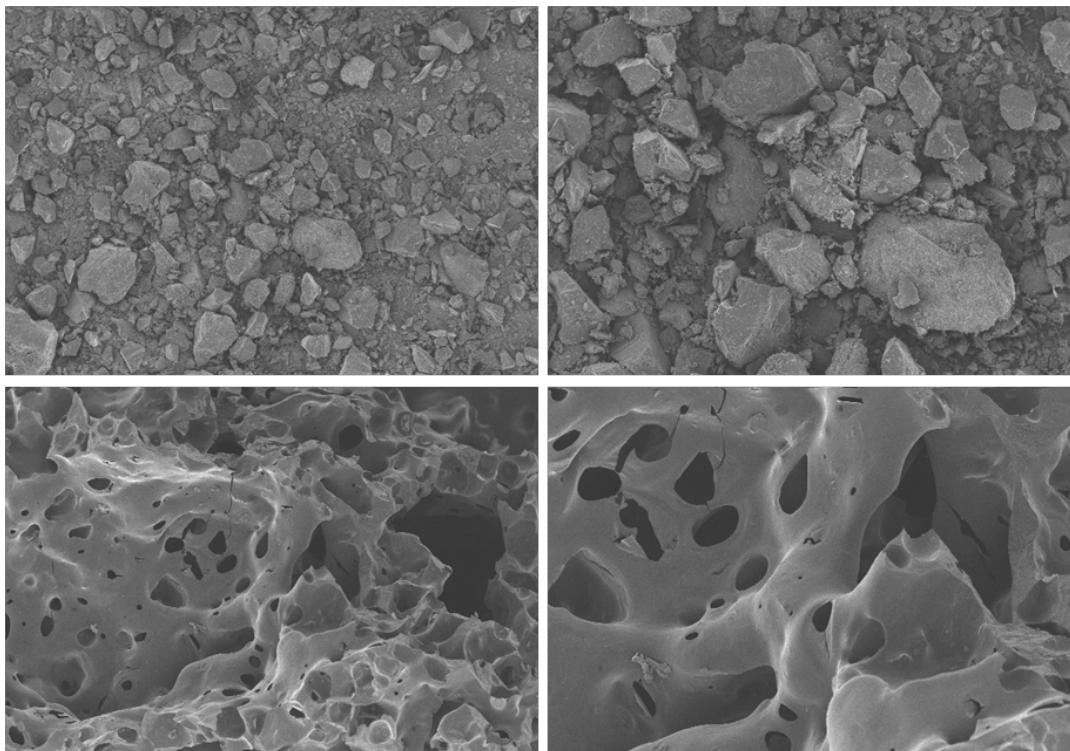


Figure 2: SEM micrographs of the original coal DECS 13 (top) and the carbon product (bottom) pictured in figure 1.

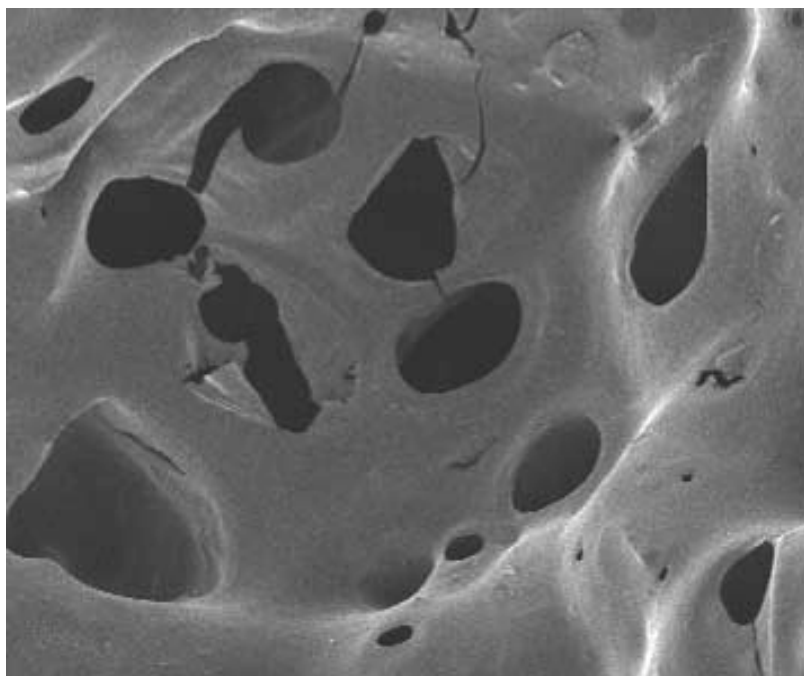


Figure 3: SEM micrographs of the carbon product shown in figures 1 and 2.

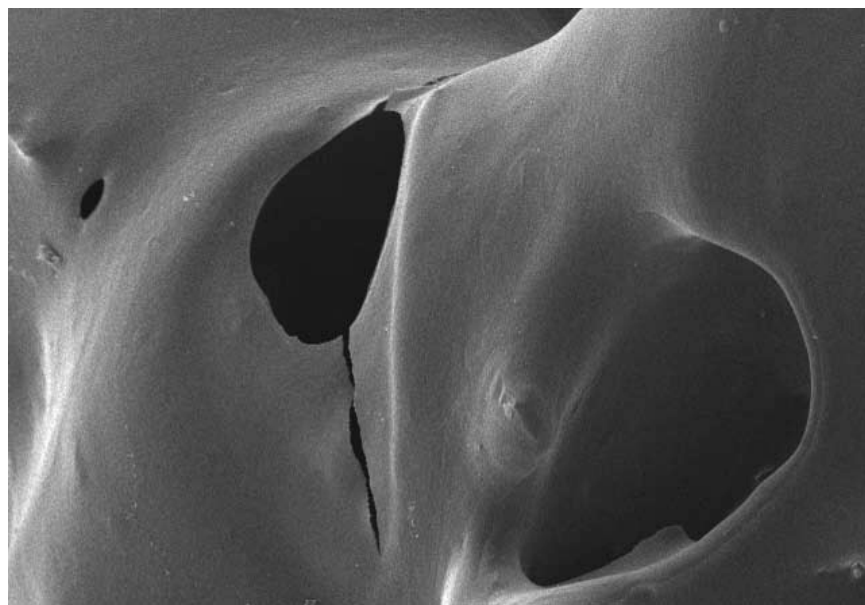


Figure 4: SEM micrographs of the carbon product shown in figures 1-3.

Figure 5 is a picture of the carbon product obtained when the coal DECS 13 was heated in the presence of sulfur using the procedure described in the experimental section. The carbon material was very hard, shiny and with a visible porosity. It was the hardest carbon material we have produced using the sulfur dehydrogenation procedure.

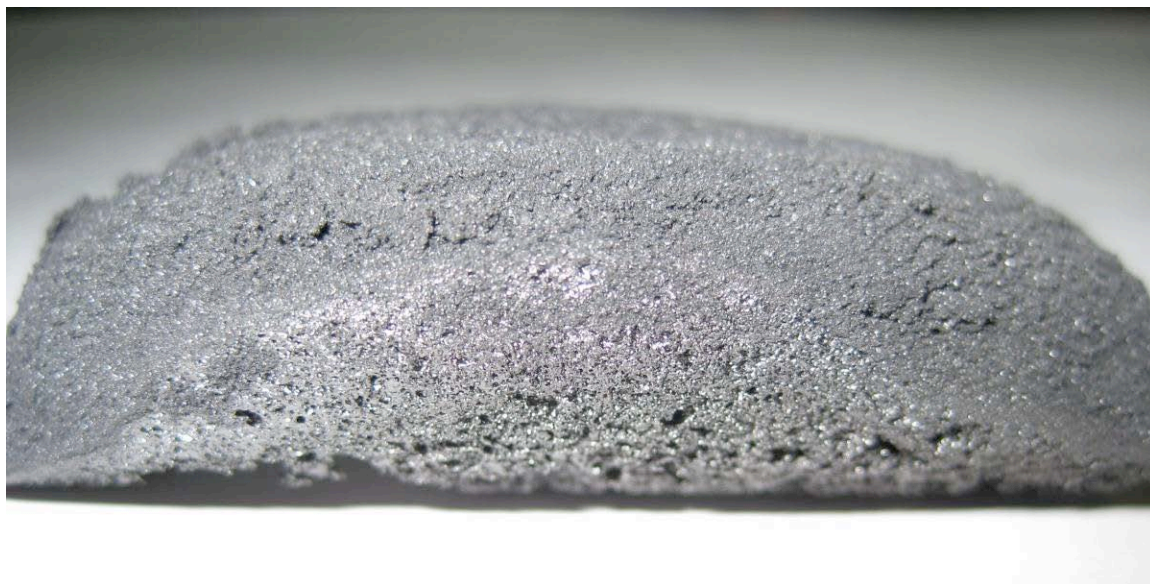


Figure 5: A picture of the carbon product obtained when coal DECS 13 was heated to 550°C and held constant for 15 minutes. The temperature was then raised slowly to 700°C and held at this temperature for 1 hour. The sulfur vapor started to sweep through the coal bed after the 550°C ramp was over and continued until the reaction was complete.

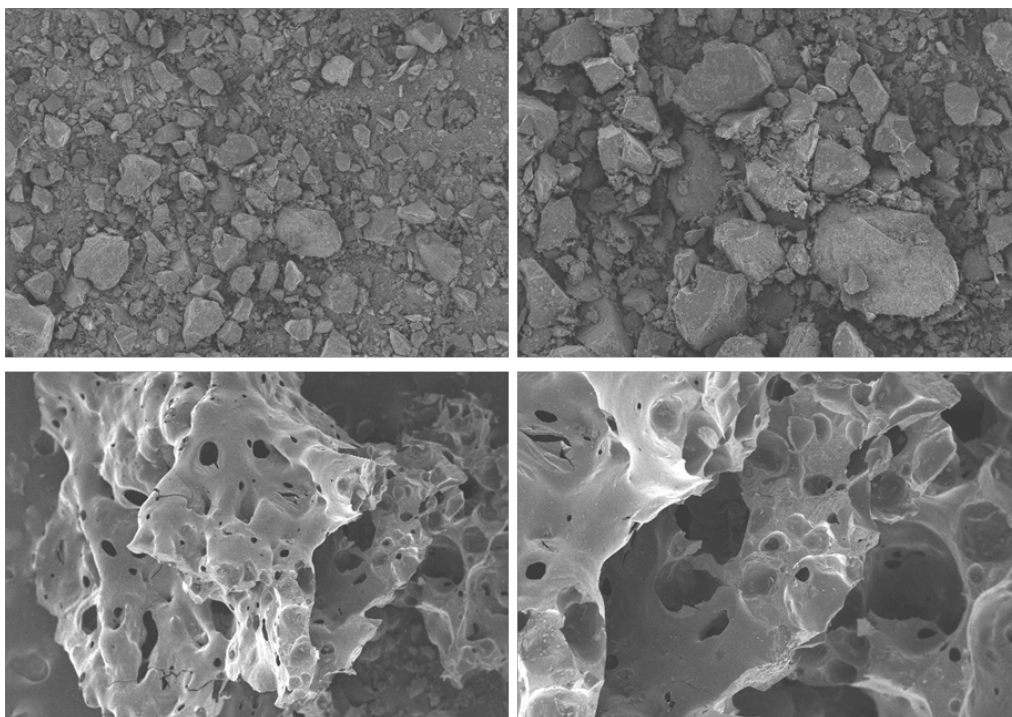


Figure 6: SEM micrographs of the original coal DECS 13 (top) and the carbon product shown in figure 5.

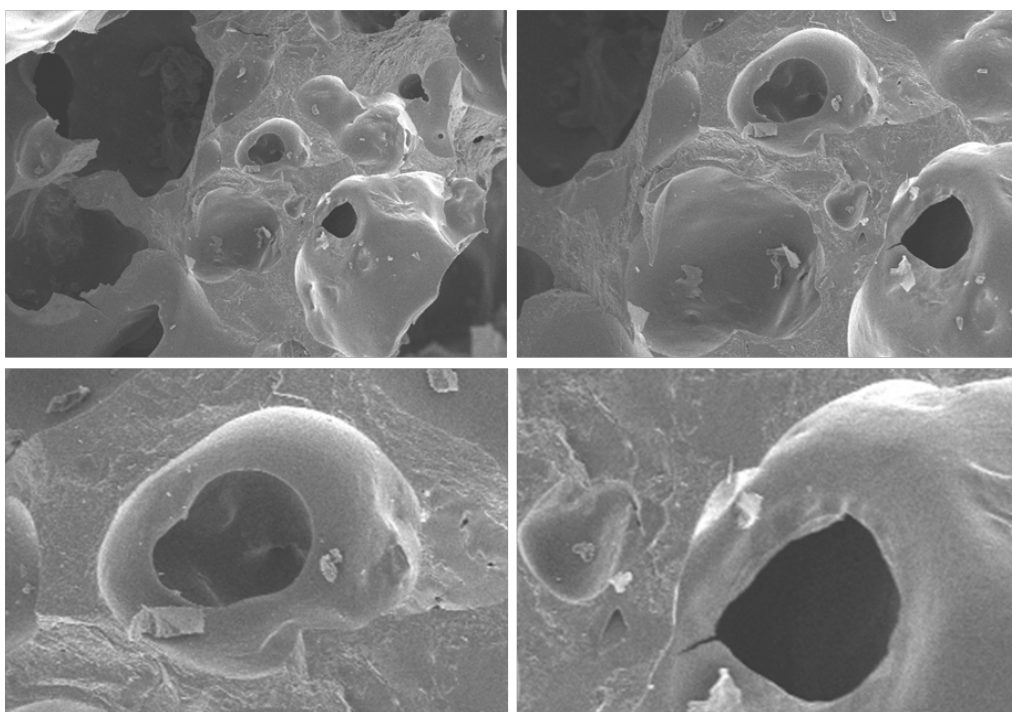


Figure 7: SEM micrographs of the carbon product shown in figures 5 and 6.

SEM micrographs of the carbon product pictured in figure 5 and the original coal DECS 13 are shown in figure 6. It can be seen that the coal passed through a liquid stage and, after consolidation, a smooth structure with porosity was developed. This is illustrated in more detail in figure 7. The walls of the pores are thick and the majority of pores are open.

In Table 2, the proximate analysis of carbon products obtained when coal DECS 13 was heated with or without sulfur are summarized and compared with those from the parent coal. A proximate analysis of the carbon product of sulfur dehydrogenation revealed a fixed carbon value of 84.9%, volatile matter of 8.0% and total sulfur of 0.7%. The proximate analysis of the carbon product obtained by heating coal without sulfur under the same conditions revealed a fixed carbon value of 80.1%, volatile matter of 11.8% and total sulfur of 1.0%. For comparison, metallurgical coke has a fixed carbon value in the range 80-90% and volatile matter between 1-5%, and sulfur ~0.5%.

Table 2: Proximate analysis of carbon products obtained from sample DECS 13.

Sample	Volatile Matter % dry	Fixed Carbon % dry	Total Sulfur % dry
Original coal DECS 13	25.0	70.5	0.6
DECS 13 alone Ramp to 550 °C, held for 15 min. Final temp 700 °C, held 1 h.	11.8	80.1	1.0
DECS 13 After S dehydrogenation. Ramp to 550 °C, held for 15 min. Final temp 700 °C, held 1 h.	8.0	84.9	0.7

The coke like material produced during sulfur dehydrogenation using mvb coal DECS 13 was the hardest coke-like material we have obtained. However, the volatile matter and sulfur contents are still too high for use as metallurgical coke. It was postulated that prolonging the holding time at the final temperature of 700°C could lower these values.

Turning now to a non-coking coal, DECS 34 was examined. Figure 8 is a picture of the carbon product obtained when this coal was heated to 550°C in the absence of sulfur and held at this temperature for 15 minutes. The temperature was then raised slowly to 700°C and held at this temperature for 1 hour. Physically, it appeared to be rather brittle material that broke into pieces while being unloaded from the oven.



Figure 8: A picture of the carbon product obtained when DECS 34 coal was heated to 550°C in the absence of sulfur and held at this temperature for 15 minutes. The temperature was then raised slowly to 700°C and held at this temperature for 1 hour.

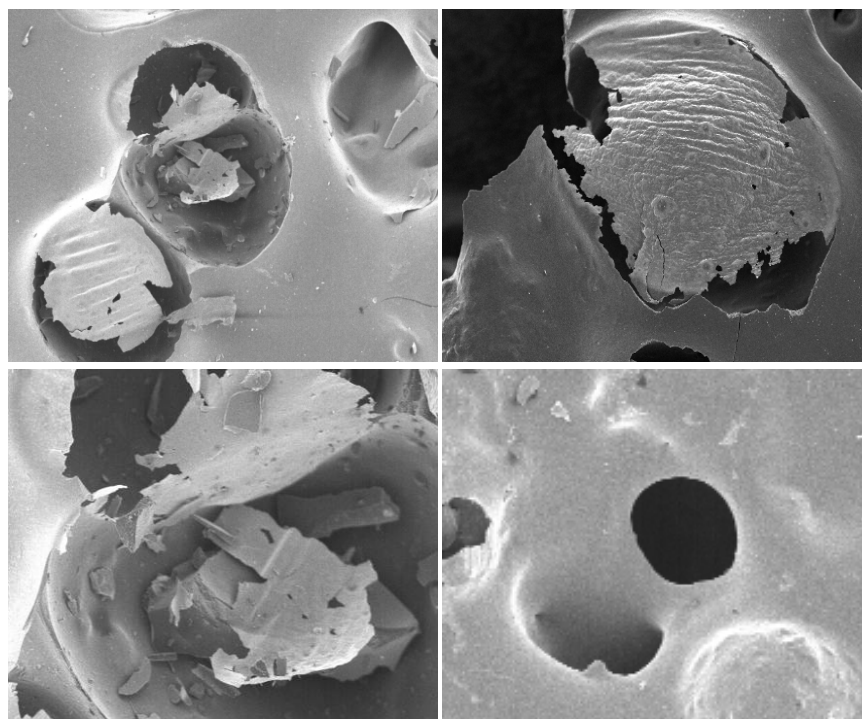


Figure 9: SEM micrographs of the carbon product shown in figure 8.

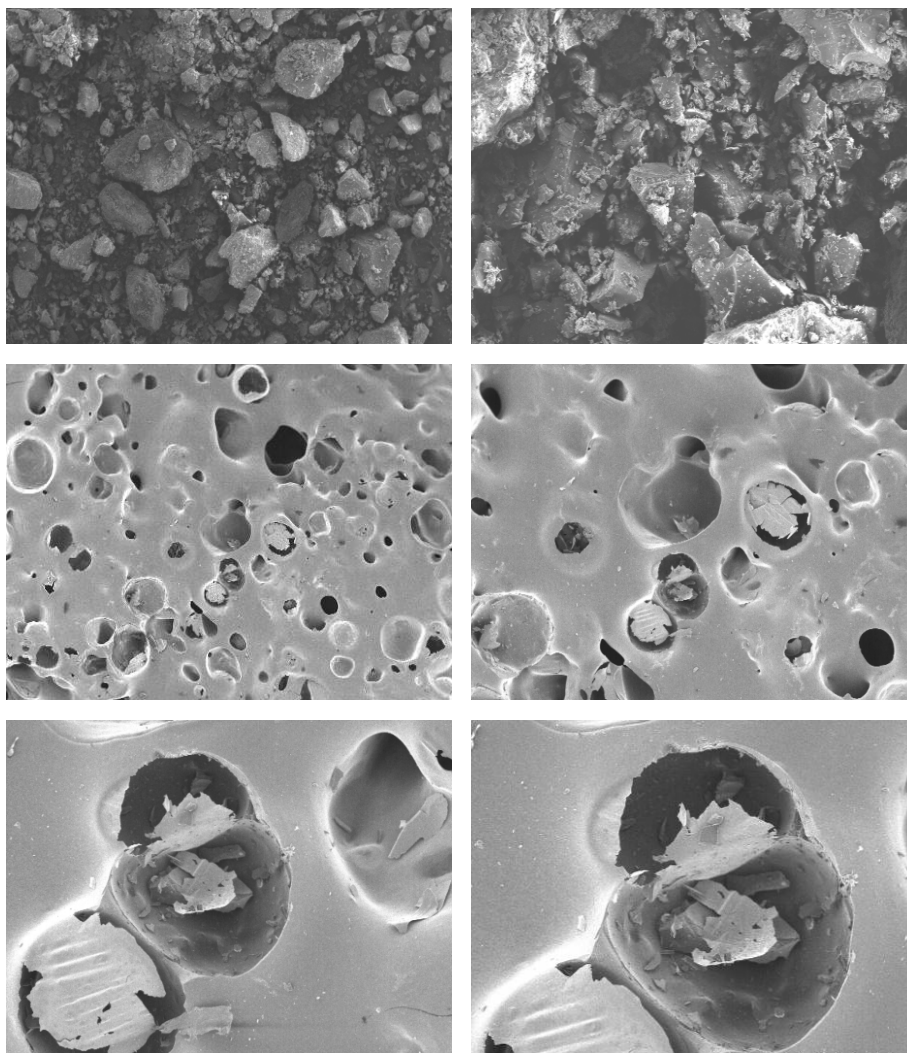


Figure 10: SEM micrographs of the carbon product shown in figures 8 and 9.

SEM micrographs of the carbon product pictured in figure 8 and the original coal are shown in figure 10. It can be seen (figure 10) that the carbon product passed through a thermal swelling stage, but produced a highly swollen, porous carbon product after consolidation. A closer examination of the carbon product (figure 9) shows that only a few pores opened. Other sections contained some debris, while many pores were closed or remained undeveloped. For comparison, SEM micrographs of the original DECS 30 (coking coal) coal (left) and the carbon product (right) produced under similar conditions as in these experiments are shown in figure 11. It can be seen that the carbon product passed through a liquid stage and after consolidation, dense smooth structures with a few pores develop.

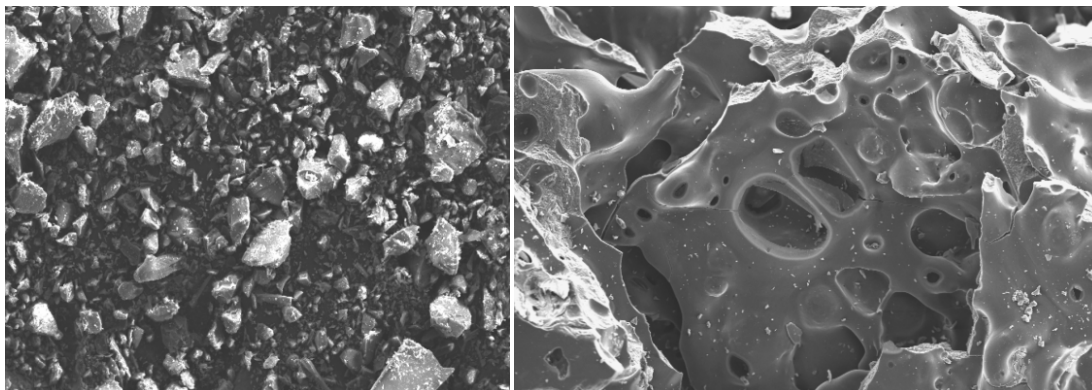


Figure 11: SEM micrographs of the original DECS 30 (coking coal) coal (left) and the carbon product (right) produced under similar conditions to the material shown in figures 8-10.

Figure 12 is a picture of the carbon product of coal DECS 34 obtained during sulfur dehydrogenation. The carbon product took the shape of the glass tube and was easily removed from the oven. However, after applying some pressure, it broke into pieces.



Figure 12: A picture of the carbon product obtained when the DECS 34 coal alone was heated to 550°C and held for 15 minutes. Temperature was then raised slowly to 700°C and held at this temperature for 1 hour. Sulfur dehydrogenation commenced at the start of this second heating ramp and continued until the reaction was complete.

SEM micrographs of the carbon product pictured in figure 12 and the original coal are shown in figure 13. It can be seen that the carbon product passed through a thermal swelling stage, but produced a highly swollen, porous carbon product after consolidation. A closer examination of the carbon product (figure 14) shows an unusual (relative to the carbons produced from DECS 30), very smooth, “glassy” almost shiny carbon surface.

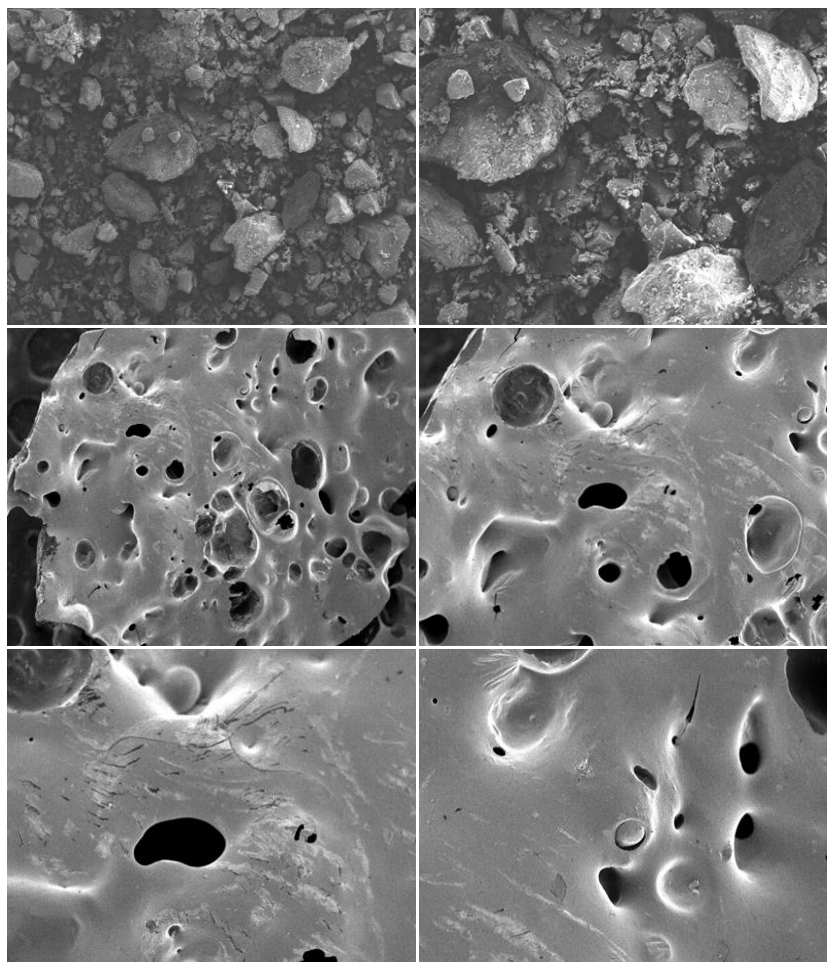


Figure 13: SEM micrographs of the original DECS 34 coal (top) and the carbon product (middle and bottom) pictured in figure 12.

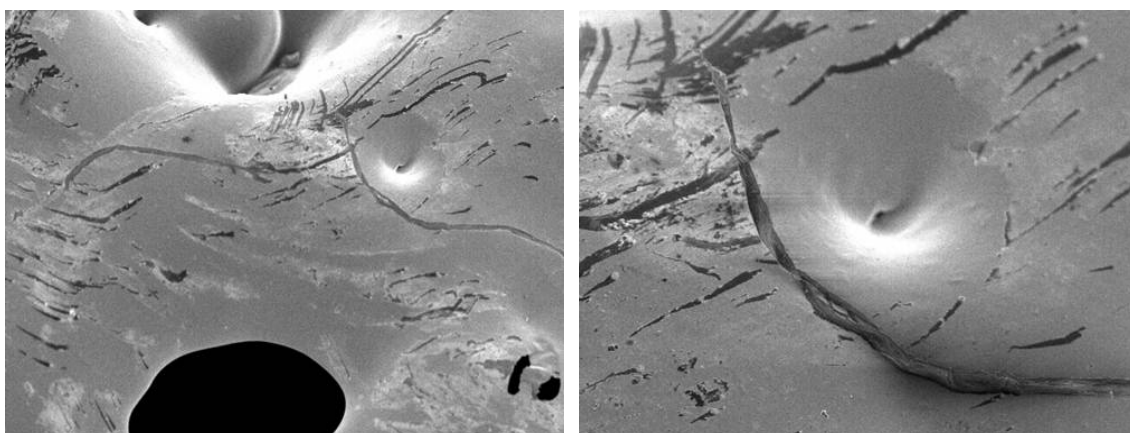


Figure 14: Additional SEM micrographs of the carbon product pictured in figure 12 and 13.

Table 3: Proximate analysis of carbon products obtained from sample DECS 34.

Sample	Volatile Matter % dry	Fixed Carbon % dry	Total Sulfur % dry
Original coal DECS 34	38.4	54.3	1.6
DECS 34 alone Ramp to 550 °C, held for 15 min. Final temp 700 °C, held 1 h.	16.7	77.0	1.4
DECS 34 after S dehydrogenation. Ramp to 550 °C, held for 15 min. Final temp 700 °C, held 1 h.	16.0	79.6	2.1

The proximate analysis of original coal DECS 34 and two carbon products are presented in Table 3. The proximate analysis of the carbon products obtained when DECS 34 coal was heated with and without sulfur under the same condition is very similar. The volatile matter is 16.0% and 16.7%, respectively. Fixed carbon values for the product obtained by sulfur dehydrogenation is slightly higher, 79.6 %, than when the coal is heated in the absence of sulfur (77%).

Coal Blends

Coal DECS 30 blended with DECS 34

In coal blending experiments, we used the same high-volatile bituminous A coal, DECS 34 (Tables 1 & 3). This bituminous coal has very good swelling properties, very similar to those of DECS 30. Both coals have an identical free swelling index. On this basis, DECS 34 appeared to be a good choice for blending with the primary coking coal, DECS 30.

Figure 15 is a picture of the carbon product of the blend (5% wt DECS 34 with 95% wt DECS 30) obtained without sulfur (holding time 15 minutes at 550°C, final temperature 700°C for 1 hour). The carbon product took the shape of the glass tube. Physically, it appeared to be a swollen mass with some visible porosity. It broke easily when pressure was applied.

SEM micrographs of the carbon product pictured in figure 15 are shown in figure 16. It can be seen that the carbon product passed through a swelling phase and produced a smooth mass with some porosity after consolidation.



Figure 15: A picture of the carbon product obtained when the coal blend (5% DECS 34 and 95% DECS 30) was heated to 550°C and held at this temperature for 15 minutes. The temperature was then raised slowly to 700°C and held at this temperature for 1 hour.

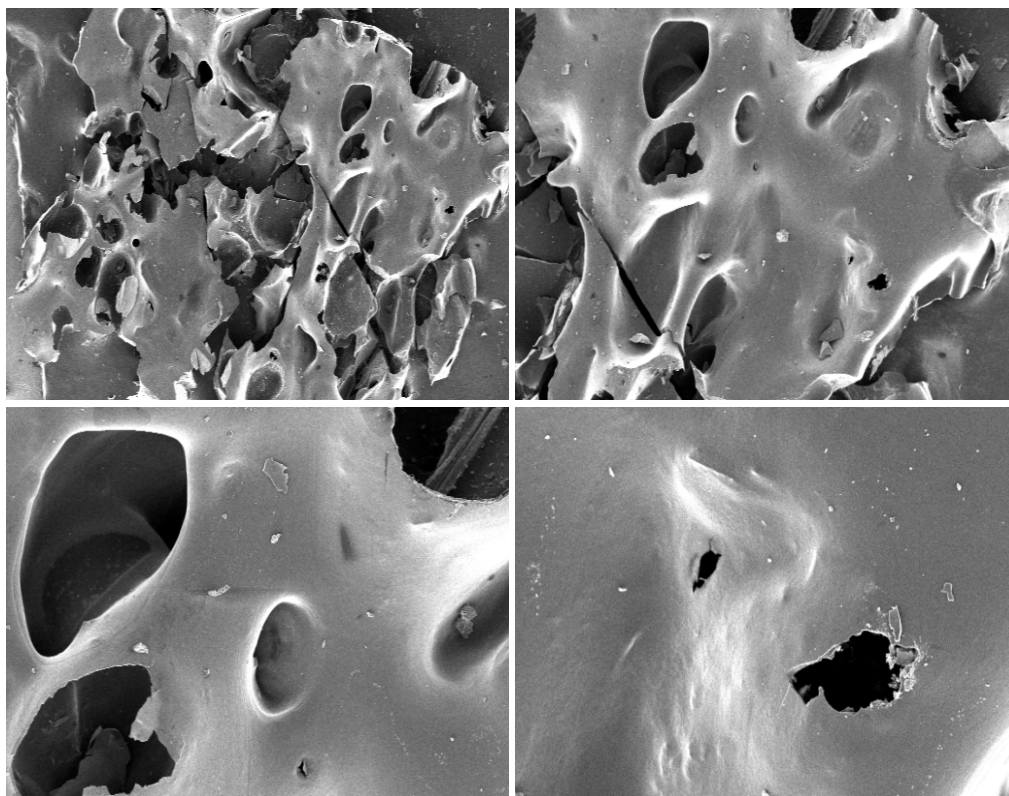


Figure 16: SEM micrographs of the carbon product pictured in figure 15.

Figure 17 is a picture of the carbon product of the blend (5% wt DECS 34 and 95% wt DECS 30) obtained during sulfur dehydrogenation (holding time of 15 minutes at 550°C, final temperature 700°C for 1 hour, sulfur dehydrogenation commenced at start of this second heating ramp and continued until the reaction was complete).

The carbon product took the shape of the glass tube. Physically, it appeared to be hard with some visible porosity. SEM micrographs of this carbon product are shown in figures 18 and 19 (bottom row). In figure 19, SEM micrographs of the carbon product produced from the blend (bottom row) are compared with those produced from coal DECS 34 (middle row, right) and DECS 30 (top, right) during sulfur dehydrogenation under the same conditions. The carbon material produced from the blend resembles the carbon produced when DECS 30 was heated without sulfur under the same conditions.



Figure 17: A picture of the carbon product obtained when the coal blend (5% DECS 34 and 95% DECS 30) was heated to 550°C and held at this temperature for 15 minutes. The temperature was then raised slowly to 700°C and held at this temperature for 1 hour. Sulfur dehydrogenation commenced at the start of this second heating ramp and continued until the reaction was completed.

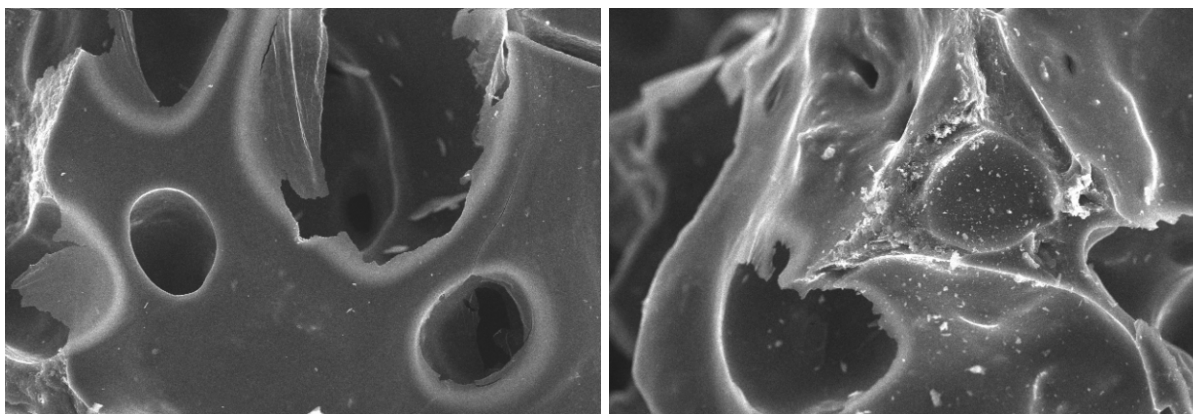


Figure 18: SEM micrographs of the carbon product pictured in figure 17.

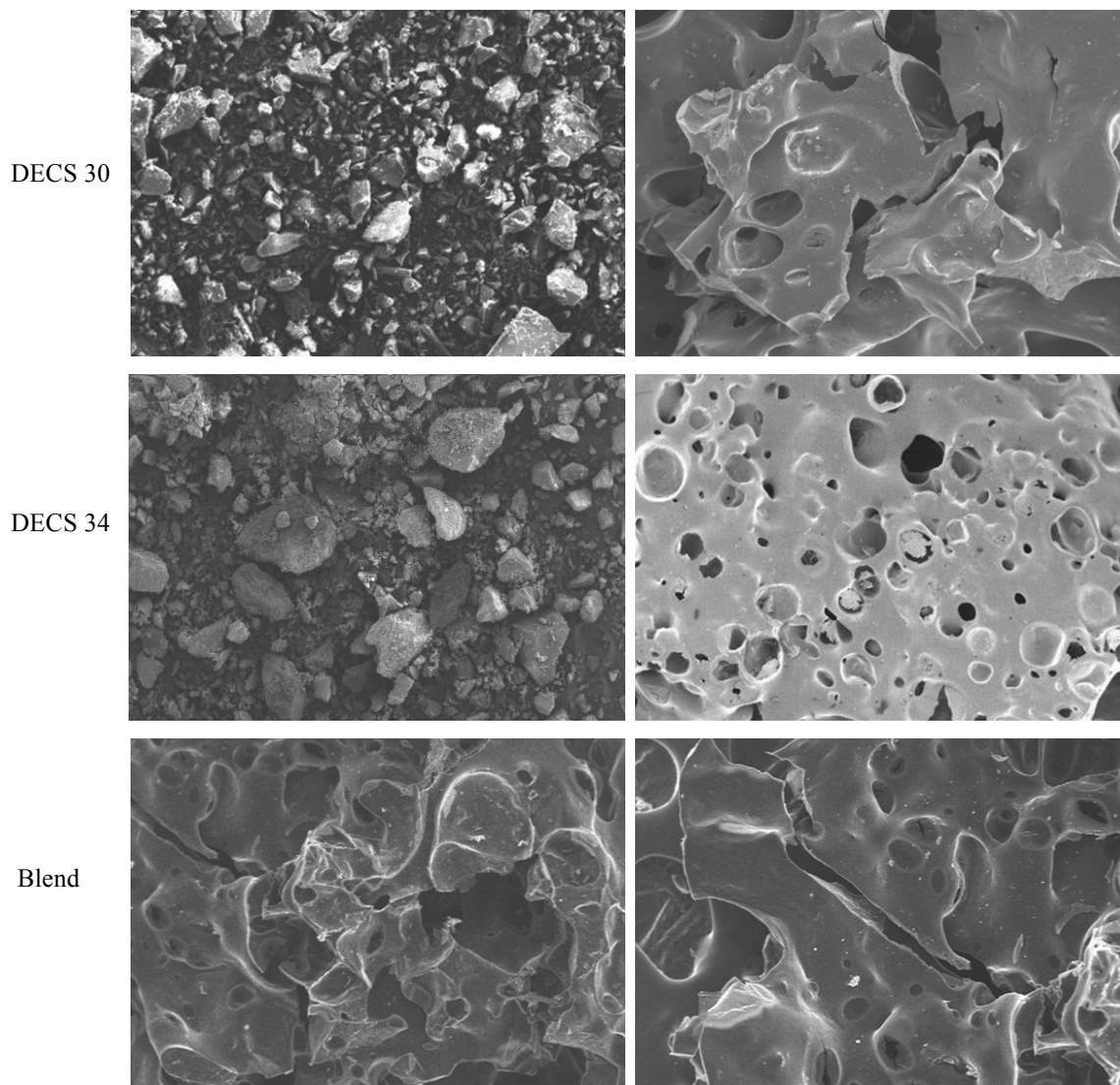


Figure 19: SEM micrographs of the carbon product pictured in figure 17 (bottom row) compared with those produced from DECS 34 (the middle row, right) and DECS 30 (top, right) under the same conditions.

Figure 20 shows a picture of the carbon product obtained from the same blend using the same temperature program as the experiment above. The only difference was that the holding time at the final temperature of 700°C was prolonged to 6 hours, instead of the 1 hour holding time used in the previous experiment. Physically, the carbon appeared to be a swollen, dull mass. It proved to be a brittle material that broke when pressure was applied. SEM micrographs of the carbon product pictured in figure 20 are shown in figure 21. It can be seen that the carbon product passed through a “melting” stage and after consolidation a highly swollen, porous carbon product was produced. Closer characterization of the carbon product (figure 22) shows that only few pores were open and many contained some debris. Most of the pores were closed or had not developed.



Figure 20: A picture of the carbon product obtained when coal (5 % wt DECS 34 blend with 95% wt DECS 30) was heated to 550°C in the absence of sulfur and held at this temperature for 15 minutes. The temperature was then raised slowly to 700°C and held at this temperature for 6 hours. Sulfur dehydrogenation commenced at the start of this second heating ramp and continued until the reaction was complete.

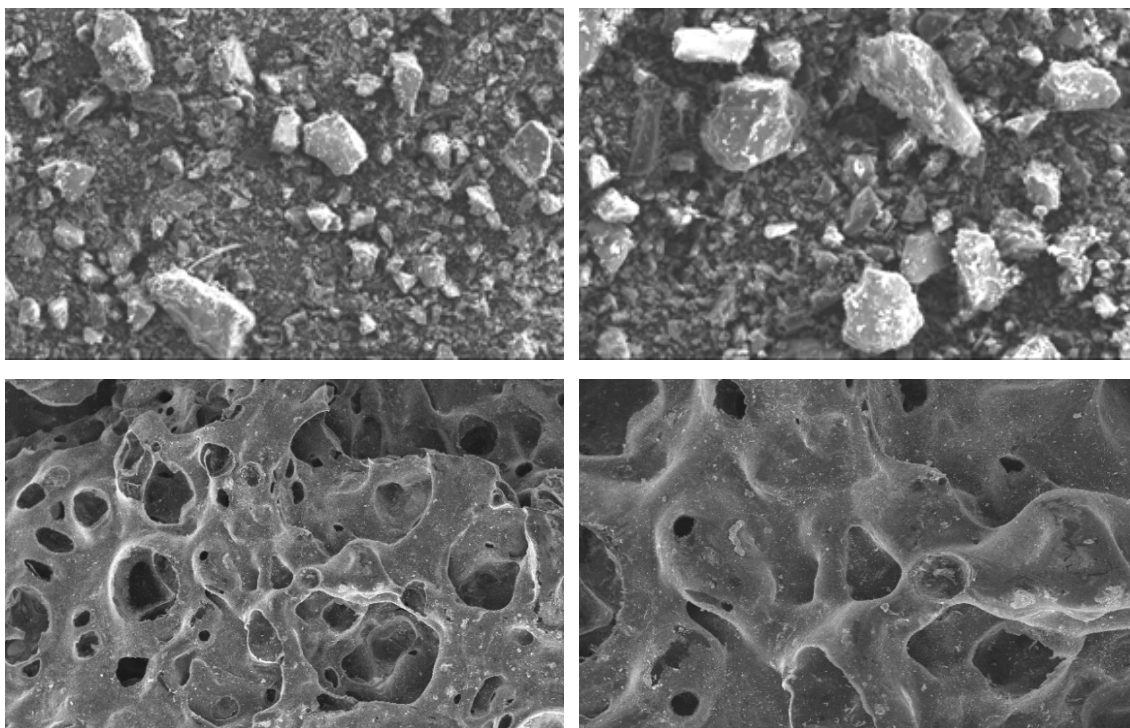


Figure 21: SEM micrographs of the carbon product shown in figures 20.

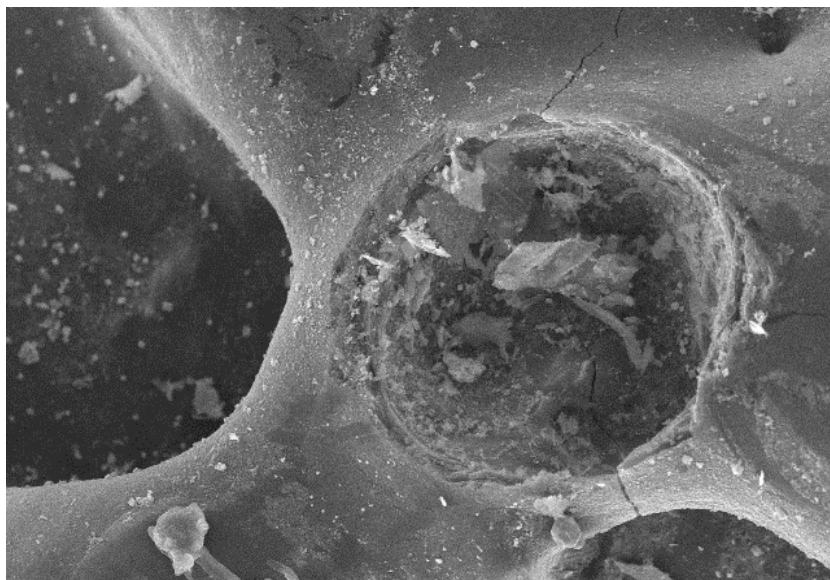


Figure 22: SEM micrographs of the carbon product shown in figures 20 and 21.

For comparison purposes, SEM micrographs of the carbon product produced from coal DECS 30 under the same conditions as the blend are shown in figure 23. It can be seen that the carbon product passed through a liquid stage and after consolidation, dense smooth structures with a few pores developed.

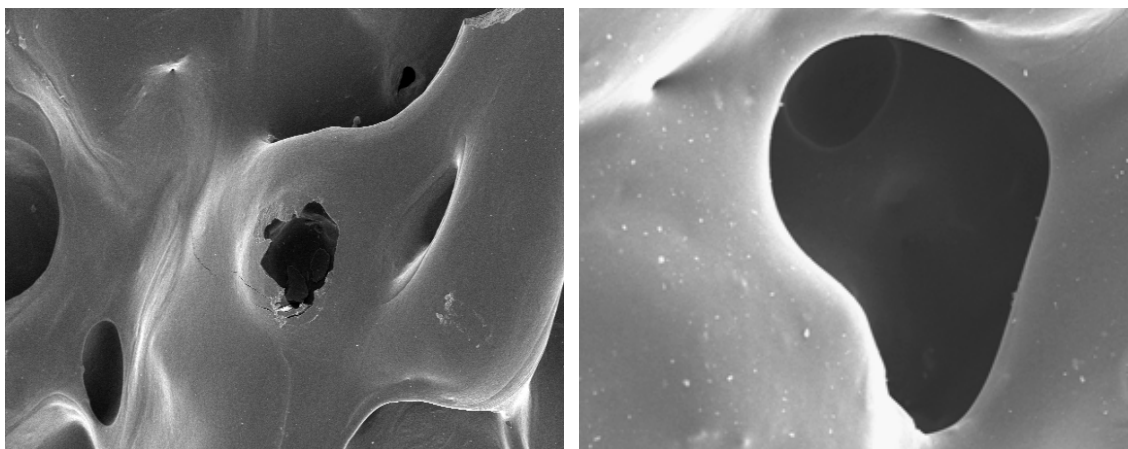


Figure 23: The carbon product produced from coal DECS 30 under the same conditions as the carbon product from the blend pictured in figures 20-22.

Table 4: Proximate analysis of carbon products obtained from coal DECS 30, DECS 34 and their blend (5 % wt DECS 34/95 % wt DECS 30), using the same temperature program.

Sample	Volatile Mater % dry	Fixed Carbon % dry	Sulfur % dry
Original coal DECS 30	30.2	65.9	0.8
DECS 30 alone Ramp to 550°C held for 15 min. Final temperature 700°C, held 1h.	11.2	82.3	0.7
DECS 30 after S dehydrogenation. Ramp to 550°C held for 15 min. Final temp 700°C held for 1 h.	10.1	84.3	0.6
Original coal DECS 34	38.4	54.3	1.6
DECS 34 alone. Ramp to 550°C held for 15 min. Final temp 700°C held for 1 h.	16.7	77.0	1.4
DECS 34 after S dehydrogenation. Ramp to 550°C held for 15 min. Final temp 700°C held for 1 h.	16.0	79.6	2.1
Coal blend (5% wt DECS 34 and 95% wt DECS 30) alone Ramp to 550°C held for 15 min. Final temp 700°C held for 1 h.	14.6	80.7	1.0
Coal blend (5% wt DECS 34 and 95% wt DECS 30) after S dehydrogenation Ramp to 550°C held for 15 min. Final temp 700°C held for 1 h.	11.7	82.6	2.9

In Table 4, a proximate analysis of the carbon products obtained from coal DECS 34 alone and in blends with coal DECS 30 is compared with that from coal DECS 30 alone. The carbon material produced from the blend by sulfur dehydrogenation resembles the carbon produced when DECS 30 was heated without sulfur under the same conditions, except for its high sulfur content. The proximate analysis of the carbon products obtained when DECS 34 coal was heated with or without sulfur under the same condition is also very similar, with the volatile matter being 16.0 and 16.7%, respectively. The fixed carbon value for the product obtained by sulfur dehydrogenation is slightly higher, 79.6 %, than when the coal is heated in the absence of sulfur (77%). The proximate analysis of the carbon product obtained from the blend after sulfur dehydrogenation has a higher fixed carbon value (82.6%), volatile matter content (11.7%) and very high sulfur content 2.9 %. The carbon material produced from its 5% wt blend with primary coking coal DECS 30 did not improve the properties of the carbon product. The fixed carbon value is lower and volatile matter content higher than the carbon product produced during sulfur dehydrogenation of the DECS 30 coal alone under the same conditions.



Figure 24: A picture of the carbon product obtained when a coal blend (20% by wt DECS 34, 80% by wt DECS 30) was heated to 550°C in the absence of sulfur, and held at this temperature for 15 minutes. The temperature was then raised slowly to 700°C and held at this temperature for 1 hour. Sulfur dehydrogenation commenced at the start of this second heating ramp and continued until the reaction was complete.

In another experiment on coal blends, the amount of coal DECS 34 was increased to 20% by weight in blend with DECS 30 coal. The carbon product was very brittle and thin as shown in figure 24. Because of its poor mechanical properties, this carbon was not characterized any further. It appears that in spite of its excellent fluidity properties, DECS 34 is not a good choice for blending experiments.

Sample DECS 36

Coal DECS 36, classified as a hvb A bituminous coal, is actually a blend of four hvb A bituminous coals. This blend has an exceptionally high fluidity and free swelling index,

Figure 25 shows a picture of the carbon product obtained when sample DECS 36 alone (in the absence of sulfur) was heated as described in the experimental section (holding time 15 minutes at 550°C, final temperature 700°C for 1 hour). Physically, it appeared to be a swollen, shiny mass. It was easy to remove from the glass tube. SEM micrographs of the carbon product pictured in figure 25 and the original coal DECS 36 are compared in figure 26. It can be seen that the carbon product passed through a liquid stage and after consolidation a smooth structure with very few pores was developed. Closer characterization of the carbon product (figure 27) shows a smooth structure with underdeveloped pores.



Figure 25: A picture of the carbon product obtained when coal DECS 36 alone was heated to 550°C and held at this temperature for 15 minutes. The temperature was then raised slowly to 700°C and held at this temperature for 1 hour.

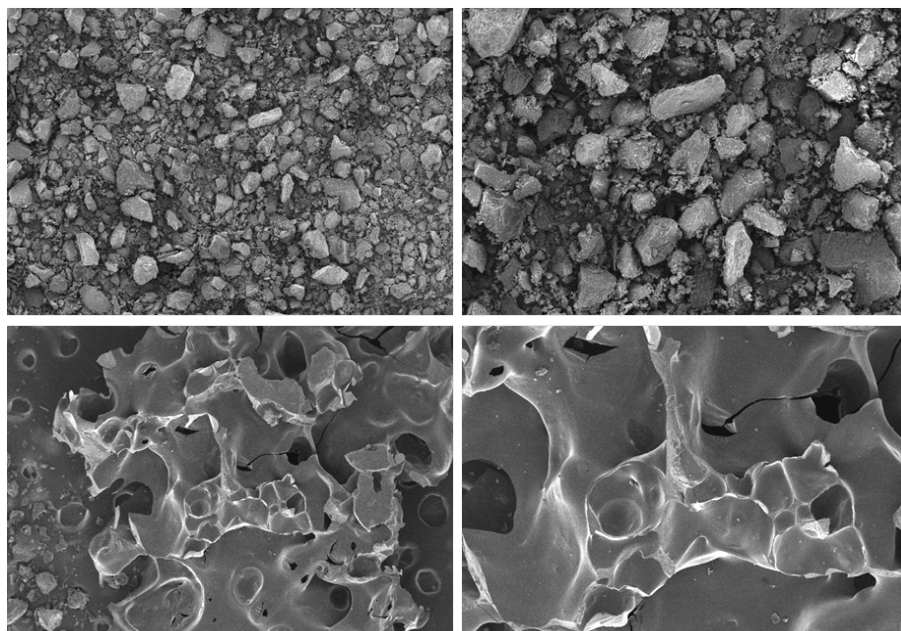


Figure 26: SEM micrographs of the carbon product shown in figures 25

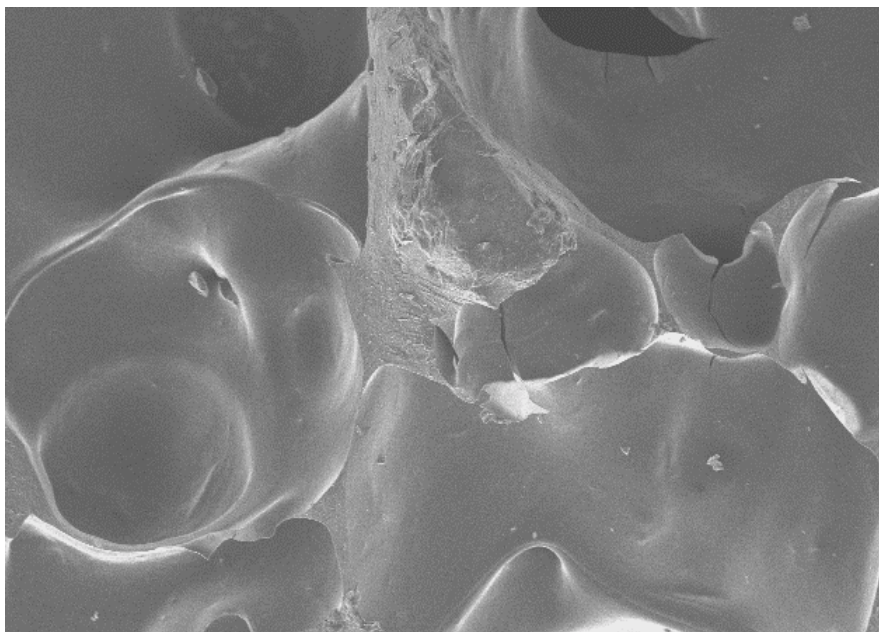


Figure 27: SEM micrographs of the carbon product shown in figures 25 and 26.



Figure 28: A picture of the carbon product obtained when coal DECS 36 was heated to 550°C in the absence of sulfur and held at this temperature for 15 minutes. The temperature was then raised slowly to 700°C and held at this temperature for 1 hour. The sulfur vapor started to sweep through the coal bed after the 550°C ramp was over and continued until the reaction was complete.

Figure 28 is a picture of the carbon product obtained when coal DECS 36 was heated to 550°C in the absence of sulfur and held at this temperature for 15 minutes. The temperature was then raised slowly to 700°C and held at this temperature for 1 hour. The sulfur vapor started to sweep through the coal bed after the 550°C ramp was over and continued until the reaction was

complete. The carbon product was hard and very shiny. SEM micrographs of the carbon product pictured in figure 28 and the original coal are shown in figure 29. It can be seen that the carbon product passed through a thermal swelling stage, and after consolidation a swollen carbon product, with some pores, was produced. A closer examination of the carbon product (figures 30 and 31) shows that the walls of the pores are very thin and some of them are only partially open.

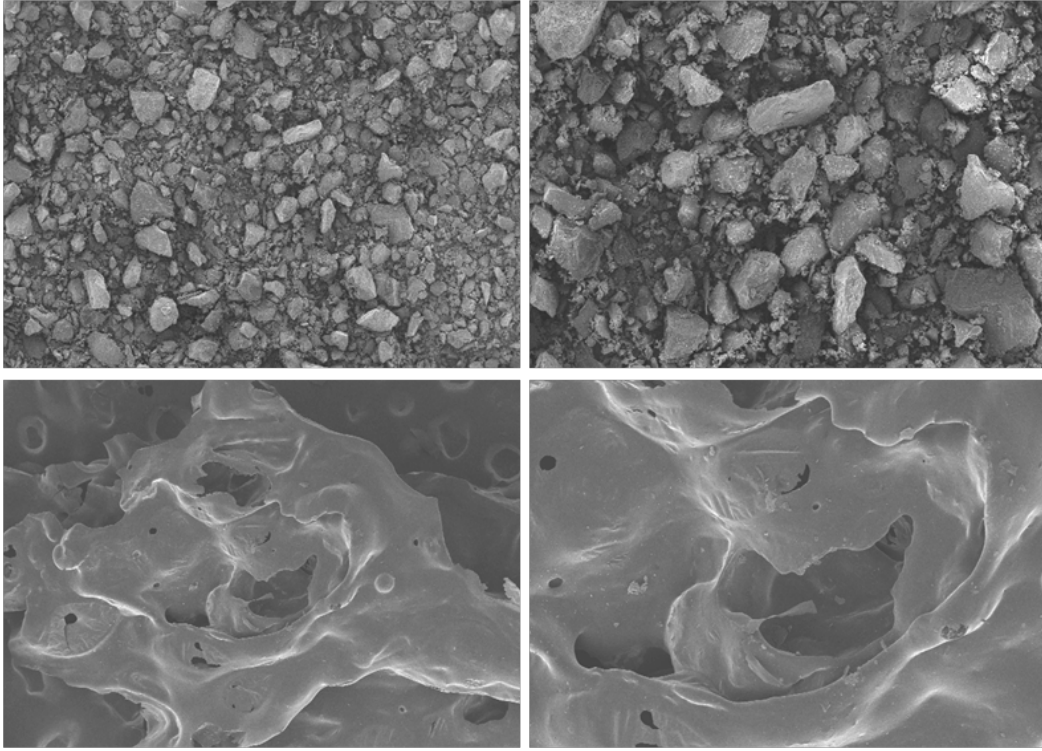


Figure 29: SEM micrographs of the original DECS 36 coal (top) and the carbon product (bottom) pictured in figure 28.

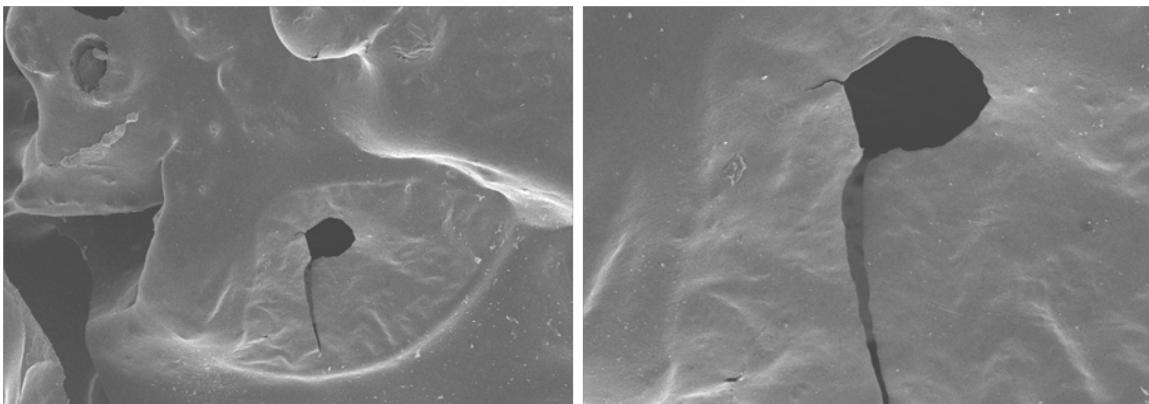


Figure 30: SEM micrographs of the carbon product pictured in figures 28 and 29.

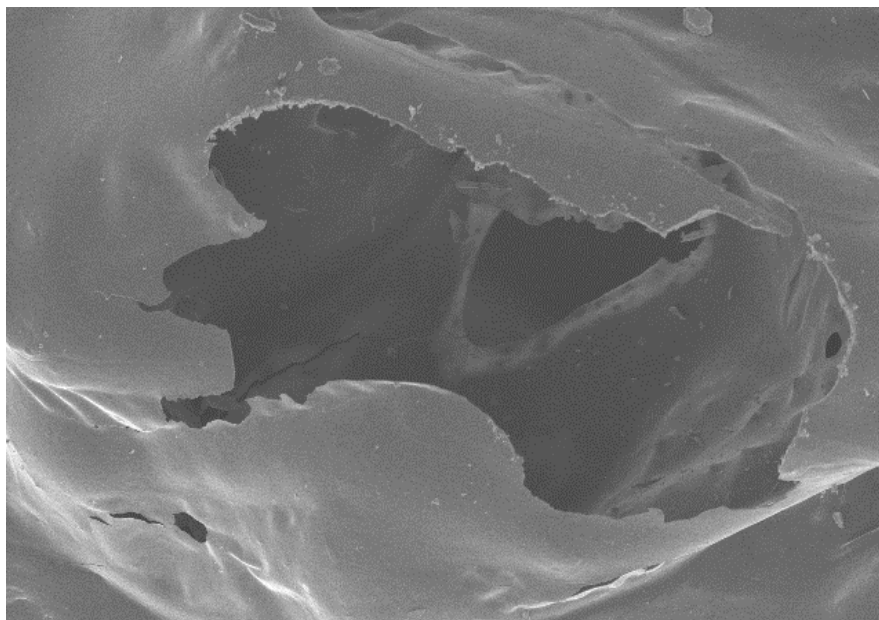


Figure 31: SEM micrographs of the carbon product pictured in figures 28-30.

Table 5: Proximate analysis of carbon products obtained from sample DECS 36.

Sample	Volatile Matter % dry	Fixed Carbon % dry	Sulfur % dry
Original coal DECS 36	34.5	58.9	1.1
DECS 36 alone Ramp to 550 °C, held for 15 min. Final temp 700 °C, held 1 h.	18.9	72.3	1.0
DECS 36 after S dehydrogenation Ramp to 550 °C, held for 15 min. Final temp 700 °C, held 1 h.	13.3	74.9	3.5

In Table 5, a proximate analysis of carbon products obtained when coal DECS 36 was heated with and without sulfur are summarized and compared with those from the original DECS 36 coal. The proximate analysis for the carbon product of sulfur dehydrogenation revealed a fixed carbon value of 74.9%, volatile matter of 13.3%% and total sulfur of 3.5%. A proximate analysis

of the carbon product obtained when coal is heated in the absence of sulfur revealed a fixed carbon value of 72.3%, volatile matter of 18.9% and total sulfur of 1.0%. For comparison, metallurgical coke has a fixed carbon value in the range 80-90% and volatile matter between 1-5%, and sulfur ~ 0.5%.

Changing the temperature program

We performed one experiment using the modified temperature program described in the experimental section. The holding time at 550°C was extended from 15 minutes (as used in previous experiments) to 120 minutes. The carbon product obtained in this study is shown in figure 32. The material was swollen, very brittle and had some porosity. SEM micrographs of the carbon product pictured in figure 32 and the original DECS 30 coal are compared in figure 33. It can be seen that the coal passed through a thermal “melting” stage and after consolidation, a swollen, porous carbon product was produced. Closer characterization of the carbon product (figure 34) shows that only a few pores were open and these have rather thin walls. Other pores contained some debris, though many of the pores were closed or undeveloped.



Figure 32: A picture of the carbon product obtained when coal DECS 30 was heated to 550°C in the absence of sulfur and held at this temperature for 120 minutes. The temperature was then raised slowly to 700°C and held at this temperature for 1 hour. The sulfur vapor started to sweep through the coal bed after 550°C ramp is over and continued until the reaction was complete.

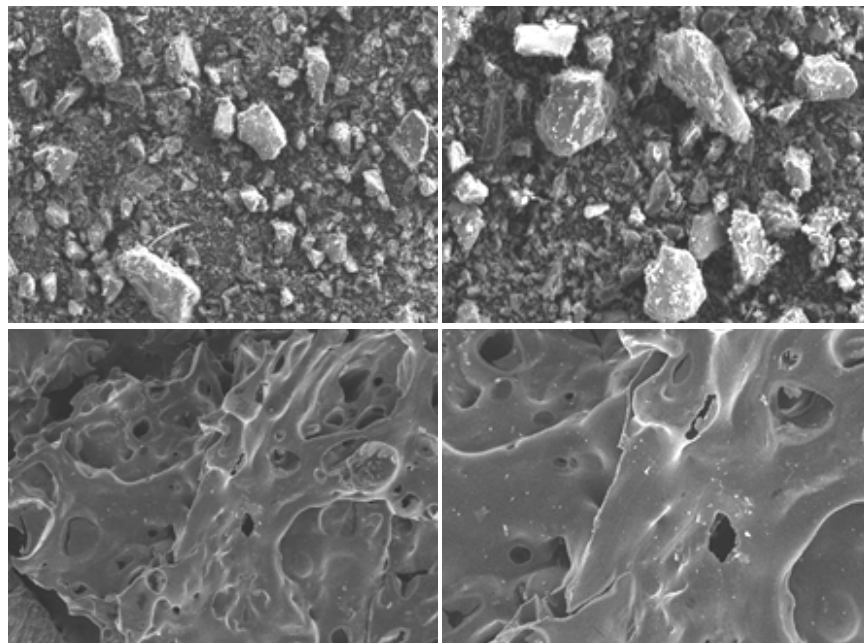


Figure 33: SEM micrographs of the original coal DECS 30 (top) and the carbon product (bottom) pictured in figure 32.

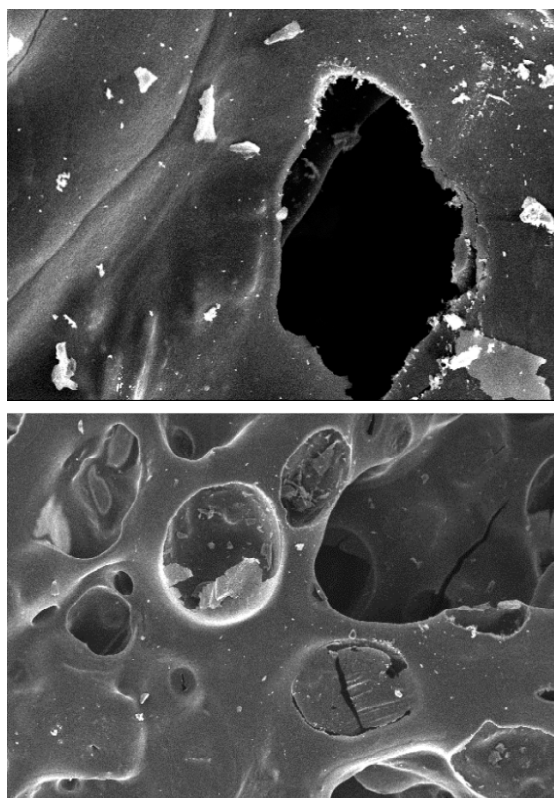


Figure 34: SEM micrographs of the carbon product shown in figures 32 and 33.

For comparison purposes, in figure 35 the carbon product obtained from the same coal (DECS 30) dehydrogenated using a similar temperature program, but with only 15 minutes holding time at 550°C temperature, is shown. SEM micrographs of this carbon product are presented in figure 36. The carbon product was solid, very hard, shiny, and the majority of the pores were open and had thick walls.



Figure 35: A picture of the carbon product obtained when coal DECS 30 alone was heated to 550°C in the absence of sulfur and held at this temperature for 15 minutes. The temperature was then raised slowly to 700°C and held at this temperature for 1 hour. The sulfur vapor started to sweep through the coal bed after 550°C ramp is over and continued until the reaction was complete.

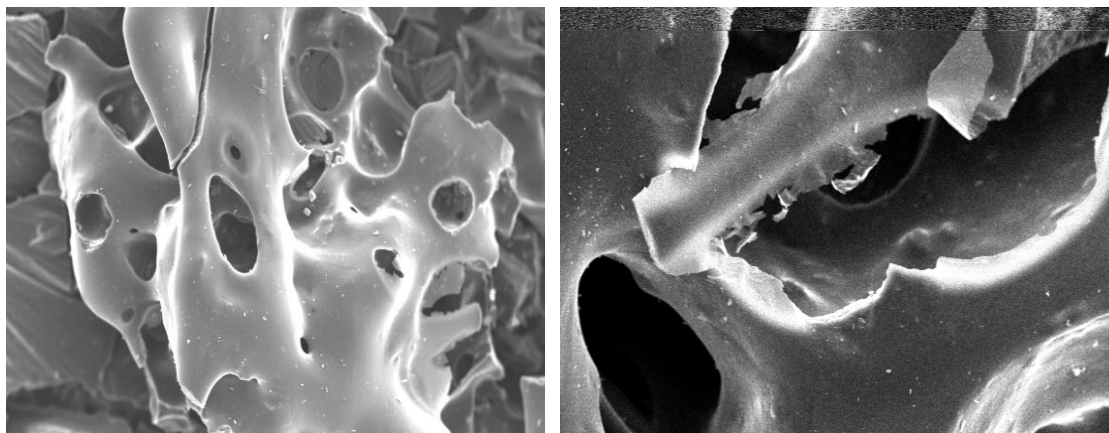


Figure 36: SEM micrographs of the carbon product shown in figure 35.

A modified temperature program did not improve the quality of the carbon product. The material was more brittle than those obtained with shorter holding times at 550°C.

Changing the design of the ovens

Figure 37 shows a picture of the carbon product obtained during the first of two experiments in the modified oven. The coal sample was loaded into the narrower 2.5 cm diameter glass tube while sulfur was placed in the second oven in a glass tube of diameter 5 cm. Physically, the carbon appeared to be swollen and shiny. It also proved to be brittle and broke easily into pieces during removal from the oven.



Figure 37: A picture of the carbon product obtained when the DECS 30 coal was loaded into the narrower 2.5 cm diameter glass tube and heated to 550°C in the absence of sulfur and held at this temperature for 15 minutes. The temperature was then raised slowly to 700°C and held at this temperature for 1 hour. The sulfur vapor started to sweep through the coal bed after the 550°C ramp was over and continued until the reaction was complete.

SEM micrographs of the carbon product pictured in figure 37 and the original DECS 30 coal are compared in figure 38. It can be seen that the carbon product passed through a liquid stage and after consolidation a highly swollen carbon product with some pores was produced. Closer examination of the carbon product (figure 39) shows that although the carbon mass looks to be highly swollen, there are only a few open pores. Some of these pores had smooth edges, but the walls were very thin. Many pores were closed and some had not developed.

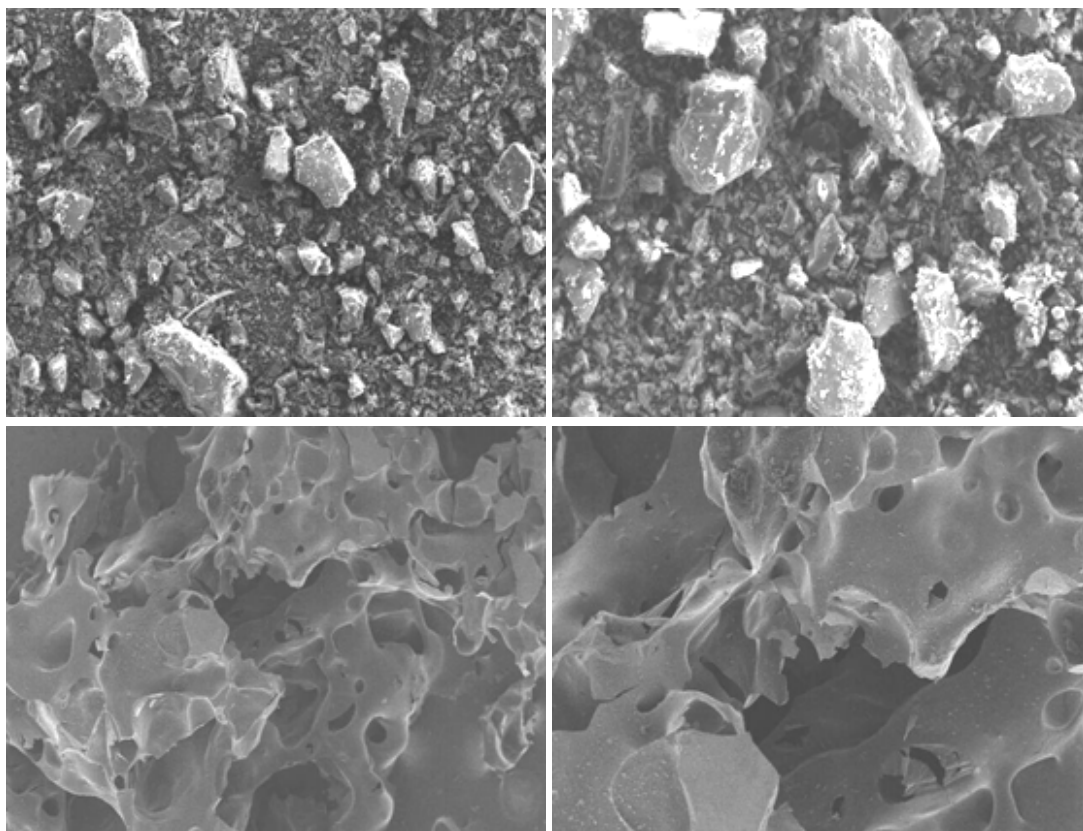


Figure 38: SEM micrographs of the original DECS 30 coal (top) and the carbon product (bottom) pictured in figure 37.

Figure 40 shows a picture of the carbon product obtained from the second experiment from this series. This time the coal sample was placed into a glass tube with a diameter of 5 cm, but the sulfur was loaded into the glass tube with a diameter of 2.5 cm. Physically the carbon took the shape of glass tube, but the product was dull with a coarse surface. After removing from the oven, the carbon broke into pieces very easily with little applied pressure.

SEM micrographs of this carbon product pictured in figure 40 and DECS 30 coal are compared in figure 41. It can be seen that the carbon product passed through a liquid state and after consolidation a swollen, carbon product with some porosity was produced. The edges of some of pores were very shaggy. Closer examination of the carbon product (figure 42) shows that very few pores were open and many contained some debris. Most of the pores were closed or had not developed.

In order to compare results, figure 35 (page 36) shows the carbon product obtained from the same coal (DECS 30) under the same temperature program, but from an experiment where the glass tubes containing the coal and sulfur had the same dimensions (diameter 5 cm). The carbon was very hard, smooth and shiny. In figure 36, SEM micrographs of this carbon product are presented. The majority of pores were open with thick walls.

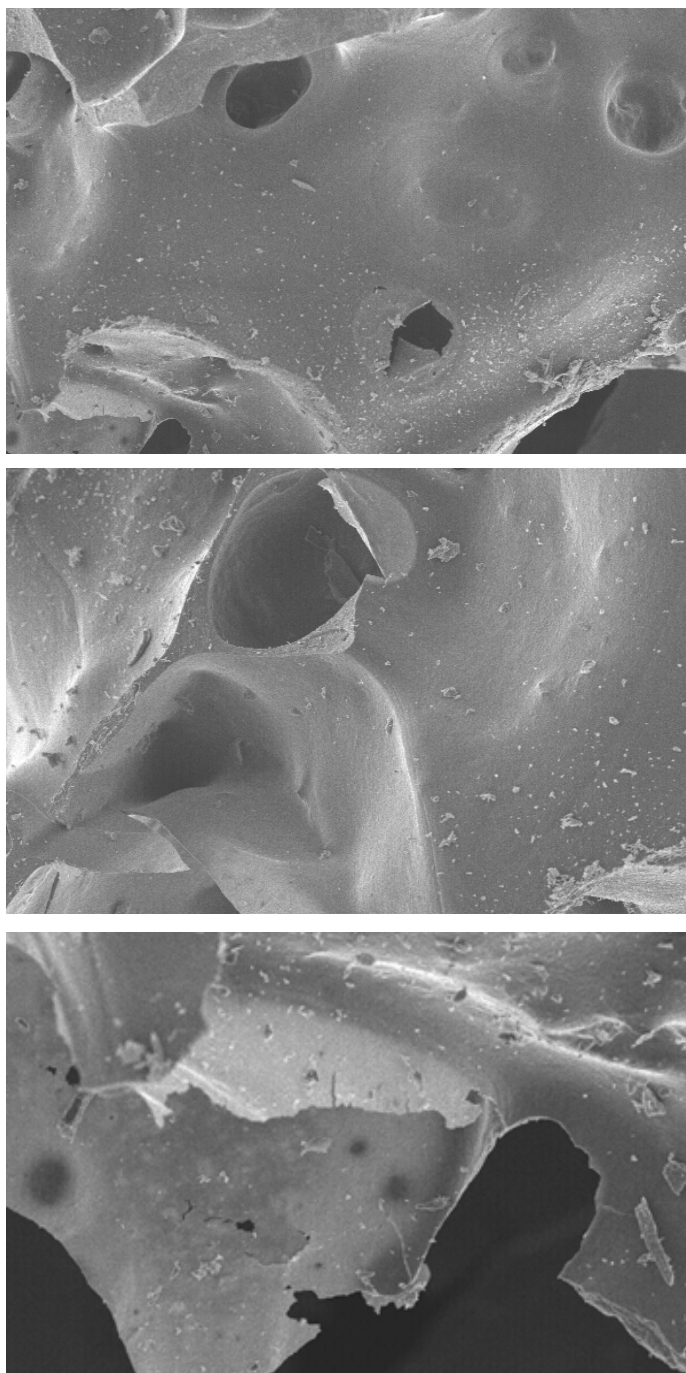


Figure 39: SEM micrographs of the carbon product shown in figures 37 and 38.



Figure 40: A picture of the carbon product obtained during the second experiment when coal DECS 30 was heated to 550°C in the absence of sulfur and held at this temperature for 15 minutes. The temperature was then raised slowly to 700°C and held at this temperature for 1 hour. The sulfur vapor started to sweep through the coal bed after the 550°C ramp was over and continued until the reaction was complete. The sulfur was loaded into the glass tube with a smaller (2.5 cm) diameter.

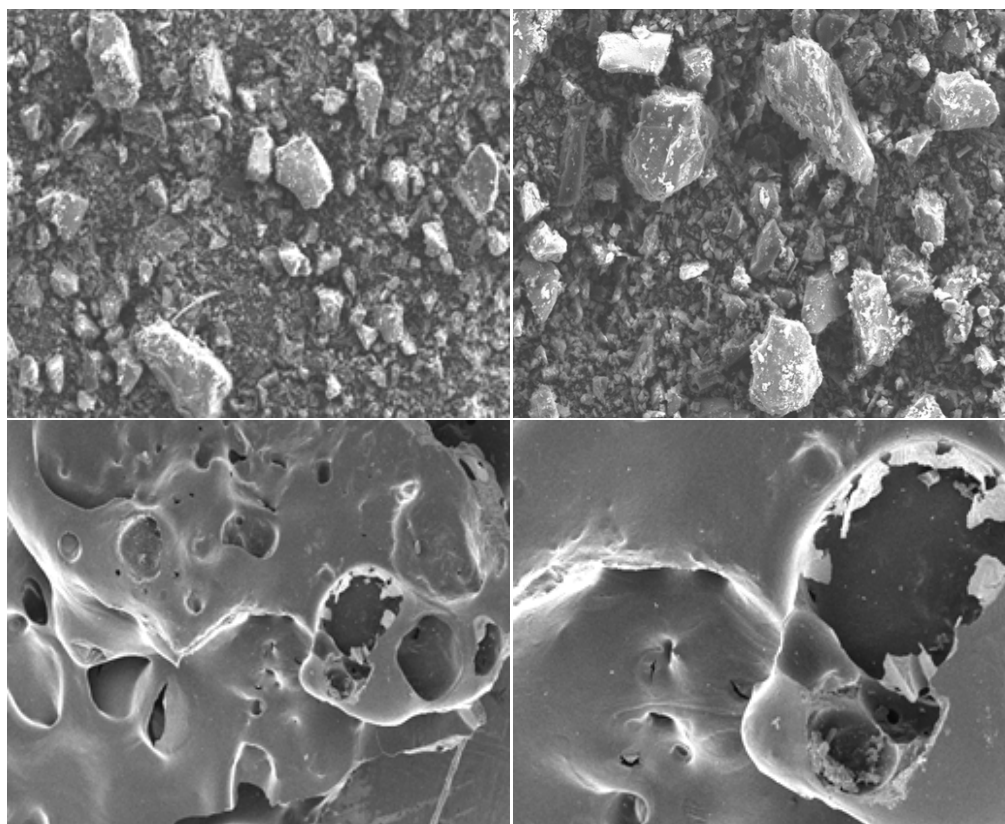


Figure 41: SEM micrographs of the original DECS 30 coal (top) and carbon product (bottom) pictured in figure 40.

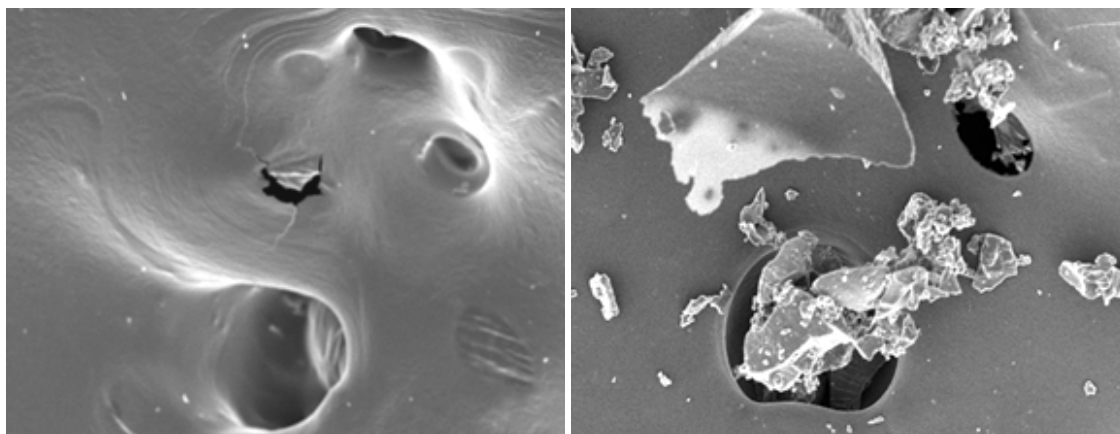


Figure 42: Additional SEM micrographs of the carbon product shown in figures 40 and 41.

The results of a proximate analysis of the carbon products obtained using the modified reactor tubes are presented in Table 5, where they are compared to those obtained in the ovens where both glass tube had the same diameter ($D = 5$ cm). The original coal has a fixed carbon content of 65.9%, a volatile matter content of 30.0% and 0.8% total sulfur, all on a dry basis. The carbon materials produced in the modified ovens had fixed carbon contents between 80.1 and 83.2%.. The content of volatile matter was 11.5% and 12.8 %, and the sulfur content 0.8% and 1.1 %. For carbon material produced in the ovens having the glass tubes of the same diameters (0.5cm) the values were 84.3%, 10.3% and 0.6%, respectively.

Although interesting carbons were produced, oven modifications did not result in the production of metallurgical coke.

Table 4: Proximate analysis of carbon products obtained when coal is heated to 550°C for 15 min and kept constant at this temperature for 15 min, then heated to a final temperature of 700°C and held there for 1 hour.

Sample	Volatile Matter % dry	Fixed Carbon % dry	Total Sulfur % dry
Original coal DECS 30	30.0	65.9	0.8
Same glass tubes in both ovens ($D=5$ cm)	10.3	84.3	0.6
Experiment #1 Coal placed into the narrower tube ($D=2.5$ cm)	11.5	83.2	0.8
Experiment #2 Sulfur placed into the narrower tube ($D=2.5$ cm)	12.8	80.1	1.1

Conclusions

The carbon produced by sulfur dehydrogenation of the mvb bituminous coal DECS 13 had a fixed carbon value of 84.9 %, volatile matter of 8.0 % and total sulfur of 0.7%. The process resulted in a coke like material in appearance. It was very hard, shiny with visible porosity. It was the hardest coke-like material we have obtained by the sulfur dehydrogenation procedure. However, the volatile matter and sulfur contents are too high for use as metallurgical coke. It is possible that prolonging the holding time at the final temperature of 700°C could lower these values.

The carbon produced from another mvb bituminous coal, DECS 30, under the same conditions resulted in a material with a fixed carbon content of 84.3%, volatile matter 9.8%, and sulfur content 0.6%. When the holding temperature at final temperature of 700°C was prolonged to 6 hours, values were slightly lower 84.7%, 8.0% and 0.5 %, respectively. The volatile matter and sulfur contents are still too high for use of this material as metallurgical coke. Metallurgical coke has a fixed carbon value in the range 80-90%, volatile matter between 1-5%, and a sulfur content of about 0.5%. Experiments using a modified temperature program as well as a modified ovens design were also performed, but did not improve the characteristics of the carbon products.

Good quality coke can be produced from coal blends, where primary coking coals are blended with non-coking coals. The non-coking DECS 34, hvb A coal has a swelling index identical to coking coal DECS 30 and an excellent fluidity index and would therefore seem to be a good choice to be used in blends. However, the carbon material produced from a 5% wt blend with the primary coking coal DECS 30 did not improve the properties of the carbon product. The fixed carbon value was lower, the volatile matter content higher, and the content of sulfur much higher than carbon product produced during sulfur dehydrogenation of DECS 30 alone under the same conditions. It appears that in spite of its excellent fluidity, DECS 34 is not a good choice for blending experiments.

Sample DECS 36 is classified as a hvb A bituminous coal, but is actually a blend of four hvb A bituminous coal. This blend has exceptionally high fluidity and a free swelling index higher than the mvb bituminous coals DECS 30 and DECS 13 used in most of the work reported here. However, this coal blend does not produce a good coke during sulfur dehydrogenation. The proximate analysis for the carbon product of sulfur dehydrogenation of coal DECS 36 revealed a fixed carbon value of 74.9%, volatile matter of 13.3% and a very high sulfur content of 3.5%. The very high sulfur content in the carbon products from hvb A coals (or their 5% blends) is probably due to their chemical structure. This type of coal contains some functional groups, which allow sulfur to react and bind to the carbon.

References

1. Jusino, A.; Schobert, H.H. 2006. Hydrogen from coal: A sulfur based approach: *International Journal of Coal Geology*, 65, 223-234.
2. Painter, P.C., Sobkowiak, M., Schobert, H. H., Premium carbon products from Coal: A sulfur approach. Final report 3/1/08–8/31/09 DOE Award Number: Subcontract 3552-TPSU-DOE-1874 under DOE Prime DE-FC26-03NT41874.
3. Painter, P.C., Sobkowiak, M., Schobert, H. H., The Production and Characterization of Metallurgical Coke Produced from Coal Using a Sulfur Dehydrogenation Process. Quarterly Report 3/1/09–5/31/09 DOE Award Number: Subcontract 3788-TPSU - DOE-1874 under DOE Prime DE-FC26-03NT41874.
4. Painter, P.C., Sobkowiak, M., Schobert, H. H., The Production and Characterization of Metallurgical Coke Produced from Coal Using a Sulfur Dehydrogenation Process. Quarterly Report 6/1/09–8/31/09 DOE Award Number: Subcontract 3188-TPSU - DOE-3788 under DOE Prime DE-FC26-03NT41874.
5. Painter, P.C., Sobkowiak, M., Schobert, H. H., The Production and Characterization of Metallurgical Coke Produced from Coal Using a Sulfur Dehydrogenation Process. Quarterly Report 9/1/09–11/30/09 DOE Award Number: Subcontract 3188-TPSU - DOE-3788 under DOE Prime DE-FC26-03NT41874.
6. Painter, P.C., Sobkowiak, M., Schobert, H. H., The Production and Characterization of Metallurgical Coke Produced from Coal Using a Sulfur Dehydrogenation Process. Quarterly Report 12/1/09–2/28/10 DOE Award Number: Subcontract 3188-TPSU - DOE-3788 under DOE Prime DE-FC26-03NT41874.
7. Painter, P.C., Sobkowiak, M., Schobert, H. H., The Production and Characterization of Metallurgical Coke Produced from Coal Using a Sulfur Dehydrogenation Process. Quarterly Report 3/1/10–5/31/10 DOE Award Number: Subcontract 3188-TPSU - DOE-3788 under DOE Prime DE-FC26-03NT41874.
8. Marsh, H., Menendez, R., Mechanisms of Formation of Isotropic and Anisotropic Carbons, Chapter 2, pp.37-73, Crelling, J.C., The Nature of Coal, Chapter 8, pp.259-284, Gray, R.J., Coal to Coke Conversion, Chapter 9, pp.285-320 In: *Introduction to Carbon Science* (Marsh, H., Ed.) Butterworth's: London; 1989.

**Development of Carbon-based “Molecular Basket”
Sorbent for CO₂ Capture from Flue Gas**

DOE Award Number: DE-FC26-03NT41874
Subcontract Number: 3789-TPSU-DOE-1874

FINAL TECHNICAL REPORT

Reporting Period

March 1, 2009 to June 31, 2010

Dongxiang Wang, Cigdem Shalaby, Eric Fillerup,
Xiaoliang Ma (PI)*, and Chunshan Song (co-PI)

Clean Fuels and Catalysis Program, EMS Energy Institute
and Department of Energy & Mineral Engineering
The Pennsylvania State University
University Park, 209 Academic Projects Building, PA 16802
*E-mail: mxx2@psu.edu/Tel: 814-863-8744/Fax: 814-863-7432

July 2010

DISCLAIMER

This report was prepared as an account of work sponsored by an agency of the United States Government. Neither the United States Government nor any agency thereof, or any of their employees, makes any warranty, expressed or implied, or assumes any legal liability or responsibility for the accuracy, completeness, or usefulness of any information, apparatus, product, or process disclosed, or represents that its use would not infringe privately owned rights. Reference herein to any specific commercial product, process, or service by trade name, trademark, manufacturer, or otherwise does not necessarily constitute or imply its endorsement, recommendation, or favoring by the United States Government or any agency thereof. The views and opinions of authors expressed herein do not necessarily state or reflect those of the United States Government or any agency thereof.

ABSTRACT

The objective of the present study was to develop a new type of inexpensive MBS by using carbon-based porous materials, instead of expensive mesoporous molecular sieves for CO₂ capture from flue gas. Our approach in this project included: 1) screening the commercial carbon-based materials for preparation of the high performance carbon-based molecular basket sorbent (CB-MBS); 2) examining the effects of properties of carbon supports, including surface oxygen-containing functional groups and pore structure of the carbon supports on the CO₂ sorption performance of CB-MBS; 3) modifying the commercial activated carbons by steam activation to tailor their pore structures for improving the CO₂ sorption performance of the prepared CB-MB; 4) examining the regenerability of the CB-MBS; and 5) estimating and comparing the preparation cost of CB-MBS. All tasks and milestones proposed for this project have been completed according to the schedule.

On the basis of the results of this project, the following conclusions can be made: 1) Some commercial carbon materials are good supports for preparation of the CB-MBS with a weight-based CO₂ sorption capacity of 135 mg-CO₂/g-sorb, which is similar to that of the second generation of MBS (MBS-2). 2) The volume-based sorption capacity of PEI(50)/C4 prepared in this study was as high as 47 mg-CO₂/ml-sorb, which is higher than that of MBS-2 by 57 %. 3) The pore volume, especially the mesopore volume, of the carbon support plays an important role in determining the CO₂ sorption performance of the CB-MBS. Many commercially available activated carbons can be modified by steam activation to increase their mesopore volume, and thus to improve the sorption performance of the prepared CB-MBS. 4) The prepared PEI(50)/C4 can be regenerated at 75 °C with more than 95% recovery of the sorption capacity after five sorption-desorption cycles. 5) The preparation cost of MBS can be substantially reduced by 90% when using a selected carbon material instead of using the silica mesopore molecular sieves, which will allow the CO₂ capture from flue gas to be conducted more cost efficiently. Due to the high CO₂ sorption capacity and low preparation cost, the carbon-based MBS could be a very promising sorbent for cost efficient CO₂ capture from flue gas.

1. Table of Contents

Disclaimer	2
Abstract	3
1. Table of Contents	4
2. List of Figures	5
3. List of Tables	6
4. Executive Summary	7
5. Introduction	8
6. Experimental	10
6.1. Carbon Samples	10
6.2. Modification of Carbon Materials	10
6.3. Preparation of Carbon-based MBS.....	11
6.4. Evaluation of Sorption-desorption Performance of Carbon-based MBS.....	12
6.5. Determination of Functional Groups on Carbon Surface	12
6.6. Characterization of Textural Structure	13
6.7. Regeneration of Carbon-based MBS	13
7. Results and Discussion	13
7.1. Screening of the Commercial Carbon-based Materials.....	13
7.2. Effect of Properties of Carbon Supports on Sorption Capacity of CB-MBS	
.....	15
7.2.1. Effect of Carbon Surface Function Groups on Sorption Capacity of	
CB-MBS	15
7.2.2. Effect of Textural Structure of Carbon Supports on Sorption	
Capacity of CB-MBS.....	17
7.3. Effect of PEI Loading on CO ₂ Sorption Capacity of CB-MBS	21
7.4. Regenerability of PEI(50)/C4.....	22
7.5. Estimation of Preparation Cost for CB-MBS	23
8. Conclusions	25
9. Project-related Publications	26
10. References Cited	26

2. List of Figures

Figure 1. TGA temperature program for evaluation of sorption-desorption performance of CB-MBS	12
Figure 2. The measured CO ₂ sorption capacity of CB-MBS in comparison with PEI(50)/MCM-41 and PEI(50)/SBA-15.....	14
Figure 3. Photo of PEI(50)/C1 sample	14
Figure 4. CO and CO ₂ evolution profiles for C3 and C3-700 samples	16
Figure 5. CO ₂ sorption capacity of PEI(50)/C3 with different treatment temperature of C3....	17
Figure 6. Comparison of CO ₂ sorption capacity of CB-MBS prepared by using steam-activated carbons under different temperature.....	18
Figure 7. Correlation between CO ₂ sorption capacity of PEI(50)/C _x and surface area of C _x ...	20
Figure 8. Correlation between CO ₂ sorption capacity of PEI(50)/C _x and pore volume of C _x ...	21
Figure 9. Pore size distribution of the parent C4 and PEI/C4 with different PEI loading	22
Figure 10. Effect of PEI loading on CO ₂ sorption capacity of PEI/C4.....	23
Figure 11. TGA curve for five sorption-desorption cycles of PEI(50)/C4 at 75 °C.....	23

3. List of Tables

Table 1. Pore properties of carbon materials used in this study	10
Table 2. Conditions for treatment of carbon samples by steam activation	11
Table 3. Product yield (wt %) of carbon samples after steam activation at different conditions	18
Table 4. Comparison of texture porosities of steam-activated AC samples and parent AC samples	19
Table 5. Textural characterization of C4 and PEI/C4 with different PEI loading	22
Table 6. The costs for preparation of CB-MBS, MBS-1 and MBS-2 in comparison with other sorbents/absorbents	24

4. Executive Summary

The objective of the present study was to develop a new type of inexpensive MBS by using carbon-based porous materials, instead of expensive mesoporous molecular sieves for CO₂ capture from flue gas. Our approach in this project included: 1) screening the commercial carbon-based materials for preparation of the high performance carbon-based molecular basket sorbent (CB-MBS); 2) examining the effects of properties of carbon supports, including surface oxygen-containing functional groups and pore structure of the carbon supports on the CO₂ sorption performance of CB-MBS; 3) modifying the commercial activated carbons by steam activation to tailor their pore structures for improving the CO₂ sorption performance of the prepared CB-MB; 4) examining the regenerability of the CB-MBS; and 5) estimating and comparing the preparation cost of CB-MBS. All tasks and milestones proposed for this project have been completed according to the schedule.

On the basis of our approaches in this project, the following conclusions can be made:

- Some commercial carbon materials are good supports for preparation of the CB-MBS with a weight-based CO₂ sorption capacity of 135 mg-CO₂/g-sorb, which is similar to that of the second generation of MBS (MBS-2).
- The volume-based sorption capacity of PEI(50)/C4 prepared in this study was as high as 47 mg-CO₂/ml-sorb, which is higher than that of MBS-2 by 57 %.
- The pore volume, especially the mesopore volume, of the carbon support plays an important role in determining the CO₂ sorption performance of the CB-MBS. Many commercially available activated carbons can be modified by steam activation to increase their mesopore volume, and thus to improve the sorption performance of the prepared CB-MBS.
- The prepared PEI(50)/C4 can be regenerated at 75 °C with more than 95% recovery of the sorption capacity after five sorption-desorption cycles.
- The preparation cost of MBS can be substantially reduced by 90% when using a selected carbon material instead of using silica mesopore molecular sieves, which will allow the CO₂ capture from flue gas to be conducted more cost efficiently.
- Due to the high CO₂ sorption capacity and low preparation cost, a carbon-based MBS could be a very promising sorbent for cost efficient CO₂ capture from flue gas.

5. Introduction

The continuous rise of the atmospheric CO₂ concentration and its linkage with climate change demand an urgent technological solution to reduce the CO₂ emission. Currently, one of the major sources of CO₂ emissions is the combustion of fossil fuels. Fossil fuels provide over 80 % of world energy usage today and they are expected to continue to dominate throughout this century.^{1,2,3,4,5} In the USA, the amount of CO₂ produced from the combustion of fossil fuels has reached nearly 6 billion metric tons with about 33% of it from the coal-fired electric power sector according to EIA.^{6,7} The anticipated increase in fossil fuel use in the coming decades will further increase CO₂ emissions with the potential impact on the global climate change. Consequently, carbon capture and sequestration (CCS) is crucial for deep reduction in greenhouse gas emissions, which is a challenging tasks for researchers. CO₂ exhausted from fossil fuel-fired energy systems is typically either too dilute (9-15 vol%) or at too low pressure (9-15 kPa of CO₂ partial pressure) to be directly stored or converted to a stable, carbon-based product. For geologic sequestration, there are three main cost components: capture, transportation, and storage. Among them, the cost of the capture is typically two or three times greater than the cost of both transportation and storage, which could increase electricity production costs by 60-100 % at the existing power plants and by 25-50 % at new advanced coal-fired power plants using IGCC technology. Thus, the first and also the most crucial step in the CCS process is to capture and separate CO₂ from flue gas to produce a concentrated CO₂ stream more energy efficiently and cost effectively.^{8,9,10}

A wide variety of research has been carried out on the removal of CO₂ from industrial processes, particularly flue gas. There are different technologies for CO₂ capture and separation from flue gas, including scrubbing by physical absorbents, adsorption by porous materials, sorption by reactive solid materials, sorption on the immobile amine sorbent, cryogenics distillation, and separation by membrane. Among these technologies, sorption on the immobile amine sorbent technology has been recognized as one of the most appealing options for CO₂ capture. In our previous study, we have developed the novel polymer sorbents by loading polyethylenimine (PEI) on the mesoporous molecular sieves (MCM-41 or SBA-15), called as Molecular-Basket Sorbent (MBS, MBS-1 for MCM-41 support and MBS-2 for SBA-15 support).^{11,12,13,14,15} In comparison with commercial or the state-of-the-art absorbents, adsorbents

and sorbents, the developing MBS has shown many potential advantages, including higher capacity (140 mg- CO₂/g-S at 15 kPa), high selectivity, no corrosion problem, high sorption/desorption rate, and good regenerability and stability.^{11,12,13,14,15}

However, we used the silica mesoporous molecular sieve, such as MCM-41 or SBA-15, as a matrix in preparation of the MBS. As is well known, the cost for preparing these materials is high, and even they are not commercially available yet. A great challenge is to reduce the MBS preparation cost substantially without significantly changing the MBS sorption performance, such as high capacity, high selectivity and low energy consumption. According to our preliminary estimation, the cost for SBA-15 accounts for about 90 % of the total cost for preparing MBS-2. Thus, the key is to reduce the cost of the support material for MBS. Carbon-based porous materials, such as activated carbon (AC) and carbon black, have attracted our attention because of their inexpensive price, well-developed pore structure, and facilitation for surface modification. Coal is a popular parent material for producing carbon-based pore materials. Coal is also the most abundant source in the world and is inexpensive for producing carbon-based porous materials. In general, the cost of the commercial coal-derived AC is only about \$7/kg. Consequently, coal may be a good choice to produce the porous material for mass production of MBS for CO₂ capture.^{16,17}

There are several studies in the literature on the preparation of modified adsorbents for CO₂ capture by PEI impregnation on the activated carbons. However, due to the absence of understanding the effect of the textural properties on sorption performance of MBS, the CO₂ sorption capacity of activated carbon-based sorbent is very low comparing to MBS-2. Maroto-Valer et al. showed that CO₂ sorption capacity of 33.5 wt % of PEI loading on activated anthracites at 75°C was 26.3 mg- CO₂/g-sorbent.¹⁸ They were able to increase the CO₂ sorption capacity from 26.3 to 49.8 mg- CO₂/g-sorbent with 39 wt % PEI loading on fly ash at 70°C.¹⁹ Arenillas et al. reported that CO₂ sorption capacity of 60 wt % PEI loading on fly ash derived activated carbon was only 40 mg- CO₂/g-sorbent.²⁰

The objective of the present study was to develop a new type of inexpensive MBS by using carbon-based porous materials, instead of expensive mesoporous molecular sieves for CO₂

capture from the fossil fuel power plant flue gas. The ultimate purpose was to substantially reduce the MBS preparation cost, thus allowing the CO₂ capture from flue gas to be conducted more cost-efficiently. This final report discusses our approach in preparing and evaluating the carbon-based MBS.

6. Experimental

6. 1. Carbon Samples

Some commercial carbon materials, including three activated carbons and a carbon black, with different pore structures were chosen for using as a support to prepare the carbon-based MBS. The porous properties of the carbon materials are listed in **Table 1**. Within these carbon samples, C1 has mainly a microporous structure, C2 is dominantly mesopore, C3 has a similar volume of micropores and mesopores, and C4 has a dominantly mesoporous structure with the highest pore volume in these carbon samples.

Table 1. Pore properties of carbon materials used in this study

Sample source ID	S _{BET} (m ² /g)	S _{micro} (m ² /g)	S _{meso} (m ² /g)	V _{total} (ml/g)	V _{micro} (ml/g)	V _{meso} (ml/g)
C1	1151	910	241	0.64	0.442	0.20
C2	1495	1000	495	1.21	0.55	0.66
C3	2320	1397	923	1.64	0.79	0.84
C4	1486	575	911	2.69	0.50	2.19

6. 2. Modification of Carbon Materials

Heat Treatment of C3 under a N₂ flow. A set of carbon samples were pretreated from C3 by heat treatment at four different temperatures, 500, 600, 700, and 800 °C, under a N₂ flow at a flow rate of 100 ml/min for 2 hours to tailor the functional groups on the surface. The carbon samples treated at 500, 600, 700, and 800 °C from C3 were denoted as C3-500, C3-600, C3-700, and C3-800, respectively. C3 was washed by the deionized water, and then heated at 110 °C in a vacuum oven overnight for drying before use.

Modification by Steam Treatment. The objective of the steam treatment was to enlarge

the pore size and/or develop more porosity in the carbon samples. The treatment was performed in a vertical tubular furnace. Typically, about 3 g of the carbon sample was placed into a quartz reactor. The treatment was first conducted by heating the reactor bed temperature to 600 °C under N₂ flow (20 ml/min). After introducing the activation agent, which contained steam in N₂, to the reactor, the reactor temperature was increased to 800 °C, 900 °C or 1000 °C, and kept at the temperature for 1 or 2 hours. After finishing the activation, the gas was switched to pure N₂ with a flow rate of 20 ml/min until the reactor was cooled down to room temperature. The carbon material prepared by the steam treatment was denoted as C_x(S_y), where C_x is the ID of the carbon material (x=1, 2, 3, and 4), and S_y represents the steam treatment at y °C. The treatment conditions, including activation temperature, activation time and the flow rate of gases, are summarized in **Table 2**.

Table 2. Conditions for treatment of carbon samples by steam activation

Activation temperature (°C)	Activation time(h)	Steam flow rate (ml/min)	N ₂ flow rate (ml/min)
800	2	0.06	10
900	2	0.06	10
1000	1	0.06	10

6.3. Preparation of Carbon-based MBS

Carbon-based MBSs (CB-MBS) were prepared by using the initial carbon samples and the treated carbon samples with the wet impregnation method. A given amount of PEI was dissolved in 20 ml methanol and stirred for about 30 min. Then, 2.5 g of carbon samples were added to the PEI solution and stirred until most of methanol was evaporated. When most of methanol was removed, the sample was put into a vacuum oven for drying at 80 °C overnight. After drying, the samples were grounded into a fine powder and then stored in a container.

A series of CB-MBS samples were prepared using different PEI loading amounts from 30 wt% to 70 wt% on the selected carbon samples. The prepared CB-MBS samples were denoted

as PEI(x)/y, where x is the PEI loading percentage and y is the ID of the support material.

6.4. Evaluation of Sorption-desorption Performance of CB-MBS

The sorption and desorption performance of the prepared CB-MBSs was evaluated by using thermogravimetric analysis (TGA) analyzer on the basis of the weight gain and loss during the sorption and desorption process. A typical TGA temperature program is shown in **Figure 1**. The evaluation procedure is described as following: Loading about 10 mg of the sample on the sample pan, increase the temperature at a rate of 10 °C/min from 30 °C to 100 °C under a N₂ flow at a rate of 100 ml/min. Keep the sample at 100 °C for 100 min to remove moisture, solvent or other adsorbate from the sample. Then, cool the sample to 75 °C, change the flow gas from N₂ to CO₂ and hold temperature at 75 °C for 100 min for CO₂ sorption. After CO₂ sorption, increase the temperature to 100 °C, and switch the flow gas from CO₂ to N₂ for desorption at 100 °C. Weight loss and gain during these two processes were recorded by the TGA analyzer. The weight-based sorption capacity (mg-CO₂/g-sorbent) was calculated according to the weight change of the sample during the sorption-desorption process.

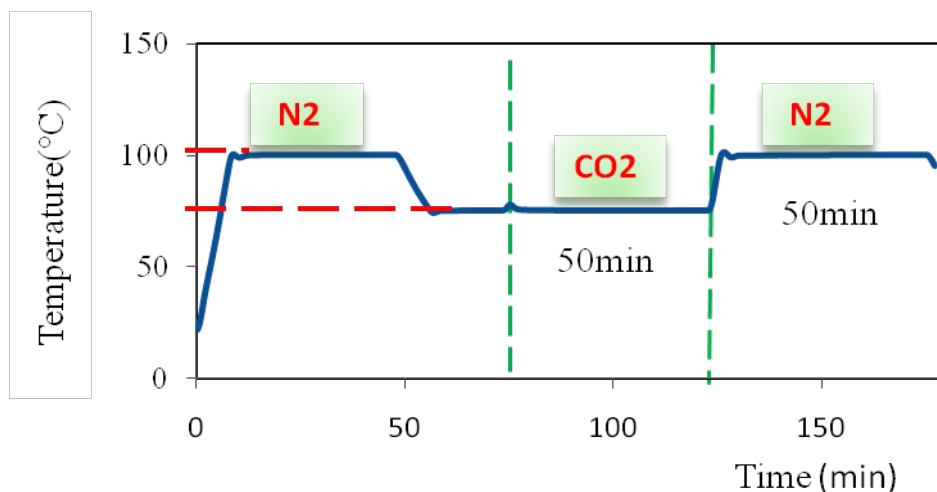


Figure 1. TGA temperature program for evaluation of sorption-desorption performance of CB-MBS

6.5. Determination of Functional Groups on Carbon Surface

The C3 and C3-700 were characterized by TPD at a temperature program with a rate of

10 °C/min from 40 to 950 °C under a He flow of 50 ml/min. The amount of the total oxygen-containing functional groups in the samples was estimated on the basis of the total evolved amount of CO and CO₂.

6.6. Characterization of Textural Structure

Characterization of the textural structure of the carbon samples and CB-MBS were carried out by physical adsorption of N₂ at -196 °C in a Micromeritics ASAP 2020 analyzer. The carbon samples were degassed at 200 °C under vacuum for 24 h. In order to avoid the degradation of PEI, CB-MBS samples were degassed at 50 °C under vacuum for 24 h.

The BET surface area (S_{BET}) was obtained from physical adsorption of N₂ using the BET equation. The total pore volume (V_t) was calculated using the N₂ absorbed at $P/P_0=0.99$. The t-plot method was used to estimate the micro-pore volume (V_M). Pore size distribution was determined by the DFT method.

6.7. Regeneration of CB-MBS

The sorption-desorption cycles of the selected CB-MBS were conducted in a TGA to evaluate the regenerability of the CB-MBS.

7. Results and Discussion

7.1. Screening of Commercial Carbon-based Materials

Figure 2 shows the measured CO₂ sorption capacity of the four CB-MBS samples, which were prepared by loading 50 wt % of PEI on C1, C2, C3 and C4, along with a comparison with the first and secondary generations of MBS, PEI(50)/MCM-41 and PEI(50)/SBA-15. PEI(50)/C1 gave the least capacity of 33 mg-CO₂/g-sorbent of the four samples. It needs to mention that PEI(50)/C1 sample appeared to be a sticky slurry, as shown in **Figure 3**, unlike the other three samples, which were solid powders. It is probably because the volume of the loaded PEI was over the pore volume of C1. The excess of PEI was coated on the external surface of the carbon particles, which allowed the particles to stick to each other. Both PEI(50)/C3 and PEI(50)/C2 showed a significantly higher CO₂ sorption capacity than that of PEI(50)/C1, but less than a half of that of PEI(50)/C4. In all tested samples, PEI(50)/C4 gave the highest CO₂ sorption

capacity of 135 mg-CO₂/g-sorbent. This capacity is significantly higher than that of PEI(50)/MCM-41, and almost the same as that of PEI(50)/SBA-15 (138 mg-CO₂/g-sorbent), which has the highest CO₂ capacity based on our previous study.

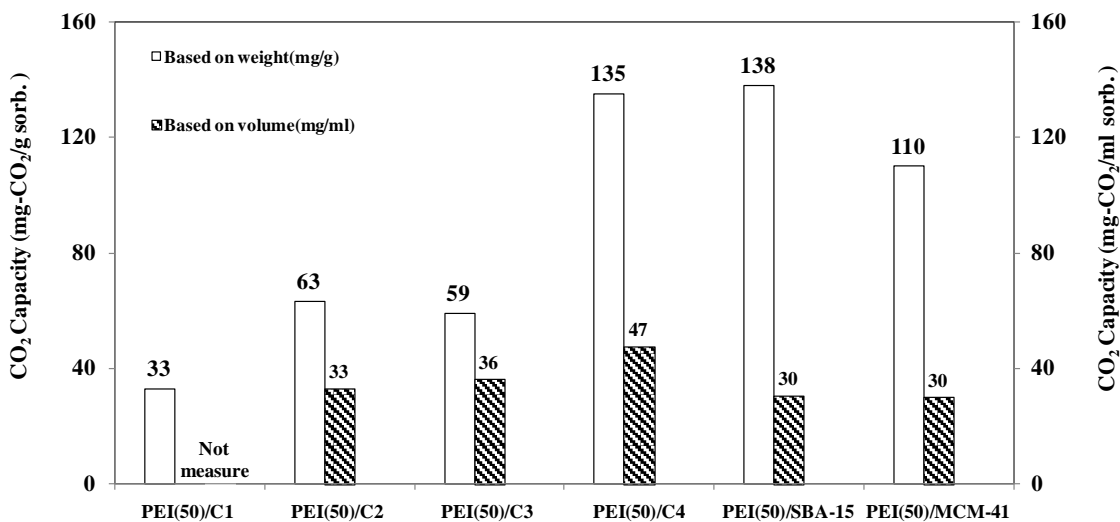


Figure 2. The measured CO₂ sorption capacity of CB-MBS in comparison with PEI(50)/MCM-41 and PEI(50)/SBA-15.



Figure 3. Photo of PEI(50)/C1 sample

Moreover, it was found that PEI(50)/C2, PEI(50)/C3, and PEI(50)/C4 had much higher packing densities of 0.52, 0.61, and 0.35 g/ml, respectively, while the packing density of PEI(50)/MCM-41 and PEI(50)/SBA-15 was only 0.22 and 0.27 g/ml, respectively. According to their packing density, the sorption capacity based on the sorbent bed volume for each sorbents was also estimated, and the results are also shown in **Figure 2**. PEI(50)/C2 and PEI(50)/C3 have a volume-based sorption capacity similar to those of PEI(50)/MCM-41 and PEI(50)/SBA-15, while PEI(50)/C4 even has a volume-based sorption capacity of 47 mg-CO₂/ml-sorbent, which is higher than that of PEI(50)/SBA-15 by 57 %. This indicates that for capturing the same amount of CO₂, the sorbent volume for PEI(50)/C4 is only about 64 % of that for PEI(50)/SBA-15, which can reduce the sorbent bed size significantly.

7.2. Effect of Properties of Carbon Supports on Sorption Capacity of CB-MBS

As determined in our previous study, sorption of CO₂ on the supported PEI is through the interaction of CO₂ with the accessible amine groups in PEI.¹⁵ Why do CB-MBS samples with the same PEI loading and different carbon supports show quite different sorption performance? The reason could be due to their different surface chemistry and/or porous structures of the carbon supports. In order to answer this question, a better understanding of the surface functional groups and textural structure of the support carbon materials on the sorption performance of CB-MBS is necessary.

7.2.1. Effect of Carbon Surface Function Groups on Sorption Capacity of CB-MBS

There are oxygen-containing functional groups on the activated carbon, such as, carboxylic groups, phenolic hydroxyl groups, etc. These weak acidic groups might consume some amine groups in PEI, resulting in the reduced CO₂ sorption capacity. In order to examine the effect of the surface oxygen-containing functional groups on the sorption performance of CB-MBS, the oxygen-containing functional groups on the C3 surface was tailored by heating at 500, 600, 700, and 800 °C, respectively, under a N₂ flow. The weight loss of the samples was 3.9, 7.2, 10.0 and 11.4 wt %, respectively. The characterization of the pore structure of the treated samples indicates that the pore volume and surface area of the samples were almost unchanged. The TPD analysis of the samples was also conducted, as shown in **Figure 4**. The TPD results indicate that more than 75 % of the oxygen-containing functional groups on the C3

surface were removed after the heat treatment at 700 °C for 2 hours. The heat-treated C3 samples were then used to prepare the PEI(50)/C3 samples, denoted as PEI(50)/C3-500, PEI(50)/C3-600, PEI(50)/C3-700, and PEI(50)/C3-800. The sorption capacities of the samples with different heat-treatment temperatures are shown in **Figure 5**. The sorption capacity had only a slight change with increasing heat-treating temperature, indicating that the oxygen-containing functional groups on the surface may have only a slight effect on the sorption performance. It suggests that the surface functional groups may not a key factor in determining the sorption performance of CB-MBS.

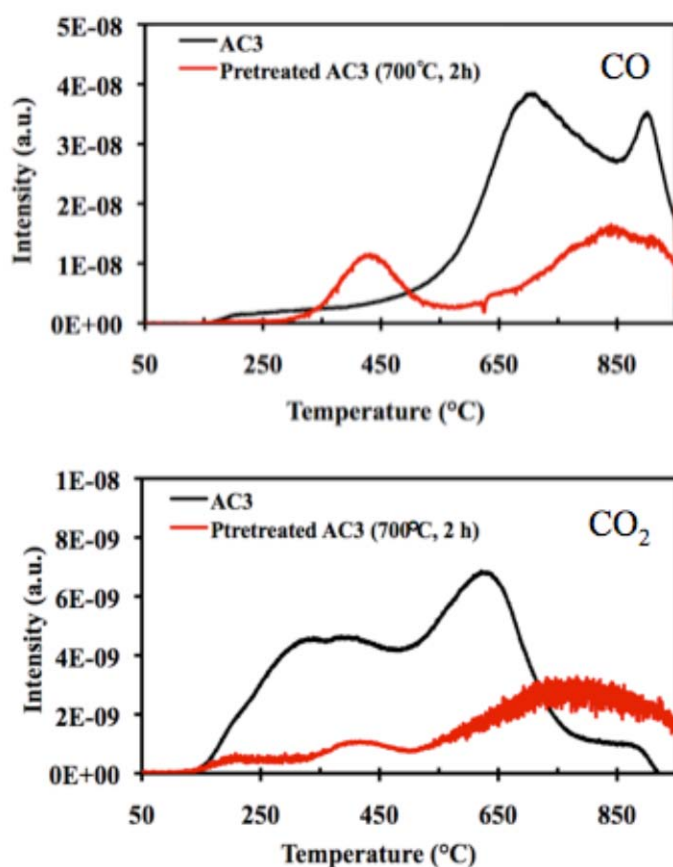


Figure 4. CO and CO₂ evolution profiles for C3 and AC3-700 samples

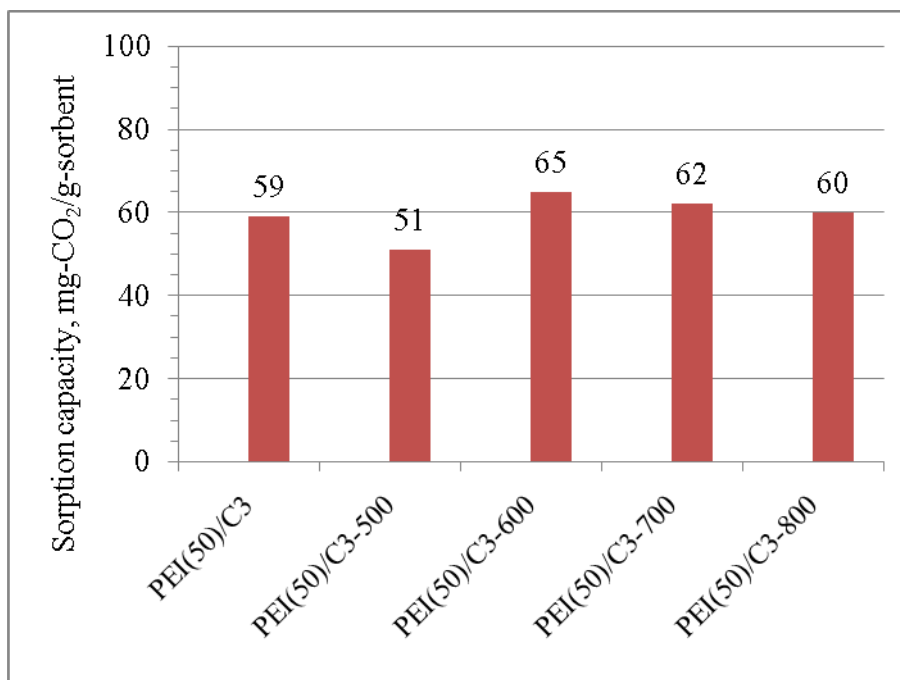


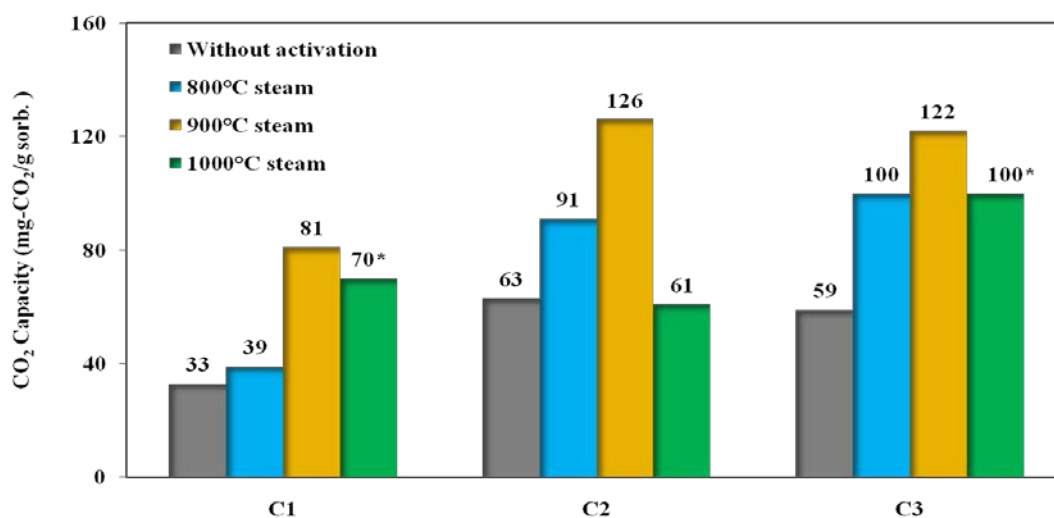
Figure 5. CO₂ sorption capacity of PEI(50)/C3 with different treatment temperature of C3

7.2.2. Effect of Textural Structure of Carbon Supports on Sorption Capacity of CB-MBS

Modification of Carbon Support by Steam Activation. As is known, steam activation is an effective method for increasing the pore size and pore volume of carbon materials. The steam activation of C1, C2 and C4 at a temperature range of 800-1000 °C and for a time of 1 to 2 hours was conducted in a fixed-bed reactor. The product yields of carbon samples modified at different conditions are listed in **Table 3**. The product yield of carbon samples decreased with increasing activation temperature. The product yield of C3 decreased from 58 wt % to 33 wt % when the activation temperature was increased from 800 °C to 900 °C for 2 hours. The increase in the temperature to 1000 °C for 2 hours resulted in a product yield of only 8.5 wt %, indicating most of the carbon sample reacted with steam at this condition. Thus, 1 hour for the activation time at 1000 °C was selected. The carbon samples obtained by the steam modified at 800 °C, 900 °C and 1000 °C were used to prepare the CB-MBS with a PEI loading of 50 wt %. The prepared CB-MBS were evaluated by using TGA for their sorption performance, and the results are shown in **Figure 6** in comparison with the CB-MBS without the steam modification of the carbon supports.

Table 3. Product yield (wt %) of carbon samples after steam activation at different conditions.

Sample ID	Activation Temperature			
	800°C (2h)	900°C (2h)	1000°C (1h)	1000°C (2h)
C1	68	44	66	-
C2	69	34	67	-
C3	58	33	52	8.5

**Figure 6.** Comparison of CO₂ sorption capacity of CB-MBS prepared by using steam-activated carbons under different temperature

It is clearly shown that the steam modification improved the sorption performance of the CB-MBS, especially for C2 and C3. The CO₂ sorption capacity of the PEI(50)/C2 increased from 63 mg-CO₂/g-sorbent for C2 without the modification to 91 mg-CO₂/g-sorbent for the modification at 800 °C and 126 mg-CO₂/g-sorbent for the modification at 900 °C. The CO₂ sorption capacity of the PEI(50)/C3 increased from 59 mg-CO₂/g-sorbent for C3 without the modification to 100 mg-CO₂/g-sorbent for the modification at 800 °C and 122 mg-CO₂/g-sorbent for the modification at 900 °C. Even for PEI(50)/C1, the modification at 900 °C was able to increase the sorption capacity to 81 mg-CO₂/g-sorbent. However, further increase in the activation temperature to 1000 °C leads to the significant decrease of the CO₂ sorption

performance of CB-MBS. The best activation temperature, regardless of the carbon samples is 900 °C. The steam modification at 1000 °C may result in the destruction of the porous structure of the carbon due to over the severe reaction, as indicated by the significant weight loss of the carbon samples shown in **Table 3**.

Correlation of Texture Structure of Carbon Supports with Sorption Capacity of CB-MBS. In order to understand the reason for the enhanced performance of CB-MBS by steam modification of the carbon supports, the texture properties of the carbon samples modified by the steam activation at 900 °C were characterized by micrometric ASAP2020. **Table 4** shows the pore physical properties of the steam modified carbon samples in comparison with their parent samples. The surface area of C1 and C2 increase slightly, but not for C3. The significant difference is the increase of the total pore volume due to the significant increase of the mesopore volume for all carbon samples. The mesoporous volume of C1, C2 and C3 was increased by 0.25, 0.35 and 0.25 ml/g, respectively. The results indicate that the steam modification is very effective for developing mesopores, but not for developing micropores, which is consistent with the reports in literature.

Table 4. Comparison of texture porosities of steam-activated AC samples and parent AC samples

Sample ID	S_{BET} (m ² /g)	S_{micro} (m ² /g)	S_{meso} (m ² /g)	V_{total} (ml/g)	V_{micro} (ml/g)	V_{meso} (ml/g)
C1	1151	910	241	0.64	0.44	0.20
C1 (S900)	1323	837	486	0.90	0.45	0.45
C2	1495	1000	495	1.21	0.55	0.66
C2 (S900)	1872	1039	833	1.57	0.56	1.01
C3	2320	1397	972	1.64	0.79	0.84
C3 (S900)	2140	1141	999	1.72	0.63	1.09

In order to further understand the relationship between the CO₂ sorption capacity and the pore property of the carbon support, a correlation between the CO₂ sorption capacity of

PEI(50)/Cx and the pore properties of their carbon support was investigated. **Figure 7** shows the CO₂ sorption capacity of PEI(50)/Cx as a function of total surface area, microporous surface area and mesoporous surface area, respectively. The correlation between the CO₂ capacity of PEI/Cx and the surface areas of Cx is very poor, and no linear relationship could be observed. It indicates that neither total surface area, nor microporous surface area, nor mesoporous surface area, are a key factor in determining the sorption performance of PEI(50)/Cx. The CO₂ sorption capacities of PEI(50)/Cx as a function of pore volume, including micro pore volume, meso pore volume, and total pore volume, are shown in **Figure 8**. It was found that the micro pore volume has a poor correlation with the CO₂ sorption capacity. However, the total pore volume, especially the mesopore volume has a good correlation with the CO₂ sorption capacity. With an increase in the mesopore volume, the CO₂ sorption capacity increased. The results strongly suggest that the total pore volume, especially the mesopore volume, plays an import role in determining the sorption performance of CB-MBS. The large mesopore volume increases the total number of accessible sorption sites.

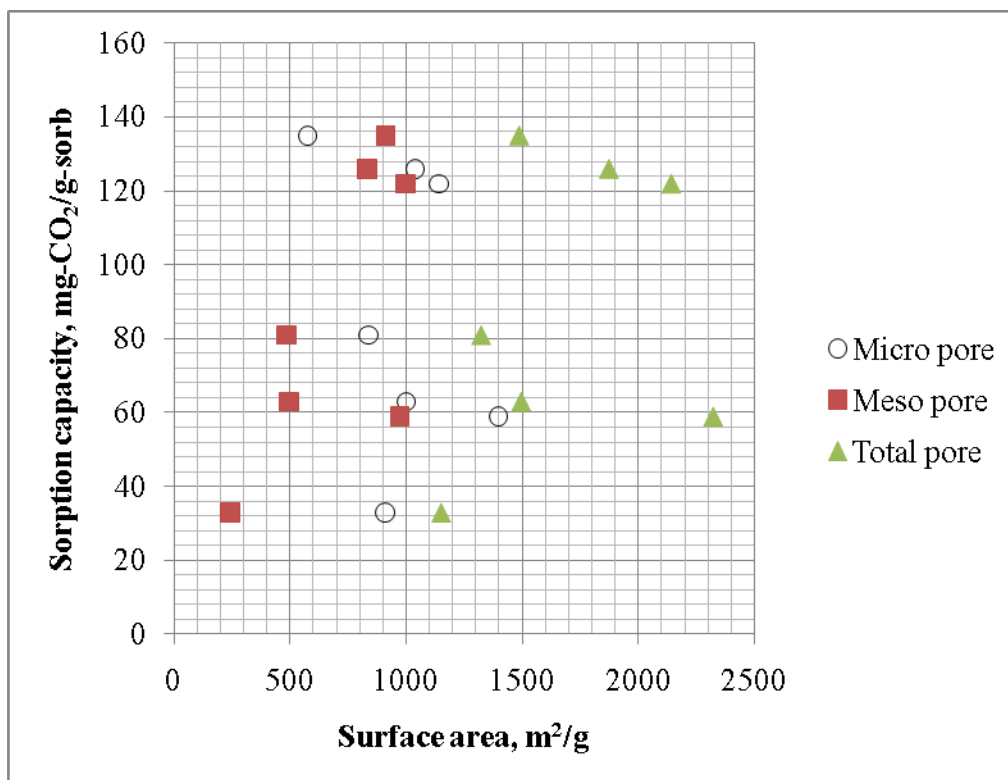


Figure 7. Correlation between CO₂ sorption capacity of PEI(50)/Cx and surface area of Cx.

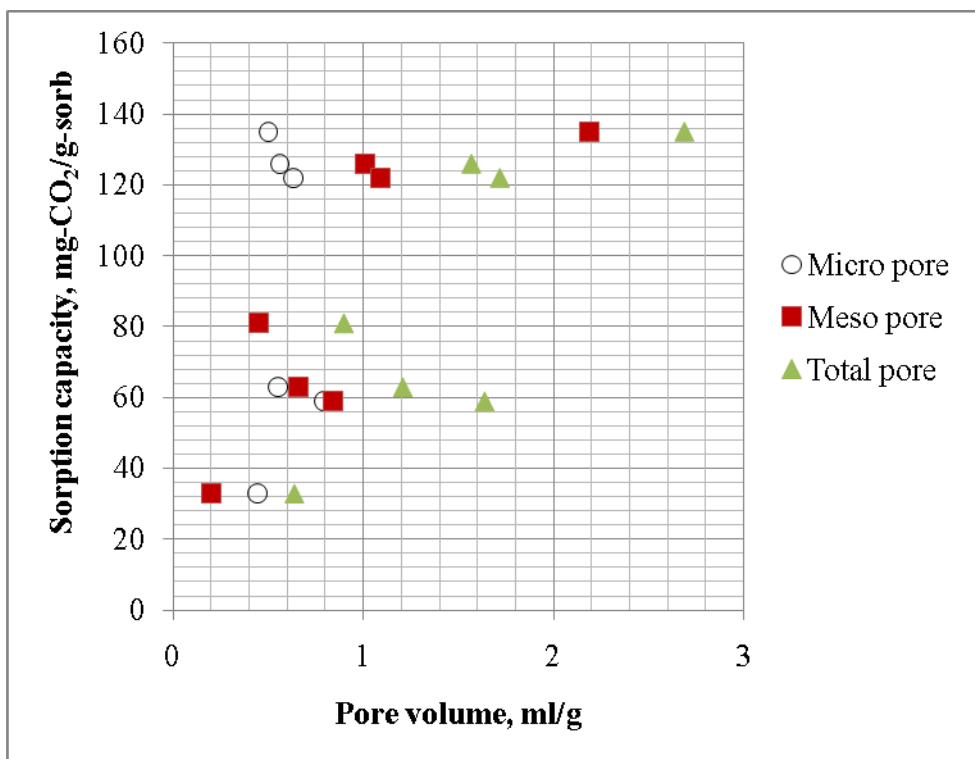


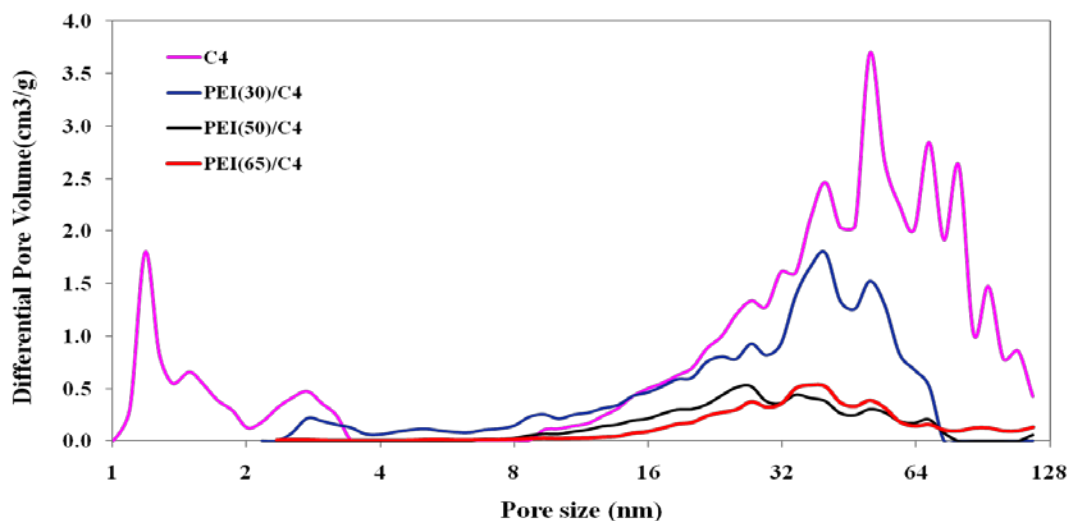
Figure 8. Correlation between CO₂ sorption capacity of PEI(50)/Cx and pore volume of Cx.

7.3. Effect of PEI Loading on CO₂ Sorption Capacity of CB-MBS

Since the CO₂ sorption capacity of CB-MBS is directly related to amount of the accessible amine groups in the PEI loaded on the carbon, the amount of the loaded PEI should play an important role in determining the CO₂ sorption capacity of CB-MBS. A series of PEI/C4 with different PEI loadings were prepared, and their textural structures were characterized. **Table 5** lists the surface area and pore volume of the parent C4 and PEI/C4 with different PEI loading. The surface area and the total pore volume of C4 were 1486 m²/g and 2.69 ml/g, respectively. The surface area and pore volume of PEI/C4 increased with increasing PEI loading. This suggests that the loaded PEI was filled into the pores of the carbon support, as indicated by the pore size distribution (see **Figure 9**) measured by the N₂ adsorption using DFT method. The apparent disappearance of the pores with porous size from 0.5 nm to 2 nm evidently suggests that the PEI molecules first filled the micro-pores, and then the mesopores.

Table 5. Textural characterization of C4 and PEI/C4 with different PEI loading

Sample ID	S_{BET} m^2/g	S_{micro} (m^2/g)	S_{meso} (m^2/g)	V_{total} (ml/g)	V_{micro} (ml/g)
C4	1486	575	911	2.69	0.50
PEI(30)/C4	321	5.40	315.60	1.31	0.14
PEI(50)/C4	37	0.60	36.40	0.33	0.02
PEI(65)/C4	27	0.45	26.55	0.29	0.01

**Figure 9.** Pore size distribution of the parent C4 and PEI/C4 with different PEI loading

The CO_2 sorption capacities of the PEI/C4 with different PEI loading were measured using TGA, and the results are shown in **Figure 10**. It was found that the carbon dioxide sorption capacity increased with the PEI loading when the PEI loading was less than 65 wt %. PEI/C4 with 65% PEI loading (PEI(65)/C4) gave the highest carbon dioxide sorption capacity of 154 $\text{mg-CO}_2/\text{g-sorb}$, even higher than that of (PEI(50)/C4). Further increases in the PEI loading resulted in a decrease of the CO_2 sorption capacity. However, the CO_2 sorption capacity of (PEI(70)/C4) was reduced to about 55 $\text{mg-CO}_2/\text{g-sorb}$. This is because the 70 wt % PEI loading is beyond the saturation pore volume of C4, which results in a decrease of the CO_2 sorption capacity.

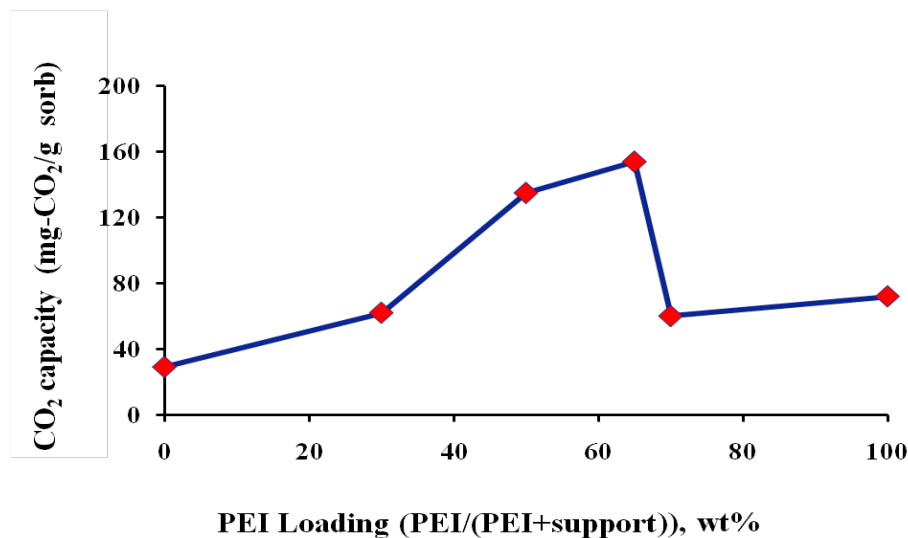


Figure 10. Effect of PEI loading on CO₂ sorption capacity of PEI/C4

7.4. Regenerability of PEI(50)/C4

For practical applications, the sorbent must possess good regenerability and long-term stability. The five sorption-desorption cycles of PEI(50)/C4 were conducted. The TGA curve for the five sorption-desorption cycles of PEI(50)/C4 at 75 °C is shown in **Figure 11**. The results indicate that the spent PEI(50)/C4 can be regenerated even at 75 °C. More than 95 % sorption capacity of PEI(50)/C4 can be recovered after five cycles, although a slight decrease of the capacity was observed. More investigations are necessary to further improve the regenerability and stability of the CB-MBS.

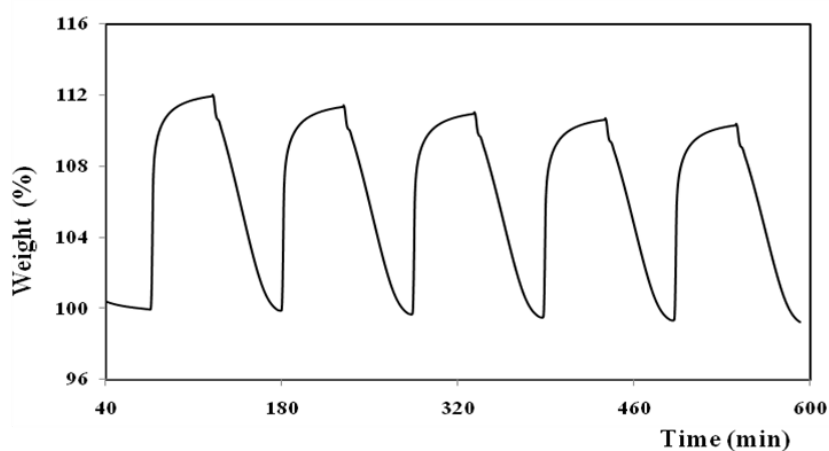


Figure 11. TGA curve for five sorption-desorption cycles of PEI(50)/C4 at 75 °C.

7.5. Estimation of Preparation Cost for CB-MBS

The costs for preparing CB-MBS on the basis of sample PEI(50)/C4 was estimated in comparison with MBS-1(PEI(50)/MCM-41) and MBS-2 (PEI(50)/SBA-15). The results are listed in **Table 6** in comparison with the some commercial absorbents. The estimated preparation cost for the previous MBS-1 and MBS-2 is \$750/kg or higher. This is about 70 times higher than that of MEA and about 25 times higher than that of the SELEXOL solvent. This is because the cost for synthesis of both MCM-41 and SBA-15 is higher than \$1300/kg. This significant disadvantage in preparing MBS-1 and MBS-2 has become a bottleneck in development of MBS, which limits the practical application of MBS-1 and MBS-2 for CO₂ capture from flue gas.

Table 6. The costs for preparation of CB-MBS, MBS-1 and MBS-2 in comparison with other sorbents/absorbents

Sorbent	Estimated Price \$/kg
Monoethanolamine (MEA)	11
Diethanolamine (DEA)	10
Polyalkylene glycol dimethyl ether (PGDE) (SELEXOL)	30
MCM-41	>1300
SBA-15	>1400
Coal-based AC	~6
Polyethylene glycol (PEG)	25.1
Polyethylenimine (PEI)	24.7
MBS-1 (PEI(50)/MCM-41)	~680
MBS-2 (PEI(50)/SBA-15)	~750
MBS-5 (PEI(50)/C4)	~31

The objective of the present study was to develop a new type of inexpensive MBS by using low cost porous material, instead of the expensive mesoporous molecular sieves. On the basis of our preliminary estimation, the cost for the support accounts for more than 90% of the

total MBS preparation expense for MBS-1 and MBS-2. Therefore, if we could find a low cost support material to replace the expensive mesoporous molecular sieves, the preparation cost of MBS will be reduced significantly. Activated carbon and carbon black are popular mass produced adsorption materials, which are applied widely in industrial and technological processes. According to our preliminary estimation, the preparation cost of PEI(50)/C4 can be reduced to \$31/kg, which is about 95% lower than that of MBS prepared by MCM-41 and SBA-15. It indicates that the CB-MBS is a very promising sorbent for cost efficient CO₂ capture from flue gas.

8. Conclusions

On the basis of our approach in this project, the following conclusions can be made:

- Some commercial carbon materials are good supports for preparation of the CB-MBS with weight-based CO₂ sorption capacity, which is similar to that of the second generation of MBS (MBS-2). The weight-based sorption capacity of PEI(50)/C4 prepared in this study was as high as 135 mg-CO₂/g-sorb.
- Many CB-MBS even give much higher volume-based CO₂ sorption capacity than those of silica-molecular-sieve-based MBS. The volume-based sorption capacity of PEI(50)/C4 prepared in this study was as high as 47 mg-CO₂/ml-sorb, which is higher than that of MBS-2 by 57 %.
- The pore volume, especially the mesopore volume, of the carbon support plays an important role in determining the CO₂ sorption performance of the CB-MBS. Many commercially available activated carbons can be modified by steam activation to increase their mesopore volume, and thus can be used to prepare CB-MBS with the weight-based sorption capacity similar to that of MBS-2 and with the volume-based CO₂ sorption capacity much higher than that of MBS-2.
- The effect of the amount of the oxygen-containing functional groups on the carbon surface on the CO₂ sorption performance of the CB-MBS is less important.
- Loading of 65 % of PEI on C4 give the highest CO₂ sorption capacity of 154 mg-CO₂/g-sorbent.
- The prepared PEI(50)/C4 can be regenerated at 100 °C. More than 95% sorption capacity can be recovered after five sorption-desorption cycles.

- The preparation cost of MBS can be substantially reduced by 90% when using the selected carbon material instead of using the silica mesopore molecular sieves in our previous study, which will allow the CO₂ capture from flue gas to be conducted more cost efficiently.
- In combination of the high CO₂ sorption capacity and low preparation cost, the carbon-based MBS could be a very promising sorbent for cost efficient CO₂ capture from flue gas.

9. Project-related Publications

1. Wang D.X.; Shalaby C.; Ma X.L.; Song C.S. Carbon-based “Molecular Basket” Sorbent for CO₂ Capture from Flue Gas 35th International Technical Conference on Clean Coal & Fuel Systems, Cleanwater, FL, USA. 2010.
2. Wang D.X.; Shalaby C.; Ma X.L.; Wang X.X.; Song C.S. Development of Carbon-based “Molecular Basket” Sorbent for CO₂ Capture from Flue Gas. 240th ACS National Meeting, Boston, 2010.

10. References Cited

- ¹ Azar, C.; Rodhe, H. *Science*, 276, 181, 1997.
- ² DOE/OS-FE Carbon sequestration. State of the Science, Office of Science and Office of Fossil Energy, U.S. Department of Energy, Washington, DC, 1999.
- ³ DOE Carbon sequestration-research and development, 1999,
http://www.fe.doe.gov/coal_power/sequestration/reports/rd/index.html
- ⁴ Ruether, J.A. FETC Programs for Reducing Greenhouse Gas Emissions, Report no. DOE/EFTC-98/1058, U.S. Department of Energy, Pittsburgh, PA, 1999.
- ⁵ Herzog, H.; Drake, E.; Adams, E. CO₂ capture, Refuse and Storage Technologies for Mitigating Global Climate Change, Report no. DOE/DE-AF22-96PC01257, Jan 1997.
- ⁶ Song, C.S.; Gaffney, A.M.; Fujimoto, K. CO₂ Conversion and Utilization, ACS Symp. Series, vol. 809, American Chemical Society, Washington, DC, 448, 2002.
- ⁷ Song, C.S. *Catalysis Today*, 115, 2–32, 2006.
- ⁸ Maroto-Valer, M. M.; Zhong, T.; Zhang, Y. Z. *Fuel Processing Technology* 86, 1487–1502, 2005.

⁹ DOE-FE Hydrogen from Coal Program – Research, Development, and Demonstration Plan, 2004-2015, September 2005.

http://www.netl.doe.gov/technologies/hydrogen_clean_fuels/refshelf/myrddp.html

¹⁰ DOE/EIA-0383 Annual Energy Outlook 2007.

¹¹ Xu, X.; Song, C.; Andresen, J. M.; Miller, B. G.; Scaroni, A. W. *Energy & Fuels*, 16, 1463, 2002.

¹² Xu, X., Song, C., Andresen, J. M., Miller, B. G., Scaroni, A. W. *Microporous and Mesoporous Materials*, 62, 29-45, 2003.

¹³ Xu, X., Song, C., Miller, B. G., Scaroni, A. W. *Ind. & Eng. Chem. Res.* 44 (21), 8113-8119, 2005.

¹⁴ Xu, X.; Song, C.; Miller, B. G.; Scaroni, A. W. *Fuel Proc. Tech.* 86 (14-15): 1457-1472, 2005.

¹⁵ Ma, X. L.; Wang, X. X.; Song, C. S. *J. Am. Chem. Soc.* 2009, 131, 5777-5783.

¹⁶ Siriwardane, R.V.; Shen, M.; Fisher, E.P.; Poston, J. *Energy Fuels*, 15, 279, 2001.

¹⁷ Burchell, T.D.; Judkins, R.R.; Rogers, M.R.; Williams, A.M. *Carbon*, 35, 1279, 1997.

¹⁸ Maroto-Valer, M.M.; Tang, Z.; Zhang, Y. *Fuel Process. Technol.* 86, 1487, 2005.

¹⁹ Maroto-Valer, M.M.; Lu, Z.; Zhang, Y.Z. *Waste Manage* 28, 2320, 2008.

²⁰ Arenillas, A.; Smith, K.M.; Drage, T.C. *Fuel* 2005, 84, 2204.

**RELATIONSHIP OF ANTHRACITE STRUCTURE TO
ISOTROPIC GRAPHITE**

Final Report

March 1, 2009 – June 30, 2010

Principle Investigator: Dr. Caroline E. Burgess Clifford

Contributions from: M. Solomon Nyathi, Harold H. Schobert, Vamsi Karri

Report Issue: July 31, 2010

Internal Agreement No. 3808-TPSU-DOE-1874,
For Award No.: DE-FC26-03NT41874

The EMS Energy Institute
Penn State University
C205 Coal Utilization Laboratory
University Park PA 16802

DISCLAIMER

This report was prepared as an account of work sponsored by an agency of the United States Government. Neither the United States Government nor any agency thereof, nor any of their employees, makes any warranty, express or implied, or assumes any legal liability or responsibility for the accuracy, completeness, or usefulness of any information, apparatus, product, or process disclosed, or represents that its use would not infringe privately owned rights. Reference herein to any specific commercial product, process, or service by trade name, trademark, manufacturer, or otherwise does not necessarily constitute or imply its endorsement, recommendation, or favoring by the United States Government or any agency thereof. The views and opinions of authors expressed herein do not necessarily state or reflect those of the United States Government or any agency thereof.

ABSTRACT

Anthracite is an abundant and inexpensive natural resource that has not been fully exploited as a carbon material. It has been known for many years that anthracites can be used as filler for low-end specialty synthetic graphite and as a precursor for activated carbons, and there is continued effort to develop new uses for anthracite. One such potential application is the use of anthracite as a filler for nuclear graphite, which is produced from isotropic coke rather than the anisotropic needle coke traditionally used for graphite electrode manufacture.

Nuclear graphite is a high-purity graphite utilized as a moderator and structural component in nuclear reactors. The function of the moderator is to slow the neutrons with high kinetic energy, reducing their kinetic energy to a range that allows for further fission. Dimensional changes occur from exposure to radiation, and include initial bulk shrinkage followed by net expansion at low and high neutron fluence, respectively. The lifetime of the graphite is defined by the dose at which the graphite shrinks and expands back to its original value. Damage by radiation is dependent on the neutron fluence and irradiation temperature. Graphite resistance to radiation damage and its structural integrity determine its lifetime in the reactor. Because of these issues, the graphite structure preferred is isotropic, because it provides better dimensional stability by attaining uniform thermal shrinkage and expansion in all directions when subjected to irradiation, therefore prolonging its lifetime. Anisotropic graphite has a shorter lifetime due to major changes occurring in the c-direction relative to the a-direction. The CTE ratio ($CTE_{c-axis}/CTE_{a-axis}$) for anisotropic graphite is high due to a high degree of crystal alignment arising from elongated particles of the precursor needle coke.

Coals were selected based on their chemical composition as well as the degree of maturity. PSOC1515 is semi-anthracite and DECS21 is anthracite. Basic characterization of these coals shows that DECS21 has more structural ordering than PSOC1515. TPO, XRD, Raman spectroscopy, and physical characterization show that DECS21 has higher structural ordering than PSOC1515. Demineralization of these anthracites was done to determine the effect of demineralization. Calcination/graphitization of the anthracites produced quality graphites – the best graphites were produced from the demineralized coals, PSOC1515-DM and DECS21-DM. In particular, DECS21-DM made the best graphite, and was expected due to the semi-crystalline nature and the demineralization of the coal. Oak Ridge National Laboratory (ORNL) nuclear graphites were also characterized in a similar fashion to our graphitized samples, as a guide to determine if the graphitized anthracites were of a high enough quality for use as filler in production of nuclear graphites. The TPO and XRD parameters of the anthracites were similar to ORNL nuclear graphites; however, Raman spectroscopy indicated that the I_D/I_G ratios for the ORNL samples were lower, ~0.3-0.5, compared to the graphitized anthracites (~0.6-0.7), therefore, the ORNL samples had fewer defects than the graphitized anthracites. However, the ORNL samples were produced specifically as nuclear graphite, while anthracites would have to go through considerably more processing to produce a graphite. Therefore, demineralized anthracites may well be a very good filler material for nuclear graphite.

GrafTech made graphite artifacts from cleaned Jeddo anthracite and Summit semi-anthracite coals – the coals were different from the original small-scale tests in order to have enough material to produce the artifacts. Compared to anisotropic control graphite, the graphites from

anthracite coals are lower in quality. However, graphites made from anthracite may be useful as a filler for isotropic graphites.

Solvent extracted cokes were also examined as potential filler for production of graphite. XRD, TPO, and Raman data of graphitized cokes indicated they were similar in quality to the anthracites. Therefore, they too may be useful as filler for isotropic graphites.

TABLE OF CONTENTS:

DISCLAIMER	ii
ABSTRACT	iii
INTRODUCTION	1
EXECUTIVE SUMMARY	5
EXPERIMENTAL	7
RESULTS AND DISCUSSION	12
CONCLUSIONS	65
REFERENCES	66

INTRODUCTION

Anthracite is an abundant and inexpensive natural resource that has not been fully exploited as a carbon material. Most anthracites contain 92–98% carbon, virtually all of which is present as aromatic carbon in large polycyclic sheets.¹⁻⁷ These sheets may contain thirty or more fused aromatic rings⁵⁻⁶ that upon processing may result in a graphitic carbon upon thermal annealing. It has been known for many years that anthracites can be used as filler for low-end specialty synthetic graphite^{1-4,8-16} and as a precursor for activated carbons,¹⁷⁻²² and there is continued effort to develop new uses for anthracite. One such potential application is the use of anthracite as a filler for manufacturing nuclear graphite, which is produced from isotropic coke rather than the anisotropic needle coke traditionally used for production of extruded graphite electrodes.

Nuclear graphite is a high-purity graphite that is utilized as a moderator and structural component in nuclear reactors. During nuclear fission, neutrons are produced as the uranium is bombarded and undergoes fission. To continue the propagation of the reaction, the additional neutrons produced must be “slowed down” enough for capture by ${}_{92}\text{U}^{235}$. The function of the moderator is to slow the neutrons with high kinetic energy to allow for this further fission.^{23,24} Under these conditions, the neutrons impinge on the graphite crystal lattice, displacing carbon atoms from their equilibrium positions. Vacancies arise due to the displaced atoms locating themselves in metastable interstitial positions between the carbon layer planes. The formation of vacancies leads to dimensional changes in the graphite structure and changes in its physical properties.^{24,25} Dimensional changes include initial bulk shrinkage followed by net expansion at low and high neutron fluence, respectively.²⁶⁻²⁹ The lifetime of the graphite is defined by the dose at which the graphite shrinks and expands back to its original value.³⁰ Damage by radiation is dependent on the neutron fluence and irradiation temperature, and graphite resistance to radiation damage and its structural integrity determines its lifetime in the reactor.^{24,28,29,31}

Because of these issues, the graphite structure preferred for nuclear applications is isotropic, because it provides better dimensional stability by attaining uniform thermal shrinkage and expansion in all directions when subjected to irradiation, therefore prolonging its lifetime. Anisotropic graphite has a shorter lifetime due to major changes occurring in the c-direction

relative to the a-direction.³² The CTE ratio ($CTE_{c-axis}/CTE_{a-axis}$) for anisotropic graphite is high due to a high degree of crystal alignment arising from the elongated particles of the precursor needle coke. **Figure 1** shows a schematic of how isotropic anthracite is produced, along with the structural aspects that are needed.³³

The question then becomes, how will the structure of anthracite be amenable to formation of an isotropic graphite, particularly when it has been shown to be useful as a filler material for anisotropic graphite? Anthracite is a non-graphitic carbon; the factors that determine whether it will be a good source are its inherent structure and the processing needed to make an isotropic graphite. Microtexture and texture of anthracite are important parameters that determine the chemical, physical, and optical properties of anthracites. Microtexture is defined by the structure of basic structural units (BSUs). A BSU is made up of a turbostratic two-dimensional arrangement stack of three to five aromatic layers. Basically a BSU is a nanometric polyaromatic material inside the domain of few tens of micrometers in diameter. The BSUs are arranged in many domains with different dimensions and spatial orientation. The collection of domains determines the texture of the anthracite. Aliphatic carbon is said to be either present in a form of cross-links that link aromatic layers of neighboring BSUs or it serves as an interstitial entity, whereby it is found in between the planes within each BSU. The interstitial carbon is attached to the planes using weak van der Waal forces.³⁴ The nature of the BSUs in anthracite, high aromaticity and alignment of planes, suggests anthracite would be a good carbon precursor for graphite. The challenge in anthracite structure transformation to graphite is the removal of aliphatic carbon, perfection of crystallites, attaining a preferred orientation of BSU, and reduction of inorganic residues.

Franklin first classified anthracite as a special non-graphitic carbon that would graphitize upon thermal annealing at temperatures of 1700-2500°C, but also qualified that the inherent structure played a role in its ability to graphitize.^{35,36} As shown in **Figure 2**, if there was already “quasi” alignment in the structure, it would be more amenable to anisotropic alignment, but if the cross-links in the structure were not aligned, the resulting carbon would be isotropic. Oberlin and Terriere graphitized thirteen anthracites and suggested that how well anthracite graphitizes anisotropically depends mainly on pore shape (anthracite with spherical pores would not

graphitize as well as an anthracite with flattened pores) and possibly on the catalytic graphitization (carbide crystal formation and decomposition).³⁷⁻³⁹ Rouzaud et al.⁴⁰ and Cohaut et al.⁴¹ supported the pore shape theory by examining the pore shape and microtexture of anthracites. They found that the weakly graphitizing coals were isotropic with spherical pores and the strongly graphitizing coals were anisotropic with flattened pores. Pusz et al.^{42,43} suggested that anthracite coal has strong potential to make graphitic carbon. They suggest that the assembly of aromatic rings and layers in anthracite structure supports a highly ordered carbon structure as well as high ultra-microporosity pore volume; given this characteristic and its low proportion to aliphatic carbon, anthracite has high potential to becoming graphite when heat treated to graphitization temperatures. They showed that the onset of changes in the structure took place at 1200-1400°C.

Another aspect to anthracite graphitization involves the inherent minerals in anthracite. Evans et al. suggested that minerals may play the dominant role in anisotropic graphite formation from anthracite, using X-ray diffraction (XRD) and transmission electron microscopy (TEM) to monitor the onset of graphitization at 1400°C.⁴⁴ Work by Pappano et al. and González et al. supported the catalysis aspect of this work.^{1-4,13-15} They both report that one of the critical factors in anthracite graphitizing was related to mineral matter content in the coal.^{1-4,13-15} González et al. reported the minerals of illite (clay), ankerite (iron carbonate), and siderite (iron carbonate) were the major contributors to graphite formation.¹⁵ In particular, Pappano et al. reported the silica, iron, and titanium in minerals of the raw coal would form carbides during heating.¹⁻⁴ Pappano's work showed that the best graphitizing anthracite out of the four he studied had a higher percentage of volatile matter (hence a greater amount of "disordered" carbon, ~10% of the organic matter) and a high mineral matter content, particularly silica (18%). Atria took a different approach, by hydrogenating anthracite with hydrogen-donor solvents and suggested this approach increased the available carbon by hydrogenating and liquefying fragments of the anthracite.^{9,10}

This leads to two fundamental problems that need to be solved in order for anthracite to be used commercially. First, there is still a need to correlate structural features and properties of

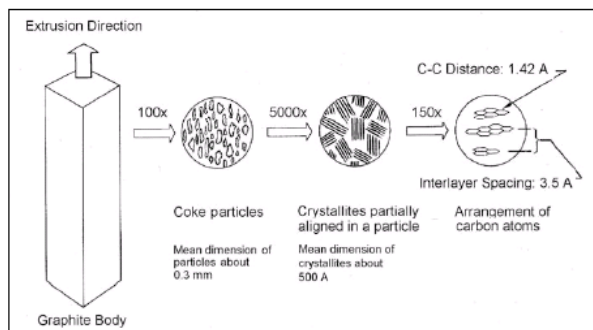


Figure 1: Schematic of isotropic graphite production.

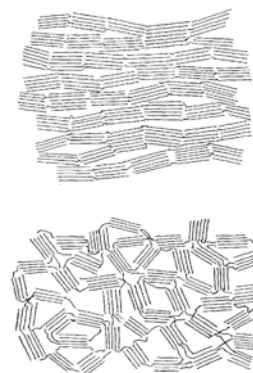


Figure 2: Schematic of anthracite structures as envisioned by Franklin.¹⁵

anthracite to synthetic graphite quality produced from anthracite, either for anisotropic or isotropic graphite. Second, we need to determine if any pretreatment is necessary to produce a good filler for isotropic graphite from anthracite.

The two main objectives for this project are: 1) to compare anthracites using numerous techniques in order to identify the best coal for use as filler for nuclear graphite and 2) to explore various pretreatments of the anthracite to produce a high-quality nuclear graphite. In order to accomplish these objectives, the following three tasks were established for the project: 1) characterization of raw coals using XRD, TEM, small-angle X-ray scattering (SAXS), pore size distribution, temperature programmed oxidation (TPO), and Raman spectroscopy to select anthracites that may be amenable to formation of isotropic graphite, 2) pretreatment of raw anthracites and characterization of the resulting products for comparison (this included heat treatment under pressure and removal mineral matter), and 3) produce synthetic graphite with particular pretreated coals to determine if a high quality nuclear graphite will be produced. This will lead to: 1) possibility of correlation between coal properties and graphitized anthracite quality, 2) production of quality nuclear graphite from anthracite, and 3) understanding of how isotropic graphitization will differ from anisotropic graphitization mechanistically.

The financial justification of the project to produce nuclear isotropic graphite from anthracite coal since isotropic graphite is more valuable than specialty anisotropic graphite. Nuclear

graphite could sell at five times the value of electrode graphite, while anthracite is less expensive than the typical graphite filler, petroleum coke. Successful graphite production depends on identification of anthracites that would be more amenable to producing anisotropic versus isotropic graphite. The use of traditional and non-traditional analytical techniques is essential to identify the best anthracites.

The report has been organized in the following manner:

1. The introduction and experimental sections are written to cover the entire report, as both sections refer to all aspects of the project.
2. The results/discussion/conclusions will be divided up into 3 parts
 - A. Small scale calcination/graphitization of two anthracite coals: The effect of anthracite structure on resulting graphite
 - B. Large scale calcination/graphitization of two anthracite coals: Generation of artifacts using anthracite coals for coefficient of thermal expansion determination
 - C. Calcination/graphitization of delayed coker cokes produced from feed generated by solvent extraction of coal

EXECUTIVE SUMMARY

Anthracite is an abundant and inexpensive natural resource that has not been fully exploited as a carbon material. It has been known for many years that anthracites can be used as filler for low-end specialty synthetic graphite and as a precursor for activated carbons, and there is continued effort to develop new uses for anthracite. One such potential application is the use of anthracite as a filler for nuclear graphite, which is produced from isotropic coke rather than the anisotropic needle coke traditionally used for graphite electrode manufacture.

Nuclear graphite is a high-purity graphite utilized as a moderator and structural component in nuclear reactors. The function of the moderator is to slow the neutrons with high kinetic energy, reducing their kinetic energy to a range that allows for further fission. Dimensional changes occur from exposure to radiation, and include initial bulk shrinkage followed by net expansion at low and high neutron fluence, respectively. The lifetime of the graphite is defined by the dose at which the graphite shrinks and expands back to its original value. Damage by radiation is dependent on the neutron fluence and irradiation temperature. Graphite resistance to radiation damage and its structural integrity determine its lifetime in the reactor. Because of these issues, the graphite structure preferred is isotropic, because it provides better dimensional stability by attaining uniform thermal shrinkage and expansion in all directions when subjected to irradiation, therefore prolonging its lifetime. Anisotropic graphite has a shorter lifetime due to major changes occurring in the c-direction relative to the a-direction. The CTE ratio (CTE_c .

α -axis/ $\text{CTE}_{\alpha\text{-axis}}$) for anisotropic graphite is high due to a high degree of crystal alignment arising from elongated particles of the precursor needle coke.

The question then becomes, how will the structure of anthracite be amenable to formation of an isotropic graphite, particularly when it has previously been shown to be a suitable filler for anisotropic graphite? Answering this question leads to two fundamental problems that need to be solved in order for anthracite to be used commercially in this application. First, there is still a need to correlate structural features and properties of anthracite to synthetic graphite quality produced from it, either for anisotropic or isotropic graphite. Second, most likely pretreatment of the anthracite will be needed to produce isotropic graphite.

Coals were selected based on their chemical composition as well as the degree of maturity. PSOC1515 is semi-anthracite and DECS21 is anthracite. Basic characterization of these coals shows that DECS21 has more structural ordering than PSOC1515. TPO, XRD, Raman spectroscopy, and physical characterization show that DECS21 has higher structural ordering than PSOC1515. Demineralization of these anthracites was done to determine the effect of demineralization. Calcination/graphitization of the anthracites produced quality graphites – the best graphites were produced from the demineralized coals, PSOC1515-DM and DECS21-DM. In particular, DECS21-DM made the best graphite, and was expected due to the semi-crystalline nature and the demineralization of the coal. Oak Ridge National Laboratory (ORNL) nuclear graphites were also characterized in a similar fashion to our graphitized samples, as a guide to determine if the graphitized anthracites were of a high enough quality for use as filler in production of nuclear graphites. The TPO and XRD parameters of the anthracites were similar to ORNL nuclear graphites; however, Raman spectroscopy indicated that the I_D/I_G ratios for the ORNL samples were lower, $\sim 0.3\text{-}0.5$, compared to the graphitized anthracites ($\sim 0.6\text{-}0.7$), therefore, the ORNL samples had fewer defects than the graphitized anthracites. However, the ORNL samples were produced specifically as nuclear graphite, while anthracites would have to go through considerably more processing to produce a graphite. Therefore, demineralized anthracites may well be a very good filler material for nuclear graphite.

GrafTech made graphite artifacts from cleaned Jeddo anthracite and Summit semi-anthracite coals – the coals were different from the original small-scale tests in order to have enough material to produce the artifacts. Compared to anisotropic control graphite, the graphites from anthracite coals are lower in quality. However, graphites made from anthracite may be useful as a filler for isotropic graphites.

Solvent extracted cokes were also examined as potential filler for production of graphite. XRD, TPO, and Raman data of graphitized cokes indicated they were similar in quality to the anthracites. Therefore, they too may be useful as filler for isotropic graphites.

EXPERIMENTAL

Procurement of Feedstocks

Four anthracite coals were selected for this project. All were obtained from the Penn State Coal Sample Bank. Two were selected to ensure differences in structure and were used in small-scale experiments (PSOC-1515 and DECS-21). Two others were selected to send to GrafTech for coefficient of thermal expansion (CTE), as 1.5 kg of coal was needed to produce test artifacts after demineralization and sizing; Jeddo and Summit anthracite coals were selected and used for this aspect of the project. Characterization data will be presented in the appropriate sections.

Three cokes produced from coking of solvent extracted coal were also calcined and graphitized.⁴⁷ Details related to the extraction and coking have been discussed in a CPCPC final report for the project “Solvent extraction of coal to produce feedstock for a laboratory scale coker.”⁴⁷ Briefly, Western Kentucky #6 coal was extracted with a Conoco-Phillips decant oil – approximately 50% of the coal was extracted, and ~15% of the total recovered liquid was coal-derived. The coal-based liquid was fed into a delayed coker: Run #142 used only decant oil as feed, Run #143 used coal extract, and Run #144 used coal extract plus a cracking catalyst that was fed inside the coker. Coke yields were ~25-33%. Details about characterization of the coke product and calcined/graphitized cokes will be included in the appropriate section.

Demineralization

The demineralization of the coals was done via a series of acid treatments to remove mineral matter inherently present in coal.⁴⁸ Eighteen grams of each coal was mixed with 120 ml of 6 M hydrochloric acid (HCl) in a 300 ml Nalgene beaker. The mixture was heated via the use of a water bath at 60 °C and kept at that temperature for one hour, while stirring every five minutes. The mixture was then left undisturbed for 24 hours. The acid was then decanted, the residue was centrifuged, and the acid further decanted. The residue was washed with de-ionized water until the water became neutral and then vacuum filtered using a grade 41 mesh ashless filter paper from Whatmann (Porosity: Coarse, Flow rate: Fast, Particle retention: 20-25 micrometer). To remove the iron content present in the form of pyrites (iron sulfide), the recovered residue was mixed with 135 ml 6 N nitric acid (HNO₃), and treated using the same procedure used for HCl treatment. The coal sample was then recovered and mixed, in a Nalgene beaker, with 120 ml of

47-52 % hydrofluoric acid (HF) for removal of silicon-based impurities. The beaker was secured on a stirring plate and a plastic-covered stirring magnet was placed in the acid/anthracite mixture. The stirring plate was set at a level where good mixing was achieved without causing any splashing of HF. The mixture was stirred for 24 hours. Following the HF treatment, the solution was again centrifuged and the acid decanted. As with the HCl treatment, the remaining mixture was vacuum filtered and the coal sample was recovered. Throughout this report the demineralized anthracites have their names suffixed with -DM.

Heat treatment

The structure of the BSU and rearrangement of the BSUs domains can be attained by thermal treatment of anthracites.^{42,43} The early work on graphitization of anthracites at graphitization temperatures was done by Franklin.^{35,36} She concluded that anthracites behave like hard-carbon (non-graphitizable carbon) at temperatures below 2000°C, whereas at temperatures above 2500°C anthracites behave like soft carbons (graphitizable carbons). Like non-graphitizing carbons, anthracites experience a decrease in microporosity when heat-treated at graphitization temperatures. The orientation, shape, and sizes of pores in the anthracite structure are now understood as main players in the transition from hard carbon to soft carbon that was observed by Franklin. Following the work of Franklin, various researchers have studied different aspects of anthracite graphitization.^{13,37,44,45} As discussed in the introduction, literature shows that factors that affect the degree of graphitization of anthracites are: cross-links, porosity, nature of microtexture and texture, and in-situ catalysis.

The heat treatments were performed in vertical microautoclave reactors, commonly referred to as tubing reactors. These tubing reactors have a nominal capacity of 25 mL. The reactors are constructed of type 316 stainless steel. Five grams of each coal were loaded into tubing reactors. The tubing reactors were then sealed and pressurized at 1000 psi with nitrogen gas in order to test for leakage. The tubing reactors were then purged three times with nitrogen gas in order to remove air. The tubing reactors were sealed at atmospheric pressure prior the reaction. The tubing reactors were immersed in a sand bath that had been pre-heated to 500 °C. The tubing reactor was kept at the reaction temperature (500 °C) for 18 hrs. The pressure of the reaction was autogenous, as a result the pressure increased to about 400 psi. At the end of the reaction time,

the tubing reactors were quenched in cold water and then the samples were collected and stored in a dessicator. The reactions were carried out in duplicates in order to ensure reproducibility. The heat-treated samples of PSOC1515 and DECS21 have an H added as a prefix to the original labels and are named HPSOC1515 and HDECS21, respectively.

Graphitization of small samples

Small samples were placed into graphite capsules and then inserted inside a high-temperature tube furnace that was purged continuously with argon. The weight of each sample was recorded. The samples were heated at $\sim 200^{\circ}\text{C}/\text{h}$ to 1420°C and held at 1420°C for 1 h – the samples were then allowed to cool overnight to ambient temperature. The “calcined” samples were weighed to determine “calcine coke” yield. Each sample was divided in half in order to keep a calcined sample and to have an additional sample for graphitization. The calcined sample (for graphitization) weight was recorded. The calcined samples were then graphitized to just above 3000°C over 24 h, then allowed to cool to ambient temperature. The graphitized samples were weighed to determine “graphite” yield.

Graphitization of large samples

Larger artifacts (for graphitization) were prepared from cleaned anthracite coals in order to determine bulk density, resistivity, and the coefficient of thermal expansion. Several hundred grams of the anthracite coals were placed in individual capsules and the weight recorded. The samples were heated to 1420°C (1 h) at $200^{\circ}\text{C}/\text{h}$, then allowed to cool to room temperature overnight. “Calcine coke” yield could not be determined because considerable quantities of coal escaped through vent openings – this was not expected because this does not happen with petroleum or pitch coke.

Using a standard mix design, each calcined anthracite was hot-mixed with conventional coal-tar binder pitch and small amounts of extrusion aids. The mixture was cooled slightly and then forced through a die to form 19-mm diameter rods. A control sample was run parallel using standard needle coke as the filler. The green rods were packed in a saggar and baked to over 900°C . After baking, the rods were transferred to a graphite capsule and the inserted inside a

high-temperature tube furnace that was purged continuously with argon. The rods were graphitized to just above 3000°C over 24 h, then allowed to cool to ambient temperature.

Characterization of Feeds, Heat-treated Materials, and Graphitized Materials

Characterization of the anthracites and products were done using ultimate analysis, proximate analysis, pore size distribution, surface area characterization, density, XRD, TEM, SAXS, TPO, and Raman spectroscopy.

Proximate analysis (moisture, volatile mater, ash and fixed carbon) and the ultimate analysis (total carbon, hydrogen and nitrogen) were conducted on a LECO 400 Proximate Analyzer and a LECO CHN 600 Analyzer, respectively. A LECO SC 132 was used to determine the total sulfur content.

The BET surface area, porosimetry, and density were measured using a Micrometrics ASAP 2000 (accelerated surface area and porosimetry) using nitrogen adsorbed at cryogenic temperatures. Adsorption and desorption isotherms were taken at incremental changes in pressure. The Materials Characterization Laboratory provided help in using the instrument.

Samples were analyzed using temperature programmed oxidation (TPO). For TPO analysis, a LECO RC 612 Multiphase Carbon Analyzer was used. In this analysis, the sample is oxidized to carbon dioxide by reaction with ultrahigh purity O₂ in a furnace over a CuO catalyst bed. The deposited metal coupon was heated at a rate of 30 °C/min (in flowing O₂ at a rate of 750 mL/min) to a maximum temperature of 900 °C with a hold period of 6 min at the 900 °C. The resulting carbon dioxide was then quantitatively measured using a calibrated IR detector as a function of the temperature in the furnace.

X-ray diffraction (XRD) was also used in studying the structural developments in the samples. Samples were ground to fine powder using mortar and pestle and then sprinkled on the surface of the quartz zero-background sample holder. The analysis was carried out using PANalytical X'Pert Pro powder diffractometer with X'celerator detector. A Ni-filtered CuK_α radiation produced at 45 KV and 40 mA was used for the analysis. A scan was continuous with a step size

of 0.01 and time per step of 100 seconds. The scan was run from 2θ of 5 to 90° . An external NIST silicon standard was used for correction of instrument broadening. Data acquisition was done using MDI Jade 9 software. Phase identification was carried out using ICDD PDF4 2008 (set 58) database. The interlayer spacing value was calculated using the Bragg equation, $n\lambda = 2d\sin\theta$, where λ is the X-ray wavelength, d is the interlayer spacing and θ is the Bragg angle. The [002] peak, which is located at $2\theta \approx 26^\circ$, is one of the important peaks for studying carbon structural organization and development. The position, intensity and shape of the peak are related to the crystal structure in a carbon material. The crystallite size and length were calculated using the Scherrer equation, $L_c = K\lambda/\beta\cos\theta$, where K is the shape factor, λ is the X-ray wavelength, β is the line broadening at half the maximum intensity (FWHM), and θ is the Bragg angle.

The Raman spectrum was recorded using the XY Raman spectrometer, with a polarized laser light at 488 nm wavelength. The spectrum was recorded in a backscattering configuration under the confocal WITec microscope attached to the instrument, using a 40- x objective. Five seconds integration was carried out over five minutes with two repetitions. The CCD camera was used for recording the spectra.

In order to study the elemental identification in the samples, scanning electron microscopy equipped with energy dispersive spectroscopy (SEM/EDS) was used to detect and semi-quantify the elements. The Hitachi S-3500 N VP SEM with PGT Princeton Gamma-tech Prism digital spectrometer was used for the analysis. The samples were ground to powder and then dispersed on a copper tape placed on a Hitachi sample holder. The sample was then inserted in the equipment. Then the instrument was set to achieve vacuum. The sample was probed at 90 magnifications for both texture and elemental identification. Various regions of the samples were probed in order to ensure fair sample representation.

Transmission electron microscopy (TEM) was performed using a JEOL 2010 LaB6 transmission electron microscope operated at 120 KeV, with a point-to-point resolution of approximately 0.23nm. High-resolution images were taken on varied magnification on a negative film in the vicinity of the optical defocus. The CCD camera was used for recording the images, and the

photographs were taken at various regions of the sample in order to have a general view of the sample structure.

Small angle x-ray scattering (SAXS) is used in studying both amorphous and crystalline materials. The sample was irradiated with x-rays, and the elastic scattering of x-rays by the sample that has inhomogeneity in the nm range is recorded at low angles, such as 0.1 to 5°. It provides information about the microstructure of regions with electronic density contrast. It also provides information on pore sizes, shapes and volumes. SAXS plots are normally presented in a form of scattering intensity as a function of the magnitude of the scattering vector, $q = 4 \pi \sin(\theta) / \lambda$. Samples were powder loaded in cell with Kapton windows, and run on the Molecular metrology with a 1.5 meter pinhole camera. The irradiation source used for the analysis was CuK_α . Background and empty cell subtraction were done on the obtained data. Transmission correction was applied before using the data for curve plotting.

RESULTS AND DISCUSSION

The report has been organized into three sections based on three aspects done during the course of the project.

A. Small scale calcination/graphitization of two anthracite coals: The effect of anthracite structure on resulting graphite

Characterization of Anthracites DECS21 and PSOC1515

Proximate and Ultimate Analysis of Raw, Demineralized, and Heat-treated Anthracite Coals

The selection of coals for this study was based on a generally accepted concept that the properties of the precursor material determine the properties of the final product and its potential use. Therefore the two anthracite coals were selected because it was expected the coals would be slightly different in carbon structure and maturity. PSOC1515 is semi-anthracite in rank, whereas DECS21 is anthracite. Both PSOC1515 and DECS21 were provided by Penn State Coal Sample Bank. PSOC1515 was collected from Penn Semi-anthracite C seam, in Sullivan county PA. DECS21 was collected from Lykens Valley No. 2 seam, in Columbia county PA. **Table 1** shows the results of ultimate, proximate, and petrographic analysis. DECS21 has a higher fixed carbon

content (84.34%) than PSOC1515 (62.39%). The ash content of DECS21 is relatively lower (11.15%) compared to the ash content of PSOC1515 (29.17%). Since nuclear graphites are typically high purity carbons, these ash contents are high; they will probably form residual metals in the resultant graphite if not removed prior to graphitization. Therefore, the anthracites were demineralized, which will be discussed in subsequent paragraphs. The goal of demineralization is to ensure high purity in resulting graphites; it is also expected that demineralization will prevent in-situ catalytic graphitization, which enhances the formation of anisotropic graphite.

Table 1: Properties of raw DECS21 and PSOC1515.

Analytical Procedure	Lyken Valley #2 DECS21	C Seam Semi-anthracite PSOC1515
Proximate Analysis: (dry)		
Fixed Carbon, %	84.34	62.39
Volatile Matter, %	4.51	8.44
Ash, %	11.15	29.17
Ultimate Analysis: (dry)		
Carbon, %	80.26	62.38
Hydrogen, %	3.56	2.77
Nitrogen, %	0.71	0.80
Sulfur, %	0.50	0.58
Oxygen, % (diff.)	3.82	4.30
Ash Mineral Composition:		
Silicon Dioxide, %	55.1	55.3
Aluminum Oxide, %	30.7	33.7
Ferric Oxide, %	4.24	2.57
Titanium Oxide, %	2.27	1.77
Phosphorus Pentoxide, %	0.04	0.13
Calcium Oxide, %	0.56	0.25
Magnesium Oxide, %	0.88	0.81
Sodium Oxide, %	0.22	0.35
Potassium Oxide, %	4.93	4.05
Sulfur Trioxide, %	0.20	0.10
Organic Petrography: (volume %)		
Total Vitrinite	87.1	90.5
Total Liptinite	0.0	0.0
Total Inertinite	12.9	9.5

Each coal sample was demineralized according to the procedure by Bishop⁴⁸ discussed in the experimental section. Proximate analysis indicates that PSOC1515 (ash content 29.17 wt. %) was demineralized to 1.92 wt % ash and DECS21 (ash content 11.15 wt %) was demineralized to 0.62 wt % ash. Demineralization caused an increase in volatile matter loss.

Heat treatment of the coals to 500°C seems to have caused raw coals to have a higher percentage of volatile matter, but heat treatment of the demineralized coals seems to have caused the carbon in the coals to become a little more stable.

Table 2: Proximate analysis of raw and demineralized anthracites, before and after heat treatment at 500°C.

Sample	Status	Fixed carbon, %	Volatile matter, %	Ash, %
PSOC-1515	Raw	62.39	8.44	29.17
HPSOC-1515	Heat-treated	55.45	15.82	28.34
PSOC1515-DM	Demineralized	64.51	33.57	1.92
HPSOC1515-DM	Heat-treated. Demineralized	79.22	15.77	5.00
DECS-21	Raw	84.34	4.51	11.15
HDECS-21	Heat-treated	71.88	16.74	10.165
DECS21-DM	Demineralized	77.22	22.16	0.62
HDECS21-DM	Heat-treated, Demineralized	84.81	12.86	2.32

Temperature Programmed Oxidation of Raw, Demineralized, and Heat-treated Anthracite Coals

TPO provides direct measurement of the amount of carbon gasified as a function of temperature. The evolution of CO₂ peaks at different temperatures during the temperature programmed analysis demonstrates the difference in reactivity of carbon species in the sample. The difference in reactivity is associated with the difference in structure of carbon species present in a sample. The CO₂ peak is usually expected to shift towards the right as the carbon structure becomes more ordered. The peak appearing at the lower oxidation temperature results from the oxidation of more reactive (less ordered) carbon species, whereas a peak appearing at higher temperature is from less reactive (more ordered) carbon species.^{45, 49}

Table 3 shows the temperature of each peak in the TPO profiles. **Figure 3a** shows the profiles for both anthracites to be within the range of amorphous carbon burn off. Each coal TPO profile shows two peaks; the peak at lower temperature is due to more disordered carbon and the peak at higher temperatures is due to more ordered carbon in the anthracites. The comparison of both profiles show that DECS21 has slightly higher structural ordering than PSOC1515 due to CO₂ signals appearing at higher temperature, indicating less reactivity of DECS21. However, since inherent metals in coals can catalyze oxidation of coal, TPO of demineralized coals may be more insightful. We anticipate that the aromatic layer planes in DECS21 have a better-organized stacking pattern compared to layer planes in PSOC1515. These results show the difference between the maturities of these two anthracites.

Figure 3a shows the profiles for both raw and demineralized anthracites, and peak temperatures are shown in **Table 3**. Both PSOC1515 and DECS21 experience a shift of the peak to the right as a result of demineralization. The demineralization of the anthracites leads to the loss of the metallic elements that catalyzes the oxidation of carbon in the sample. This leads to the reduction of reactivity of the anthracites. Even under demineralization, DECS21 still has a more ordered carbon structure than PSOC1515. The profile for DECS21 shows that its peaks are at higher temperatures than peaks for PSOC1515. This is the case at both raw and demineralization states.

The profiles for heat-treated versions show that both anthracites undergo some structural organization on heat treatment at 500 °C, as shown by shift of signals to higher oxidation temperatures in **Figures 3b and 3c and Table 3**. However, both anthracites do not show major changes in their structural ordering upon heating at 500 °C based on TPO observations.

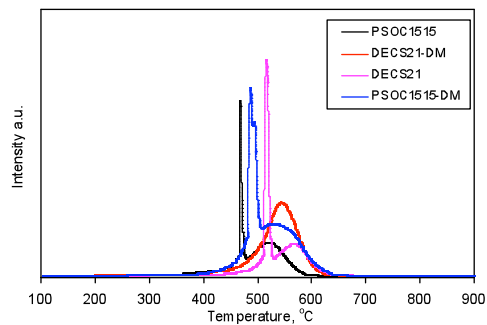
The demineralized anthracites were heat treated in order to understand their response on treatment at temperatures as low as 500 °C, hence have a better understanding of their structure at demineralized state. In previous findings, we reported that both coals at their raw state experience minor changes in their structural ordering when heat-treated at 500 °C. **Figure 3d** shows the TPO patterns of demineralized anthracites and their heat-treated versions. Both coals show an increase in reactivity upon heat treatments, as manifested by a shift of the oxidation peak to lower temperatures. This increase in reactivity when the demineralized anthracites are

heat-treated can be explained in ash content terms. **Table 2** shows the ash content of demineralized anthracites and their heat-treated versions. The ash content of DECS21-DM is 0.62 %, whereas upon heat-treatment it is 2.32 %. The ash contents for PSOC1515 are 1.92 % and 5.0 % on demineralization and heat-treatment, respectively. The increase in ash content on heat-treatment of demineralized anthracites is thought to be due to a loss of carbon in a form of low molecular weight hydrocarbon gases during the reaction. This is thought to be aliphatic chains linked to the aromatic structure. As a result the percent of ash content increases on heat-treatment, possibly because little of the inorganic elements are lost at this temperature.

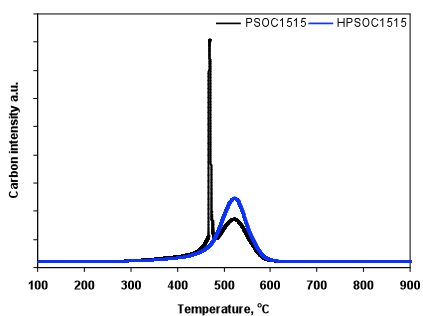
Table 3: Peak Temperatures for TPO Samples

Samples	Sample Status	Peak Temperatures			
PSOC1515	Raw			475	510
HPSOC1515	Heat-treated				510
PSOC1515-DM	Demineralized			490	525
HPSOC1515-DM	Heat-treated, Demineralized	350	390	410	490
DECS-21	Raw			505	580
HDECS-21	Heat-treated			510	580
DECS21-DM	Demineralized				560
HDECS21-DM	Heat-treated, Demineralized		430	510	

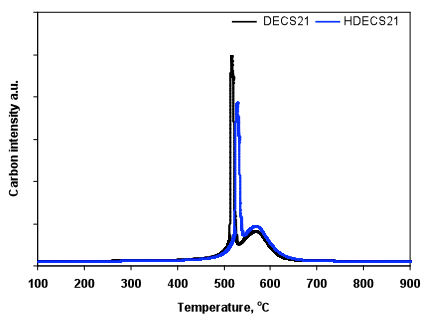
a) TPO of PSOC1515, PSOC1515-DM, DECS21, DECS21-DM



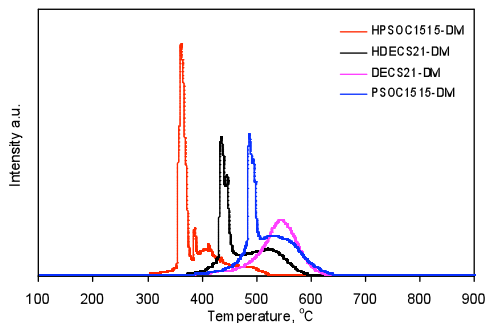
b) TPO of PSOC1515, HPSOC1515



c) TPO of DECS21, HDECS21



d) TPO of PSOC1515-DM, HPSOC1515-DM, DECS21-DM, HDECS21-DM

**Figure 3:** TPO of raw, demineralized, and heat-treated (500°C) samples

SEM/EDS of Raw and Demineralized Anthracite Coals

In order to establish changes in elemental composition, SEM/EDS was performed; the data are shown in **Table 4**. This technique is used for elemental identification in material science studies. It has an advantage of scanning a broad area on the sample, hence a fair representation of the sample. It has a detection limit of about 1000 ppm; as a result, any of the elements that are of lower concentration than 1000 ppm are not detected. In this technique, the sample is bombarded with the electron beam, x-rays are emitted from the sample, and the energy of each x-ray is characteristic of the element from which it was emitted. Although this technique can be used with confidence qualitatively, it is a semi-quantitative technique that can provide a rough view of elemental changes. **Table 4** lists the elements that are present in demineralized anthracites and their heat-treated version, as determined using SEM/EDS. It can be seen from the table that the percentage of carbon elements decreases upon heat treatment. It is also apparent that the heat-treated sample contains the element iron, which is not detected before heat-treatment. The presence of iron is attributed to possible reactor contamination. This leads to a sudden increase in ash content. The copper element shown in HPSOC1515-DM is due to the copper tape that was used for EDS analysis.

Table 4: Elemental composition, in percentages, of demineralized anthracites

Element	C	Al	S	Cl	Ti	Ni	Si	Fe	O	Cu	Total
DECS21-DM	80.1	1.4	3.5	9.1	3.4		1.2				99.0
HDECS21-DM	71.8	1.1	3.6	6.6	1.2	3.7	0.1	10.0	1.5		100
PSOC1515-DM	78.6	1.2	3.1	8.6	2.6		2.3		3.2		100
HPSOC1515-DM	69.6	3.0	3.0	4.7	1.8			13.0		4.61	99.9

X-ray Diffraction of Raw, Demineralized, and Heat-treated Anthracite Coals

XRD was used in order study the extent of crystallographic arrangement as well as identification of phases in raw, demineralized, and heat-treated anthracites.

Figures 4a1 and 4a2 show the XRD patterns of raw and demineralized versions of DECS21 and PSOC1515, respectively. Raw DECS21 and PSOC1515 have many peaks throughout the XRD pattern indicating various mineral phases present in each coal. However, the demineralized

versions, for both coals, have much cleaner patterns. **Table 5** lists the phases identified in both raw coals.

Table 5: Minerals identified in XRD of coals

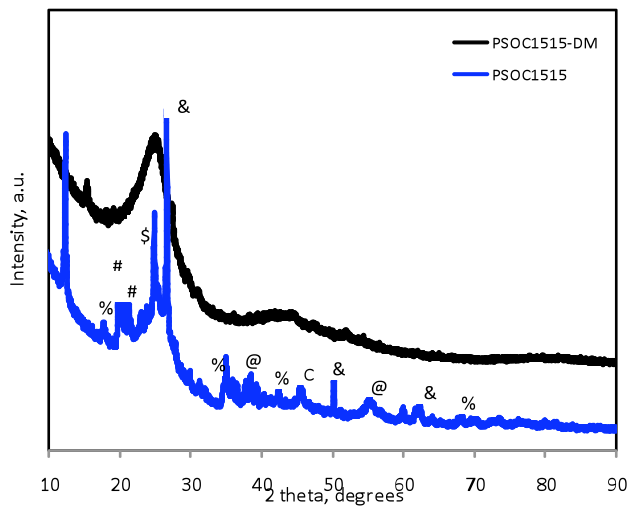
Symbol	Mineral	Reference number and Chemical formula
*	Muscovite-3T	99-000-2554 $KAl_2(Si_3Al)O_{10}(OH, F)_2$
#	Kaolinite 1A	01-078-1996 $Al_2(Si_2O_5)(OH)_4$
&	Quartz	98-000-0369 SiO_2
%	Dolomite	00-011-0078 $CaMg(CO_3)_2$
@	Fuchsite	99-000-1267 $K(Al, Cr)_2AlSi_3O_{10}(OH, F)_2$
\$	Nacrite-1Md	00-029-1488 $Al_2Si_2O_5(OH)_4$

The most obvious peak is the quartz peak that is located at $2\theta=26.68^\circ$. Upon demineralization, the quartz peak and other inorganic peaks identified are largely diminished, indicating the removal of this mineral during demineralization, or reduction beyond detection on XRD analysis. Both raw coals show the weak and broad carbon [002] peak located at 2θ of about 26° . For both coals profiles, the [002] peak is broad and short in intensity. The XRD diffraction parameters are shown in **Table 6**. There is a slight reduction in the interlayer spacing of the [002] peak upon demineralization experiments. Demineralized anthracites also have larger crystallite sizes than raw anthracites. Both parameters, interlayer spacing and crystallite size, either imply improvement on the structural ordering upon demineralization or less interference from minerals. This is in agreement with TPO results.

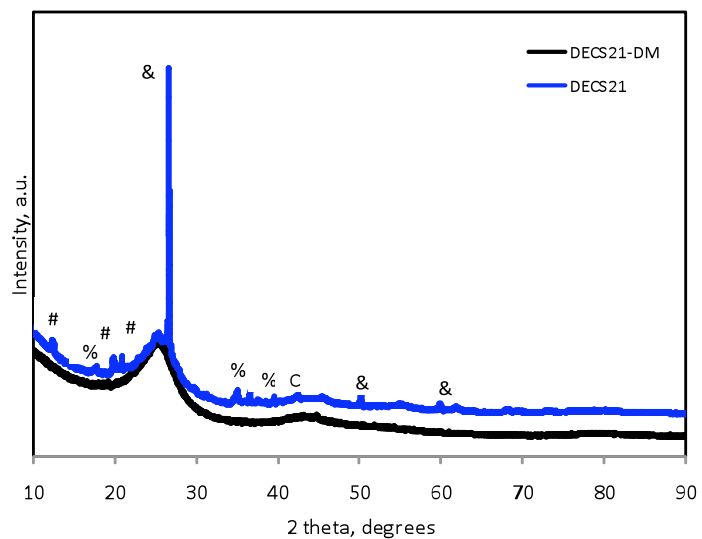
Table 6: XRD and Raman parameters of coals

Sample	Status	d-spacing (Å)	L_c (Å)	I_D/I_G
PSOC1515	Raw	3.5226	14	0.75
HPSOC1515	Heat-treated	3.5190	19	0.68
PSOC1515-DM	Demineralized	3.5211	28	0.81
HPSOC1515-DM	Heat-treated. Demineralized	3.5239	21	0.75
DECS-21	Raw	3.5210	17	0.74
HDECS-21	Heat-treated	3.5168	31	0.68
DECS21-DM	Demineralized	3.4984	31	0.77
HDECS21-DM	Heat-treated, Demineralized	3.5149	24	0.72

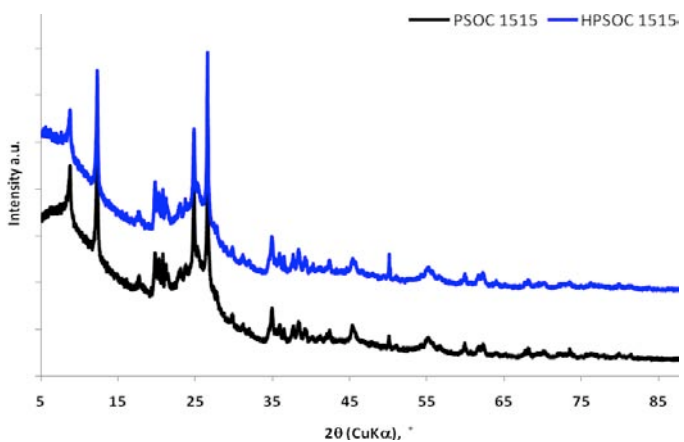
a1) XRD of PSOC1515, PSOC1515-DM and



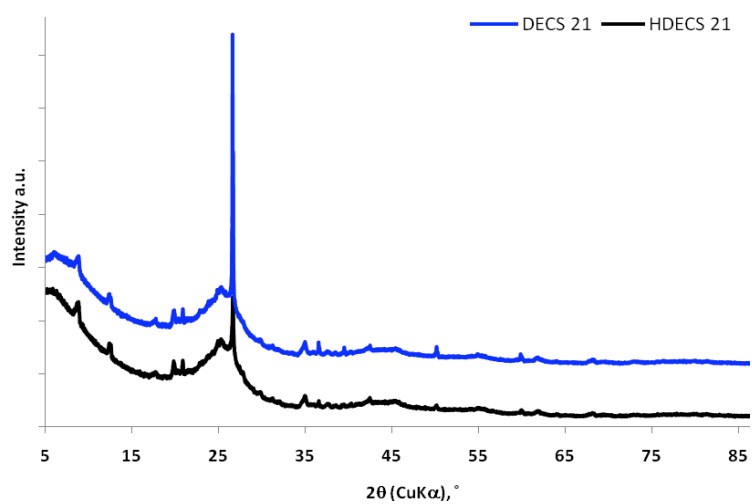
a2) DECS21, DECS21-DM



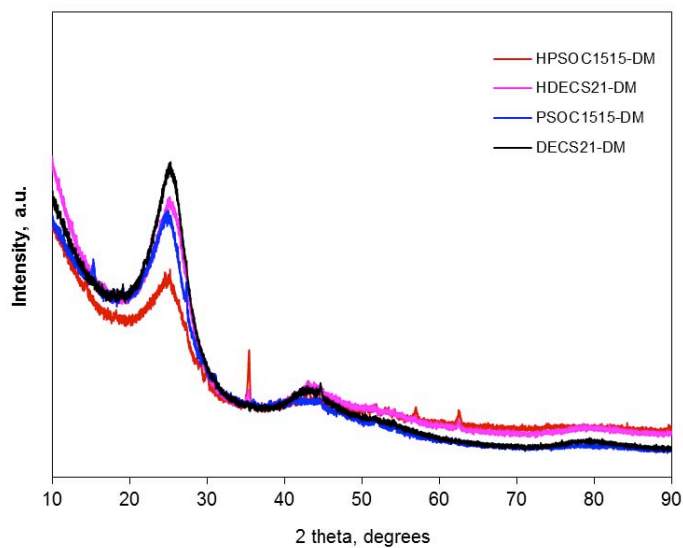
b) XRD of PSOC1515, HPSOC1515



c) XRD of DECS21, HDECS21



d) XRD of PSOC1515-DM, HPSOC1515-DM, DECS21-DM, HDECS21-DM

**Figure 4:** XRD of raw, demineralized, and heat-treated (500°C) samples

Figures 4b and 4c show the comparison of raw and heat-treated versions of PSOC1515 and DECS21, respectively, and **Table 6** has the d_{002} and L_c for the heat-treated coals as well. Both spectra do not appear to show any difference in the profiles of raw and heat-treated anthracites; however, there are slight differences in d_{002} and L_c ; the low temperature heat treatment causes the anthracite to become slightly more ordered. Additional characterization techniques may also reflect subtle differences in density and pore structure.

The XRD patterns of demineralized anthracites and their heat-treated versions are shown in **Figure 4d**. All patterns have a fairly visible, yet broad [002] peak. PSOC1515 experiences more ash content increase than DECS21 on heat treatment. Heat-treated anthracites experience a loss of carbon, and an increase in ash content. The inorganic matter can cause strain on the crystallographic structure of the heat-treated anthracites, hence a decrease in the carbon peak intensity, and an increase interlayer spacing and decrease in crystallite size as shown in **Table 6**.

Raman Spectroscopy of Raw, Demineralized, and Heat-treated Anthracite Coals

Raman spectroscopy is typically used alongside other techniques in determining the degree of crystallinity in carbon materials. It is used for characterizing a wide range of carbon materials varying from amorphous to highly crystalline structures. The most common signals in carbon materials Raman spectra are D- and G-peaks. The D-peak is located around 1300 cm^{-1} wavenumber and its evolution is associated with the presence of disordered structure, impurities or finite structure in a carbon material. The G-peak is located around 1500 cm^{-1} wavenumber and is associated with the presence of crystalline structure in a carbon material.⁵⁰

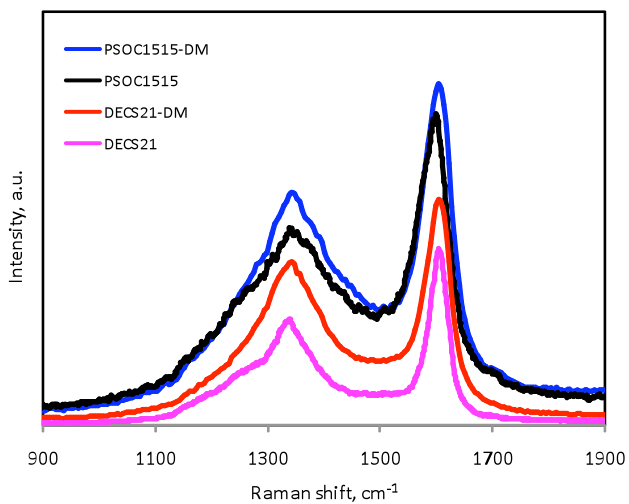
Figure 5 shows the Raman spectra of raw, demineralised, and heat-treated coals. Both coals show the presence of both D and G-peaks. The relative intensity, as given by the ratio of intensity of D- to G- peak, is dependent on the degree of crystallinity. The smaller the ratio, the more organized the structure is. **Table 6** shows the relative intensities of the D- and G-peaks for both raw coals. The relative intensities do not show much difference within the structure of both coals. The difference between raw and demineralized coals is the intensity of the peaks. The variation of the peak intensity is utilized in probing the structural differences between raw and demineralized coals. The most apparent observation is that the demineralized coals have higher

peak intensities than raw anthracites. This is mostly likely an indication of the dominance of carbon structure that is free of minerals. However, the I_D/I_G ratio (**Table 6**) indicated that the carbon in the demineralized samples is slightly more disordered.

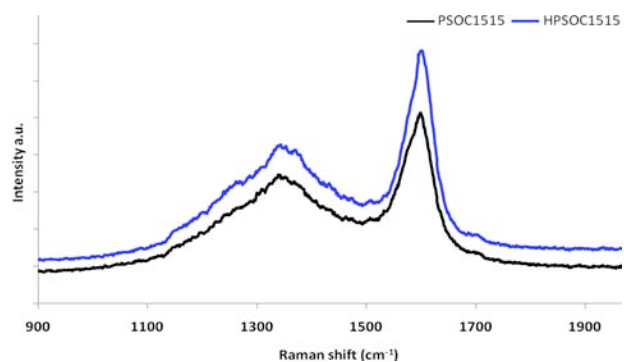
Figures 5b and 5c show raw and heat-treated versions of both coals. Both plots show that heat treatment enhances the intensity of the G-peak over the intensity of D-peak. This is indicated by the smaller relative intensities of heat-treated versions than raw anthracites. This is another indicator that the structural arrangements in these two anthracites can affect the carbon structure at low heat-treatment temperatures.

Figure 5d shows the Raman spectra for the demineralized and heat-treated demineralized coals. As already seen in TPO and XRD analysis, the heat treatment of demineralized anthracites led to a decrease in the structural ordering of both anthracites. The heat-treated demineralized samples have lower peak intensities than unheated samples. However there is a slight decrease in the D-peak intensity on heat-treatment. The I_D/I_G intensity ratio is given in **Table 6**. This is an indication that although both anthracites experience an increase in ash contents during heating, both samples experience a loss of disordered carbon upon heat-treatment. In the characterizations carried out, DECS21 still maintains a higher structural ordering than PSOC1515, with or without minerals.

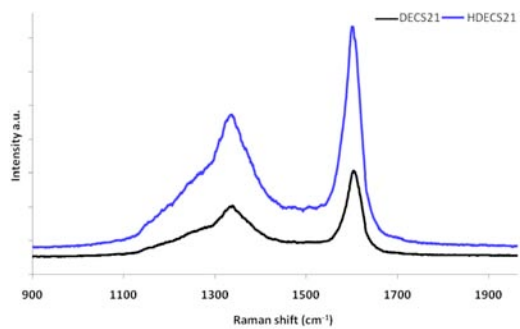
a) Raman spectroscopy of PSOC1515, PSOC1515-DM, DECS21, DECS21-DM



b) Raman spectroscopy of PSOC1515, HPSOC1515



c) Raman spectroscopy of DECS21, HDECS21



d) Raman spectroscopy of PSOC1515-DM, HPSOC1515-DM, DECS21-DM, HDECS21-DM

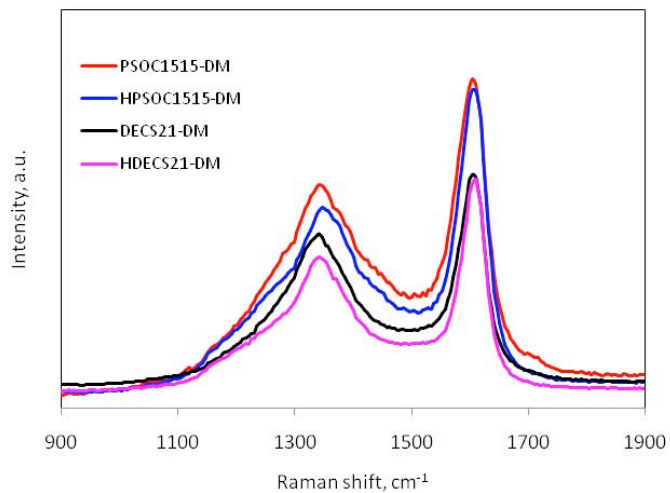


Figure 5: Raman spectroscopy of raw, demineralized, and heat-treated (500°C) samples

TEM and Surface Area Characterization of Raw Coals

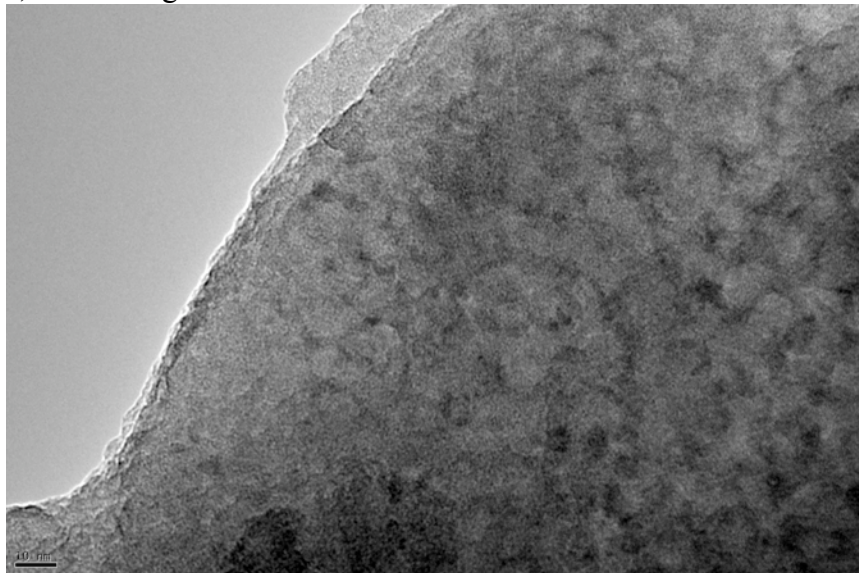
Figure 6 shows the TEM images of PSOC1515 and DECS12. Both samples seem to have coexistence of both lamellar and amorphous carbon, however the lamellar structure in DECS12 is more vivid than in PSOC1515. The PSOC1515 image is largely dominated by amorphous carbon, and has large dark spots. The dark spots are associated with the porosity in the sample. The observed image for PSOC1515 suggests the presence of large pore sizes with a circular shape. It is hard to see the basic structural units in the image, and this is suspected to be due to a lack of ordering in the semi-anthracite. The DECS12 image shows a lamellar texture extending on a long scale, and flat pores between the lamellar structures. The lamellar structure can also be seen as the pore wall. This is because the basic structural units tend to align themselves around the pores, hence a strong presence of lamellar structure with preferred orientation suggest the flattening of pores.¹⁴ However, the DECS12 also shows the presence of some amorphous carbon, and presence of circular pores in the region of amorphous carbon.

The pores in the amorphous carbon are small in size compared to the pores observed in the PSOC1515. This is in agreement with our BET surface area measurements (**Table 7**), that PSOC1515 has larger pore sizes in comparison to DECS12. It is also worth noting that DECS12 has a large percentage of the flattened pores relative to circular pores. It will be interesting to see the extent of pore flattening in both samples after graphitization treatments. These obvious difference in these two anthracites reinforce our prior observation in our previous reports that we are indeed working with two distinctly different anthracites, and it is our hope to come to a conclusion with a better starting point for isotropic graphite in terms of anthracite maturity.

Table 7: Data obtained from surface area characterization.

Sample	BET Surface Area (m ² /g)	Total Pore Volume (cm ³ /g)	Average Pore Size (Å)	Density (g/cm ³)
PSOC-1515	1.162	0.002851	214.3	1.096
HPSOC-1515	1.695	0.002961	183.1	1.205
DECS-21	2.071	0.003916	89.43	1.194
HDECS-21	1.666	0.002701	171.3	1.206

a) TEM image of PSOC-1515



b) TEM image of DECS-12

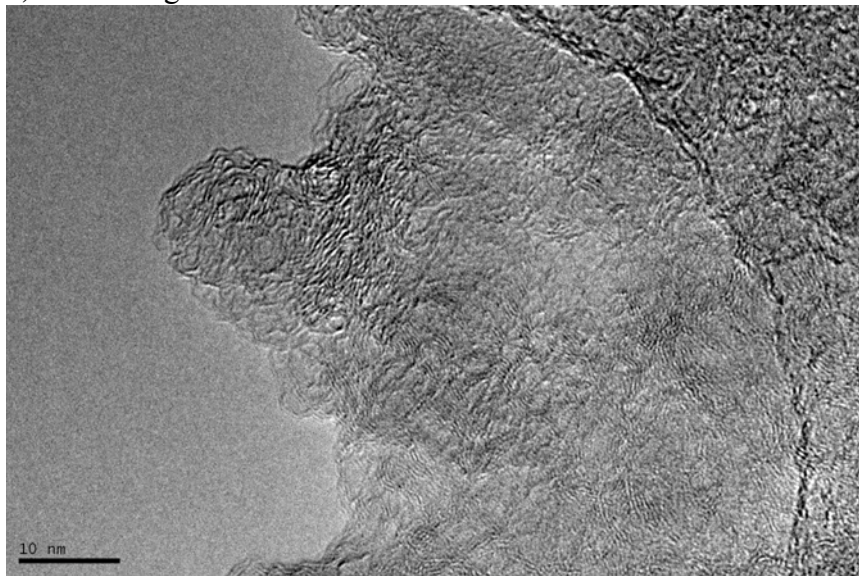
**Figure 6:** TEM of raw coals, to determine pore shape*SAXS of Raw Anthracite Coals*

Figure 7 shows the log-log plots of SAXS intensity curves of raw PSOC1515 and DECS21. The plot does not show any differences in the scattering intensity at q values less than 0.05 \AA^{-1} . At scattering q values higher than that, we observe a difference in the intensity values with DECS21 maintaining a higher intensity than PSOC1515. The shape and the slope of the scattering curve in the Poroid region are dependent on the differences in pore shape and interface properties. This

difference reflects differences in electron densities contrasts or pore volumes found in these two samples. It is thought that the upturn seen in the DECS21 curve suggest more order in lamellae domains found in pore walls than found in the POSC1515 structure.

Given the fact that the instrument used for this analysis can only observe domains in a range of 5 – 60 nm, pore size determination was impossible because the dominant size fraction are outside the low q angle; the sized particles are mostly larger than 60 nm. In order to obtain more information on this data, instrumental calibration would be required.

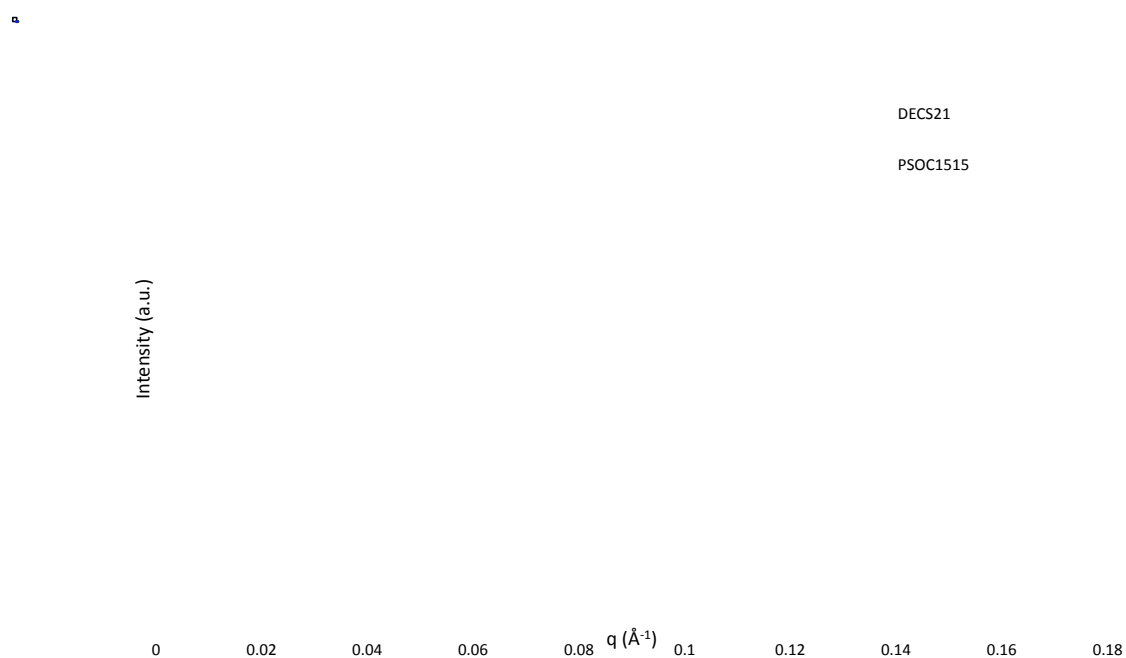


Figure 7: SAXS of PSOC1515 and DECS21 raw anthracite coals.

Summary of data for raw, demineralized, and heat-treated (500°C) PSOC1515 and DECS21 coals

All the characterization done on raw, demineralized, and heat-treated PSOC1515 and DECS21 indicated that DECS21 is a more ordered anthracite coal than PSOC1515; the results confirm that the higher rank coal, DECS21 (anthracite), is more ordered than the semi-anthracite. Proximate analysis, SEM/EDS, and XRD indicated that the process to remove the minerals in the coal was successful. XRD and TPO indicated demineralization of the coals slightly improved the crystallinity of the coals, but Raman suggested that loss of minerals created a slight increase in disorder. Heat-treatment caused some slight increases in carbon crystallinity, but not enough to warrant a change in graphitization behavior. Based on the data, it is expected that the demineralized coals will produce an isotropic graphite.

Characterization of Calcined Anthracite Samples

In graphite synthesis, calcination is a step that is done before mixing the filler coke with the binder. Calcination removes the volatiles from the coke. It is important to note that upon calcination, DECS21 has a higher recovery yield than PSOC1515, in both raw and demineralized anthracites (**Table 8**). This is due to differences in the structural composition and arrangements in the carbon in these two anthracites. It is apparent that the demineralized anthracites have a lower recovery yield than their corresponding raw anthracite. Proximate analyses of the calcined coals (**Table 9**) indicate a significant reduction in volatile matter compared to the raw and demineralised coals, an expected result.

Table 8: Weight changes during *calcination*

Sample	wt before, g	wt after, g	Yield, %
PSOC1515	19.55	15.98	81.74
PSOC1515-DM	10.41	6.96	66.86
DECS21	14.45	12.34	85.4
DECS21-DM	12.45	9.25	74.3

Table 9: Proximate analysis of *calcined* samples

Sample	Status	Moisture %	Fixed carbon, %	Volatile matter, %	Ash, %
PSOC1515	Raw	0.1	64.9	3.0	32.0
PSOC1515-DM	Demineralized	0.2	90.1	7.8	1.9
DECS21	Raw	0.3	85.2	3.3	11.2
DECS21-DM	Demineralized	0	94.0	5.1	0.9

Figure 8 shows the TPO profiles of our calcined anthracites, and **Table 10** shows the peak temperatures. There is a shift to the right in the oxidation peaks when comparing the calcined samples to unheated or anthracites heat-treated at 500 °C (compare to **Figure 3 and Table 3**). Samples heat-treated at 500 °C have an oxidation peak appearing at 640-810°C. This shows that the carbon structure becomes more ordered as the anthracites are calcined. It is interesting that PSOC1515-DM has an intense peak at the lowest oxidation temperature than other samples. This indicates that PSOC1515-DM has a less ordered structure than DECS21-DM.

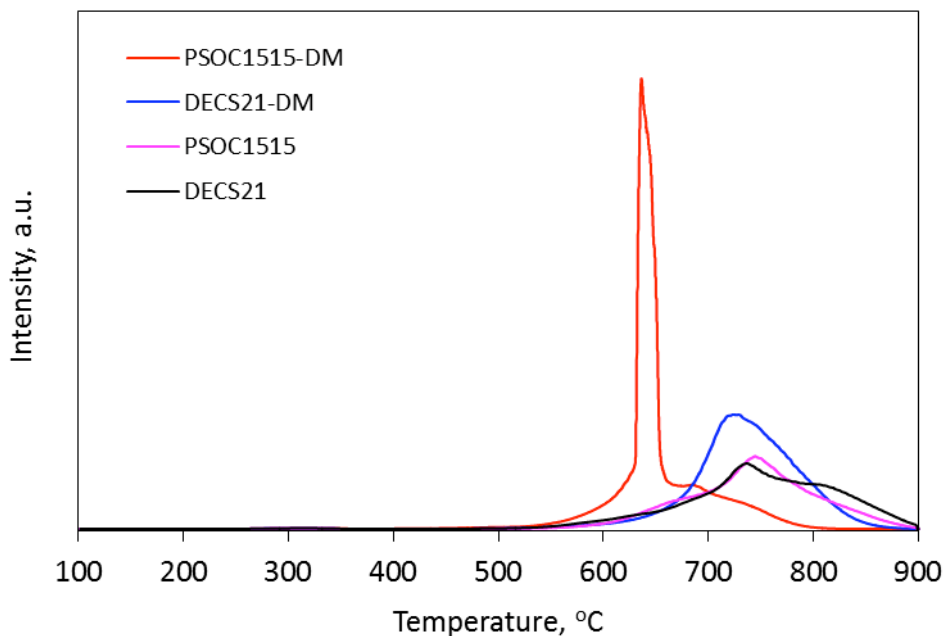
**Figure 8:** TPO of *calcined* (1420°C) PSOC1515 and DECS21 before and after demineralization

Table 10: TPO data regarding peak temperatures for *calcined* anthracite coals

Samples	Sample Status	Peak Temperatures		
PSOC1515	Calcined, Raw			740
PSOC1515-DM	Calcined, Demineralized	640	695	705
DECS-21	Calcined, Raw		735	810
DECS21-DM	Calcined, Demineralized		705	750

Figure 9 shows the XRD profiles of the calcined anthracites. All the samples have the [002] peak located at $\sim 26^\circ$. For the calcined raw samples, the carbon [002] peak is intertwined with the mullite peak. The other obvious observation is that the calcined demineralized samples have much cleaner patterns than their corresponding raw anthracites. The phases identified in the patterns are given in **Table 11**.

There is a dominance of complex carbon and iron minerals combined with aluminium- and silicon-based phases. Since the phases identified in these calcined samples are not present in raw anthracite, they are obviously the result of possible reactions taking place during calcination. Significant phase transitions are said to be occurring at temperatures below 1500°C .⁵¹ In addition, Imperial et al. showed that calcination conducted under chlorination slowly removes minerals that are located in closed pores or within crystals when done at temperatures between 1000 and 1400°C .⁵² It is therefore apparent that aluminium and silicon containing minerals in raw coals undergo some phase transition, leading to the reaction of aluminium and silicon forming the phases shown in **Table 11**. It is also interesting that the silicon carbide peak is identified in the calcined raw anthracites. It has been theorized that silicon carbides decompose to graphitic carbon and free element upon graphitization.^{3,44,45}

As a result of removing minerals, the calcined demineralized anthracites have a slightly higher structural ordering as shown by the larger crystallite size than their corresponding calcined raw anthracite. The interlayer spacing values and crystallite sizes are shown in **Table 12**. Calcined demineralized anthracites also have a more visible peak for the [10] band, which appears at 43° . This peak at graphitization temperature is known to split into [100] and [101] peaks. In terms of [002] peak intensity, interlayer spacing and crystallite size, the carbon in DECS21 appears to be more ordered structurally than PSOC1515, even at the calcinations temperature.

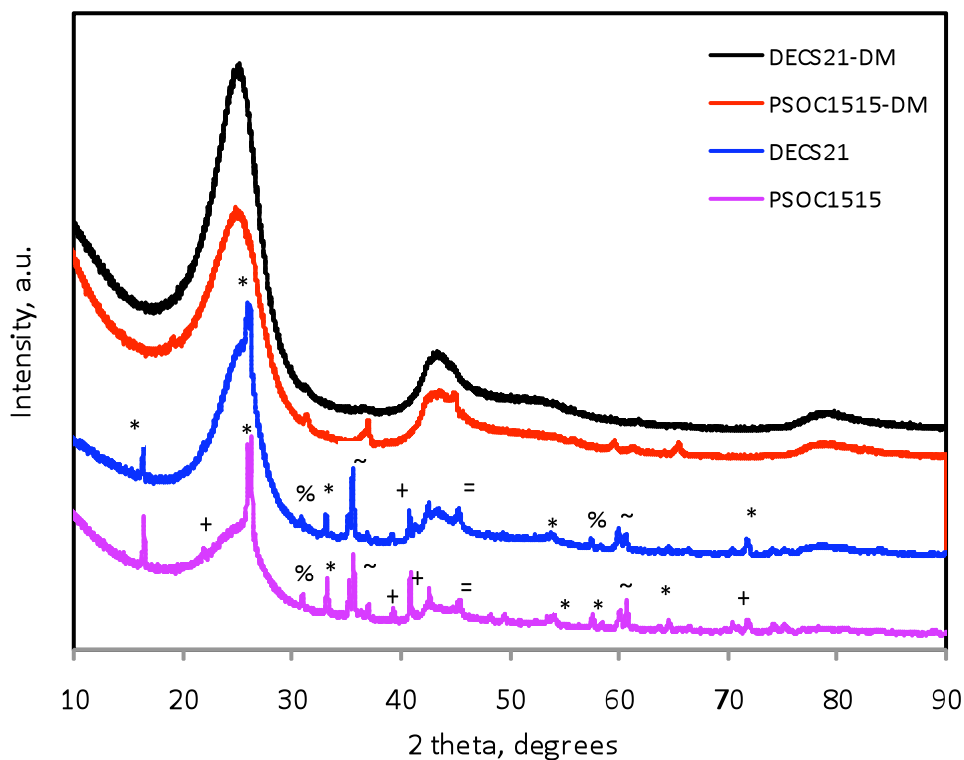


Figure 9: XRD spectra of *calcined* PSOC1515, PSOC1515-DM, DECS21, DECS21-DM.

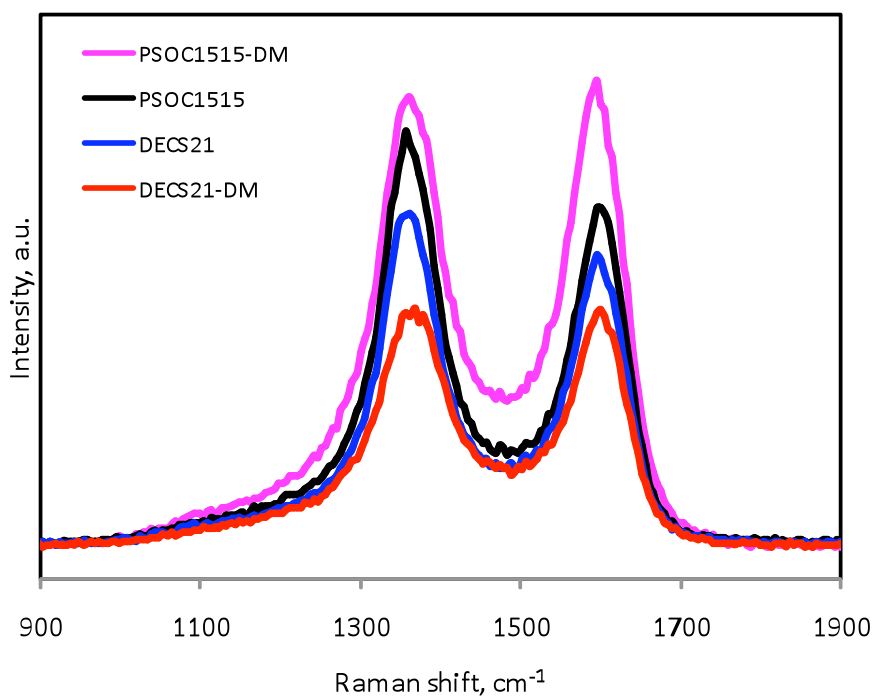
Table 11: Phases identified in *calcined* anthracites

Symbol	Mineral	Reference number and Chemical formula
*	Mullite	97-007-4008 $\text{Al}_2(\text{Al}_{2.5}\text{Si}_{1.5})\text{O}_{2.75}$
+	Aluminium Silicon Oxide	97-015-2983 $\text{Al}_2(\text{Al}_{2.58}\text{Si}_{1.42})\text{O}_{2.71}$
%	Mullite	97-004-3298 $\text{Al}(\text{Al}_{0.82}\text{Si}_{1.08}\text{O}_{4.55})$
=	Iron silicide	97-041-2842 $(\text{Fe}_{2.502}\text{Si})_{1.11}$
~	Molssanite	97-002-8389 SiC

Table 12: Interlayer spacing, crystallite size and Raman intensity ratio of *calcined* anthracites

Sample	d_{002} , Å	L_c , Å	I_D/I_G
PSOC1515	3.4357	28	1.06
PSOC1515-DM	3.4365	36	0.98
DECS21	3.4369	46	1.03
DECS21-DM	3.4053	48	1.00

The calcined anthracites were also characterized using Raman spectroscopy. As already indicated by XRD analysis, the raw anthracites contain inorganic components. This is shown by the D-peak that has a higher intensity than the G-peak, as shown in **Figure 10 and Table 12**. The I_D/I_G ratios for the calcined coals, before and after demineralization, are actually higher than the samples before calcination. Raman spectroscopy indicates that there is more disordered carbon than crystalline carbon, contrary to what the XRD and TPO data suggests (that calcination is beginning to crystallize the carbon in the anthracites). The D-peak is theoretically known to be due to structural defects, finite crystallite size and presence of impurities. It is therefore most likely that high intensity of D-peak in the raw anthracites is probably due to the presence of impurities and the lack of crystallinity in calcined samples.

**Figure 10:** Raman spectra of *calcined* anthracites

Characterization of Graphitized Anthracite Samples

There is an interesting contrast between the weight changes during calcination (**Table 10**) and graphitization (**Table 13**). During calcination, the demineralized anthracites have a lower recovery yield than raw anthracites, whereas in graphitization the demineralized anthracites have a higher recovery yield than the raw anthracites. This is an indication that minerals are lost at graphitization temperatures. However, proximate analysis (**Table 14**) indicates little volatile matter loss once the samples are graphitized, so the produced graphites are fairly stable – PSOC1515 has a slightly higher volatile matter loss than the other samples, so the sample may contain a little more disordered carbon.

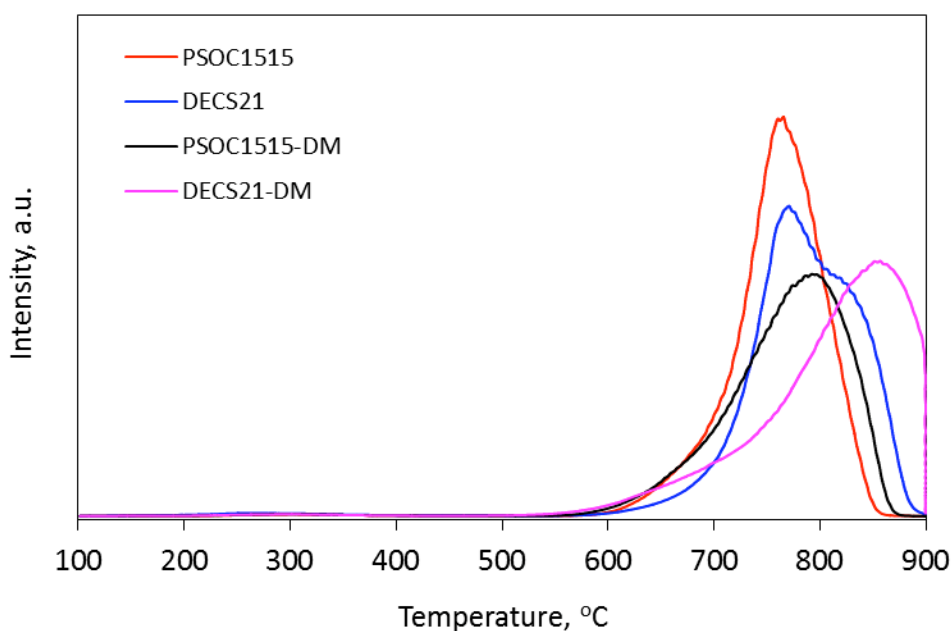
The graphitized samples were characterized using the techniques used for characterization of raw, demineralized, heat-treated and calcined anthracites. **Figure 11** shows the TPO profiles of the graphitized anthracites, and **Table 15** shows the peak temperatures. In comparison to calcined anthracites, the graphitized anthracites have their oxidation peaks appearing at higher temperature. Their peaks appear at 690-800°C, and therefore are considered to be graphitic according to TPO theory.⁴⁹ Graphitized DECS21-DM shows higher structural ordering as shown by its peak at highest temperature. This is indicative of homogeneity in the carbon structure. Graphitized DECS21 has two peaks overlapping, indicating the presence of two carbon species with different oxidation reactivity. The presence of these two peaks is indicative of the coexistence of two crystalline carbons in DECS21. This is important to note since it will be involved in XRD and Raman spectroscopy analysis discussions.

Table 13: Weight changes during *graphitization*

Sample	wt before, g	wt after, g	Yield, %
PSOC1515	8.49	4.74	55.83
PSOC1515-DM	4.2	3.82	90.95
DECS21	5.85	4.89	83.59
DECS21-DM	4.85	4.67	96.29

Table 14: Proximate analysis of *graphitized* samples

Sample	Status	Moisture %	Fixed carbon, %	Volatile matter, %	Ash, %
PSOC1515	Raw	0.2	92.3	7.5	0.0
PSOC1515-DM	Demineralized	0	95.0	4.9	0.2
DECS21	Raw	0	95.9	4.1	0.0
DECS21-DM	Demineralized	0	95.2	4.6	0.2

**Figure 11:** TPO spectra of *graphitized* coals, before and after demineralization**Table 15:** TPO data regarding peak temperatures for *graphitized* anthracite coals

Samples	Sample Status	Peak Temperatures	
PSOC1515	Graphitized, Raw		750
PSOC1515-DM	Graphitized, Demineralized	695	800
DECS-21	Graphitized, Raw	750	810
DECS21-DM	Graphitized, Demineralized	700	850

XRD was used to follow the structural developments in graphitized anthracites. This is a useful technique for determining the degree of graphitization in graphitized samples. **Figure 12** shows the XRD spectra of the graphitized anthracites. All spectra show a sharp, intense and narrow, hence small full width at half maximum (FWHM), for the [002] peak located at 26° . All patterns show the [004] and [110] reflections appearing at 55° and 77° , respectively. According to the spectra, these samples are graphitic since these peaks that are considered to be the signal of three-dimensionality observed in the patterns. Other typical graphitic peaks are: 1) [100] at 42° , 2) [101] at 44° , 3) [004] at 55° , 4) [110] at 77° , 5) [112] at 83° , and 6) [006] at 87° . The presence of [112] band shows a miller index (hkl) with $l \neq 0$, another important peak.¹⁴ **Table 16** lists the XRD parameters. Although the samples are graphitic, it can be seen in **Table 16** that all samples have the interlayer spacing that is larger than the perfect graphite interlayer spacing 3.354 \AA . The interlayer spacing values were used to calculate the degree of graphitization (DOG) using the following formula: $\text{DOG} = (3.440 - d_{002}) / (3.440 - 3.354)$, where 3.440 is the interlayer spacing of carbon with no graphitic order and 3.354 being the interlayer spacing of graphite.

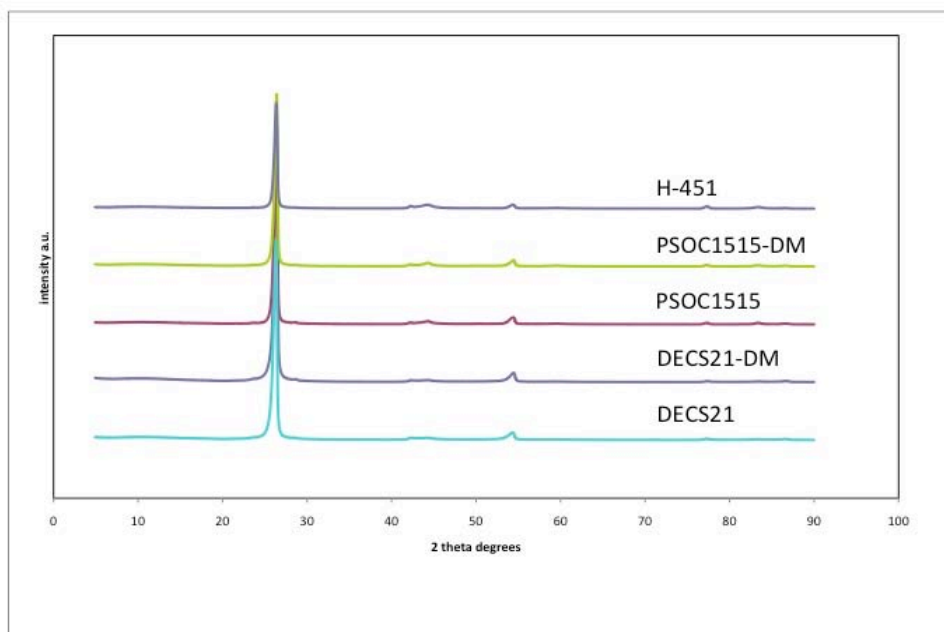


Figure 12: XRD of *graphitized* anthracite coals and nuclear graphite H-451

Table 16: XRD parameters and Raman intensity ratio of *graphitized* anthracites

Sample	d_{002} , Å	Rank	DOG	L_c , Å	Rank	L_a , Å	Rank	I_D/I_G	Rank	Total
PSOC1515	3.3753	3	0.75	195	3	204	1	0.674	4	11
PSOC1515-DM	3.3726	2	0.78	210	2	193	2	0.651	3	9
DECS21	3.3833	4	0.65	182	4	189	3	0.642	1	12
DECS21-DM	3.3713	1	0.79	216	1	168	4	0.646	2	8

The decrease in interlayer spacing and increase in L_c and L_a are indicative of improvements in crystallographic structure. In order to have a fair comparative crystallographic analysis, the samples are ranked in each category. For interlayer spacing, 1 to 4, representing smaller to largest, for L_c and L_a , 1 to 4, representing largest to smallest. The rank in each category is summed up to give a total value. This count includes the Raman I_D/I_G ratios; these values will be discussed in a subsequent paragraph. As a result, the most crystalline sample exhibits the lowest total score. It is interesting that the graphitized demineralized anthracites have smaller interlayer spacing values, hence higher degree of graphitization than their corresponding graphitized raw anthracites. It is widely accepted that the inherently present minerals in anthracites promote catalytic graphitization. In fact, DECS21-DM has the lowest score followed by PSOC1515-DM. This is ironic given a widely accepted view that minerals catalyze graphitization. However, it has been noted that the nature of the minerals inherently present in the coal are a factor in determining its ability to catalyze graphitization.^{8,44} Pappano demineralized anthracites and remineralized them with specific minerals of interest and specific concentrations. In that study, it was concluded that kaolinite ($Al_2Si_2O_5(OH)_4$) has no graphitization-enhancing ability. It was pointed out that kaolinite reduced the crystallite size of the resulting graphite.³ Interestingly, kaolinite was detected in our raw anthracites by XRD. It is important to note that the element that potentially inhibits graphitization is aluminum, as the coals also have silicon, which has the ability to catalyze graphitization. It is therefore dependent on relative concentrations between these two elements. In our calcined anthracite, we detected the dominance of aluminum based phases, as discussed in the calcination section. It is therefore assumed that the presence of aluminum led to reduced catalytic graphitization, and in fact may have existed as a species that

caused defects in the structure, at least before its evaporation. In our study, the demineralized anthracites therefore have the advantage over the raw anthracites for improved graphitization.

In agreement with TPO results, XRD and Raman parameters of DECS21-DM indicate a higher crystallinity than the other samples. DECS21 showed two overlapping peaks in TPO analysis; it can be seen in **Table 16** that the graphitized sample has the best interlayer spacing value and lowest total score. The other interesting feature about this sample is that it has the L_a that is almost equal to L_c . In fact, both graphitized raw anthracites have L_c almost equal to L_a in comparison to their demineralized counterparts. It seems as though demineralization led to an increase in the crystallite size but a decrease the crystallite length. Since it is in the interest of nuclear graphite manufacturers to have highly crystalline but not long range preferred orientation, but more importantly there should be a balance between the CTE values, leading to low CTE ratio ($CTE_{c-axis}/CTE_{a-axis}$), it might be of interest to look at the graphites that have a small difference between the L_a and L_c values. Isotropic graphite possesses a low CTE value which enables it to experience stability during neutron irradiation.

Figure 13 shows the Raman spectra of graphitized anthracites. The Raman intensity ratio (I_D/I_G) values are shown in **Table 16**. The plot shows that the samples are graphitic, as shown by a low intensity D-peak (around 1300 cm^{-1}), high intensity G-peak (around 1500 cm^{-1}), and the presence of a strong peak in the second-order region of Raman spectra ($2000 - 3000\text{ cm}^{-1}$). The higher G-peak intensity is associated with an increase in structural ordering. The graphitized demineralized anthracites have higher peak intensity than the graphitized raw anthracites. This is in agreement with the XRD results that showed that graphitized demineralized anthracites achieve a higher degree of graphitization than those that were not demineralized. Graphitized DECS21 has the lowest I_D/I_G ratio value, followed the graphitized DECS21-DM. This can be linked to the overlapping peaks in the TPO analysis. While the TPO result may not be reflected in XRD, it may be reflected in the Raman I_D/I_G ratio value.

Low ash content is of utmost importance in nuclear graphite. A good moderator, while ensuring minimum neutron loss and not undergoing major structural changes, slows down the neutrons with high kinetic energy, thus enabling them to cause further fission. Inorganic elements present

in graphite in a form of ash constituents tend to absorb the neutrons during the reactor operation. Though all elements should be reduced greatly, boron and cadmium are of usually of major concern in this regard because of their major neutron absorbers. The absorption of neutrons by the elements in graphite reduces the multiplication factor of the reactor, hence its reduced efficiency. The graphitized samples were analyzed using SEM/EDS for elemental identification. It would be best to have a rigorous elemental identification in these samples, since EDS has a detection limit of 1000 ppm. Therefore any element that is in concentration lower than 1000 ppm is not detected by this technique. In the EDS analysis, the graphitized anthracites did not have any element detectable. **Figure 14** shows an example of EDS scan obtained for the graphitized anthracites. The scan shows a strong carbon peak and copper peaks. The copper peak observed is from the tape that was used for mounting the sample for the analysis, therefore it is not from the sample. All graphitized anthracites showed scans that were very similar. The reasonable conclusion was that these samples have elements that are below the EDS detection limit.

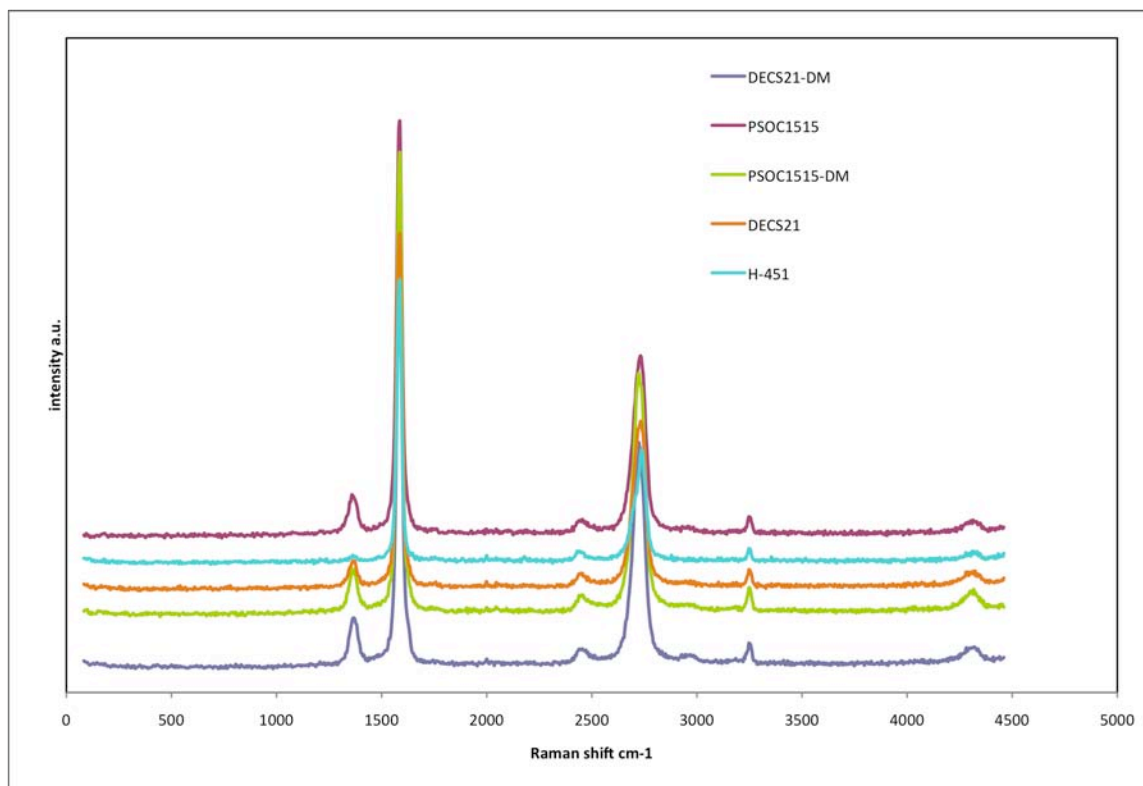


Figure 13: Raman of *graphitized* anthracite coals and nuclear graphite H-451

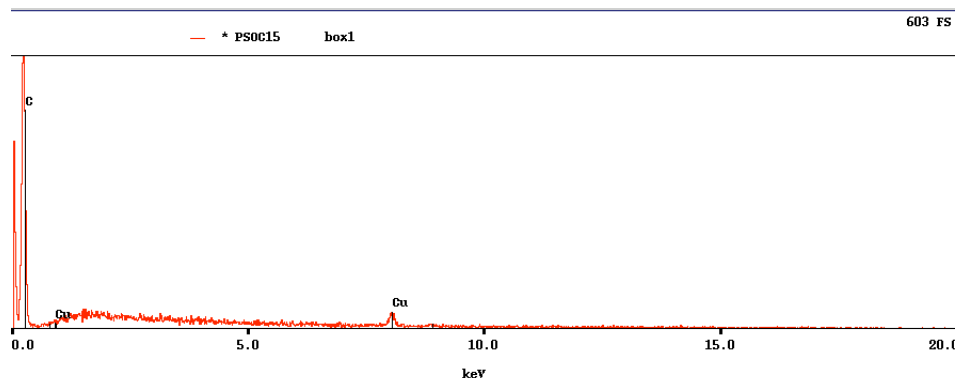


Figure 14: Typical EDS of graphitized anthracites – no metals, indication of less than 1000 ppm of various elements – particular EDS scan for graphitized PSOC1515

Summary of Graphitized Anthracites

The most graphitic sample was produced by graphitization of the DECS21-DM coal, and the least graphitic was DECS21. Demineralization possibly removed metal oxides that inhibit graphitization (alumina). Once demineralized, the more ordered coal produced the most graphitic material. However, to determine how well these samples would serve as fillers for isotropic graphites, the graphitized samples should be compared known nuclear graphites.

Characterization of Graphites Provided by Oak Ridge National Laboratory

Graphite samples were provided by Oak Ridge National Laboratory (ORNL). The intention was to compare, at least at the carbon structural level, our graphitization products to nuclear graphites (also known as isotropic graphites). These samples are among the several candidates that have been chosen for the Next Generation Nuclear Plant (NGNP) program. The selected candidates will be tested in the AGC-1 irradiation capsule. The AGC-1 irradiation capsule will provide irradiation creep design data, and data for the effects of irradiation creep on key physical properties of these candidates.^{53,54} For this work we selected only five of the NGNP candidates for comparison to our graphite products. The five selected graphite candidates are NBG-10, NBG-17, IG-430, IG-110 and H-451. H-451 is considered to be reference graphite because of its superior properties, and was used as a moderator in the Fort St-Vrain reactor in Colorado. These graphite samples have been categorized by ORNL as major grades because they will serve as

reactor vendors for the core structure in the NGNP. These grades are most likely to receive reasonably large neutron doses in their lifetime and will be subjected to significant stresses in operation. Consequently, these grades occupy the stressed and companion unstressed positions in the AGC-1 capsule and hence yield irradiation creep data.

In this work, we are interested in the diversity in the NGNP candidates; therefore we selected five NGNP candidates based on their precursor material, method of processing, manufacturer, and country of origin. **Table 17** gives the description of the five graphite candidates that have been selected for the work. According to ORNL characterization, vibrationally molded and isostatically pressed graphites exhibit higher density and strength, whereas extruded graphite have lower values in this parameters, in comparison. Graphites synthesized from pitch coke also possess greater density than petroleum synthesized graphites. It therefore seemed reasonable to compare our products to grades of diverse backgrounds.

Table 17: Description of selected graphite candidates

Sample	Source	Country of origin	Process
NBG-17	SGL carbon	Germany/France	Pitch coke, vibrationally molded, medium grain
H-451	SGL carbon	USA	Petroleum coke, extruded, medium grain
IG-110	Toyo Tanso	Japan	Petroleum coke, isostatically pressed, fine grain
IG-430	Toyo Tanso	Japan	Pitch coke, isostatically pressed, fine grain
NBG-10	SGL carbon	France	Pitch coke, extruded, medium grain.

The five selected ORNL graphite samples were characterized using these the same techniques and under similar characterization conditions as our graphite products. It should be noted that these techniques cannot by themselves alone determine whether our anthracite synthesized graphite products qualify to be used as a moderator in a nuclear reactor; to come to such a conclusion would require more characterization, particularly mechanical properties (i.e., tensile properties, compressive properties, thermal conductivity, and the coefficient of thermal expansion (CTE)). An irradiation test would be required as a final test. However, characterization carried out in our work is meant to provide a guide to the status of our graphite

products in comparison to nuclear graphites, hence paving a way to successful synthesis of nuclear graphite from anthracites. It is also important to note that the selected five ORNL graphites were synthesized using a traditional composite synthesis method by mixing filler coke with a binder. The anthracites would replace filler coke. However, in this work, anthracites were graphitized without mixing with a binder. It is important to understand how anthracite can graphitize to nuclear graphite even before mixing them with a binder.

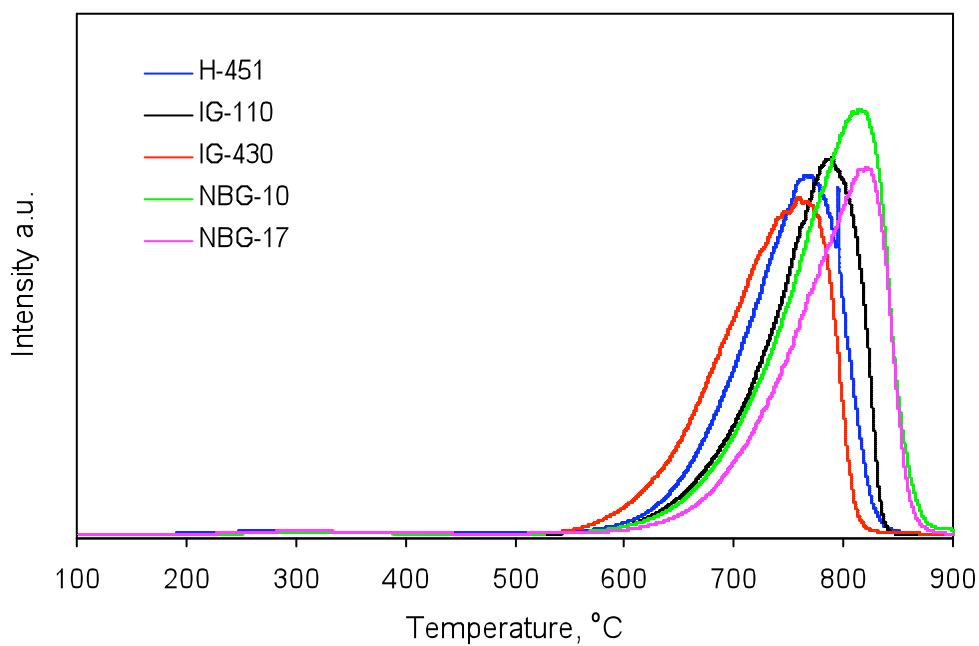
The details about calcination conditions, impregnation, baking, graphitization temperature and time were not provided due to the proprietary nature of nuclear graphite manufacture. Nevertheless, comparison still provides useful implications about our graphitized anthracites in terms of their ability to transform to nuclear graphite on graphitization.

In order to do the comparison, the ORNL graphite samples were analysed using the same characterization techniques as our graphitized anthracites. The TPO profiles of ORNL graphite samples are shown in **Figure 14**, and **Table 18** shows the TPO peak temperature of each graphite. All profiles show the oxidation peak at graphitic structure oxidation region, with IG-430 being most reactive as its oxidation peak at about 770 °C and NBG-10 being the least reactive, its oxidation peak appearing at about 830 °C. These samples show structural homogeneity demonstrated by the single peak in the profile. According to these results, NBG-10 possesses higher structural ordering than the other ORNL samples.

The graphitized anthracites are compared to NBG-10 using temperature programmed oxidation as shown in **Figure 15**. NBG-10 was selected because it showed less reactivity when compared to the rest of ORNL samples. Graphitized samples are shown to be within the oxidation range of ORNL samples, although the graphitized raw anthracites have lower oxidation temperatures. DECS21-DM has an oxidation peak showing up at higher oxidation temperature than NBG-10. This signals a higher structural ordering on this sample than ORNL samples. The summary of this graph is that our graphitized samples are within the same oxidation range as ORNL graphite samples.

Table 18: TPO data regarding peak temperatures for calcined anthracite coals

Samples	Sample Source	Peak Temperatures
H-451	SGL carbon	760
IG-110	Toyo Tanso	790
IG-430	Toyo Tanso	770
NBG-10	SGL carbon	825
NBG-17	SGL carbon	830

**Figure 14:** TPO of ORNL graphite samples

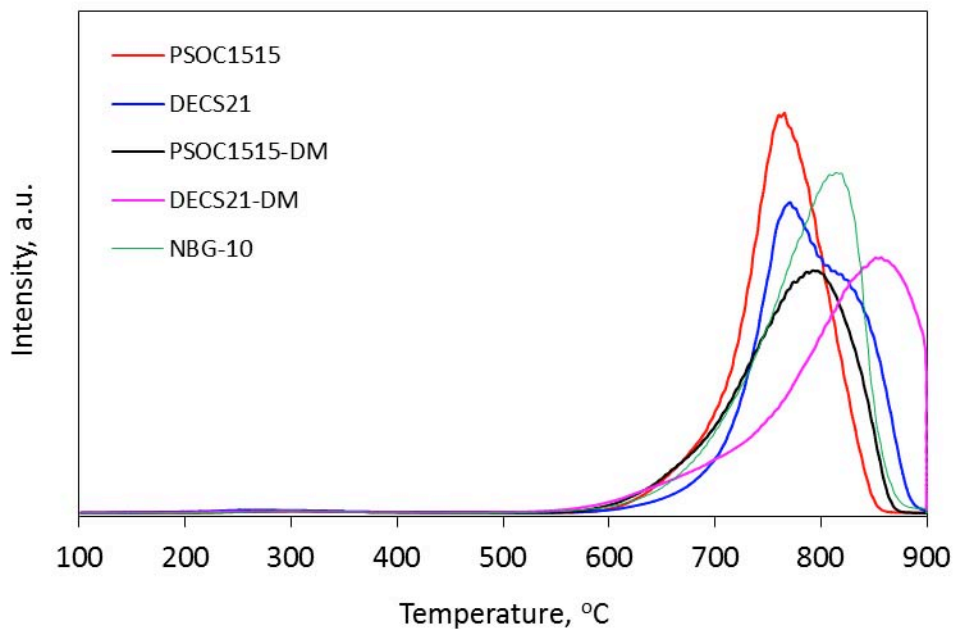


Figure 15: TPO of graphitized anthracites and NBG-10 for comparison

The ORNL graphite samples were also analysed using XRD under the similar conditions with our graphite products. **Figure 16** shows the XRD spectra of the ORNL graphite samples. All of them show the peaks that are characteristic of three-dimensionality in the structure; these peaks were mentioned earlier in this report. They have a sharp and narrow [002] peak located $\sim 26^\circ$. Interestingly the H-451, the reference graphite, has the highest peak intensity. The interlayer spacing, crystallite size and crystallite length are shown in **Table 19**. The samples are also ranked according their values for comparison purposes.

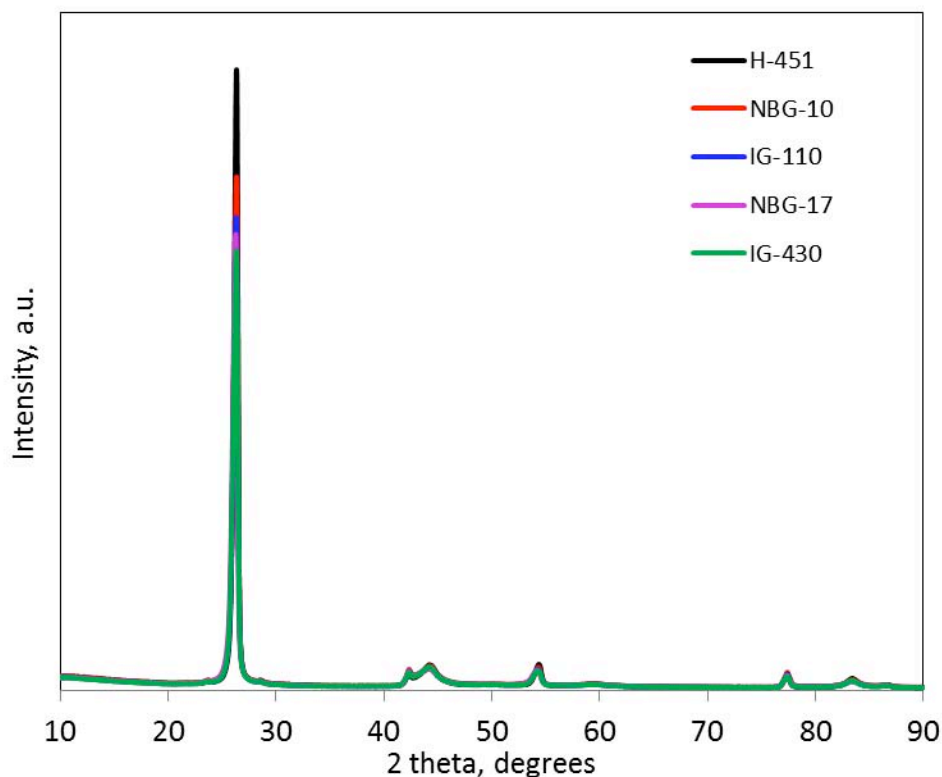


Figure 16: X-ray diffraction pattern of graphitized anthracites

Table 19: X-ray diffraction parameters and Raman intensity ratio of ORNL graphite samples

Sample	d_{002} , Å	DOG	Rank	L_c , Å	Rank	L_a , Å	Rank	I_D/I_G	Rank	Total
H-451	3.379	0.70	2	219	1	208	2	0.344	1	6
NBG-10	3.378	0.72	1	192	2	210	1	0.416	3	7
NBG-17	3.388	0.60	5	190	3	196	4	0.465	4	16
IG-110	3.383	0.66	4	188	4	199	3	0.531	5	16
IG-430	3.382	0.67	3	172	5	186	5	0.345	2	15

These samples have the interlayer spacing larger than that of graphite, 3.354 Å. The interlayer spacing values given in **Table 19** are higher than the values reflected in the document that was sent to us along with the samples. This difference could be due to a number of reasons, including the instrument that was used and the sample preparation method. The document indicates that the XRD analysis of the ORNL samples were done on the solid samples, whereas in this work we ground the samples to fine powder for analysis. For the sake of comparison, we used similar analysis conditions as our graphitized samples.

Table 19 shows that H-451 and NBG-10 have the lowest total scores, implying higher crystallinity than the other ORNL graphite samples, and NBG-17 and IG-110 being at the lowest crystallinity ranking. It is interesting to note that extrusion was used during the manufacture of H-451 and NBG-10.

Figure 12 shows the comparison of graphitized anthracites to H-451 (the XRD values in **Table 16** can be compared to the XRD values in **Table 19**). Our graphitized anthracites have interlayer spacing values within the range of the ORNL graphite samples. The same can be said about the crystallite size and length values.

As in XRD results, H-451 shows the highest peak intensity in Raman spectroscopy analysis (**Figure 17, Table 19**). All samples show an intensity G-peak and a short D-peak located at 1500 and 1300 cm^{-1} , respectively. There is also a strong in the second-order region of the Raman spectra. This is indicative of graphitic structure.

The Raman I_D/I_G ratio peak values are shown in **Table 19**. Although H-451 has the highest G-peak intensity, it has the lowest I_D/I_G ratio. **Figure 13** shows the Raman spectra comparison of graphitized anthracites with H-451. As it was observed in the XRD analysis, H-451 has the shortest G-peak intensity compared to the graphitized anthracites. However, the plot shows that H-451, hence all ORNL graphite samples, have the lowest D-peaks compared to graphitized anthracites. This is evidenced by the Raman I_D/I_G ratio values. The graphitized anthracites have Raman intensity ratio values are within 0.642 and 0.674, whereas the ORNL graphite samples

have their values within 0.344 and 0.531. High I_D/I_G ratio values indicate greater carbon graphite disordering in graphitized anthracites, and are greater than the I_D/I_G ratio values in the ORNL samples.

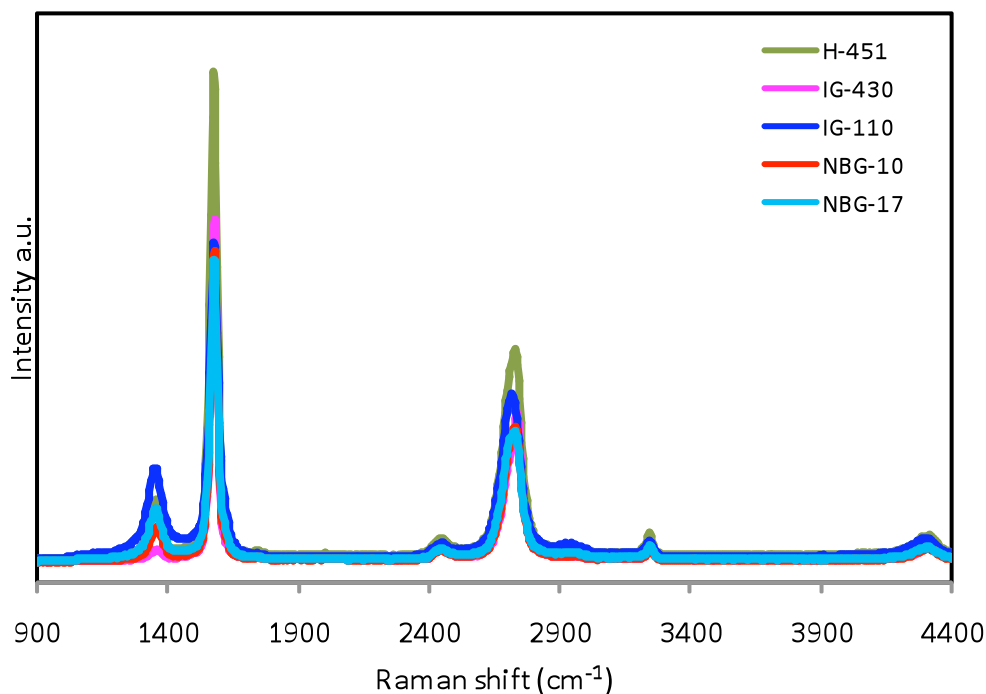


Figure 17: Raman spectra of graphitized anthracites

For comparison purposes, the scanning electron microscope (SEM) images that were taken and scanned during EDS elemental identification were collected for comparison of different samples. SEM is a useful technique in studying the texture of materials texture and morphology. The shapes and sizes in the surface of the sample can be studied using SEM. SEM utilizes a beam of electron to probe the materials surface composition and topology. A beam of electrons is shone into the sample, and the electrons either undergo elastic or inelastic interaction with the sample electron cloud. The electrons are collected in the detector and manipulated to create signal from which the image is obtained.

According to Raman spectroscopy and XRD analysis, H-451 is the most crystalline graphite and IG-110 is the least crystalline of all the five ORNL graphite samples examined in this work. The SEM images of these two graphite samples were then collected for comparison with the

graphitized anthracites. The images were taken under similar conditions, with a magnification of 90 for all samples. **Figure 18** shows the SEM images of H-451, IG-110 and graphitized anthracites. The image for H-451 seems to have a coarser texture than that of IG-110. The large particles seen in the H-451 are not found in the IG-110 image. There is also a significant difference in the images of PSOC1515 and PSOC1515-DM. The demineralization of this anthracite seems to have led to a much finer surface upon graphitization. However, this effect is not seen with DECS21 as its surface is not too different when raw or demineralized.

Summary of Part A

DECS21 is a more crystalline coal than PSOC1515. Demineralization of DECS21 (DECS21-DM) produced the most crystalline carbon. In comparison to ORNL graphites, the graphitized coals had similar XRD and TPO values; however, the ID/IG ratios for the graphitized coals were higher than the ORNL samples, an indication of more defects in graphitized anthracites. However, the graphitized anthracite would be used as a filler to produce graphite, so the additional processing would most likely lead to a higher quality graphite.

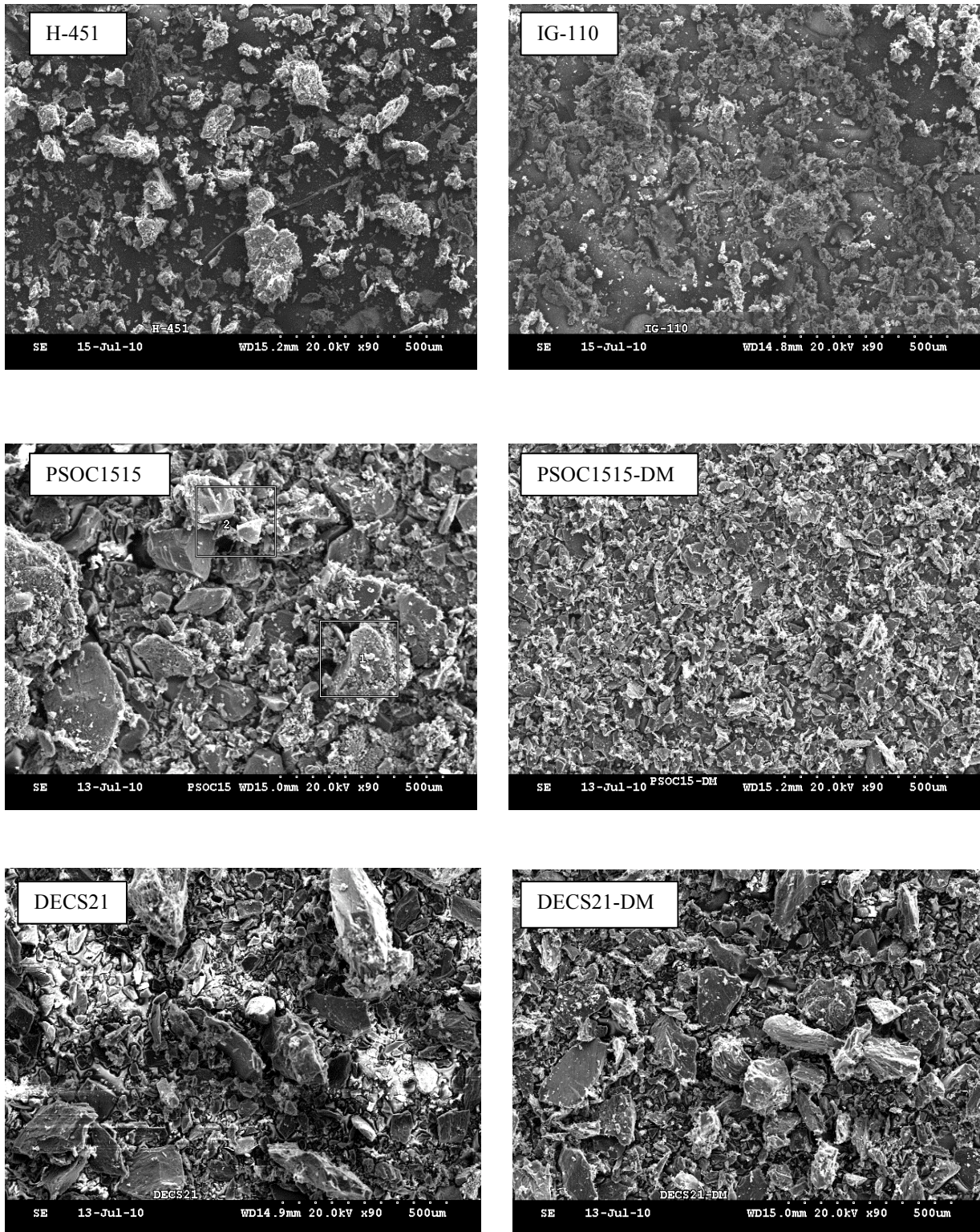


Figure 18: SEM images of two ORNL graphite samples and graphitized anthracites.

B. Large scale calcination/graphitization of two anthracite coals: Generation of artifacts using anthracite coals for coefficient of thermal expansion determination

Part of any graphite product qualification requirement for use as a moderator in the nuclear reactor is a low CTE ratio ($CTE_{c-axis}/CTE_{a-axis}$). It has been shown numerous times that isotropic graphites contract and expand to all directions during neutron irradiation, unlike anisotropic graphite which tends to experience more dimensional change in the c-axis.⁵⁵⁻⁵⁷ Although we were unable to do any neutron irradiation tests on our graphitized anthracites, it was deemed important to have the CTE measurements carried out. However, in order to have this measurement done, a large quantity of the raw anthracites is needed (1.5 kg) for making test rods.

Unfortunately, the two coals that we have been working with throughout this work (PSOC1515 and DECS21) were not available in such large quantities. We then selected two coals that would be used for this test. Summit and Jeddo are both anthracites named after the mines where they were mined. These coals were provided by Penn State sample bank. These two coals were used by Pappano for graphitization studies.³ In Pappano's study, the Summit anthracite was found to have circular pore structure with very little pore flattening and be a semi-anthracite in rank, whereas the Jeddo anthracite showed no circular pores under high resolution transmission electron microscopy (HRTEM) and was anthracite in rank. Pappano found Summit anthracite produced a more crystalline graphite than Jeddo anthracite.³ This was interesting since the flat pores in the raw Jeddo might have been assumed to be signaling a higher degree of graphitization than that of Summit which had circular pores. However, inherent minerals played a role in graphitizing the coals. As Summit and Jeddo anthracite coals are similar to the coals we used for small scale studies, we selected these two coals for graphitization and CTE measurements. The CTE measurements might shed some light about coals' ability to convert to nuclear graphite.

We obtained both the Summit and Jeddo anthracites as run-of-mines unprocessed. Both samples were provided at a -1/4 in particle size. They were ground to -60 mesh. The coals were subjected to a series of float/sink tests on representative aliquots in order to provide the specific gravity solution of tetrachloroethylene and toluene that would provide products with low ash contents.

These coals were then subjected to float/sink experiments, and the ash contents were reduced from 17.6 to 7.5% (Summit) and 8.0 to 4.31% (Jeddo). The proximate analysis of the cleaned coals are provided in **Table 20**. These anthracites were then sent to Dr Peter Stansberry of GrafTech for processing and CTE measurements.

Table 20: Proximate analysis of Jeddo and Summit anthracite coals

Anthracite	Fixed carbon, %	Volatile matter, %	Ash, %
Summit	70.62	18.03	7.58
Jeddo	82.63	10.6	4.31

Both Summit and Jeddo were characterized using TPO. Characterization of these unheated anthracites is useful for comparison and understanding their degrees of graphitizability. **Figure 19** shows the TPO profiles of cleaned Jeddo and Summit anthracites, and **Table 21** has the peak temperatures. The Summit anthracite is more reactive than the Jeddo anthracite. This is evidenced by the appearance of oxidation peaks at higher oxidation temperatures. Both coals show two overlapping peaks, the peak at lower temperature is due to disordered carbon whereas the peak at higher temperature is due to more ordered carbon. The data imply higher structural ordering in the Jeddo coal than Summit coal.

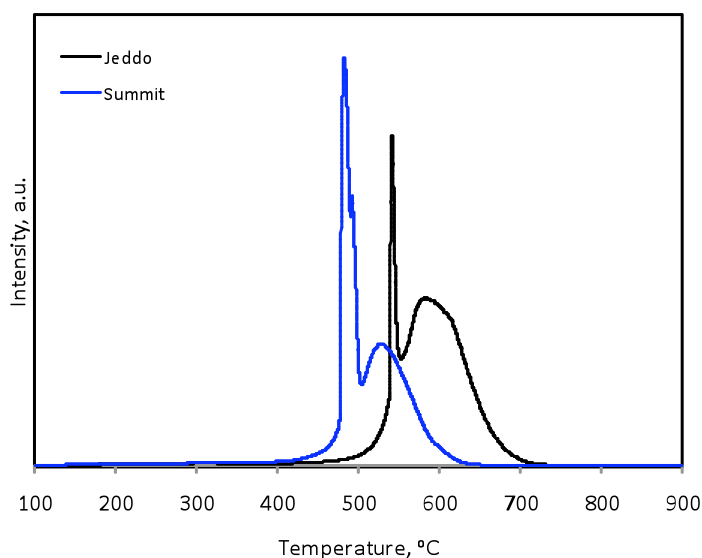
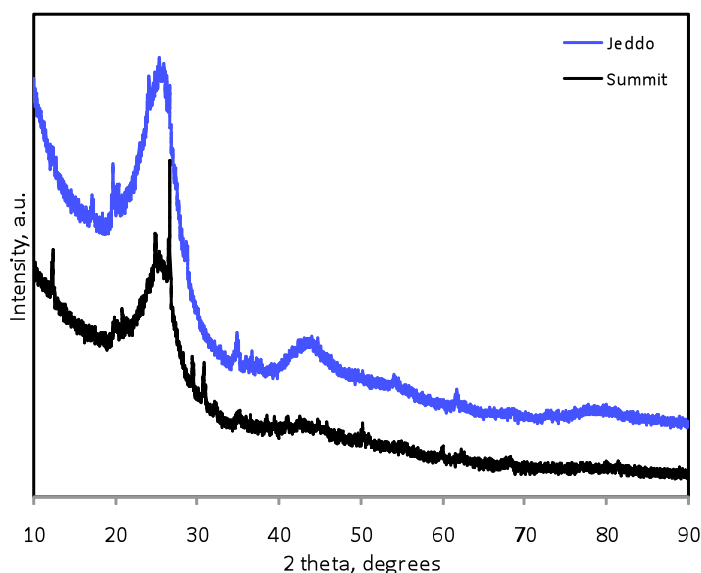


Figure 19: TPO of Jeddo and Summit anthracite coals

Table 21: TPO data regarding peak temperatures for *graphitized* anthracite coals

Samples	Sample Status	Peak Temperatures	
Jeddo	Raw, demineralized	550	600
Summit	Raw, demineralized	490	525

This is confirmed by the XRD spectra shown in **Figure 20** and the data shown in **Table 22**. Although both coal patterns have many peaks, indicating the presence of minerals, the Jeddo coal seems to have a higher [002] peak intensity than the Summit. Jeddo also has a smaller interlayer spacing value for the [002] peak (3.3520 Å) whereas the Summit has 3.3531 Å. The Jeddo spectrum also shows the presence of the [10] peak around 43°; this peak is known to split into [101] and [100] peaks at graphitization temperatures. This peak is not seen in the Summit coal. These results are indicative of higher crystallinity in Jeddo than Summit.

**Figure 20:** XRD of Jeddo and Summit anthracite coals**Table 22:** XRD spectra of Jeddo and Summit raw cleaned anthracites.

Sample	d_{002} , Å	L_c , Å	I_D/I_G
Jeddo	3.3520	26	0.700
Summit	3.3531	23	0.783

Figure 21 shows the Raman spectra of Jeddo and Summit coals. Both coals have both the D- and G-peak located at about 1300 cm^{-1} and 1500 cm^{-1} , respectively. The plot shows that Jeddo has more structural ordering than Summit as shown by its shorter D-peak relative to its G-peak. The TPO, XRD, and Raman spectroscopy results obtained in this work are in agreement with Pappano's findings, that Jeddo has more flattened pores than the Summit. Flattened pores are normally linked to a preferred orientation in the basic structural units of the anthracites, which is indicative of structural ordering.

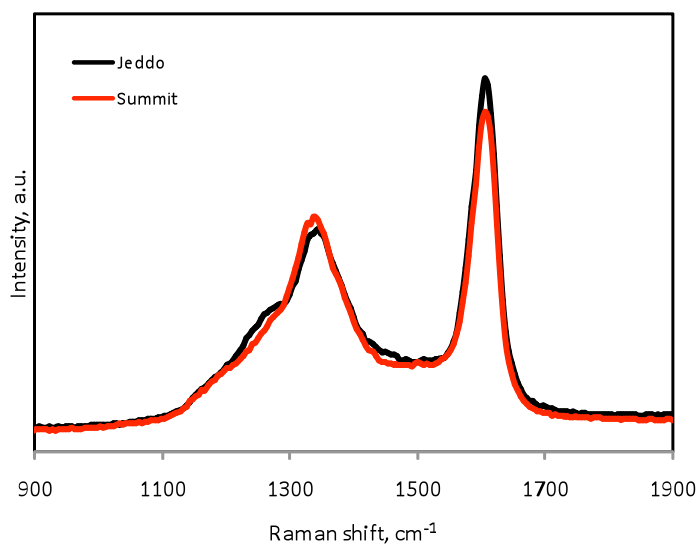


Figure 21: Raman spectra of anthracites

Table 23 shows the data collected on the 19-mm diameter graphite test rods. The control rod was made to be typical of an anisotropic graphite, and the tests rods from the cleaned anthracites were not all that similar. Because the CTE ratio could not be determined (only the CTE in the c-direction was determined), it is hard to determine if the coal samples meet the CTE ratio of ~ 1 .

Table 23: Summary of 19-mm diameter graphite test rods

Test	Control	Jeddo	Summit
Bulk density, g/cm^3	1.43	1.14	1.17
Specific resistivity, $\mu\Omega\text{-m}$	9.04	36.43	37.46
Coefficient of Thermal Expansion, $10^{-6}/^\circ\text{C}$	0.130	2.331	2.011

C. Calcination/graphitization of delayed coker cokes produced from feed generated by solvent extraction of coal

In another CPCPC project, bituminous coals were extracted with decant oil, and the extract was fed into the delayed coker.⁴⁷ Part of the impetus for doing this project was to produce a coke that had coal-derived material in it (coal-derived pitches are good materials for producing graphitic materials and sell at a fairly high value), but was lower in ash and unreactive organic coal particles when co-coking coal and decant oil (in co-cokes, the ash content was too high for use to produce anode and graphite grade materials).^{59,60} While the solvent extracted cokes were evaluated for anode use (and better in character than co-cokes), we thought it also of value to evaluate the cokes for generation of anisotropic and isotropic graphites.

As discussed in the experimental section, three cokes produced from coking of solvent extracted coal were also calcined and graphitized.⁴⁷ Details related to the extraction and coking have been discussed in the CPCPC final report for the project “Solvent extraction of coal to produce feedstock for a laboratory scale coker” and in the experimental section.⁴⁷ The coal-based liquid was fed into a delayed coker: Run #142 used only decant oil as feed, Run #143 used coal extract, and Run #144 used coal extract plus a cracking catalyst that was fed inside the coker. The details about characterization of the coke product and calcined/graphitized cokes will be discussed in this section.

Table 24 shows the proximate and ultimate analyses of the cokes generated from solvent extract of Western Kentucky #6 coal. The proximate analyses indicates that the ash content of runs #142 and #143 are lower than the amount of ash in the co-cokes when using cleaned coals. The ash content of #142 and #143 is a result of the ash content in the decant oil – decant oils can contain some residue from the catalysts used in fluid catalytic cracking, and are typically silica. The silica in the ash could be beneficial to graphite generation, as discussed in previous sections of the report. The ash content in run #144 is almost double the other runs; #144 had a cracking catalyst added to the coking run, therefore, there would be more ash in the coke. The catalyst in the coke is alumina-based, which was chosen because the generated coke was evaluated for the production of aluminum; however, alumina is expected to be detrimental to graphite formation.

Table 24: Proximate and ultimate analyses of cokes generated from solvent extract of bituminous coals

Sample Id.	Proximate Analysis, dry				Ultimate Analysis, dry				
	% Moisture	% Ash	% Volatile Matter	% Fixed Carbon	% Carbon	% Hydrogen	% Nitrogen	% Sulfur	% Oxygen (diff)
142	0.30	0.54	6.20	93.26	92.78	3.03	0.12	1.31	2.76
143	0.27	0.57	7.21	92.22	93.00	3.20	0.16	1.65	1.99
144	0.29	1.01	7.88	91.11	93.77	3.32	0.19	1.53	1.19

Table 25: TPO data regarding peak temperatures for cokes generated from solvent extract of bituminous coals

Samples	Sample Status	Peak Temperatures
142	Raw coke	508 536
143	Raw coke	549 560 568
144	Raw coke	508 536 560

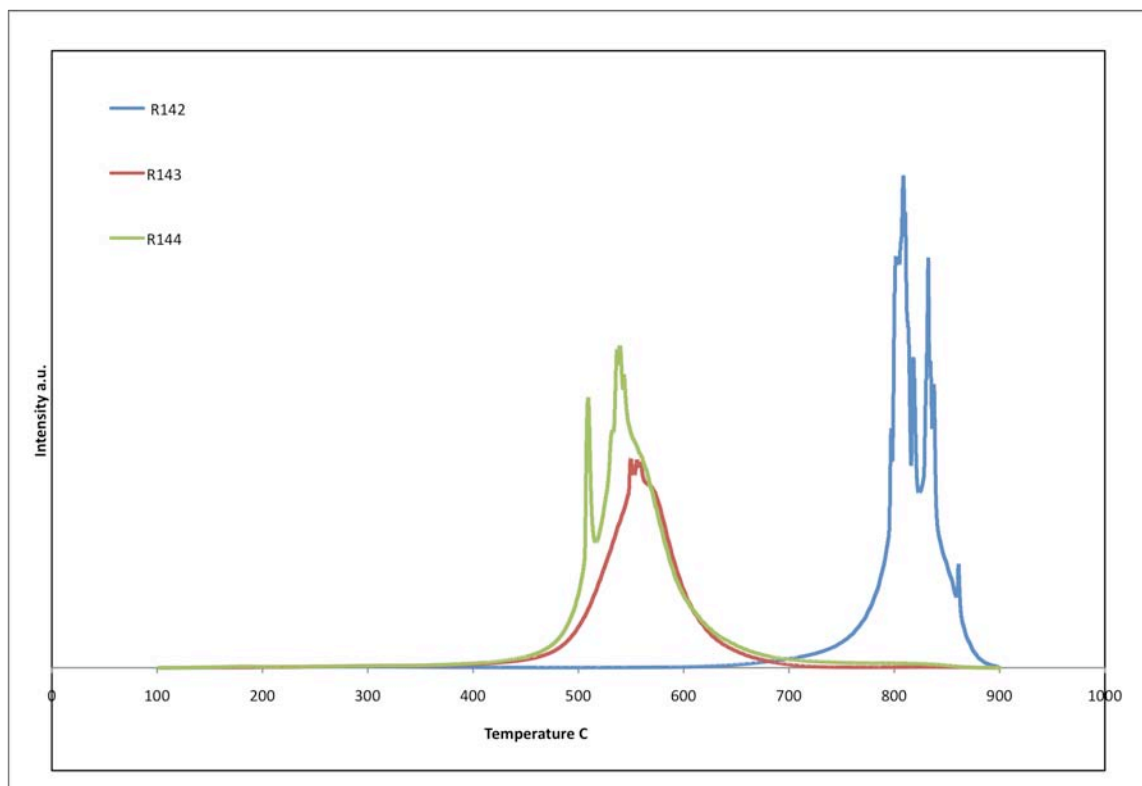


Figure 22: TPO of cokes from solvent extract of bituminous coal

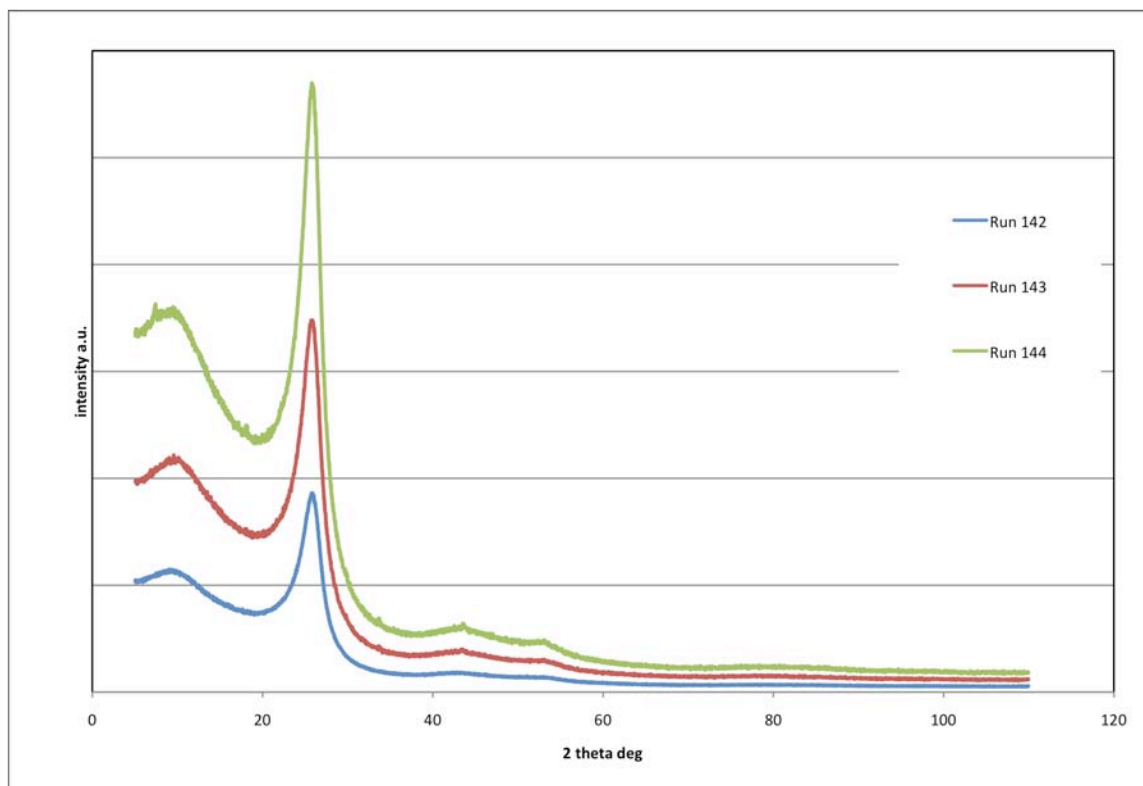
Optical microscopy was done on the solvent extract cokes.⁴⁷ Optical microscopy indicated the cokes generated were of similar quality, the cokes from runs #142 and #143 were very similar. In order to evaluate the cokes for graphitization behavior, XRD and TPO were done on the cokes.

TPO profiles of the cokes are shown in **Figure 22**, and peak temperatures are shown in **Table 25**. TPO of the raw cokes for 143 and 144 indicate that the cokes are similar in structure to the anthracites DECS-21 and Jeddo, and have similar organized structure to an anthracite coal. However, the profile for 142 is very similar to the TPO of calcined 142, so there is suspicion that the wrong sample was run. However, based on other results, we would expect the TPO of 142 raw coke to be similar to 143 and 144.

XRD spectra of the cokes are shown in **Figure 23**, and XRD parameters are shown in **Table 26**. The XRD of the raw cokes also indicate the cokes generated are very similar in structure. Raman was not done on the raw cokes due to time constraints.

Table 26: XRD parameters of cokes generated from solvent extract of bituminous coals

Sample	2θ	d_{002} , Å	L_c , Å
142	26.03	3.4204	27
143	26.017	3.4221	27
144	26.037	3.4194	28

**Figure 22:** XRD of cokes from solvent extract of bituminous coal

Calcination

The cokes were calcined to 1420°C, as discussed in the experimental section. The interesting comparison of these cokes is that the yield (**Table 27**) after calcination is significantly higher than what was seen from anthracite coals. Proximate analysis (**Table 28**) also indicates the low ash content and volatile matter content of the cokes after calcination.

Table 27: Yield of *calcined* cokes

Sample	wt before, g	wt after, g	Yield, %
R142	36.5	34.36	94.14
R143	38.6	35.76	92.64
R144	34.2	31.53	92.19

Table 28: Proximate analyses of *calcined* cokes

	Moisture %	Volatile Matter %	Ash %	Fixed Carbon
Run 142	0.02	4.74	0.235	95.005
Run 143	0.9	6.545	0.67	91.885
Run 144	0.95	6.285	0.59	92.175

TPO was done on the calcined cokes 142, 143, and 144. The TPO profiles are shown in **Figure 24** and the data on the peak temperatures are shown in **Table 29**. While there are some small differences in peak temperatures, the calcined cokes oxidize from ~760-885°C. The calcined coke from #143 oxidizes at the lowest temperature. An interesting feature of the calcined cokes is there are more peaks than with the raw cokes – this is most likely due to the fact that the cokes are in between a coke and a graphite and in a transformative stage.

Table 29: TPO of calcined cokes 142, 143, and 144, with peak temperatures listed

Samples	Sample Status	Peak Temperatures			
142	Calcined coke	800	810	832	868
143	Calcined coke	757	790	813	835
144	Calcined coke	790	805	845	885

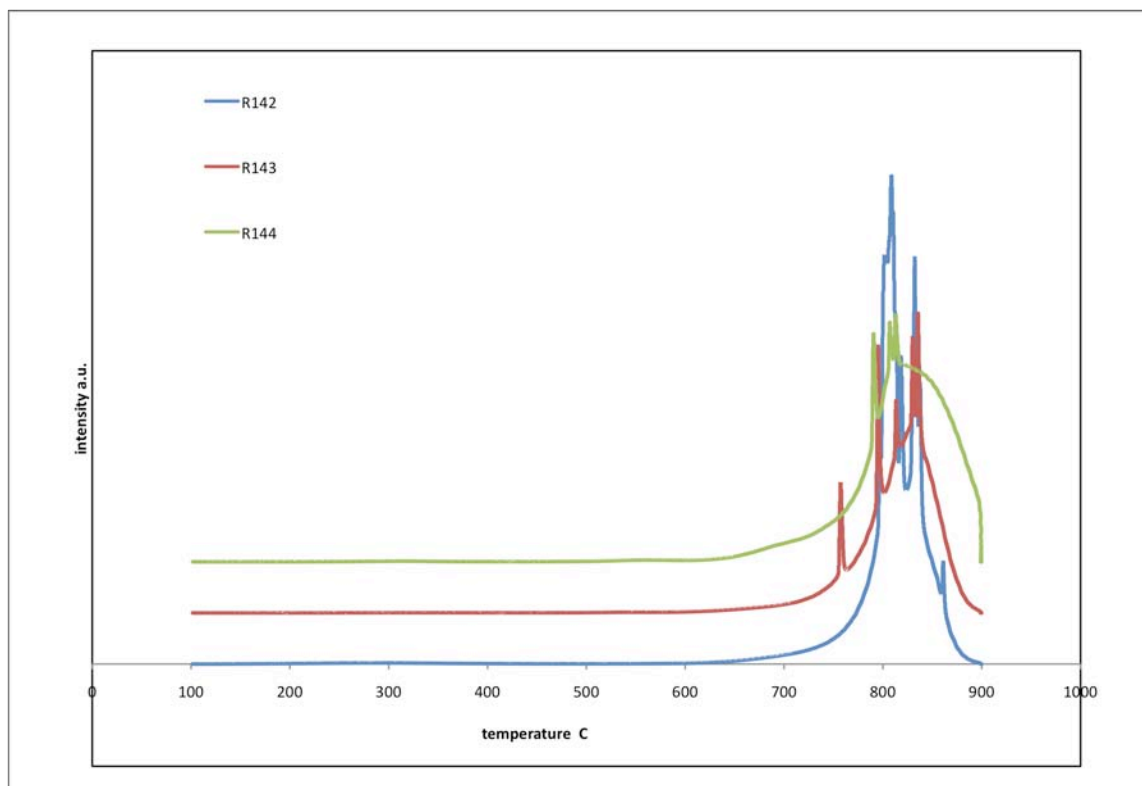


Figure 24: TPO profiles of *calcined* cokes 142, 143, and 144

XRD and Raman spectroscopy was done the calcined cokes. XRD spectra and Raman spectra are shown in **Figures 25 and 26**, and XRD/Raman parameters are shown in **Table 30**. Again, the data for all the cokes are very similar, with the d_{002} and Raman I_D/I_G ratio indicating that the carbon in the calcined coke in Run #142 was slightly more disordered, different from the TPO.

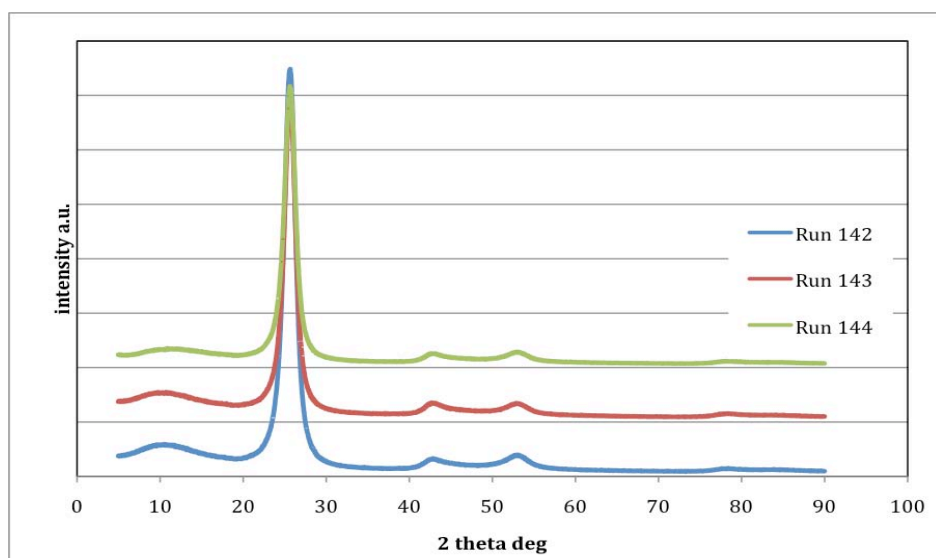


Figure 25: XRD spectra of *calcined* cokes from solvent extract of bituminous coal

Table 30: XRD and Raman parameters of *calcined* cokes from solvent extract of bituminous coal

Sample	2θ	d_{002} , Å	L_c , Å	I_D/I_G
Run 142	26.654	3.4697	48	0.965
Run 143	26.675	3.4669	50	0.956
Run 144	26.677	3.4666	50	0.954

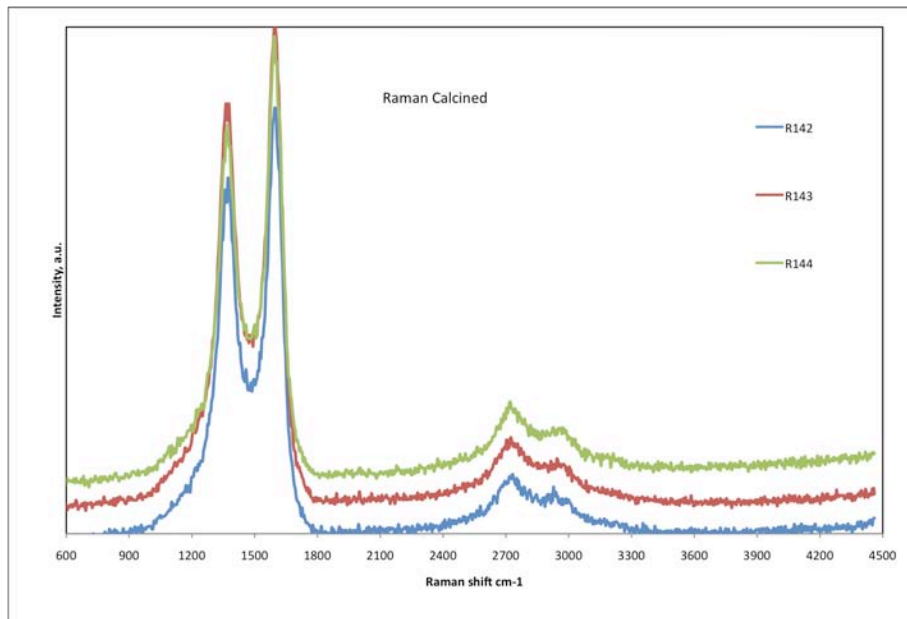


Figure 26: Raman spectra of *calcined* cokes from solvent extract of bituminous coal

Graphitization

The solvent extract cokes were graphitized according to the procedure described in the Experimental section. Yield data are shown in Table 29, and proximate analyses are shown in Table 30. The graphitization yield was high, an indication that the carbon in the cokes was not lost and instead transformed into graphitic material. The loss of volatile matter and the low ash content of the graphitized cokes make these cokes good candidates for filler in graphite.

Table 29: Yield data for cokes that were graphitized after being calcined.

Sample	wt before, g	wt after, g	Yield, %
R142	17.39	16.87	97.01
R143	17.35	16.72	96.37
R144	17.75	17	96.9

Table 30: Proximate analysis of graphitized cokes.

	Moisture %	Volatile Matter %	Ash %	Fixed Carbon
Run 142	0	3.685	0.145	96.17
Run 143	0	2.495	0.065	97.44
Run 144	0	3	0.02	96.98

TPO of graphitized cokes was done. TPO profiles are shown in **Figure 27** and data are shown **Table 31**. The TPO indicates the samples have become more uniform in carbon structure since only one peak is emitted during oxidation. The peak temperatures also indicate the oxidation resistance of the graphitized cokes, oxidation taking place at temperatures of 823-851°C. The graphitized coke from this process is quite stable. TPO indicates the graphitized coke of the highest quality was produced by the delayed coking of decant oil, Run #142.

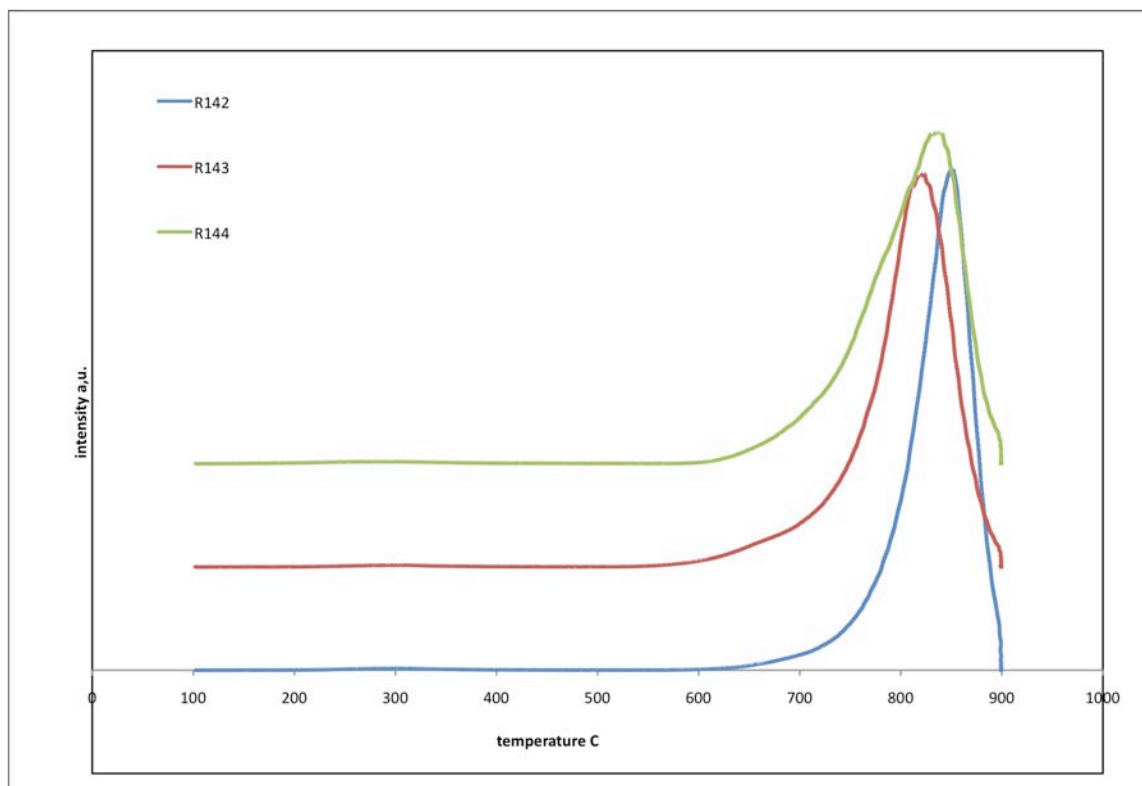


Figure 27: TPO profiles of graphitized cokes for cokes from 142, 143, and 144.

Table 31: TPO of graphitized cokes from solvent extraction of W. Kentucky #6 coal

Samples	Sample Status	Peak Temperatures
142	Graphitized coke	851
143	Graphitized coke	823
144	Graphitized coke	840

XRD spectra of the graphitized cokes are shown in **Figure 28**, and XRD parameters are shown in **Table 32**. The graphitized cokes were all of similar quality according to XRD, and may be good as a filler for nuclear graphite since the L_c and L_a are similar in size (~ 200 Å). Again, the best graphitized coke seems to be produced from delayed coking of decant oil alone; adding coal liquid to the solution does not improve the XRD parameters. Raman indicates a similar scenario, that the graphitized coke generated from delayed coking of decant oil is the best (**Figure 29** and **Table 32**).

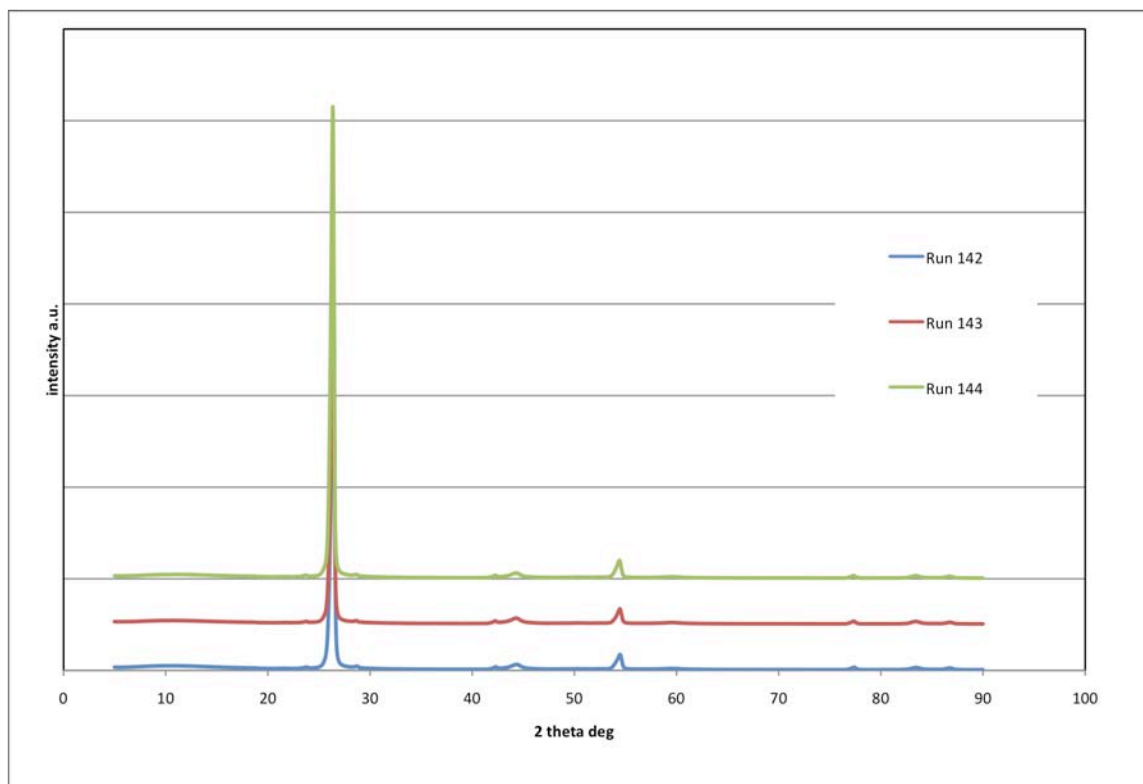


Figure 28: XRD spectra of *graphitized* cokes from solvent extract of bituminous coal

Table 32: XRD and Raman parameters of *graphitized* cokes from solvent extract of bituminous coal

Sample	2θ	d_{002} , Å	L_c , Å	L_a , Å	I_D/I_G
Run 142	26.413	3.3717	234	217	0.644
Run 143	26.381	3.3756	243	218	0.701
Run 144	26.645	3.3802	249	216	0.657

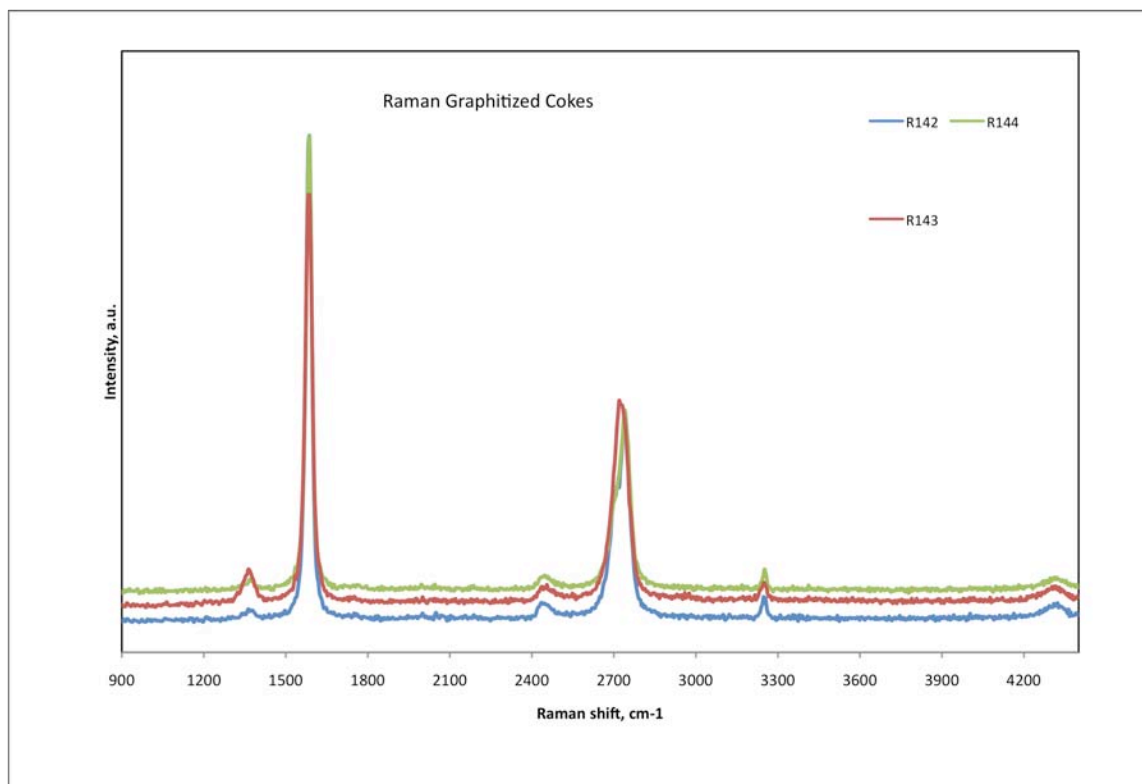


Figure 29: Raman spectra of *graphitized* cokes from solvent extract of bituminous coal

Summary of Part C

The cokes generated from solvent extraction of Western Kentucky #6 coal are good quality and all of similar quality. XRD, TPO, and Raman indicate the cokes produce a good quality graphitic material, similar in quality to graphitized anthracites and ORNL graphites, although the I_D/I_G from Raman for the graphitized cokes are higher than the ORNL graphites. However, the cokes would be used a filler to produce a graphite, so additional processing would improve the properties of a graphite produced from the cokes.

CONCLUSIONS

Coals were selected based on their chemical composition as well as the degree of maturity. PSOC1515 is semi-anthracite and DECS21 is anthracite. Basic characterization of these coals shows that DECS21 has more structural ordering than PSOC1515. TPO, XRD, Raman spectroscopy, and physical characterization show that DECS21 has higher structural ordering than PSOC1515. Heat treatment of these coals to 500°C seems to induce small structural changes as indicated in XRD, Raman, TPO, and physical characterization. Demineralization of these anthracites was done to determine the effect of demineralization. Calcination/graphitization of the anthracites produced quality graphites – the best graphites were produced from the demineralized coals, PSOC1515-DM and DECS21-DM. In particular, DECS21-DM made the best graphite, and was expected due to the semi-crystalline nature of the coal and the demineralization. Oak Ridge National Laboratory (ORNL) nuclear graphites were also characterized in a similar fashion to our graphitized samples, as a guide to determine if the graphitized anthracites were of a high enough quality for use as filler in production of nuclear graphites. The TPO and XRD parameters of the anthracites were similar to ORNL nuclear graphites; however, Raman spectroscopy indicated that the I_D/I_G ratios for the ORNL samples were lower, ~0.3-0.5, compared to the graphitized anthracites (~0.6-0.7), therefore, the ORNL samples had fewer defects than the graphitized anthracites. However, the ORNL samples were produced specifically as nuclear graphite, while anthracites would have to go through considerably more processing to produce a graphite. Therefore, demineralized anthracites may well be a very good filler material for nuclear graphite.

GrafTech made graphite artifacts from cleaned Jeddo anthracite and Summit semi-anthracite coals – the coals were different from the original small-scale tests in order to have enough material to produce the artifacts. Compared to anisotropic control graphite, the graphites from anthracite coals are lower in quality. However, graphites made from anthracite may be useful as a filler for isotropic graphites.

Solvent extracted cokes were also examined as potential filler for production of graphite. XRD, TPO, and Raman data of graphitized cokes indicated they were similar in quality to the anthracites. Therefore, they too may be useful as filler for isotropic graphites.

REFERENCES

1. Pappano, P.J., Mathews, J.P., Schobert, H.H., *Preprints, Amer. Chem. Soc. Div. Fuel Chem.* **44**, 567, 1999.
2. Pappano, P.J., M.S. Thesis, The Pennsylvania State University, University Park, PA, 2000.
3. Pappano, P.J., PhD. Thesis, The Pennsylvania State University, University Park, PA, 2003.
4. Andrésen, J.M., Burgess, C.E., Pappano, P.J., Schobert, H.H., *Fuel Proc. Tech.*, **85** (12), 1373, 2004.
5. Gerstein, B.C., Murphy, P.D., Ryan, L.M., In: *Coal Structure*. Academic Press, New York, 1982, Chapter 4.
6. van Krevelen, D.W., *Coal: Typology–Chemistry–Physics–Constitution*. Elsevier, Amsterdam, 1981.
7. Bratek, K., Bratek, W., Gerus-Piasecka, I., Jasienko, S., and Wilk, K., *Fuel*, **81**, 97-108, 2002.
8. Zheng, S., Rusinko, Jr., F., Schobert H.H., Penna. Energy Devel. Auth. Report, PEDDA 9303-4019, 1996.
9. Atria, J.V., M.S. Thesis, The Pennsylvania State University, University Park, PA, 1995.
10. Atria, J.V., Rusinko, F., Schobert, H.H., *Energy Fuels*, **16** (6), 1343-1347, 2002.
11. Conrad, B., Principal Investigator, Final Report for “Anthracite Feedstocks for Specialty Graphite Production,” CPCPC, DOE Prime Award No.: DE-FC26-98FT40350, July 1, 2000.
12. Stansberry, P., Principal Investigator, Final Report for “Anthracite Filler and Coal Extract Binder for Development of Isostatically-Molded Graphite,” CPCPC, DOE Prime Award No.: DE-FC26-98FT40350, July 1, 2003.
13. González, D., Montes-Morán, M.A., Garcia, A.B., *Energy Fuels*, **17**, 1324, 2003.
14. González, D., Montes-Morán, M.A., Suárez-Ruiz, I., Garcia, A.B., *Energy Fuels*, **18**, 365, 2004.
15. González, D., Montes-Morán, M.A., Garcia, A.B., *Energy Fuels*, **19**, 263, 2005.
16. Andrésen, J.M., Zhang, Y., Burgess, C.E., and Schobert, H.H., *Fuel Proc. Tech.*, **85** (12), 1361, 2004.
17. Bessant, G.A.R., Walker Jr., P.L. *Carbon*, **32** 1171, 1994.
18. Walker Jr., P.L., Almagro, A., *Carbon*, **33**, 239, 1995.
19. Walker Jr., P.L., Imperial, G.R., *Fuel*, **74**, 179, 1995.
20. Gergova, K., Eser, S., Schobert, H.H., *Energy Fuels*, **7**, 661, 1993.
21. Gergova, K., Eser, S., Schobert, H.H., Klimkiewicz, M., Brown, P.W., *Fuel*. **74** 1042, 1995.
22. Maroto-Valer, M.M., Tang, Z., Zhang, Y.Z., *Fuel Proc. Tech.*, **86** (14-15), 1487-1502, 2005.
23. Baker, D.E., *Nuclear Engineering and Design*, **14**, 413-444, 1970.
24. Reynolds, W.N., *Chemistry and Physics of Carbon*, **Vol. 2**, Ed. Philip L. Walker, Jr., Marcel Dekker, Inc.: New York, p. 121, 1966.
25. Reynolds, W.N., *Physical Properties of Graphite*, Elsevier Publishing, LTD.: New York, Ch. 7, p. 147, 1968.
26. Helm, J.W., Davidson, J.M., *Carbon*, **1**, 435-439, 1964.
27. Burchell, T.D., Eatherly, W. P., *J. Nucl. Mater.*, **205**, 179-181, 1991.
28. Burchell, T.D., Snead, L.L., *J. Nucl. Mater.*, **371**, 18-27, 2007.
29. Mitchell, B.C., Smart, J., Fok, S.L., and Marsden, B.J., *J. Nucl. Mater.*, **322**, 126-137a, 2003.
30. Kelly, B.T., *Progress in Nucl. Energy*, **2**, 219-269, 1978.

31. Isihiyama, S., Burchell, T.D., Strizak, J.P., and Eto, M., *J. Nucl. Mater.*, **230**, 1-7, 1996.
32. Kelly, B.T., *Physics of Graphite*, Applied Science Publishers:Englewood, London, and New Jersey, p. 477, 1981.
33. Nightngale, R.E., *Nuclear Graphite*, Academic Press: New York, Ch. 5, p. 88, 1962.
34. Maire, J., Mering, J., Graphitization of Soft Carbons, in *The Chemistry and Physics of Carbon*, P.L. Walker, Jr., Editor, Marcel Dekker, Inc.:New York, 125-190, 1970.
35. Franklin, R., *Acta Cryst.*, **4**, 253, 1951.
36. Franklin, R., *Proc. Roy. Soc. Ser. A.*, **209**, 196, 1951.
37. Oberlin, A., Terriere, G., *Carbon*, **13** 367, 1975.
38. Oberlin, A., *Carbon*, **17**, 7, 1979.
39. Oberlin, A., *Carbon*, **22**, 521, 1984.
40. Bustin, R., Rouzaud, J.N., Ross, J., *Carbon*, **33**, 679, 1995.
41. Couhaut, N., Blanche, C., Dumas, D., Guet, J.M., Rouzaud, J.N., *Carbon*, **38**, 1391, 2000.
42. Pusz, S., Kwiecinsak, B.K., Duber, S., *Fuel Processing Tech.*, **77-78**, 173-180, 2002.
43. Pusz, S., Kwiecinsak, B.K., Duber, S., *Int. J. of Coal Geology*, **54**, 115-123, 2003.
44. Evans, E., Jenkins, J., Thomas, J., *Carbon*, **10**, 637, 1972.
45. Gonzales, D., Altin, O., Eser, S., Garcia, A.B., *Materials Chemistry and Physics*, **101**, 137-141, 2007.
46. Burgess Clifford, C.E., M. Solomon Nyathi, Harold Schobert, "Relationship of Anthracite Structure to Isotropic Graphite," CPCPC, Quarterly report, Grant No. DE-FC26-03NT41874, Internal Agreement No. 3808-TPSU-DOE-1874, September 1 – November 30, 2009, December 31, 2009.
47. Burgess Clifford, C.E., "Solvent extraction of coal to produce feedstock for a laboratory scale delayed coker," CPCPC, Final report, Grant No. DE-FC26-03NT41874, Internal Agreement No. 3553-TPSU-DOE-1874, March 1, 2008 – December 31, 2009, February 28, 2009.
48. Bishop, M. and D.L. (1958) Ward, *The direct determination of mineral matter in coal*. Fuel. **37**: p. 191 - 200.
49. McCarty, J. G.; Hou, P. Y.; Sheridan, D.; Wise, H.; Albright, L. F.; Baker, R. T. K.; Eds. (1982). ACS Symposium Series
50. Tuinstra F. and Koenig J. L. (1970). Raman spectrum of graphite. *The Journal of Chemical Physics*, Vol. 53 (3), pages 1126-1130.
51. Tsai, S.C., (1982) *Fundamentals of coal beneficiation and utilization*. Elsevier, Amsterdam, Chapter 1.
52. Imperial, R.G. (1962). PhD thesis, the Pennsylvania State University.
53. Burchell, T.D. and Bratton, R. (2005). ORNL/TM-2005/505. Graphite Irradiation Creep Capsule AGC-1 Experimental Plan.
54. Burchell T.D. (2009) A Revised AGC-1 Creep Capsule Layout, ORNL/TM-2009/009.
55. Kelly B T, *Nuclear Reactor Materials in Material Science and Technology*, Vol. 10A, Cahn R W, Haasen, P and Kramer E J, Academic Press, London, 1981.
56. Isihiyama S., Burchell T.D., Strizak J.P. and Eto M. (1996).The effect of high fluence neutron irradiation on the properties of a fine-grained isotropic nuclear graphite. *Journal of Nuclear materials*, 230.
57. Burchell T.D. (1999), Carbon materials for advanced technologies, *Oak Ridge National laboratory*, Pergamon, USA, page 429.

58. Gonzalez, D.; Altin, O.; Eser, S.; Garcia, A. B. (2007). Temperature-programmed oxidation studies of carbon materials prepared from anthracites by high temperature treatment. *Materials chemistry and physics*, 101, 137.
59. Burgess Clifford, C.E., Principal Investigator, Boehman, A., Miller, B.G., Mitchell, G., Rudnick, L.R., Song, C., Schobert, H.H., co-PIs, "Refinery Integration of By-Products from Coal-Derived Jet Fuels", Final Report, Grant No. FC26-03NT41828, September 18, 2003 – March 31, 2008, Date Issued: July 25, 2008.
60. Burgess Clifford, C.E., Gul, O., Principle Investigators, "Production of graphite from coke obtained from delayed coking of decant-oil blends," CPCPC Final Report, Grant No. DE-FC26-03NT41874, Internal Agreement No. 3550-TPSU-DOE-1874, March 1 – October 31, 2009, December 31, 2009.

Spectrally Selective Coal-Derived Coatings for Solar Collectors

Final Report

CPCPC Contract 3836-WVU-DOE-1874

Prime Contract: DE-FC26-03NT41874
Contract Dates: 3/01/2009 to 02/28/2010

Principal Investigators:

Elliot Kennel
Alfred H. Stiller

Additional Authors:

Poornima Chateker
Naveen Kumar Bogum
Chandar Prasad Subramanian Palamadai
Santhoshi Dixit

Report Issued: 28 April 2010

West Virginia University

Department of Chemical Engineering
College of Engineering and Mineral Resources
PO Box 6102
Morgantown, WV 26506-610

Disclaimer

This report was prepared as an account of work sponsored by an agency of the United States Government. Neither the United States Government nor any agency thereof, nor any of their employees, makes any warranty, express or implied, or assumes any legal liability or responsibility for the accuracy, completeness, or usefulness of any information, apparatus, product, or process disclosed, or represents that its use would not infringe privately owned rights. Reference herein to any specific commercial product, process or service by any trade name, trademark or manufacturer otherwise does not necessarily constitute or imply its endorsement, recommendation, or favoring by the United States Government or any agency thereof. The views and opinions of authors expressed herein do not necessarily state or reflect those of the United States Government or any agency thereof.

Abstract

The objective of this research is to test the suitability of spectrally-selective coal-derived coatings for solar collectors. Solar collectors convert solar radiation into thermal energy for the purpose of heating a liquid, usually water. Solar collectors are often used as swimming pool heaters or domestic water heaters. Because coal-derived coatings tend to be absorptive of solar radiation, but transmissive in the infrared regime, it is conceivable that coal-derived coatings might be used to increase the economic attractiveness and enhance the performance of solar collectors. In addition coal-derived coatings can be of interest because of their ability to resist damaging effects of ultraviolet (UV) radiation. Accordingly, UV/VIS Spectrophotometer testing was used to verify the spectral characteristics of coatings derived from coal tar. The absorption spectrum verified that the coal-derived coatings are transmissive in the IR region but absorptive at shorter wavelengths. Tests were also conducted to measure the temperature rise of panels coated with the manufacturer's own absorptive coating, as well as identical panels coated with coal tar derived binder pitch. Glass (reflective of IR) as well as plastic (transparent) was trialed as cover plates for different materials and configurations. The results suggest that coal tar derived pitch can be a low-tech material for achieving spectrally selective coatings for enhanced performance and reduced cost for solar collectors of different types.

WVU and SolarRoofs.com will continue to explore the possibility of developing commercial applications of coal derivatives in solar heating products.

Table of Contents

LIST OF FIGURES.....	5
I. EXECUTIVE SUMMARY.....	7
2.1 Types of Solar Collectors.....	8
3.1 Tasks:	12
3.2 Experiments with Coal Tar Pitch for Task 1	12
3.3 Conclusions from Preliminary Experiments	15
3.4 Final set of experiments with coal tar pitch.....	15
IV. ANALYSIS.....	18
4.1 True Coal Enamel versus Diluted Pitch.....	18
4.2 Possible Alternate Configurations.....	19
4.3 Comparison of Manufacturer's Panels and CPCPC Panel	24
V. RESULTS	34
VI. CONCLUSION AND SUMMARY.....	39
VII. REFERENCES	41

LIST OF FIGURES

Figure 1. Flat Plate Solar Collector. ²	8
Figure 2. Evacuated Tubes Collector.	8
Figure 3. Skyline Solar Collector (SolarRoofs.com Product).	9
Figure 4. Energy balance for the manufacturer’s panel.	10
Figure 5. Preferred configuration for solar collector. The cover glass reflects infrared energy, righting in an immediate efficiency.	11
Figure 6. Absorption Spectra of Coal Tar Pitch Dissolved in THF.	13
Figure 7. Absorption Spectra of Black Paint Dissolved in THF.	13
Figure 8. Aluminum Panels placed in the sun.	14
Figure 9. Aluminum Panels placed in sun with glass sheets covered.	15
Figure 10. SolarRoofs.com solar collector, including the “Black Crystal” coating which maximizes thermal efficiency.	16
Figure 11. The backside of the tube fin assembly is believed to be pure copper. This was spray painted with a coating prepared at WVU.	16
Figure 12. Solar Collector with Coal Tar Pitch coating and glass cover mounted on a test stand on the roof of Engineering Research Building at West Virginia University.	17
Figure 13. Skyline Solar Collector (Flat Plate Collector) and the modified collector.	17
Figure 14. SolarRoofs.com geometry. Polycarbonate Cover plate over welded fin/tube assembly.	19
Figure 15. Cross-Section of SolarRoofs.com Tube/fin subassembly.	20
Figure 16. Modified Free Convection Geometry. Is it possible to avoid welding the fin to the tube?	22
Figure 17. Graduate student Poornima Chateker and technician Bob Badley from SolarRoofs.com.	25
Figure 18. Summary of Trials.	26
Figure 19. Performance of the modified and unmodified panel was measured for different flow rates using the same input water source at about 20 °C.	35
Figure 20. Repeated experiment of Figure 19.	36
Figure 21. Comparison of output thermal temperature at 1 liter per minute water flow.	37

LIST OF TABLES

Table 1. Koppers Coal-Tar Pitch Properties.....	12
Table 2. Conditions for WVU Panel with Glass Cover.....	27
Table 3. Calorimetry for WVU Panel with Glass Cover.....	27
Table 4. Conditions for SolarRoofs.com with Glass cover	27
Table 5. Calorimetry for SolarRoofs.com with Glass cover	27
Table 6. Conditions for SolarRoofs.com with glass cover.....	28
Table 7. Calorimetry for SolarRoofs.com Panel with glass cover.	28
Table 8. Conditions for WVU panel with glass cover.....	28
Table 9. Calorimetry for WVU Panel with glass cover.	28
Table 10. Conditions for WVU Panel with glass cover.....	29
Table 11. Calorimetry for WVU Panel with glass cover.....	29
Table 12. Conditions for SolarRoof.com panel with carbonate cover.....	29
Table 13. Calorimetry for SolarRoof.com panel with carbonate cover.....	29
Table 14. Conditions for SolarRoof.com panel with carbonate cover.....	30
Table 15. Calorimetry for SolarRoof.com panel with carbonate cover.....	30
Table 16. Conditions for SolarRoof.com panel with carbonate cover.....	30
Table 17. Calorimetry for SolarRoof.com panel with carbonate cover.....	31
Table 18. Conditions for SolarRoof.com panel with carbonate cover.....	31
Table 19. Calorimetry for SolarRoof.com panel with carbonate cover.....	31
Table 20. Conditions for WVU Panel with glass cover.....	32
Table 21. Calorimetry for WVU Panel with glass cover.....	32
Table 22. Conditions for WVU Panel with glass cover.....	33
Table 23. Calorimetry for WVU Panel with glass cover.....	33

I. EXECUTIVE SUMMARY

The objective of this DOE NETL-funded research via the Consortium for Premium Carbon Products from Coal (CPCPC) is to develop inexpensive coal derived coatings which offer high absorptivity of solar radiation, with low emissivity of thermal (infrared) radiation. Results show superior results compared to state of the art nano-coatings used by industry leaders, with lower manufacturing cost. Solar collectors convert solar radiation into thermal energy for the purpose of heating a liquid, usually water. Solar collectors are often used as swimming pool heaters or domestic water heaters. Because coal-derived coatings tend to be absorptive of solar radiation, but transmissive in the infrared regime, it is conceivable that coal-derived coatings might be used to increase the economic attractiveness and enhance the performance of solar collectors. In addition coal-derived coatings can be of interest because of their ability to resist damaging effects of ultraviolet (UV) radiation. Full scale testing of solar collectors resulted in increased thermal output when the solar collector used the CPCPC coating in place of the manufacturer's coating. Performance and low cost have been achieved using a diluted coal tar pitch sprayed as a variable emissivity coating. This has been shown to be higher performance, when used with a glass cover, compared to the state of the art nanocoating with a polycarbonate cover.

However, the current coating exhibits problems with delamination from copper fins. Thermal expansion coefficient mismatch and lack of compliance in the coating likely contribute to this issue. In addition the coating was probably not completely cured, as condensate was noted on the inside of the cover. The possibility of replacing copper fins with steel fins (known to be an excellent host for coal tar enamel coatings) was considered. The possibility was raised that adequate coupling between fin and tube might be achieved via free convection from air in the collector, but this appears to be too weak. Hence, it is tentatively concluded that the manufacturer's presumed high quality weld is indeed an essential feature of the apparatus, and thus copper is the material of choice.

The results of testing, while carried out under less than ideal conditions due to variable cloud cover, verified that the CPCPC modified unit probably performs slightly better than the manufacturer's unit. If the manufacturer's unit is modified by replacing the polycarbonate cover with an IR-reflective glass cover, there is also some performance enhancement. Repeated testing under better conditions is necessary in order to distinguish between the CPCPC-best and SolarRoofs.com-best configurations. Irrespective of that hair-splitting exercise, the salient point is that the coal derived spectrally selective coating is very competitive in terms of thermal performance, while also offering potential benefits in cost.

WVU and SolarRoofs.com will continue to explore the possibility of developing commercial applications of coal derivatives in solar heating products.

II. INTRODUCTION

A solar collector is a device for extracting the energy of the sun directly into a more usable or storable form. The energy in sunlight is in the form of electromagnetic radiation from the infrared (long) to the ultraviolet (short) wavelengths. The solar energy striking the earth's surface at any one time depends on weather conditions, as well as location and orientation of the surface, but overall, it averages about 1000 watts per square meter under clear skies with the surface directly perpendicular to the sun's rays. The direct radiation is captured using a dark colored surface which absorbs the radiation as heat and conducts it to the transfer fluid. Metal makes a good thermal conductor, especially copper and aluminum. In high performance collectors, a "selective surface" is used in which the collector surface is coated with a material having properties of high-absorption and low-emissivity. The selective surface reduces heat-loss caused by infrared radiant emission from the collector to ambient. Another method of reducing radiant heat-loss employs a transparent window such as clear UV stabilized plastic or Low-emissivity glass plate¹.

2.1 Types of Solar Collectors

There are various types of solar collectors like flat plate collectors, evacuated tube collectors, pool or unglazed collectors. Flat plate and evacuated tube solar collectors in this section are typically used to collect heat for space heating or domestic hot water.

Flat Plate Collector:

A flat plate is the most common type of solar thermal collector, and is usually used as a solar hot water panel to generate solar hot water. Figure 1 shows a typical flat plate collector, used in this study.

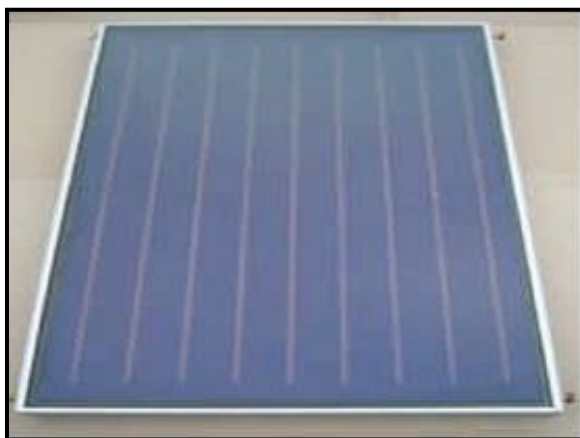


Figure 1. Flat Plate Solar Collector.²

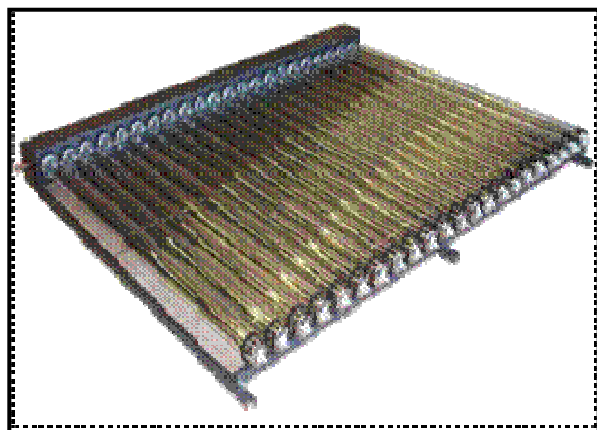


Figure 2. Evacuated Tubes Collector.

Evacuated Tube Collector:

These collectors have multiple evacuated glass tubes which heat up solar absorbers and, ultimately, solar working fluid (water or an antifreeze mix -- typically propylene glycol) in order to heat domestic hot water, or for hydronic space heating. The vacuum within the evacuated tubes reduce convection and conduction heat losses, allowing them to reach considerably higher temperatures than most flat-plate collectors. The evacuated tubes draw their energy from the available light rather than outside temperature .Figure 2 shows a typical evacuated tube collector³.

Pool or unglazed Collector:

This type of collector is much like a flat-plate collector, except that it has no glazing/transparent cover. It is used extensively for pool heating, as it works quite well when the desired output temperature is near the ambient temperature (that is, when it is warm outside). As the ambient temperature gets cooler, these collectors become ineffective¹.

Coal Tar Pitch and its Properties

A modified variable-emissivity coating was produced by the West Virginia University Chemical Engineering Department, Carbon Products Group. Our intent was to create a coating that could achieve nearly equivalent performance in terms of solar absorption with inhibited thermal re-radiation. As a target, we considered Skyline™ solar collectors, obtained from SolarRoofs.com Inc, in Sacramento California as shown in Figure 3. The high solar absorptivity assures that solar energy is converted into sensible heat (hot water), and the low emissivity in the infrared regime minimizes thermal losses.



Figure 3. Skyline Solar Collector (SolaRoofs.com Product).

The SolarRoofs.com device consists of copper tubes with welded fins, as shown in Figure 3. The fins are black in color due to a “Black Crystal” coating from Thermafin, which is understood to be a nanocrystalline metal alloy. This is considered to be a “spectrally selective” surface. According to the Thermafin.com web site, the solar absorptance ranging from 0.94 to 0.96 and the thermal emissivity ranges from 0.07 to 0.10.

Thermafin indicates that “the minimal thickness of the bimetallic alloy allows for almost complete transparency in the infrared spectrum allowing the coating to exhibit excellent thermal emittance properties⁵. A quartz encapsulation layer is said to protect the dendritic structure, and to impede optical reflection losses, though specifics are not given.

The energy balance for the solar collector system is not given. However, it is presumed that the polycarbonate material may allow most of the radiation from the sunlight to pass through, and that infrared radiation is not trapped, or at least not to the same degree that it might be in a greenhouse. Once absorbed, the low absorptivity of the coating and high reflectivity results in lower thermal energy rejected as graybody heat at a given temperature. This situation is shown qualitatively below (see figure 4 below).

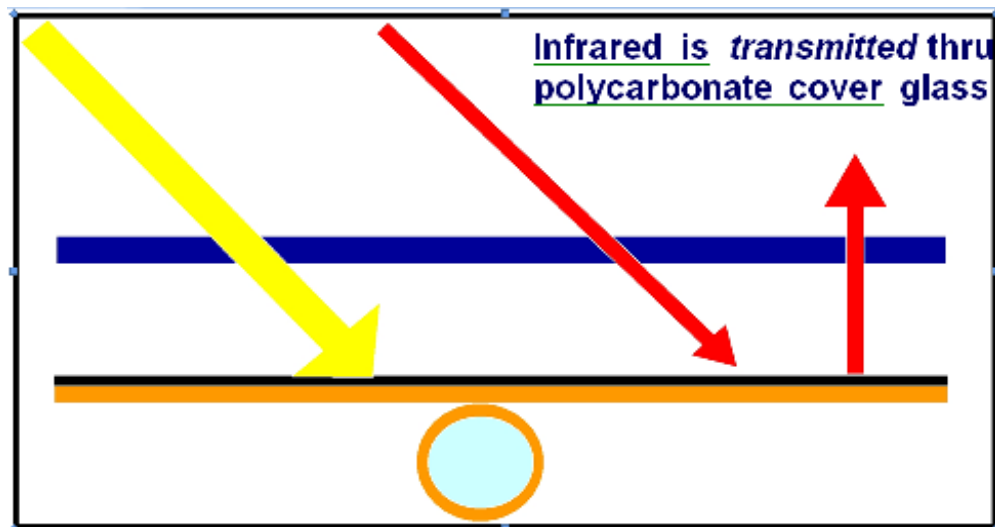


Figure 4. Energy balance for the manufacturer's panel.

The CPCPC variant uses a coal derived coating for the fins and pipe surface exposed to sunlight (see Figure 5 below). Like the nanocoating, the absorptivity for solar radiation is high. Unlike the nanocoating, however, the coal-derived coating is largely transparent to IR rather than reflective. Hence the IR emissivity is controlled by the copper metal underneath. Typically smooth metallic surfaces have poor emissivity. The IR-reflective window results in trapping thermally radiated energy that would otherwise be lost.

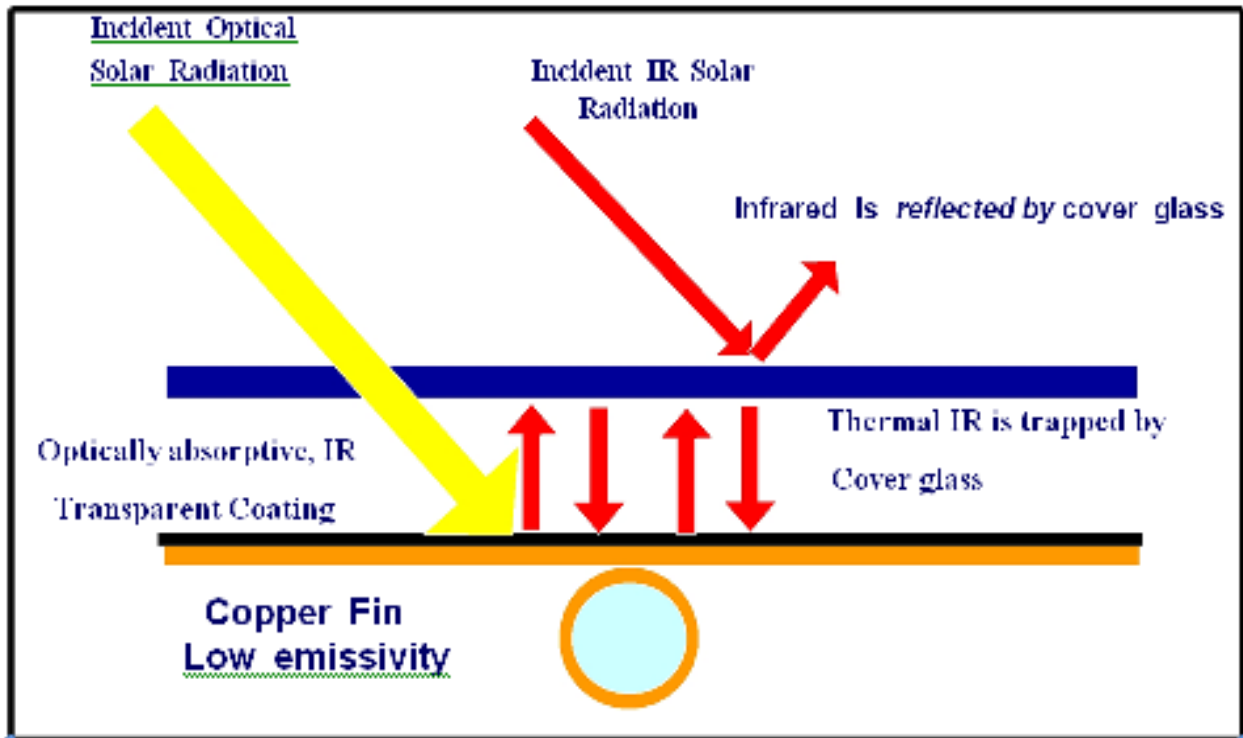


Figure 5. Preferred configuration for solar collector. The cover glass reflects infrared energy, resulting in an immediate efficiency.

III. EXPERIMENTAL

3.1 Tasks:

The major tasks involved the demonstration of:

- a) Ability of coal-derived coatings to screen ultraviolet (UV) radiation.
- b) Satisfactory bond strength between coal-derived coatings and polymeric substrate.

The selected material for these experiments was a coal tar binder pitch supplied by Koppers Inc. The coal tar binder pitch from Koppers has softening point of 109 °C. The chemical description of that pitch follows in Table 1. Tetrahydrofuran (THF) was used as solvent to dissolve the coal-tar pitch.

Table 1. Koppers Coal-Tar Pitch Properties.

	As Received	Post-filtration
Mettler Softening Pt. (°C)	109.9	108.1
Ash (%)	0.18	0.05
WVU Coke Yield (%)	-	53.95
Conradson Coke Yield (%)	-	48.0
Toluene Insolubles (%)	28.8	17.0
Quinoline/NMP Insolubles (%)	12.8	Nil

3.2 Experiments with Coal Tar Pitch for Task 1

The preliminary tests in this research began with attempts to study the ability of coal tar pitch to screen the ultraviolet (UV) radiation. Samples of coal-tar pitch and black paint dissolved in Tetrahydrofuran (THF) were analyzed by a UV/VIS spectrophotometer in the wavelength range of 190-1100 nm using 1mm cuvettes. It was seen from preliminary tests that coal-tar pitch was more sensitive in ultraviolet radiation than the black paint. The absorption spectrum of both coal tar pitch and black paint are shown in the Figures 6 and 7 respectively.

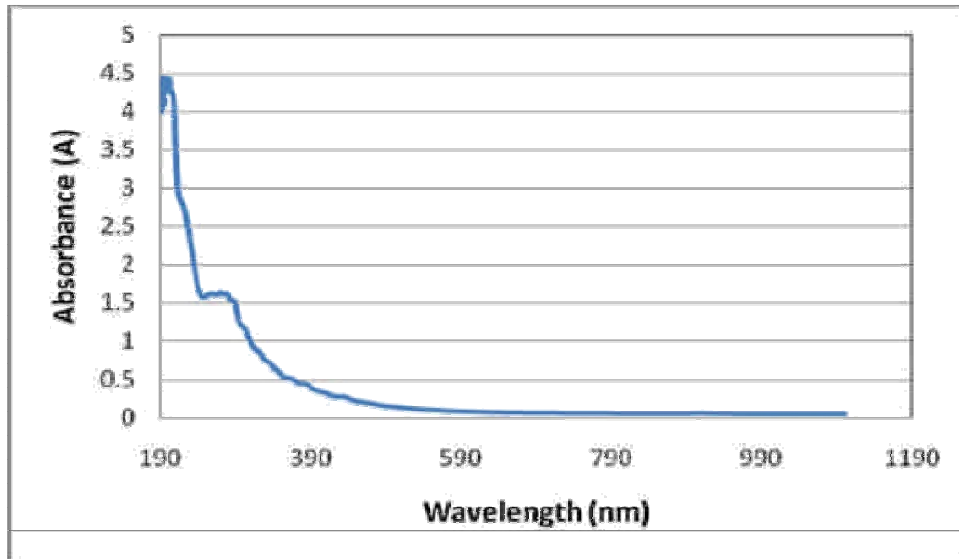


Figure 6. Absorption Spectra of Coal Tar Pitch Dissolved in THF.

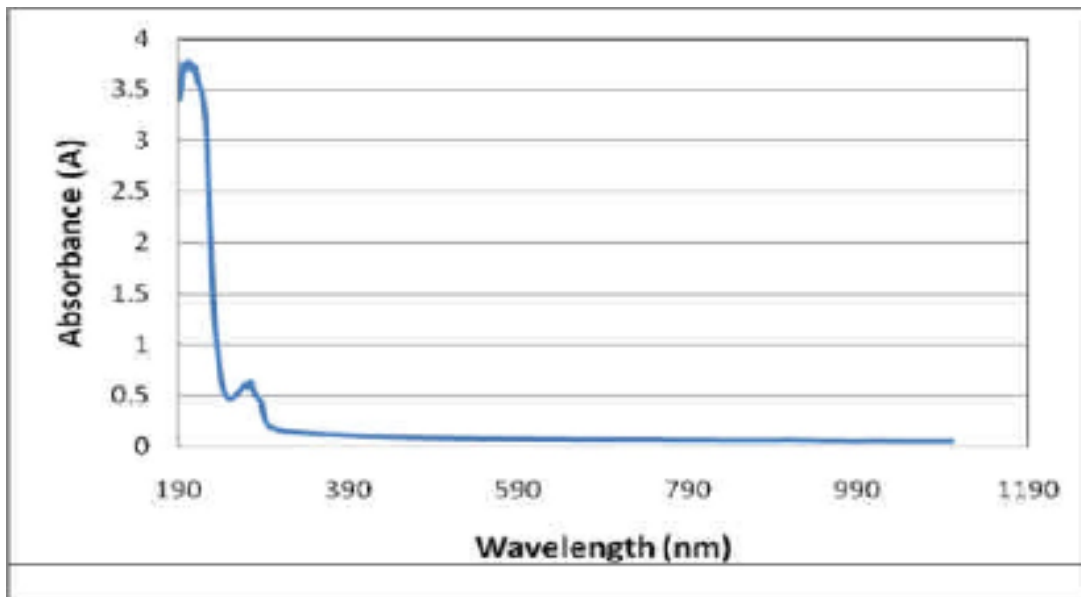


Figure 7. Absorption Spectra of Black Paint Dissolved in THF.

The other set of preliminary tests were conducted by measuring the temperature rise of aluminum panels coated with coal-tar pitch and black paint. In this test three aluminum panels, each of 1 ft² area, were used. One of these panels was coated with black paint, the second one with coal tar pitch (dissolved in THF) and the third one was left as it is (blank). These panels were placed outside in the sun with thermocouples attached to monitor the temperature rise continuously on a sunny day as shown in the Figure 8. It was seen that the coal tar pitch coated panel was as hot as the black paint. The temperature of the coal tar pitch coated panel was 63.69°C while that of the black paint was 64.89°C. The blank panel was at 31.64°C.

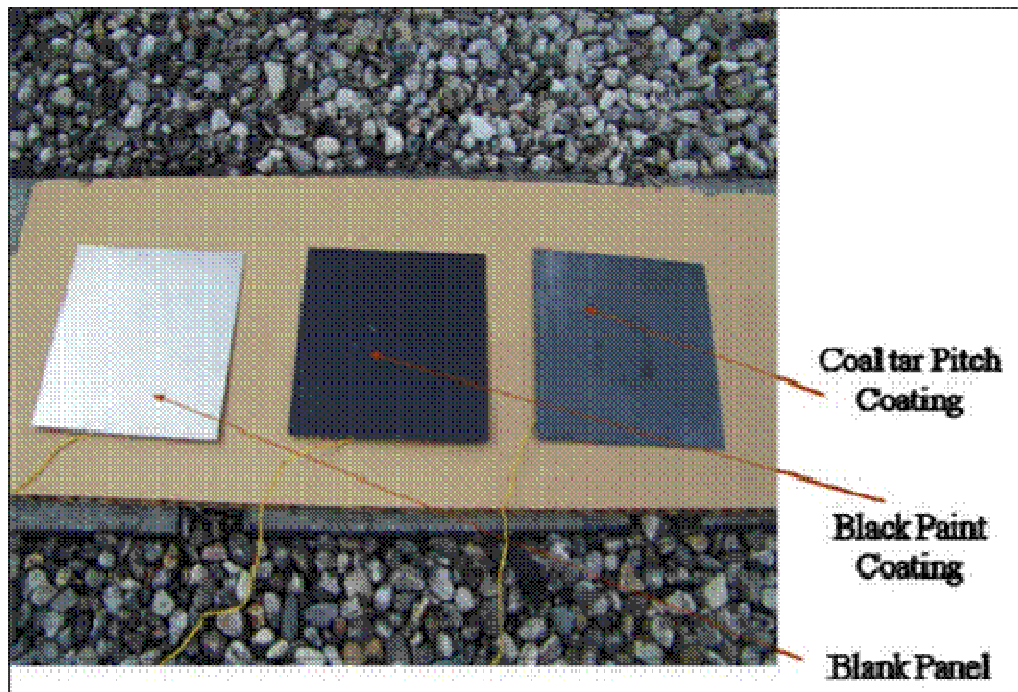


Figure 8. Aluminum Panels placed in the sun.

The final set of preliminary tests was done by modification of the above test. In this case the three panels, as mentioned above, were covered by a glass sheet using wooden spacers as shown in the Figure 9. The temperature rise of each panel was monitored using thermocouples attached to them. It was seen that the coal tar pitch coated panel was hotter than the black paint. The temperature of the coal tar pitch coated panel was 73.86°C while that of the Black Paint 71.29°C . The blank panel was at 20.23°C .

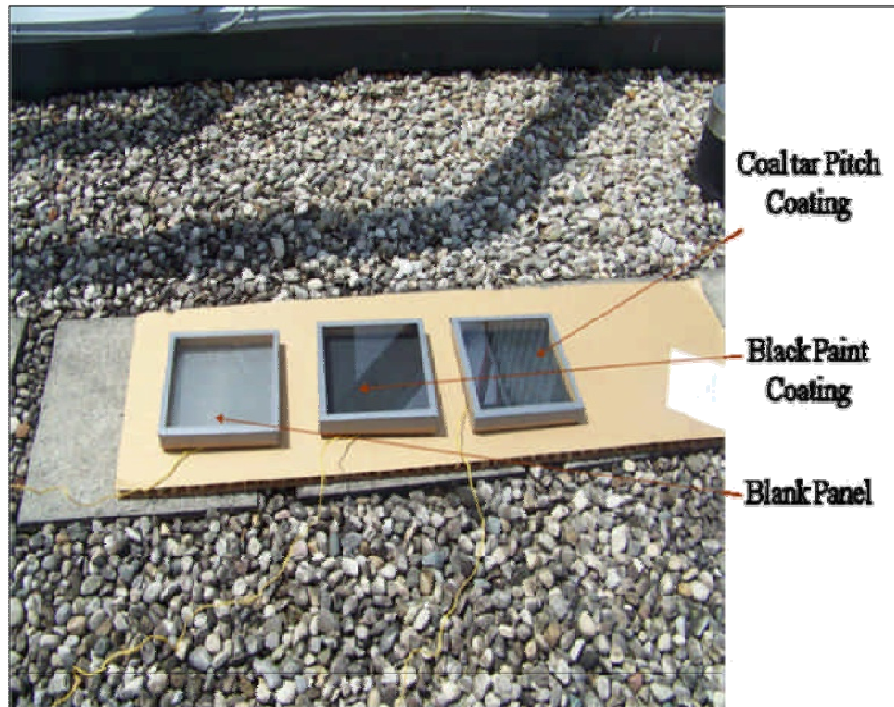


Figure 9. Aluminum Panels placed in sun with glass sheets covered.

The main idea in covering with the glass sheets was that, the glass plate placed above the collector plate will trap the radiated heat within the airspace below it. This exploits the so-called greenhouse effect, which is in this case a property of the glass: it readily transmits solar radiation in the visible and ultraviolet spectrum, but does not transmit the lower frequency infrared re-radiation very well. The glass plate also traps air in the space, thus reducing heat losses by convection. This idea was clearly illustrated in Figure 5.

3.3 Conclusions from Preliminary Experiments

The original idea to use coal tar pitch as an alternative spectral coating was successful, as it was seen from preliminary tests that coal-tar pitch was more sensitive in ultraviolet radiation than the black paint. Also the use of a glass sheet instead of a plastic shield was quantified as the temperature of the coal tar pitch coated aluminum panel was higher by 10°C when covered with glass. This demonstrates the ability of coal-tar pitch to offer tailored spectral emissivity and low emissivity and high transmissivity in infrared (IR) region of spectrum.

3.4 Final Set of Experiments with Coal Tar Pitch

After some discussion concerning the best way to apply a coating to the copper unit, the WVU approach was simply to flip over the manufacturer's panel, an illustration of which is shown in Figure 10 below, and to spray paint the uncoated side with our own spectrally selective emissivity coating. The uncoated side is shown in Figure 11. The final set of experimentation

was done to compare the efficiency of two solar collectors, first one coated with coal-tar pitch on its fins and the second one as received. These collectors were placed outside in the sun with water flowing through them and the temperature rise in the outlet water for each of these panels was measured. By difference in the temperature of the inlet and outlet water, the energy flow from the tubes to the water was calculated and hence the efficiency was compared.

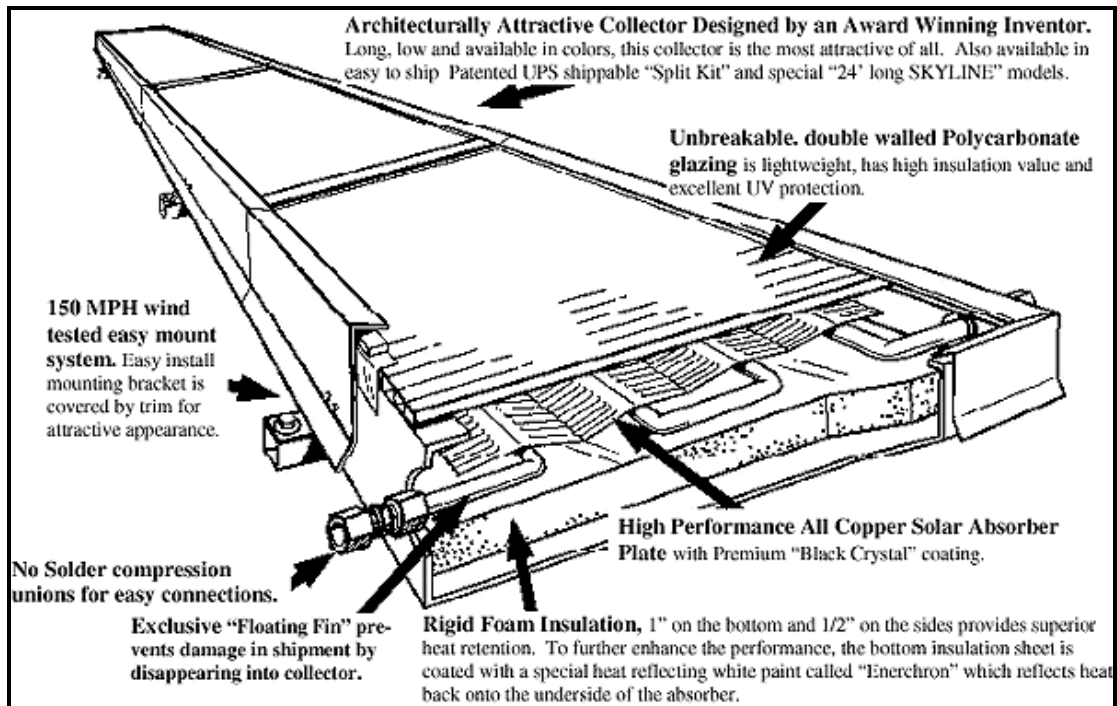


Figure 10. SolarRoofs.com solar collector, including the "Black Crystal" coating which maximizes thermal efficiency.



Figure 11. The backside of the tube fin assembly is believed to be pure copper. This was spray painted with a coating prepared at WVU.



Figure 12. Solar Collector with Coal Tar Pitch coating and glass cover mounted on a test stand on the roof of Engineering Research Building at West Virginia University.

The all day thermal performance of the panels, one coated with coal-tar pitch and the other one as received was measured by monitoring the temperature rise of outlet water through the panels. It was seen that the temperature rise of water through the coal-tar coated panel was significantly higher than the manufacturer's panel. For water flow rate of about 500 ml/min, the outlet water temperature of coal-tar pitch coated panel was about 46°C and that of the manufacturer's panel was about 40°C.

Referring to Figure 13, the unit on the left is the modified unit, mounted on the test stand, held at a 45 degree angle, facing approximately due south. It is interchangeable with the unit on the right, so that the modified panel can be taken down and the control panel mounted on the test stand within five minutes, with another ten minutes to achieve thermal equilibrium. All tests indicated more thermal energy from the modified collector than the unmodified collector.



Figure 13. Skyline Solar Collector (Flat Plate Collector) and the modified collector.

IV. ANALYSIS

The results of the preliminary experiments showed that the coal derived coatings can screen the UV radiation when compared to black paint. As these coatings are effective UV shields, additives to increase the thermal stability of solar collectors can be utilized without a net drop in UV resistance. Also the use of glass sheets instead of plastic shields can greatly improve the efficiency of solar collectors by trapping the radiated heat within the airspace below it. The results of the final tests are also as hypothesized, the result will be an increase in renewable energy usage at lower cost.

It was expected that approximately equivalent performance would be observed, with the primary advantage to the CPCPC concept being that the capital cost could be reduced if a low-tech replacement for nanocoatings were to be made available.

4.1 True Coal Enamel versus Diluted Pitch

Experimental results clearly show that there is a distinct advantage in the suggested coal tar enamel based coating. However, there are several technical points that need to be resolved before a commercial product can be realized.

First, the coatings tested were intended to mimic the properties of coal tar enamel, which is used as a pipeline coating, and has literally decades worth of data in a variety of weathering conditions ranging from salt water to arctic conditions to desert conditions. However, the formulation for pipeline applications includes the use of additives such as gypsum, which serves to create a more compliant material.

These additives would have made data collection from ultraviolet-visible spectroscopy difficult to obtain due to the non-homogeneous nature of the coating with additives. For that reason, it was decided to carry out spectroscopic studies with coal tar derived pitch, in order to verify the spectrally-variable emissivity of the coatings.

Two problems were introduced by that substitution, however. First, the toluene-soluble pitch had a softening temperature of 110 °C, which is reasonably close to the operating condition of the solar absorption panel. Solvent condensation was noted on the inner surface of the glass cover. This raises the possibility that the toluene may be partially bound to the coating, and that it might devolatilize over time once the panel is in unattended operation. Although the observed condensate seemed to be clear, it is possible that some discoloration might occur in the future, and if so there could be an effect on the performance of the panel. The solution to this is to use industry standard coal tar enamel, and to bake out the coating at a temperature of some 300 °C.

Another deficiency in the coating as tested was that the coating was friable and could actually flake off during handling. This is no doubt due in part to the fact that a pure coal tar pitch was used rather than the true coal tar enamel, as described above. However, there may be some differences between the pipes traditionally protected by coal tar enamel coatings, and the commercial grade copper uses in the solar collector.

First, the coal tar enamel may not adhere well to copper compared to pipeline steel. Coal tar enamel coatings are typically used with ferrous alloy piping and tubes. Coal tar enamel may not adhere as well to copper based alloys. In addition, copper alloys are notorious for thermal expansion problems. The thermal expansion coefficient for copper is about $17 \times 10^{-6}/^{\circ}\text{C}$, whereas steel is usually less than $11 \times 10^{-6}/^{\circ}\text{C}$. The potential mismatch, then, suggests that loss of integrity of the interface may be possible.

4.2 Possible Alternate Configurations

The current design of the SolarRoofs.com collector, as well as other similar units, relies on a weld between the copper pipe, and thin copper fin materials. The reason for preferring copper is obvious. With a thermal conductivity of about 400 W/mK versus a paltry 16 W/mK for steel, it seems obvious that copper should be the preferred candidate. Based on conductivity ratios, a copper fin would replace a steel fin of 25 times its mass. The geometry is shown in Figures 14 and 15.

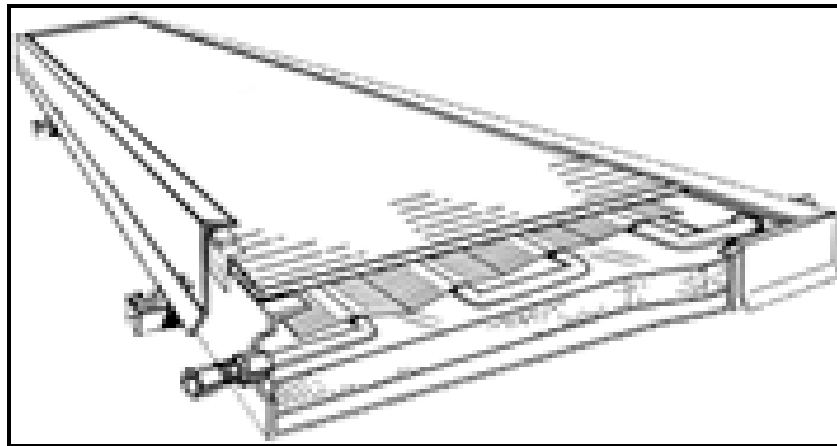


Figure 14. SolarRoofs.com geometry. Polycarbonate Cover plate over welded fin/tube assembly.

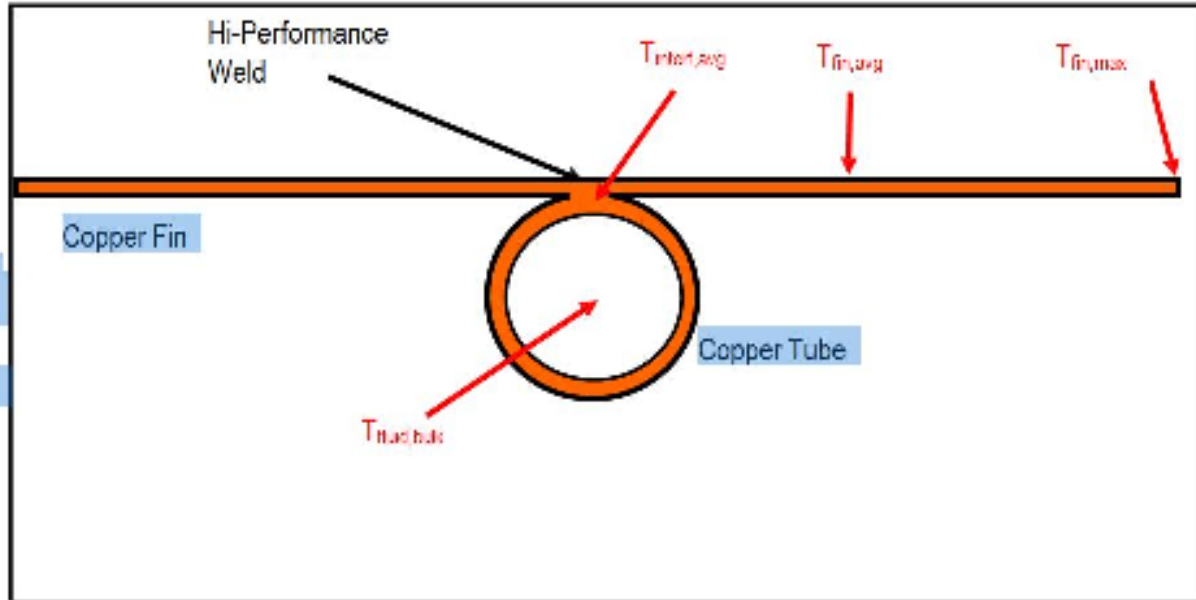


Figure 15. Cross-Section of SolarRoofs.com Tube/fin subassembly.

The question was raised whether the gossamer thin fin can actually transfer heat via conduction through the welded interface to the tube. Welded interfaces are notoriously poor conductors of heat if not created with utmost care. Hence an alternative possibility is envisioned. In this case the fin is thermally decoupled from the tube. Heat transfer is thus via free convection between the hot atmosphere within the unit and the pipes passing through an air interface, which for purposes of illustration are assumed to be in an isothermal air atmosphere at 100 °C

This reduces to a Grashoff number problem, requiring some estimate of the cooling coefficient that can exist at the fin surface as well as the outer surface of the tubes.

Although numerical estimates of the actual heat transfer coefficients in this complex geometry are very difficult, by solving the problem backwards, we can suggest constraints for the problem.

a. Conduction Problem. It is first assumed that the fins collect solar radiation and transfer heat mainly by conduction (negligible convection effects). As a representative case, the following data are used:

Temperature of the inlet water: 23 °C = 296 K

Temperature of the outlet water: 46 °C = 319 K

Volumetric flow rate of water through copper tubes = 500 ml/min

Average Temperature of the Water flowing through the panels is :

$$T_{fluid,bulk} = (23+46)/2 = 34.5 \text{ } ^\circ\text{C}$$

The amount of energy flowing from tubes through water is given by

$$\dot{Q} = \dot{m}C_p\Delta T$$

Where,

A is the effective collector area, 70 inches by 18 inches or 1260 in² or 8130 cm²;
 m is the mass flow rate of water flowing through the tubes, 0.50 kg/min = 8.3 g/sec;
 C_p is the specific heat of water = 4.186 joule/gram °C

□□□□□ΔT is the rise in water temperature = 319 K - 296 K = 23 K

Therefore,

$$\dot{Q} = 8.3 \frac{\text{g}}{\text{sec}} \cdot 4.186 \frac{\text{joule}}{\text{gm} - \text{sec}} \cdot 23 \text{ K} = 798 \text{ Watts}$$

The average heat flux for the collector can be measured as:

$$\frac{\dot{Q}}{A} = \frac{798 \text{ Watts}}{8130 \text{ cm}^2} = 982 \frac{\text{W}}{\text{m}^2}$$

This is very close to the expected value.

Working the problem backward, the average fin temperature can be estimated knowing that the length of tubing is 70 inches or 177.8 cm. There are four lengths of tubing with fins on both sides. Thus the total fin base is 1422 cm long.

Assuming a fin thickness of 0.5 mm, the fin area is 711 cm². The fin height is 5.7 cm, meaning that the average conduction path would be 2.8 cm. This allows the fin average temperature to be estimated by the conduction equation (equating the fin interface temperature with the bulk fluid temperature), with the thermal conductivity of copper at 400 W/mK.

$$798 = 400 * 0.0711 * \left[\frac{T_{fin,avg} - 34.5 \text{ } ^\circ\text{C}}{0.028} \right]$$

Therefore,

$$T_{fin,avg} = 35.3 \text{ } ^\circ\text{C}$$

and by symmetry,

$$T_{fin,avg} \approx 36 \text{ }^{\circ}\text{C}$$

One might then ask whether it is possible to transfer that same amount of energy via free convection to the air in the unit, and then by free convection to the tubing, as shown in Figure 16.

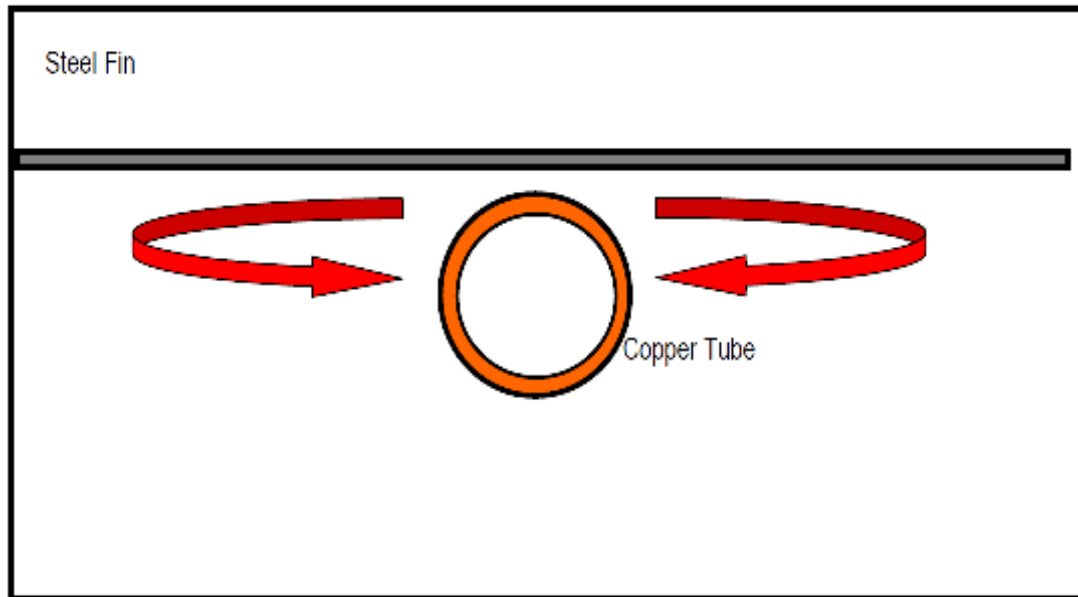


Figure 16. Modified Free Convection Geometry. Is it possible to avoid welding the fin to the tube?

In this case, the total heat for the panel should be approximately the same, or 798 W. The heat flux at the fin surface likewise remains equal to about 982 W/m². However, the outer area of the pipes is calculated knowing that the diameter of the tubes is 3/8" O.D., with length 6 feet x 4 feet. Hence the outer area of the tubing is

$$A_2 = 3.14 * .375'' \times 24 \times 12'' = 339 \text{ in}^2 \text{ or } 2189 \text{ cm}^2.$$

The wall heat flux from gas to tubing is thus:

$$Q'' = \frac{\dot{Q}}{A_2} = \frac{798 \text{ W}}{2189 \text{ cm}^2} = 4486 \frac{\text{W}}{\text{cm}^2}$$

A thermal impedance formulation can be written based on a fin temperature or 36 °C. Specifically, applying Newton's Law of Cooling to both interfaces,

$$\dot{Q} = h_1 A_1 (T_{fin,max} - T_{air}) = h_2 A_2 (T_{air} - T_{fluid,bulk}) = 798 \text{ W}$$

Solving for T_{air} ,

$$(T_{fin,max} - T_{air}) = \frac{798 \text{ W}}{h_1 A_1}$$

or

$$T_{air} = \left(T_{fin,max} - \frac{798 \text{ W}}{h_1 A_1} \right)$$

This can then be substituted in the convection equation, yielding an expression containing only the fin temperature and bulk fluid temperature,

$$h_2 A_2 \left(T_{fin,max} - \frac{798 \text{ W}}{h_1 A_1} - T_{fluid,bulk} \right) = 798 \text{ W}$$

Substituting the desired result, $T_{fin,max} = 36 \text{ }^\circ\text{C}$ and $T_{fluid,bulk} = 34.5 \text{ }^\circ\text{C}$, along with $A_1 = 8130 \text{ cm}^2$ and $A_2 = 2189 \text{ cm}^2$

$$h_2 \cdot 0.2189 \text{ m}^2 \left(36 \text{ }^\circ\text{C} - \frac{798 \text{ W}}{h_1 0.8130 \text{ m}^2} - 34.5 \text{ }^\circ\text{C} \right) = 798 \text{ W}$$

The term in the brackets must be non-zero in order for a meaningful result to exist. Hence

$$\left(\frac{798 \text{ W}}{h_1 0.8130 \text{ m}^2} \right) < 1.5 \text{ }^\circ\text{C}$$

Thus,

$$h_1 > \left(\frac{798 \text{ W}}{0.8130 \text{ m}^2 \cdot 1.5 \text{ }^\circ\text{C}} \right)$$

$$h_1 > \left(\frac{650 \text{ W}}{\text{m}^2 \text{ }^\circ\text{C}} \right)$$

Clear et al. suggested correlations for free convection from flat roofs, which yielded heat transfer coefficients lower by at least an order of magnitude.⁴

This suggests indeed that a metallic conduction path (i.e. a welded joint) is necessary for reasonable performance. A remaining experimental need would be to check whether the fin temperature is indeed as close to the water outlet temperature as expected.

4.3 Comparison of Manufacturer's Panels and CPCPC Panel

It was decided to attempt to duplicate the side-by-side comparison of the modified panel at the manufacturer's facility (see Figure 17). There are several reasons for this. One is that to establish a long term working relationship it is obviously useful to work onsite. Second, the performance of solar panels is a fairly complex function of latitude, cloud cover, orientation, etc., and there may be some differences in experiments carried out in Morgantown WV versus Carmichael CA. If so, these differences need to be understood. Third, and most important, there may be different understandings on how the panels should be designed, and these need to be resolved.

It became obvious that there were actually two variables changed for the CPCPC project. The first, obviously, is the coating material, in which WVU used a coal tar derivative versus a spectrally selective emissivity nanocoating, which we understood would absorb virtually all incident solar energy (including IR), but radiate poorly in the infrared regime; i.e., at a 100 °C graybody spectrum. WVU researchers presumed that this meant that the SolarRoofs.com coating is mainly *absorptive* in the IR, while the CPCPC coating is mainly *transmissive* in the IR.

Hence the CPCPC coating is presumed to be a poor absorber of IR, and so is the smooth copper surface underneath. Thus an IR-transmissive polycarbonate cover would not result in much additional initial absorption of thermal energy in the system. Conversely a IR-reflective glass cover would not result in additional losses from incident radiation, it was decided early on in this project to use a borosilicate glass cover.

It was further perceived that the situation would be different for the nanocoated SolarRoofs.com coating, since that coating might well absorb incoming IR radiation, but re-

radiate with lower emissivity. This assumption was based on reading the company's literature, and was not tested experimentally due to the lack of a sample (a nanocoated cuvette would have been needed for the UV-vis characterization). For that reason, it made sense that an IR transmissive cover could be used.

During discussions with Mr. Al Rich, the President of SolarRoofs.com, it was apparent that some of our assumptions of the spectrally selective characteristics of the nanocoating were perhaps incorrect. Specifically, Mr. Rich is of the belief that indeed better performance is obtainable from nanocoated copper using glass covers rather than polycarbonate. However, the reason for preferring polycarbonate is or it is believed to be lighter and thus easier to install for do-it-yourself solar collector installers; it is more durable in adverse weather conditions; and it is less susceptible to breakage. These commercial factors may outweigh the scientific and engineering advantages of higher efficiency.

Hence an apples-to-apples comparison needs to be done with the SolarRoofs.com collector using a borosilicate glass cover.



Figure 17. Graduate student Poornima Chateker and technician Bob Badley from SolarRoofs.com.

Graduate student Poornima Chateker, Elliot Kennel, worked directly with Al Rich, Bob Badley and Rob Van Heck of SolarRoofs.com. As shown in Figure 17, a movable test stand was placed in a southern orientation to compare panels. Although two panels are shown, in actuality only the lower panel was operated in order that any effects from the difference in position be mitigated.

It was decided that we would operate the panel, collecting data to perform calorimetry, and then switch from one configuration and back again to ensure that a trend could be observed. Obviously, in a solar panel, a maximum power generation is expected under cloud

free conditions when the sun as in its highest point versus the orientation of the panel.

The conditions were not optimal during the days we chose to visit, although we did have one day with only intermittent cloud cover. The data is shown in Tables 2 – 23. The data is summarized graphically in Figure 18 below.

Ideally it would have been better to repeat the experiments over many days in order to make an evaluation of the “best performance.” It is very likely that the CPCPC panel with glass cover achieved higher performance than the SolarRoofs.com panel with polycarbonate cover. Due to cloud cover, the data comparing the CPCPC panel with glass cover and the SolarRoofs.com Panel with glass cover is ambiguous. We could not reach a definite conclusion as to which is actually the higher performance, although it can be said that the CPCPC panel was at least comparable to the best possible performance attainable from the SolarRoofs.com panel in any configuration. Likely these tests will be repeated in the future.

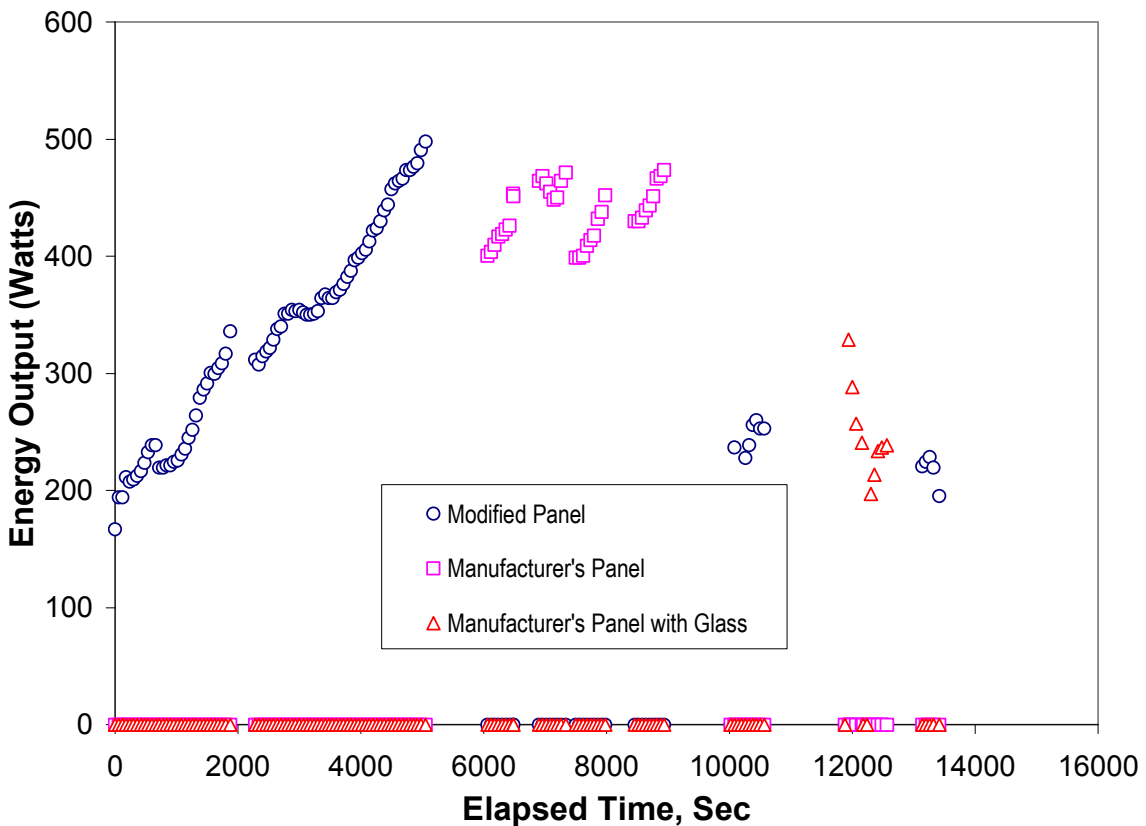


Figure 18. Summary of Trials.

Table 2. Conditions for WVU Panel with Glass Cover.

Ambient Air	hours	min	sec	
Flow rate start time	14	56		
Flow rate stop time	15	0	38	
Flow rate delta time			278	
Flow rate volume	27.8	ounces	1209.40048	mL
Volumetric flow rate			4.350361437	mL of water per sec
Mass flow rate			4.350361437	grams/sec
Panel being tested:	WVU panel with glass cover			

Table 3. Calorimetry for WVU Panel with Glass Cover.

	Hours	min	Sec	Temp Water IN	Temp Water Out	Watts
Time (total seconds)						
53760	14	56		63.8	85.6	220.5508
53820	14	57		63.8	86	224.5976
53880	14	58		63.8	86.4	228.6444
53940	14	59		63.8	85.5	219.5391
54038	15	0	38	63.8	83.1	195.2582

Table 4. Conditions for SolarRoofs.com with Glass cover

Ambient Air	hours	Min	sec	
Flow rate start time	14	35		
Flow rate stop time	14	40	37	
Flow rate delta time			337	
Flow rate volume	27.8	Ounces	1209.40048	mL
Volumetric flow rate			3.588725459	mL of water per sec
Mass flow rate			3.588725459	grams/sec
Panel being tested:	SolarRoofs.com Panel with glass cover			

Table 5. Calorimetry for SolarRoofs.com with Glass cover

	hours	min	Sec	Temp Water IN	Temp Water Out	Watts
Time (total seconds)						
52500	14	35	0	63.8	0	0
52560	14	36		63.8	96.3	328.8027
52620	14	37		63.8	92.3	288.3347
52680	14	38		63.8	89.2	256.972
52778	14	39	38	63.8	87.6	240.7848
52800	14	40			87.6	

Table 6. Conditions for SolarRoofs.com with glass cover.

Ambient Air	hours	min	sec	
Flow rate start time	14	41		
Flow rate stop time	14	46	23	
Flow rate delta time			323	
Flow rate volume	27.8	ounces	1209.40048	mL
Volumetric flow rate			3.744273931	mL of water per sec
Mass flow rate			3.744273931	grams/sec
Panel being tested:	SolarRoofs.com Panel with glass cover			

Table 7. Calorimetry for SolarRoofs.com Panel with glass cover.

				Temp	Temp	
Time(total seconds)	hours	min	sec	Water IN	Water Out	Watts
52860	14	41		66.9	85.8	0
52920	14	42		66.9	86.4	197.2816
52980	14	43		66.9	88	213.4689
53040	14	44		66.9	90	233.7029
53100	14	45		66.9	90.3	236.738
53183	14	46	23	66.9	90.5	238.7614

Table 8. Conditions for WVU panel with glass cover.

Ambient Air	hours	min	sec	
Flow rate start time	14		2	
Flow rate stop time	14		6	57
Flow rate delta time				297
Flow rate volume	27.8	ounces	1209.40048	mL
Volumetric flow rate			4.072055487	mL of water per sec
Mass flow rate			4.072055487	grams/sec
Panel being tested:	WVU Panel with glass cover			

Table 9. Calorimetry for WVU Panel with glass cover.

				Temp	Temp	
Time (total seconds)	hours	min	sec	Water IN	Water Out	Watts
50520	14		20	63.5	63.5	0
50580	14		3	63.5	63.5	0
50640	14		4	63.5	63.5	0
50700	14		5	63.5	86.9	236.738
50760	14		6	63.5	81.7	184.1295
50817	14		6	63.5	81.5	182.1061

Table 10. Conditions for WVU Panel with glass cover.

Ambient Air	hours	min	sec	
Flow rate start time	14	8		
Flow rate stop time	14	13	5	
Flow rate delta time			305	
Flow rate volume	27.8	ounces	1209.40048	mL
Volumetric flow rate			3.965247474	mL of water per sec
Mass flow rate			3.965247474	grams/sec
Panel being tested:	WVU Panel with glass			

Table 11. Calorimetry for WVU Panel with glass cover.

				Temp	Temp	
Time(total seconds)	hours	min	sec	Water IN	Water Out	Watts
50880	14	8	0	63.5	86	227.6327
50940	14	9		63.5	87.1	238.7614
51000	14	10		63.5	88.8	255.9603
51060	14	11		63.5	89.2	260.0071
51120	14	12		63.5	88.5	252.9252
51185	14	13	5	63.5	88.5	252.9252

Table 12. Conditions for SolarRoof.com panel with carbonate cover.

Ambient Air	hours	min	sec	
Flow rate start time	12	58		
Flow rate stop time	13	5	27	
Flow rate delta time			447	
Flow rate volume	27.8	ounces	1209.40048	mL
Volumetric flow rate			2.705593914	mL of water per sec
Mass flow rate			2.705593914	grams/sec
Panel being tested:	SolarRoofs.com panel with carbonate cover			

Table 13. Calorimetry for SolarRoof.com panel with carbonate cover.

				Temp	Temp	
Time(total seconds)	hours	min	sec	Water IN	Water Out	Watts
46680	12	58	0	63	102.6	400.6335
46740	12	59		63	102.9	403.6686
46800	13	0		63	103.5	409.7388
46860	13	1		63	104.2	416.8207
46920	13	2		63	104.4	418.8441
46980	13	3	0	63	104.8	422.8909
47040	13	4		63	105.1	425.926
47100	13	5		63	107.8	453.2419
47105	13	5	5	63	107.6	451.2185

Table 14. Conditions for SolarRoof.com panel with carbonate cover.

Ambient Air	hours	min	sec	
Flow rate start time	13		11	
Flow rate stop time	13		19	17
Flow rate delta time				497
Flow rate volume	27.8	ounces	1209.40048	mL
Volumetric flow rate			2.433401367	mL of water per sec
Mass flow rate			2.433401367	grams/sec
Panel being tested:	SolarRoofs.com panel with carbonate cover			

Table 15. Calorimetry for SolarRoof.com panel with carbonate cover.

				Temp	Temp	
Time(total seconds)	hours	min	sec	Water IN	Water Out	Watts
47460	13	11		65.1	65.1	0
47520	13	12		65.1	111	464.3706
47580	13	13		65.1	111.4	468.4174
47640	13	14		65.1	110.8	462.3472
47700	13	15		65.1	110.1	455.2653
47760	13	16		65.1	109.4	448.1834
47820	13	17		65.1	109.6	450.2068
47880	13	18		65.1	111	464.3706
47957	13	19	17	65.1	111.7	471.4525

Table 16. Conditions for SolarRoof.com panel with carbonate cover.

Ambient Air	hours	min	sec	
Flow rate start time	13		21	
Flow rate stop time	13		30	0
Flow rate delta time				540
Flow rate volume	27.8	ounces	1209.40048	mL
Volumetric flow rate			2.239630518	mL of water per sec
Mass flow rate			2.239630518	grams/sec
Panel being tested:	SolarRoofs.com panel with carbonate cover			

Table 17. Calorimetry for SolarRoof.com panel with carbonate cover.

Time(Total seconds)	hours	min	sec	Temp	Temp	Watts
				Water IN	Water Out	
48060	13	21	0	67.8	67.8	0
48120	13	22		67.8	107.2	398.6101
48180	13	23		67.8	107.2	398.6101
48240	13	24		67.8	107.4	400.6335
48300	13	25		67.8	108.2	408.7271
48360	13	26	0	67.8	108.7	413.7856
48420	13	27		67.8	109.1	417.8324
48480	13	28		67.8	110.5	431.9962
48540	13	29		67.8	111.1	438.0664
48600	13	30		67.8	112.5	452.2302

Table 18. Conditions for SolarRoof.com panel with carbonate cover.

Ambient Air	hours	min	sec	
Flow rate start time	13		37	
Flow rate stop time	13		45	57
Flow rate delta time				537
Flow rate volume	27.8	ounces	1209.40048	mL
Volumetric flow rate			2.25214242	mL of water per sec
Mass flow rate			2.25214242	grams/sec
Panel being tested:	SolarRoofs.com panel with carbonate cover			

Table 19. Calorimetry for SolarRoof.com panel with carbonate cover.

Time(total seconds)	hours	min	sec	Temp	Temp	Watts
				Water IN	Water Out	
49020	13	37	0	65.5	65.5	0
49080	13	38		65.5		108429.9728
49140	13	39		65.5		108429.9728
49200	13	40		65.5	108.3	433.0079
49260	13	41		65.5	108.9	439.0781
49320	13	42	0	65.5	109.3	443.1249
49380	13	43		65.5	110.1	451.2185
49440	13	44		65.5	111.6	466.394
49500	13	45		65.5	111.8	468.4174
49557	13	45	57	65.5	112.3	473.4759

Table 20. Conditions for WVU Panel with glass cover.

Ambient Air	hours	min	sec	
Flow rate start time	11		17	
Flow rate stop time	11		48	17
Flow rate delta time			1877	
Flow rate volume	320	ounces	1209.40048	mL
Volumetric flow rate			0.644326308	mL of water per sec
Mass flow rate			0.644326308	grams/sec
Panel being tested:	WVU Panel with glass cover			

Table 21. Calorimetry for WVU Panel with glass cover.

Time(total seconds)	hours	min	sec	Temp	Temp	Watts
				Water IN	Water Out	
40620	11	17		56.5	73	166.9306
40680	11	18		56.5	75.7	194.2465
40740	11	19		56.5	75.7	194.2465
40800	11	20		56.5	77.4	211.4455
40860	11	21		56.5	77	207.3986
40920	11	22	0	56.5	77.2	209.422
40980	11	23		56.5	77.5	212.4572
41040	11	24		56.5	77.9	216.504
41100	11	25		56.5	78.6	223.5859
41160	11	26	0	56.5	79.5	232.6912
41220	11	27		56.5	80.1	238.7614
41280	11	28		56.5	80.1	238.7614
41340	11	29		58.6	80.3	219.5391
41400	11	30		58.6	80.3	219.5391
41460	11	31		58.6	80.5	221.5625
41520	11	32		58.6	80.5	221.5625
41580	11	33		58.6	80.8	224.5976
41640	11	34		58.6	80.9	225.6093
41700	11	35		58.6	81.4	230.6678
41760	11	36		58.6	81.9	235.7263
41820	11	37		58.6	82.8	244.8316
41880	11	38		58.6	83.5	251.9135
41940	11	39		58.6	84.7	264.0539
42000	11	40		58.6	86.2	279.2294
42060	11	41		58.6	86.9	286.3113
42120	11	42		58.6	87.4	291.3698
42180	11	43		58.6	88.3	300.4751
42240	11	44		58.6	88.2	299.4634
42300	11	45		58.6	88.7	304.5219
42360	11	46		58.6	89.1	308.5687
42420	11	47		58.6	89.9	316.6623
42497	11	48	17	58.6	91.8	335.8846

Table 22. Conditions for WVU Panel with glass cover.

Ambient Air	hours	min	sec	
Flow rate start time	11		50	
Flow rate stop time	12		41	15
Flow rate delta time			3075	
Flow rate volume	320	ounces	1209.40048	mL
Volumetric flow rate			0.393300969	mL of water per sec
Mass flow rate			0.393300969	grams/sec
Panel being tested:	WVU Panel with glass cover			

Table 23. Calorimetry for WVU Panel with glass cover.

				Temp	Temp	
Time(total seconds)	hours	min	sec	Water IN	Water Out	Watts
42600	11	50	0	59.9	59.9	0
42660	11	51		59.9	59.9	0
42720	11	52		59.9	59.9	0
42780	11	53		59.9	59.9	0
42840	11	54		59.9	59.9	0
42900	11	55	0	59.9	90.7	311.6038
42960	11	56		59.9	90.3	307.557
43020	11	57		59.9	91	314.6389
43080	11	58		59.9	91.4	318.6857
43140	11	59	0	59.8	91.6	321.7208
43200	12	0		59.8	92.3	328.8027
43260	12	1		59.8	93.2	337.908
43320	12	2		59.8	93.4	339.9314
43380	12	3		59.8	94.5	351.0602
43440	12	4		59.8	94.5	351.0602
43500	12	5		59.8	94.8	354.0953
43560	12	6		59.9	94.8	353.0836
43620	12	7		59.9	94.9	354.0953
43680	12	8		59.9	94.7	352.0719
43740	12	9		59.9	94.5	350.0484
43800	12	10		59.9	94.5	350.0484
43860	12	11		59.9	94.6	351.0602
43920	12	12		59.9	94.8	353.0836
43980	12	13		59.9	95.9	364.2123
44040	12	14		59.9	96.2	367.2474
44100	12	15		59.9	95.9	364.2123
44160	12	16		60.1	96.1	364.2123
44220	12	17		60.1	96.6	369.2708
44280	12	18		60.1	96.8	371.2942

44340	12	19		60.1	97.3	376.3527
44400	12	20		60.1	97.9	382.4229
44460	12	21		60.1	98.4	387.4814
44520	12	22		60.1	99.3	396.5867
44580	12	23		60.1	99.5	398.6101
44640	12	24		60.1	99.9	402.6569
44700	12	25		60.1	100.2	405.692
44760	12	26		60.1	100.9	412.7739
44820	12	27		60.1	101.8	421.8792
44880	12	28		60.1	102	423.9026
44940	12	29		60.1	102.6	429.9728
45000	12	30		60.1	103.5	439.0781
45060	12	31		60.1	104	444.1366
45120	12	32		60.1	105.3	457.2887
45180	12	33		60.1	105.8	462.3472
45240	12	34		60.1	106	464.3706
45300	12	35		60.1	106.2	466.394
45360	12	36		60.1	106.9	473.4759
45420	12	37		60.1	106.9	473.4759
45480	12	38		60.1	107.2	476.511
45540	12	39		60.1	107.5	479.5461
45600	12	40		60.1	108.6	490.6748
45675	12	41	15	60.1	109.3	497.7568

Efforts to date have shown that coal tar pitch diluted in solvent, in order to make it sprayable results in an optically black coating, with reduced emissivity in the IR band. Our concept relies on the coating being transparent in the IR band, meaning that IR emission actually comes from the smooth metal surface underneath. A reflective borosilicate glass cover sheet is used. The SolarRoofs.com panel uses a polycarbonate cover which is transmissive in the IR band. The fin coating is a nanocoating which is presumed to have low emissivity in the same band.

The combination of glass cover and coal derived fin coating is not only less expensive, but also appears to have significantly better output. This firmly established proof of concept. High temperature stability and thermal cycling resistance can be achieved from a true coal tar enamel coating than with the coal tar pitch coating.

V. RESULTS

The results of the preliminary experiments showed that the coal derived coatings can screen the UV radiation when compared to black paint. As these coatings are effective UV –shields, additives to increase the thermal stability of solar collectors can be utilized without a net drop in UV resistance. Also the use of glass sheets instead of plastic shields can greatly improve the

efficiency of solar collectors by trapping the radiated heat within the airspace below it.

It was expected that approximately equivalent performance would be observed, with the primary advantage to the CPCPC concept being that the capital cost could be reduced if a low-tech replacement for nanocoatings were to be made available. Surprisingly, however, a significant performance advantage was also observed, as shown in Figures 19-21. Figures 19 and 20 were determined using a single test stand, and replacing one panel with another and sequentially recording the data. Figure 21 was produced using both panels operating simultaneously in separate test stands. In all cases, thermal power output from the modified collector was 25% higher than in the case of the manufacturer's collector.

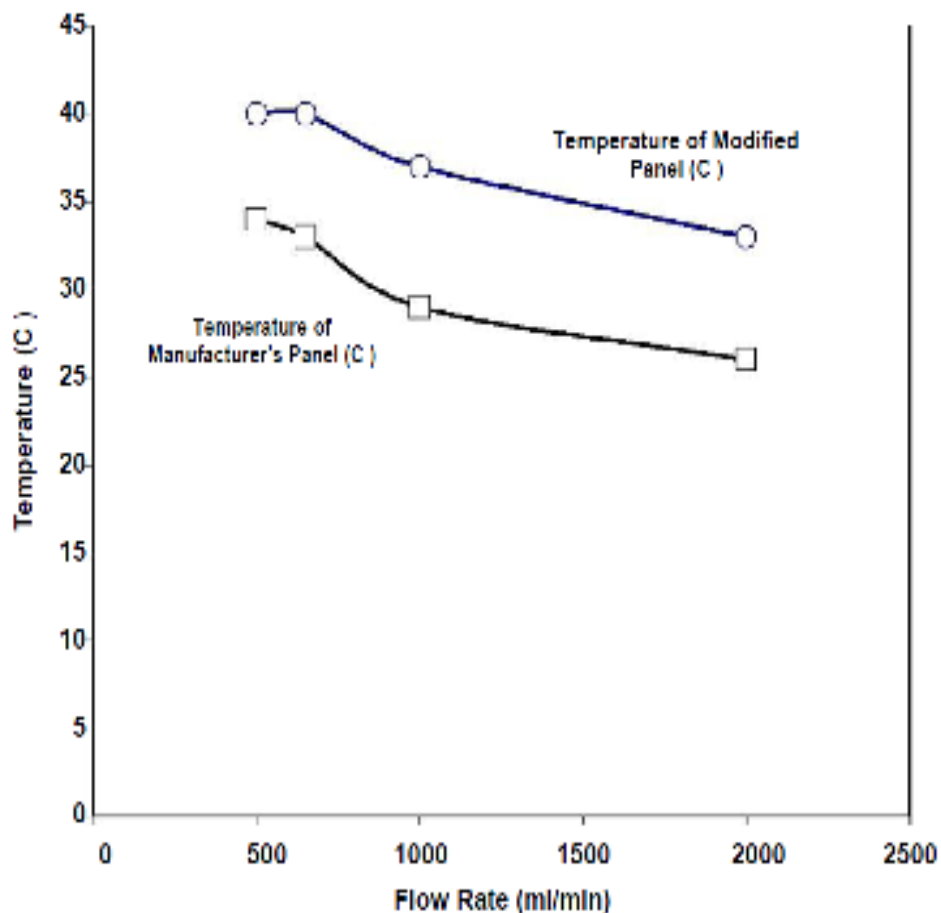


Figure 19. Performance of the modified and unmodified panel was measured for different flow rates using the same input water source at about 20 °C.

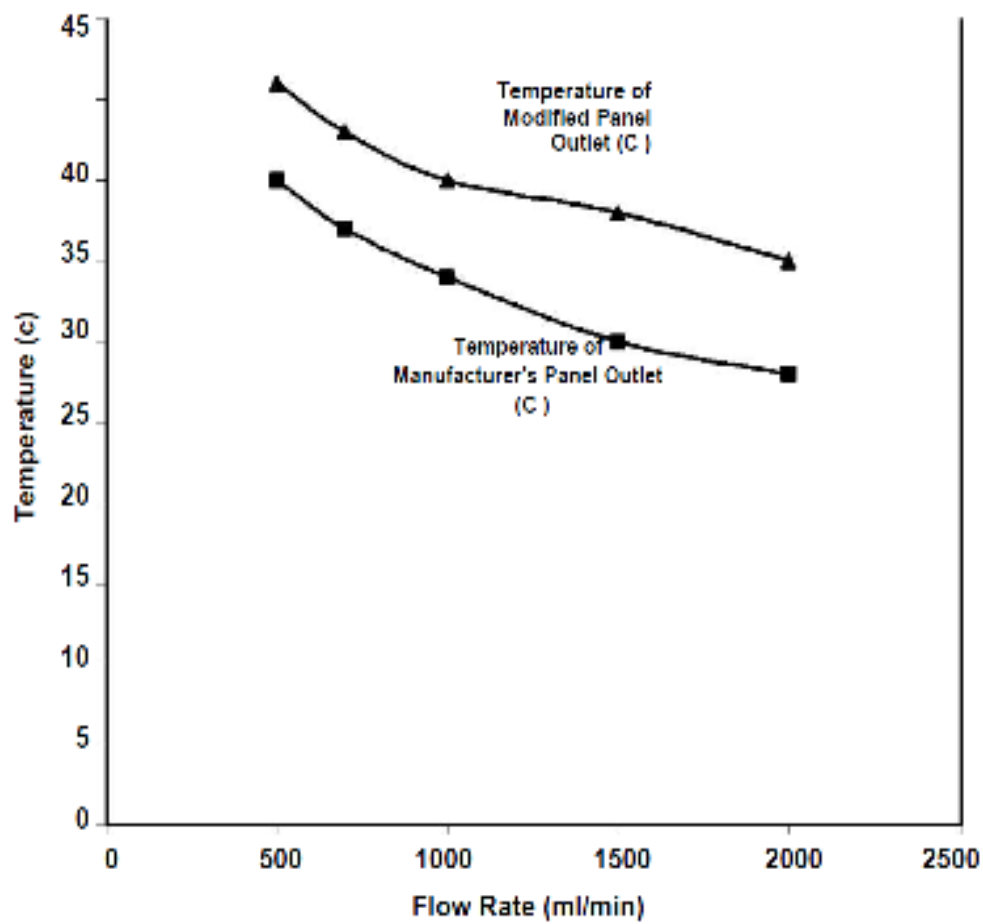


Figure 20. Repeated experiment of Figure 19.

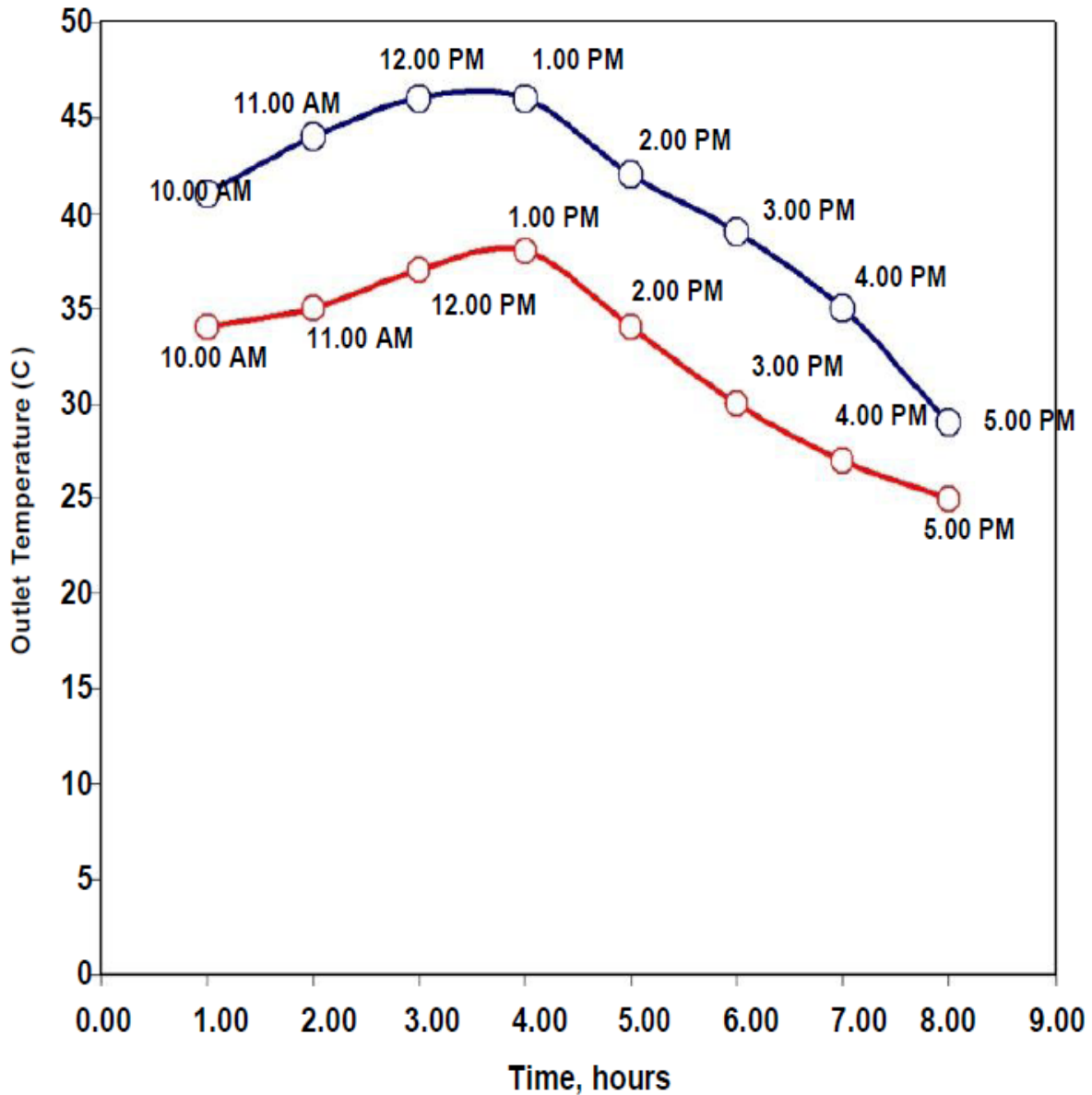


Figure 21. Comparison of output thermal temperature at 1 liter per minute water flow.

Referring to Figure 21, the lower curve shows the performance of an ACR Skyline Solar Panel. The upper curve shows an otherwise identical panel with a variable emissivity coating designed by WVU for CPCPC.

Efficiencies are estimated below:

Coal Tar Pitch Coated Panel

- Temperature of the inlet water: 23 °C = 296 K
- Temperature of the outlet water: 46 °C = 319 K

- Volumetric flow rate of water through copper tubes = 500 ml/min

Average temperature of the water flowing through the panels is $(23+46)/2 = 34.5^{\circ}\text{C}$.

Amount of energy flowing from tubes through water (Q):

$$Q = mC_p dT$$

Where,

m is the mass flow rate of water flowing through the tubes

C_p is the specific heat of water = 4.186 joule/gram $^{\circ}\text{C}$

dT is the rise in water temperature = 319 K - 296 K = 23 K

Mass flow rate of water flowing through the tubes is volumetric flow rate x density of water.

Therefore,

$$\text{Flow rate (m)} = 500 \text{ ml/min} \times 0.9948 \text{ gm/cc}$$

$$m = 497.4 \text{ gm/min}$$

Therefore,

$$Q = 497.4 \times 4.186 \times 23$$

$$47888.67 \text{ joules/min}$$

$$798.144 \text{ Watts}$$

Manufacturer's Panel

- Temperature of the inlet water: $23^{\circ}\text{C} = 296 \text{ K}$
- Temperature of the outlet water: $39^{\circ}\text{C} = 312 \text{ K}$
- Volumetric flow rate of water through copper tubes = 500 ml/min

Average temperature of the water flowing through the panels is $(23+39)/2 = 31^{\circ}\text{C}$. Amount of energy flowing from tubes through water (Q):

$$Q = mCpdT$$

Where,

dT is the rise in water temperature = 312K - 296 K = 16 K Therefore,

$$Q = 497.4 \times 4.186 \times 16 = 3313.86 \text{ Joules/min}$$

$$= 555.231 \text{ Watts}$$

Efficiency:

Amount of total radiation incident on the panel during a sunny day (corrected for angle of incidence) is 972 Watts in West Virginia region.

Therefore the efficiency of panel becomes

$$\text{Efficiency } (\eta) = (\text{Total energy out/Total energy in}) * 100$$

Coal tar pitch coated panel:

$$\text{Efficiency } (\eta) = (798.144 / 972) * 100$$

$$= \underline{82.11 \%}$$

Manufacturer's panel:

$$\text{Efficiency } (\eta) = (555.231 / 972) * 100$$

$$= \underline{57.12\%}$$

These values suggest that the coal tar pitch is not only effective in reducing the cost of the equipment but also improves the performance of the panel by 25 %. This high efficiency values suggest that coal tar pitch can replace the existing nano-coatings both for improved efficiency and for reducing the total cost.

VI. CONCLUSIONS AND SUMMARY

Coal-tar pitch dissolved in THF was analyzed by UV/VIS spectrophotometer and was seen that it has an effective UV-shielding ability. This allows the use of additives to increase the thermal stability of solar collectors without a net drop in UV resistance. Increased thermal stability would allow solar collectors to expand their market presence in glazed applications. Also this suggests that coal-derived coatings could increase the life span, and therefore value, of solar collectors. It is also anticipated that the coal-derived coatings may also increase the efficiency of solar collectors. Also it has been quantified that the coal-derived coatings are robust enough to resist extended weathering.

All the data taken is consistent with the view that the modified panel has lower thermal losses than the manufacturer's panel. It is premature to conclude that the modified panel offers superior performance at all temperature regimes, latitudes, angle of inclination etc., but in no case was the performance better for the manufacturer's as-delivered panel. It is likely that the observed performance increase is due to the reduced loss of infrared radiation from the panel. The use of a "finless" geometry; i.e., using close spaced pipes with no fins would result in simplified manufacturing, and might allow the use of PVC pipes instead of the integrally-welded fin and tube assembly in use in the manufacturer's unit. Lower cost and higher efficiency might result from use of the CPCPC-sponsored modifications to solar panels.

However, the current coating exhibits problems with delamination from copper fins. Thermal expansion coefficient mismatch and lack of compliance in the coating likely contribute to this issue. In addition the coating was probably not completely cured, as condensate was noted on the inside of the cover. The possibility of replacing copper fins with steel fins (known to be an excellent host for coal tar enamel coatings) was considered. The possibility was raised that adequate coupling between fin and tube might be achieved via free convection from air in the collector, but this appears to be too weak. Hence, it is tentatively concluded that the manufacturer's presumed high quality weld is indeed an essential feature of the apparatus, and thus copper is the material of choice.

The results of onsite testing (Sacramento, California) while carried out under less than ideal conditions due to variable cloud cover, verified that the CPCPC modified unit probably performs slightly better than the manufacturer's unit. If the manufacturer's unit is modified by replacing the polycarbonate cover with an IR-reflective glass cover, there is also some performance enhancement. Repeated testing under better conditions is necessary in order to distinguish between the CPCPC-best and SolarRoofs.com-best configurations.

Irrespective of that hair-splitting exercise, the salient point is that the coal derived spectrally selective coating is very competitive in terms of thermal performance, while also offering potential benefits in cost.

WVU and SolarRoofs.com will continue to explore the possibility of developing commercial applications of coal derivatives in solar heating products.

VII. REFERENCES

1. http://en.wikipedia.org/wiki/Solar_collector
2. http://greenterrafirma.com/images/flat_panel_collector.jpg
3. http://en.wikipedia.org/wiki/Solar_thermal_collector
4. R.D. Clear, L. Gartland, F.C. Winkelmann, *An empirical correlation for the outside convective air-film coefficient for horizontal roofs*, Energy and Buildings, 35(8), pp. 797-811, 2003.
5. http://www.thermafin.com/coat_tech.html

APPENDIX J: MANUSCRIPTS SUBMITTED TO THE 2009 CLEARWATER COAL CONFERENCE

Consortium for Premium Products from Coal: An Industry/ Government/University Collaboration

Bruce G. Miller and Sarah E. Haner.....1762

Mesophase Pitches Derived from Coal Tar Distillates

Peter G. Stansberry, Doug J. Miller, John C. F. Chang, Irwin C. Lewis and Richard T. Lewis1768

Graphitization Behavior of Pretreated Anthracite Coal

Caroline E. Burgess-Clifford, Deepa L. Narayanan, Dirk T. Van Essendelft, Puja Jain, Apurba Sakti, and Angela D. Lueking1779

Centrifugation of Coal Liquefaction Products

Charles W. Kling, Elliot B. Kennel, J. Joshua Maybury, Alfred H. Stiller, and Robert C. Svensson1791

Fabrication of Electrochemical Double Layer Capacitors Using Carbon Derived from Coal Tar Pitch/ Polyethylene Glycol Diacid Blends

Ramakrishnan Rajagopalan, Keith Perez and Henry C. Foley.....1801

Mild Coal Extraction for the Production of Anode Coke

Rodney Andrews, David Jacques, Terry Rantell and James C. Hower.....1805

Premium Carbon Products from Coal: A Sulfur-Based Approach

Maria Sobkowiak, Harold Schobert, and Paul Painter.....1817

Consortium for Premium Products from Coal: An Industry/ Government/ University Collaboration

Bruce G. Miller and Sarah E. Haner
Energy Institute
The Pennsylvania State University
C211 Coal Utilization Laboratory
University Park, PA 16802

Abstract

Since 1998, The Pennsylvania State University has been successfully managing the Consortium for Premium Carbon Products for Coal (CPCPC), which is a vehicle for industry-driven research on the promotion, development, and transfer of innovative technology on premium carbon products from coal to United States industry. The U.S. Department of Energy's National Energy Technology Laboratory provides the base funding for CPCPC, while The Pennsylvania State University and West Virginia University share charter membership and collaborate with numerous affiliate members from industry and academia to form a dedicated and productive team, effectively carrying out innovative research and development of high-value carbon products derived from coal. Penn State is responsible for consortium management, with activities ranging from membership recruitment to proposal solicitation to awarding and monitoring subcontracts to members. Another key responsibility is providing a forum in which its industry-led council selects proposals submitted by members to ensure CPCPC target areas have strong industrial support. CPCPC and its members are fully committed to fulfilling the consortium mission and vision to promote the use of secure, domestic coal resources to produce environmentally sound, affordable carbon products that would reduce dependence on foreign imports. Since its inception, CPCPC continues to strive for the sustainable development of the U.S. carbon industry and the recognition of coal as a valuable resource for producing premium carbon products. This paper, examines, in-depth, the mission that drives CPCPC and summarizes the cutting-edge research and success stories that have resulted from its existence.

Introduction

The objective of the industry-driven Consortium for Premium Carbon Products from Coal (CPCPC) is to investigate alternative technologies for the non-fuel uses of coal. Research, development, demonstration and commercial application programs are conducted to investigate technologies for non-fuel uses of coal, including production of coke and other premium carbon products from coal, and production of coal-derived feedstocks that will be precursors of value-added premium carbon products. The intent of this program is greater recovery of mined coal, the recovery of lost carbon materials from waste generated during coal processing, and the development of the technology for producing premium carbon products for the industrial market. The development of advanced technologies designed to improve the efficiency, economics, and environmental performance of coal-based feedstocks was performed, reduction of hazardous air pollutants were investigated, and work toward bringing high-value premium carbon products to the marketplace was pursued. The CPCPC has been funded over a period of nine years, with 88 projects either completed or on-going to fulfill this objective. Total funding for these 88 projects, which has involved nearly 100 companies/universities, is over \$10 million.

CPCPC is promoting the use of secure, domestic coal resources to produce environmentally-benign, high-value carbon products, such as carbon fibers, activated carbons, binder pitches, cokes for baked anodes and graphite, carbon foams, and carbon nanotubes. Although coal is the largest domestic fossil fuel hydrocarbon resource of the U.S., estimated to last over 200 years at the present consumption rate, most of the premium carbon products developed and manufactured in the U.S. derive mainly from petroleum, thus creating dependence on foreign imports to manufacture essential carbon products for the domestic market. To ensure sustainable development of the carbon product, the inherent potential of the great abundance of coal in the U.S. must be pursued to supply and introduce environmentally benign and affordable premium carbon products to the general public. The CPCPC has, since 1998, strived for the recognition of coal as a valuable resource for producing premium carbon products. Through its implementation, the industrial-driven consortium is committed to promote projects that use coal to ensure a sustainable development of the U.S. carbon industry.

Consortium Structure

The CPCPC is an initiative led by Penn State, West Virginia University (WVU), and the U.S. Department of Energy, National Energy Technology Laboratory (NETL), with Penn State responsible for consortium management. Each CPCPC member appoints a representative to an Advisory Committee, which serves as a steering committee for the consortium. The Executive Council is composed of one representative each from Penn State and WVU, together with seven elected industrial members who evaluate and select those research projects that will be of most benefit to the CPCPC membership.

Projects are solicited from the CPCPC membership. Each member is eligible to submit projects and compete for financial support. Successful projects usually have general applicability to all members so that the entire membership will benefit. Research projects require a minimum 30% cost share.

The organizational structure of the CPCPC underscores that the consortium is industry-driven. Industry identifies, selects, and partially funds projects that it deems as having near-term potential for producing competitively priced premium carbon products from coal or coal-derived feedstocks.

The scope of Penn State's activities includes managing the process of attracting and maintaining consortium members, soliciting proposals, providing the forum for the CPCPC council in selecting proposals from members for technical work in the subject area, awarding and monitoring subcontracts to members to accomplish the selected technical work, and disseminating the results of the technical work via meetings of the consortium and a Web site.

Members and Membership Benefits

Membership in CPCPC fluctuates each year and has varied from 30 to 60 members per year. Members include anthracite and bituminous coal producers, manufacturers of specialty carbon and graphite products, activated carbon producers, municipally-owned water treatment facilities, anthracite filter media producers, carbon fiber and composite producers, aluminum producers, carbon black and coal tar pitch producers, battery manufacturers, coal-fired electric utilities, humic acid producers, firms specializing in coal cleaning and plant construction, and academia. There are currently 28 members of CPCPC including:

Industrial Participants

Alcoa Primary Metals
 Asbury Graphite Mills, Inc.
 CII Carbon, LLC.
 Carbon Sales
 Carbone of America
 Caterpillar, Inc.
 Comalco Aluminum Ltd.
 Fisher Mining Co.
 GrafTech International, Ltd.
 Graphite Metallizing Corp.
 Greater Cincinnati Water Works
 HYCET, LLC.
 Inorganic Specialists, Inc.
 Jeddo Coal
 Koppers Industries, Inc.
 Morgan AM&T Pure Carbon
 Neenah Foundry Company
 Premium Anthracite Wales
 Premium Carbon Products, LLC
 Preptech, Inc.
 Pure Carbon Company
 Reading Anthracite Company
 RJ Lee Group, Inc.
 West Materials, Inc.

Location

Pittsburgh, Pennsylvania
 Asbury, New Jersey
 Kingwood, Texas
 Wilkes-Barre, Pennsylvania
 St. Marys, Pennsylvania
 East Peoria, Illinois
 Thomastown, Australia
 Montoursville, Pennsylvania
 Parma, Ohio
 Yonkers, New York
 Cincinnati, Ohio
 Apex, North Carolina
 Miamisburg, Ohio
 Wilkes-Barre, Pennsylvania
 Pittsburgh, Pennsylvania
 St. Mary's Pennsylvania
 Neenah, Wisconsin
 Strand, London
 Morgantown, West Virginia
 Apollo, Pennsylvania
 St. Mary's, Pennsylvania
 Pottsville, Pennsylvania
 Pittsburgh, Pennsylvania
 Warren, Ohio

University Participants

Pennsylvania State University	University Park, Pennsylvania
University of Florida	Gainesville, Florida
University of Kentucky	Lexington, Kentucky
West Virginia University	Morgantown, West Virginia

The benefits of being a member include:

- Members steer research into areas that are of strategic importance to the coal and carbon/graphite industries;
- Members gain immediate access to low-cost technology transfer on projects valued at \approx \$1.5 million annually as well as the final reports for all projects conducted since CPCPC's inception;
- Coals, carbon products, and other materials that are used, produced, or sold by members can be used as part of CPCPC projects; and
- CPCPC-sponsored events serve as an ideal networking opportunity.

Funded Research

Since CPCPC's inception, there have been 88 projects funded. These projects can be categorized into eight overall objectives:

- (1) To find alternative methods to alleviate the problems associated with the decline in metallurgical and petroleum coke production;
- (2) To determine new methods of utilizing fly ash from power plants;
- (3) To produce high-quality and low-cost products from anthracite;
- (4) To better understand and integrate the use of carbon fibers into new technologies;
- (5) To find additional uses for activated carbons;
- (6) To integrate the use of carbon foams into industry;
- (7) To better understand the characteristics of coal and specialty coal products such as nanofibers and turbostratic carbon; and
- (8) To increase environmental responsibility by reducing harmful waste products from coal-fired power plants.

A full listing of all projects, the company that performed the funding, and the project principal investigator can be found at <http://www.energy.psu.edu/cpcpc/>. Currently, CPCPC is funding nine research projects with a total project value of nearly \$1.0 million. These projects include:

- **Removal of SO₂ and NO_x Over Coal-Petroleum Based Activated Carbons** - The main objective of this research is to understand the properties (surface area, porous texture, pore volume) of activated carbons produced from different carbonization and activation methods using blends of decant oil and bituminous coal. An in-depth study is being conducted to correlate optical textures of cokes after carbonizing the blends using various activated carbon properties, investigate the effect of different carbonization and activation conditions on activated carbon production and properties, and correlate these properties with SO₂ and NO_x adsorption capacity.
- **Investigation of Carbon Foams Produced from Pitch via Blowing Agents** - It has been demonstrated that blowing agents can produce carbon foam from coal tar pitch, but important information is absent. Several objectives must be met before the technology is commercially viable. In this study, the following will be performed: 1) estimate the cost of one cubic foot of carbon foam produced with this technology; 2) determine requirements for implementing this technology on a large scale; 3) investigate potential applications of carbon foam; 4) research and model the rheology of coal tar pitch plasticized with blowing agents; 5) relate the system rheology to the cell morphology of the resultant carbon foam; 6) test mechanical and electrical properties of the carbon foam; and 7) model foam properties as a function of morphology and treatment temperatures.
- **Coal Derived Carbon Foam as an Energy Attenuator** - Energy attenuators function by absorbing kinetic energy, which transforms high acceleration impacts into lower acceleration impacts. They can be used to prevent head injuries during automobile accidents, improve survivability in airplane crashes, and protect delicate equipment during shipping. This research project hypothesizes that energy attenuating coal derived carbon foams weigh less, require less space, and cost less than current state-of-the-art energy attenuating materials. The main objective of this research is to develop low cost coal-derived energy attenuating carbon foams.

- **Catalytic Extraction of Coal for the Development of Highly Oriented Cokes** - This research seeks to demonstrate that catalytic coal extraction can make feedstocks that can be processed into highly crystalline cokes. The objective of this work is to demonstrate that coal has the ability to fulfill the role in non-fuel uses, in that suitable coal-derived cokes can be used in graphite electrodes, materials supplying critical markets.
- **Enhanced Pyrolysis of Coal Derivatives** - This project seeks to produce high quality nanocarbon structures, such as acetylene black as well as carbon nanofibers using coal derivatives augmented with high pressure plasma.
- **Needle Coke from Nitrogen Removed and Coal-Derived Feedstock** - Needle coke is the most important raw material for making graphite electrodes, which are used in electric furnaces in industry for making steel from scrap metals. Currently, there are no coal-based needle coke producers in the United States. If treated properly, needle coke for coal-based feedstock could be superior to that of petroleum needle coke. In this study, a coal-based feedstock will be used for making needle coke, after removing the nitrogen from the feedstock.
- **Premium Carbon Products from Coal: A Sulfur-Based Approach** - The goal of the project is to develop new methods for producing marketable forms of carbon from coals using a sulfur dehydrogenation process. If successful, this research could allow for the development of a new, environmentally-cleaner process for coke and carbon production, expanding the number of coals that can be used to make these products and allowing the development of a carbon dioxide-free, carbon-neutral, source of hydrogen.
- **Bituminous Coal for Cincinnati Water Treatment** - Granular Activated Carbon (GAC) that is derived from coal effectively removes organic contaminants from drinking water in hundreds of municipalities in the United States. The focus of this research project is to devise a thermal reactivation protocol that allows reactivated carbon to remove organic compounds for longer durations, than can be achieved conventionally, by employing low-temperature steam preconditioning and curing, so as to create reactivated carbon that hosts more micropores, more mesopores, less chemisorbed oxygen, and less negative charge.
- **Activated Carbons for CO₂ Capture from Coal-Derived Pitch/ Polymer** - The main objective of this investigation is to produce activated carbons from coal-derived pitch/ polymer blends that offer the potential for successful implementation as CO₂ adsorbents. These porous materials will offer a viable and economic route to meeting carbon dioxide emission limits, particularly for existing and aging coal-fired power generation plants

Technology Transfer

Semiannual meetings are sponsored by the CPCPC, and are held in the spring and fall of each year, with a short tutorial typically taking place in the summer. Fall meetings are usually dedicated to project solicitation, while spring meetings are reserved for project reviews. Members are provided with a comprehensive final report at the conclusion of each project.

Success Stories

Several success stories have been funded so far including, but not limited to, low-cost carbon fibers from coal for lighter vehicles, large production of inexpensive activated carbon for water and air treatment, high-quality binder pitches and cokes from coal, production of nanocrystalline diamond from anthracite, development of a hydrogen storage and production technique using anthracite, use of high surface area carbon for ultracapacitors and other applications, and carbon foam production using coal tar binder pitch. Detailed discussions of these projects can be found at <http://www.energy.psu.edu/cpcpc/> in the members-only site. In some cases, provisional patents have been filed.

Closing Statements

CPCPC has strived, since 1998, for the recognition of coal as a valuable resource for producing premium carbon products. Coal is the largest domestic fossil hydrocarbon resource of the United States estimated to last over 200 years at the present usage rate. Yet, much of the premium carbon products developed and manufactured in the United States are derived from fossil hydrocarbon sources other than coal, mainly petroleum, creating dependence on foreign imports to manufacture essential carbon products for the domestic market.

The goal of CPCPC is to simulate the development, commercialization and promotion of the technologies necessary for producing value-added carbon products using coal and coal-derived feedstocks. CPCPC is an industry-driven consortium whose members propose research initiatives in areas they identify as being strategically important to the coal and carbon industries.

Just as the CPCPC seeks to advance the carbon and coal industries through its research, the success of the consortium relies heavily upon the active involvement and leadership of its industrial participants. Currently, the CPCPC is comprised of ≈ 30 industrial and university members, among which are manufacturers of specialty carbon and graphite products, activated carbon producers, coal-fired electric utilities, coal producers and firms specializing in coal cleaning and plant construction.

MESOPHASE PITCHES DERIVED FROM COAL TAR DISTILLATE

Peter G. Stansberry, Doug J. Miller, John C. F. Chang, Irwin C. Lewis, Richard T. Lewis
GrafTech International, Ltd.
12900 Snow Road
Parma, OH 44130

INTRODUCTION

Mesophase pitch is an important raw material for producing premium carbon products, such as high-modulus carbon fibers, high-conductivity graphite foams, binders and matrices for carbon-carbon composites, and meso-carbon microbeads. In the U.S.A, manufacturers of mesophase pitch do so for their internal use only, usually from petroleum-based feedstocks. Unfortunately, there currently is no domestic source of mesophase pitch generally available to industry or consumers, although Mitsubishi Gas Chemical Co. produces AR mesophase pitch from naphthalene in commercial quantities. Thus, there is motivation to seek alternative sources of quality feedstocks for mesophase pitch production.

The goal of this DOE-funded Consortium for Premium Carbon Products from Coal project was to demonstrate process routes for producing mesophase pitch from coal-derived distillates. GrafTech has an extensive background in the chemistry and processes involved in the production of mesophase pitch and the equipment necessary for processing distillate materials to pitch and mesophase. The basic concept was to obtain a commercial coal tar distillate material, which is free of solids and highly aromatic, and to demonstrate its suitability as a precursor for mesophase pitch. A key first step was to transform the distillate thermally into a tar that would provide an acceptable yield of pitch after distillation. The thermal route was developed at Union Carbide for obtaining petroleum pitch-derived mesophase pitch for carbon fibers.⁽¹⁾ Batch heat treatments under pressure were used to polymerize the polynuclear aromatic components of the distillate to potential mesophase-forming species. The goal was to obtain a tar with a high Modified Conradson Carbon (MCC) value while avoiding the formation of mesophase or coke. The presence of mesophase in the product thermal tar is undesirable because it could cause premature coking in commercial operations. On the other hand, the highest feasible MCC coking value in the thermal tar ensures an acceptable yield of pitch after distillation.

Another element of the project was to utilize solvent extraction concepts to produce the final mesophase pitch and to compare this approach to that of thermal treatment. The solvent extraction route was first reported by Riggs and Diefendorf⁽²⁾ and was employed by ConocoPhillips to transform petroleum pitch to mesophase.⁽³⁾ The solvent extraction route requires preparation of a precursor pitch with a high concentration of high molecular weight species capable of forming mesophase. These components will transform to mesophase after they are separated from the lower molecular weight non-mesophase formers by extraction. The intricate phase behavior of the anisotropic and isotropic phases in a mesophase pitch and the interaction between

high and low molecular weight components is highly complex and has recently been modeled by Hurt and co-workers.⁽⁴⁾

For mesophase pitch production by either the thermal or extraction route, precise control of the production process is critical. First, the mesophase pitch yield should be high. Second, both the mesophase content and the mesophase viscosity need to be acceptable for further processing. For example, for petroleum-derived mesophase pitch for fiber spinning, it was shown that near 100% mesophase could be achieved at a softening point of less than 350 °C.⁽⁵⁾ In this way, fiber spinning could be carried out below reaction temperatures. A schematic representation for transforming coal tar distillate to mesophase pitch by both the thermal and extraction routes is shown in Figure 1.

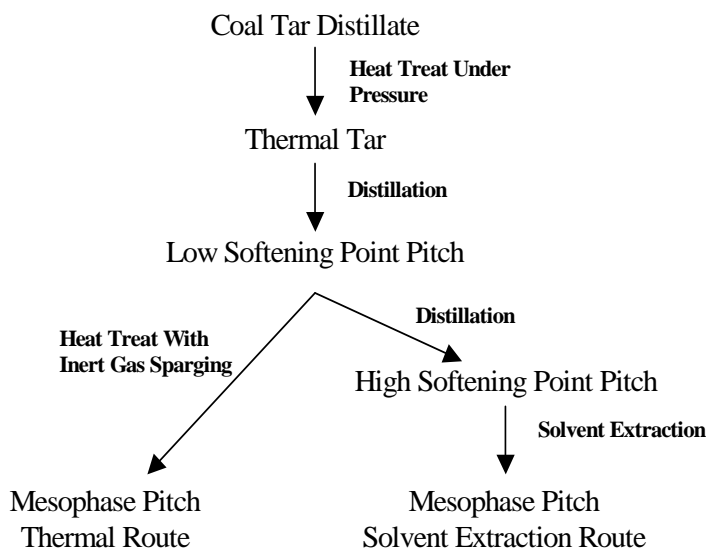


Figure 1: Schematic Representation of Mesophase Pitch Formation Using Thermal and Extraction Routes.

EXPERIMENTAL

Analytical Methods

Koppers Incorporated provided the coal tar distillate for this work. Additional details on the characterization of the distillate material and other experimental procedures have been reported elsewhere⁽⁶⁾. A standard coking value test, Modified Conradson Carbon (ASTM D-2416), was used to estimate the amount of very high boiling material present in the material before heat treatment. Softening point temperature was determined using a Mettler apparatus and weight loss versus temperature was measured using thermal gravimetric analysis (TGA). Samples were also evaluated by elemental analysis, density or specific gravity (ASTM D-71), and QI content (ASTM D-2318). The

elemental analysis (C,H,N) was obtained using a LECO CHN instrument. A LECO SC132 instrument was used to measure the sulfur content. For the mesophase pitches, mesophase contents were estimated from polarized light photomicrographs on annealed samples or by hot-stage microscopy.⁽⁷⁾ Number average molecular weights for some tar and pitch samples were measured for pyridine solutions using vapor phase osmometry (VPO).

Mesophase Pitch Development

Pilot-scale pressure heat treatments were performed in an autoclave system with dimensions of 29.8 cm I.D. by 144.8 cm inside length. The autoclave is capable of 1500 psig pressure and up to 600 °C operating temperature. The temperature can be computer controlled for a pre-determined ramping rate, final hold temperature, and hold time. Gas pressure was maintained during a run with an automatic pressure control system. The pressure heat treatments were carried out on material contained in a covered stainless steel vessel with a capacity of about 4 liters. The vessel was partially filled with approximately 1550 g of coal tar distillate.

The pressure heat-treated coal tar distillate (CTD) was converted to pitches with different softening points by vacuum distillation. The distillation was performed in resin flasks using inert argon gas sparge. Final temperatures were kept below 350 °C to minimize further reaction. In the initial distillations, 1000 g of tar was converted to 120-130 °C SP pitch. This product was then used as a precursor for higher SP pitches for use in solvent extraction. The same gas sparging system was used to produce the higher SP pitches.

Small-scaled solvent extractions with toluene were used to determine the conditions for obtaining mesophase from the vacuum-distilled pitches. The toluene insolubles were examined by hot-stage microscopy and annealed at 350-400 °C for examination by polarized light microscopy. Once these small-scale scoping studies were completed, larger-scale extractions were performed using 50 g of pitch in 1000 ml of toluene. Following extraction, the insolubles were heated under nitrogen with stirring to 350-360 °C to remove residual solvent and to homogenize the mesophase pitch. The thermal transformations of isotropic pitch to mesophase were carried out in a specially designed lab-scale reactor using ~200 g quantity of starting material. The reactions were performed at temperatures of 390-400 °C with nitrogen gas sparging using published procedures.⁽¹⁾

RESULTS AND DISCUSSION

Characterization of Coal Tar Distillate

The TGA curve for the coal tar distillate is shown in Figure 2. The extrapolated onset and endset temperatures were 312° and 419 °C, respectively. Approximately 98% of the sample had volatilized by 450 °C. This is consistent with the 1.2% MCC value measured for this material.

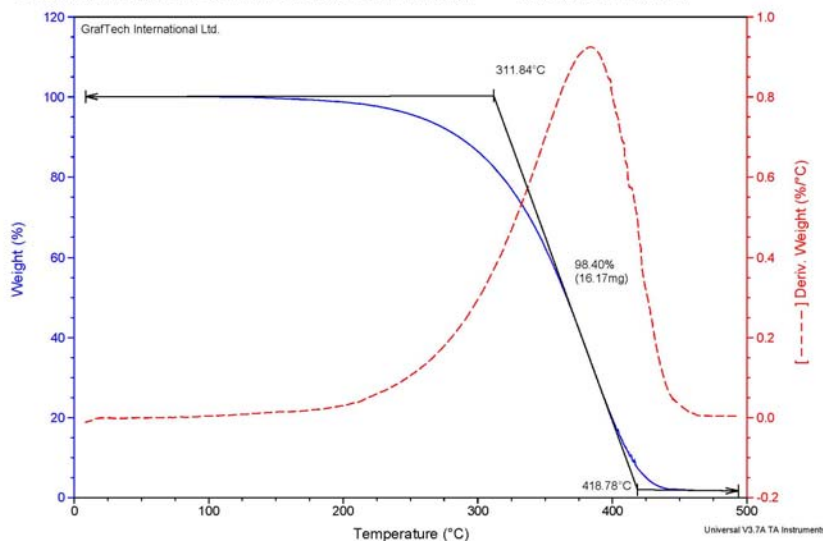


Figure 2: TGA of Coal Tar Distillate.

Pilot-Scale Pressure Heat Treatment of Coal Tar Distillate

Initially, laboratory trials were undertaken to guide in the selection of processing conditions for the larger pilot-scale studies⁽⁶⁾. After the laboratory trials, pilot-scale pressure heat treatments were then performed, nominally between 430°-435 °C for 5 hours at 100 psig. The exceptions are runs PHT-2, which was conducted at a significantly higher temperature, and PHT-6, which was for a longer residence time. These two samples were both found to contain mesophase and were not examined further. The results are summarized in Table I.

Table I
Summary of Pilot-Scale Pressure Heat Treatment Runs PHT-1 to PHT-5

Run No.	Estimated Temp, °C	Yield, Wt %	MCC, Wt %	Mesophase Content, Vol. %
PHT-1	435	94.0	19.2	0
PHT-2	441	84.5	24.5	1-5
PHT-3	431	95.8	14.3	0
PHT-4	434	92.7	20.4	0
PHT-5	432	90.5	22.1	0
PHT-6	435 (7 hr. hold)	90.5	23.4	1-5
PHT-7	435	95.0	19.1	0

Distillation of Tars to Isotropic Precursor Pitches

The tar obtained from the first pressure heat treatment (PHT-1) was initially distilled to a 128 °C SP pitch. This pitch was to be used as the precursor for higher SP pitches for scoping experiments for the solvent extraction route to mesophase. The objective was to establish the requirements for achieving an isotropic pitch that would provide an acceptable yield of mesophase using toluene as a solvent.

Properties of this 128 °C SP pitch (13-22) are presented in Table II along with those obtained for the precursor CTD. As expected, the aromaticity and average molecular weight have increased considerably as a result of the pressure heat treatment and distillation processes.

Table II
Properties of Coal Tar Distillate and Derived 128 °C SP Pitch

Test	Coal Tar Distillate	Pitch 13-22
C, %	92.3	92.7
H, %	5.44	4.59
Atomic C/H Ratio	1.43	1.70
N, %	1.03	1.13
S, %	0.58	0.44
MCC, %	1.2	61.4
RT Density, g/cc	1.16	NM
QI, %	0.0	NM
TI, %	NM	15.5
Number Average Molecular Wt. (VPO)	163	304

In a second distillation, the 128 °C SP pitch was used to prepare smaller quantities (~50 g) of higher SP pitches with softening points ranging up to 220 °C. The pitch yields and softening points for the various products are summarized in Table III. The pitch yields are based on the original coal tar distillate.

Table III
Pitches From Distillation of Pressure Treated CTD – PHT-1

Pitch ID Number	Overall Yield , Wt %	SP , °C
13-22	32.1	128.5
13-38	26.1	164.9
13-50	23.6	187.2
13-52	22.8	194.0
13-54	19.7	204.2
13-81	17.9	220.6

The pitch softening points are directly related to the amount of distillate removed. This conclusion is apparent from Figure 3, where the pitch softening point is plotted versus yield. The filled squares represent the data from Table III.

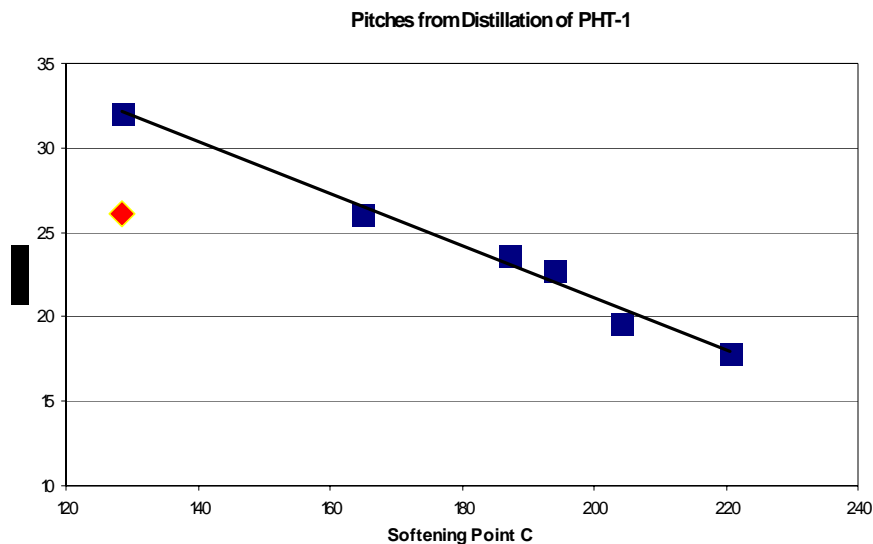


Figure 3: SP vs. Yield for Pitches from Distillation of PHT-1.

In order to obtain more pitch material, a distillation on the tar product from PHT-3 was also performed. As seen in Table I, this material was less severely treated and had a lower MCC value than the tar from PHT-1. The tar PHT-3 was distilled to produce about 350 g of pitch with a softening point of 132 °C. The pitch yield was 26.1%. The red diamond-shaped symbol in Figure 3 represents the data point for this pitch and, as can be seen, it deviates from the plot of the pitches derived from the PHT-1 tar. The pitch yield is evidently related to the severity of the thermal treatment in conversion of CTD to tar. The 132 °C SP pitch was used as a precursor for the thermal mesophase pitch and also used for assessing the potential mesophase domain size.

Thermally Produced Mesophase Pitch

Mesophase pitches were prepared using direct thermal treatment of isotropic pitches from the distillation of the heat-treated coal tar distillate. The process involves heat treating at a high enough temperature to effect chemical polymerization while sparging with an inert gas to remove the low molecular weight species and reaction by-products.⁽¹⁾ In a first trial, the 132 °C SP pitch (distilled tar PHT-3) was used as the starting material and heat treated in a reaction vessel for 24 hours at 390 °C to produce a product with a softening point of 338 °C. The mesophase pitch yield was 53%, based on the precursor isotropic pitch. Shown in Figure 4a is a polarized light photomicrograph of the annealed mesophase pitch. The anisotropic mesophase is the continuous phase with small spherical isotropic regions uniformly distributed throughout the bulk coalesced

mesophase. The mesophase content is estimated at about 75%. This appearance is typical for pitches suitable for fiber spinning in that the rheology is controlled by the continuous mesophase and the material does not undergo significant phase separation at spinning temperatures⁽⁵⁾. In contrast, Figure 4b shows the appearance of a mesophase pitch with a lower mesophase content (~50%) which exhibits phase separation and is unsuitable for production of carbon fibers.

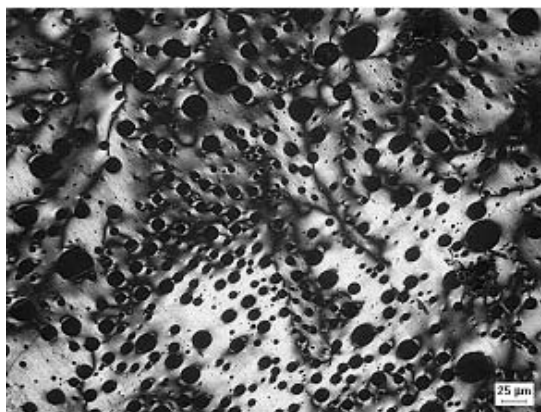


Figure 4a: Thermal Mesophase Pitch (13-84), 338 °C SP, ~75% Mesophase

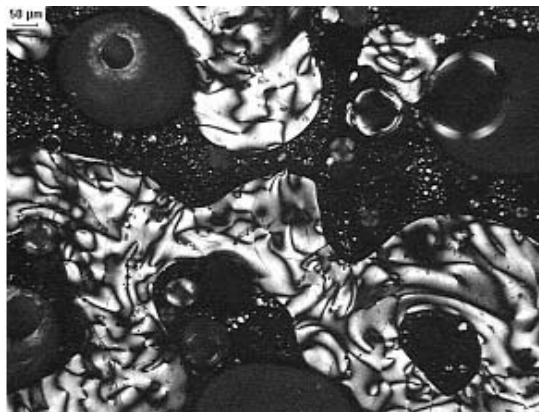


Figure 4b: Segregated 2-Phase Mesophase Pitch, ~50% Mesophase

A second thermal mesophase pitch was prepared after combining tars from PHT-4 and PHT-5 and distilling them to a 129 °C SP pitch. In this case, the heat treatment was increased to 26 hours at 390 °C followed by 2 hours at 400 °C. About 180 g of mesophase pitch product was obtained in a yield of 53%. The mesophase pitch softening point was 343 °C. From examination of the mesophase pitch by polarized light microscopy, the mesophase content was estimated as 85%. A polarized light photomicrograph of the annealed mesophase pitch is shown in Figure 5.



Figure 5: Thermal Mesophase Pitch, 343 °C, 85% Mesophase.

This mesophase pitch appears to be an acceptable precursor for products such as high performance carbon fibers and carbon foam. In order to obtain more detailed information about the processability of the material, particularly for fiber spinning, its viscosity versus temperature was measured. Shown in Figure 6 is a plot of viscosity versus temperature for the thermal mesophase pitch. An activation energy plot of log viscosity versus $1/T(K)$ is presented in Figure 7. An activation energy of 24.2 kcal/mole was calculated from this plot.

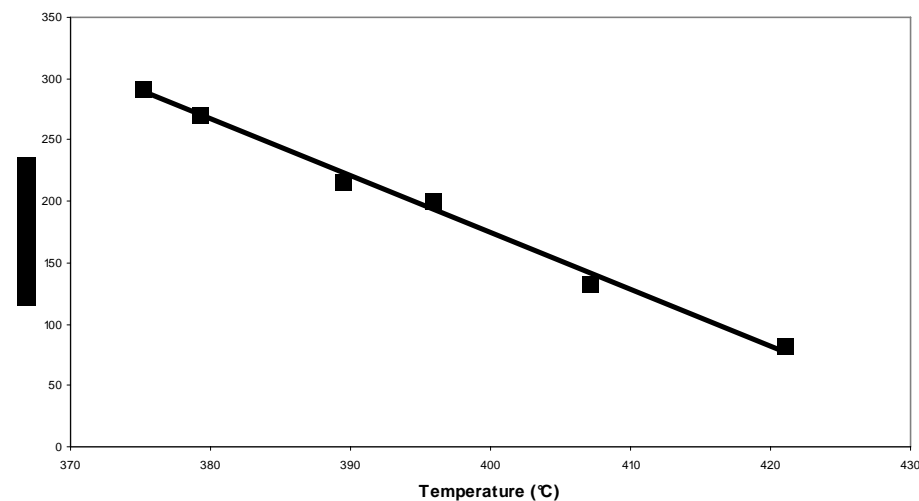


Figure 6: Viscosity vs. Temperature for Thermal Mesophase Pitch.

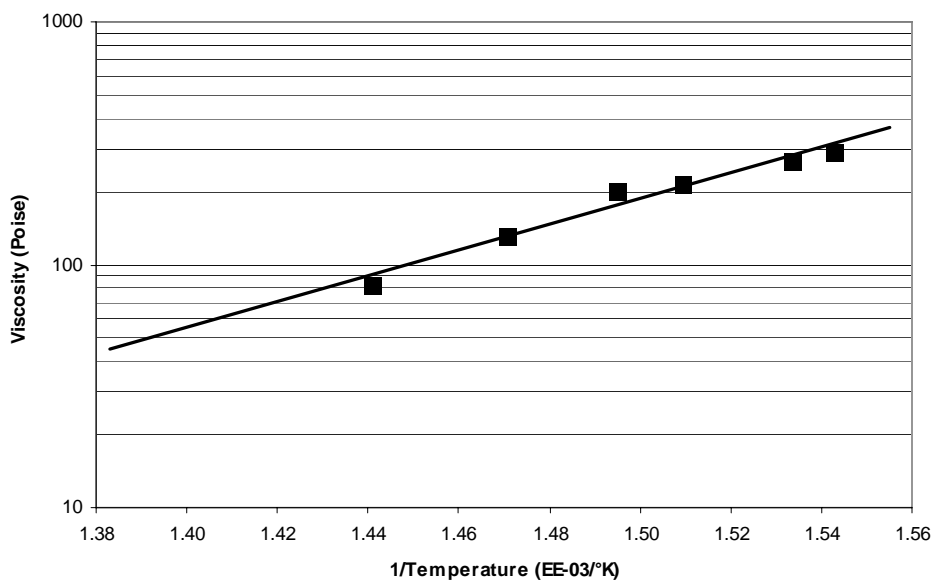


Figure 7: Viscosity vs. $1/T(K)$ for Thermal Mesophase Pitch.

MESOPHASE PITCH BY SOLVENT EXTRACTON

Small-Scale Extractions of 204 °C SP Pitch (13-54)

We performed some initial small-scale toluene extractions with the 204 °C SP pitch (13-54, Table III) in order to determine the quantity of low molecular weight components that need to be removed in order to develop mesophase. Examination of the original pitch by hot-stage microscopy showed that it was completely isotropic. Extractions were performed with toluene at room temperature and with heated toluene at 75 °C. The room temperature extracted residue was re-extracted a second time with toluene at room temperature in order to determine if more material could be removed using the fixed ratio of 25 g solid to 500 ml of solvent. The extraction residues were screened initially by hot-stage microscopy to obtain a quick estimate of mesophase content and viscosity. They were also annealed by heating at 350 °C and examined by conventional optical microscopy to determine the amount of mesophase more accurately. The hot toluene extract residue was also annealed at 400 °C. The results are summarized in Table IV.

Table IV
Yields and Mesophase Contents from Toluene Extraction of Pitch (13-54)

Treatment	Yield, Wt. %	Estimated Mesophase Content, Vol. %
1x at 25 °C	64	10-20
2x at 25 °C	50	40-50
1x at 75 °C*	45	70-80
1x at 75 °C**	44	90-95

*Annealed at 350 °C, **Annealed at 400 °C

The results in Table IV show how sensitive the mesophase concentration is to the amount of low molecular weight material removed. At least 45% removal is required in order to obtain > 80% mesophase from the 204 °C SP pitch. The hot toluene extraction residue gave an ~ 70-80% anisotropic phase content after being annealed at 350 °C. When the same material was annealed at 400 °C, the mesophase content increased to a value of over 90% as a result of only an additional 1% weight loss. The mesophase derived from the pitch extraction exhibited a very large average domain size. A polarized light photomicrograph for the mesophase from the 1X cold toluene extraction is shown in Figure 8. Figure 9 presents a photomicrograph of the mesophase from the pitch extracted with toluene at 75 °C. The insolubles from the hot toluene extraction, after annealing at 350 °C to remove any residual solvent, gave a Mettler softening point of 357 °C.

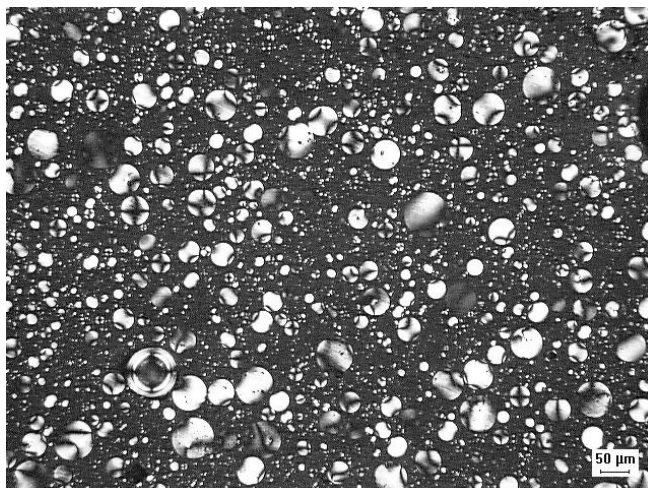


Figure 8: Polarized Light Photomicrograph of Mesophase from 1X Toluene Extraction of 204 °C SP Pitch (13-54).



Figure 9: Polarized Light Photomicrograph of (400 °C) Annealed Mesophase from Hot Toluene Extraction of 204 °C SP Pitch (13-54).

CONCLUSIONS

A coal tar distillate was shown to be an acceptable precursor for mesophase pitch suitable for producing high performance carbon products. The key initial step involves a pressure heat treatment for polymerizing the low molecular weight aromatic components to higher molecular weight molecules capable of forming mesophase. For a commercial continuous process, it is necessary to carry out these reactions while maintaining a homogeneous liquid state free of solid mesophase and coke.

Physical separation procedures of distillation and solvent extraction can then be used to concentrate the high molecular weight components and allow the formation of mesophase. Distillation to a high softening point pitch, followed by extraction with

toluene, was shown to provide a route to mesophase. Mesophase content can be altered by choice of extraction conditions.

Higher mesophase pitch yields were obtained using the thermal route where an intermediate softening point pitch was heated treated at temperatures sufficient to effect thermal reaction. The thermal treatment can effectively polymerize low molecular weight components of the pitch into molecules capable of incorporating into the mesophase. Viscosity versus temperature measurements for the thermal mesophase pitch show that it is suitable for spinning fibers. It attains a viscosity which is suitable for spinning (~200 poise) below reaction temperature.⁽⁸⁾

REFERENCES

1. U.S. Patent 3,976,729 I.C. Lewis et al., (1976).
2. D.M.Riggs and R.J. Diefendorf, Carbon 80, Deutsche Keramische Gesellschaft, Baden Baden, 326, (1980).
3. U.S. Patent 5,259,947 W.M.Kalback et al, (1993).
4. R.H. Hurt and Y. Hu, Carbon 37, 281 (1999), Carbon 39, 887, (2001).
5. F. Nazem and I.C. Lewis, Mol. Cryst., Liq. Cryst. 139,195,(1986).
6. D. J. Miller et al., DOE Final Report DE-FC26-03NT41874, March 31, 2005.
7. R.T.Lewis, Ext. Abs. for the 12th Biennial Carbon Conference,(1975), p215.
8. B. Rand, "Handbook of Composites" Vol. 1, 495 (1985).

GRAPHITIZATION BEHAVIOR OF PRETREATED ANTHRACITE COAL

Caroline E. Burgess-Clifford*, Deepa L. Narayanan, Dirk T. Van Essendelft, Puja Jain, Apurba Sakti, and Angela D. Lueking
The Energy Institute, Penn State University, C211 Coal Utilization Laboratory, University Park, PA 16802

INTRODUCTION

Anthracite coal, a non-graphitic carbon, is known to graphitize from 1700-3000°C. Several researchers have suggested anthracite will graphitize so long as the anthracite coal has a basic structure that will align and inherent mineral matter that catalyzes graphitization upon thermal annealing at high temperature.¹⁻¹¹ Most researchers have suggested that two factors must be present for anthracite to graphitize: 1) the carbon structure in the anthracite must be partially aligned to allow for graphitization¹⁻⁸ and 2) certain minerals must be present to catalyze graphitization of anthracite by carbide formation and decomposition.³⁻¹¹ Mechanical pretreatment of the coal to small particles and in the presence of solvent may affect graphitization behavior of the coal, and in work published elsewhere, have shown that other carbons (i.e., nanocrystalline diamond) and hydrogen are other products of the reaction.¹²⁻¹⁵ In this particular research, we report differences in behavior for low temperature graphitization, depending on whether anthracite coal was pretreated with or without solvent.

EXPERIMENTAL METHODS

Synthesis of Samples – Materials, Ball Milling and Heat Treatment. The coal used is PSOC-1468 from the Penn State University coal sample bank. The coal is an anthracite coal from the Buck Mountain seam, bottom of the Llewellyn formation, collected from Luzerne Co., PA, near Eckley. Henceforth, it will be labeled as BMT. It has a fairly low ash content coal, with low volatile matter content and high fixed carbon content. Details of the ultimate and proximate analysis are included in Table 1. Cyclohexene (99 % purity) was purchased from JT Baker.

BMT was milled both under dry conditions and in the presence of a cyclohexene solvent as a wetting agent. All milling occurred with an argon purge to minimize oxidation effects and water contamination during processing. Ball milling was done on a Fritsch Pulveristte LC-106A at 400 rpm, using 6 g of BMT and 20 mL of cyclohexene solvent in the 250 mL bowl and 15 balls (each 15 mm diameter) in the mill. The grinding bowl and balls were made of 316 stainless steel. The coal was ball-milled for 80 h, with and without cyclohexene. The ball milling time was selected based on preliminary work in our laboratory.¹² The milled samples are denoted BMT-dry when no solvent was used and BMT-wet when cyclohexene was used.

After milling, samples were heated in a tube furnace at 1400°C for 3 h under 1 L/min of argon. The temperature ramp rate was 2.5°C/min to 1400 °C. The 1400°C annealing temperature was selected based on previous reports of annealing ball-milled graphite to form MWNTs.¹⁶⁻¹⁷ The thermally-annealed samples are labeled BMT-HT, BMT-dry-HT and BMT-wet-HT, respectively, with BMT-HT denoting thermal anneal without ball milling.

Characterization of Samples: Several electron spectroscopy methods were used to examine the milled samples. Scanning electron microscopy (SEM) was used for analysis of milled coal. Samples were analyzed on a Hitachi S 3000-H, under high vacuum and 20 eV. Energy dispersion spectrometry was done on a Hitachi S 3500N, under low vacuum and 20 eV, and

images were obtained from background scattering SEM. Transmission electron microscopy (TEM) was done on a JEOL 2020F 200kV field emission transmission electron microscope at the Materials Research Institute at the Penn State University.

Samples were analyzed via temperature programmed oxidation (TPO) on a Perkin Elmer 7 thermogravimetric analyzer (TGA) using purified air as the oxidant and a heating rate of 10°C/min. The TPO figures shown are the negative derivative of the mass loss over time, thus the TPO figures represent the rate of mass loss. TPO is a technique being used more widely to distinguish different carbon morphologies. It easily distinguishes crystalline graphite from amorphous carbon, as amorphous carbon oxidizes at ~150-200 °C while graphite oxidizes at ~850°C or above. Carbon nanotubes and nanofibers typically oxidize around 500 °C, with the oxidation temperature dependent upon orientation of graphene layers, particle size, and metal content.

XRD was performed on a Phillips X'Pert MPD with Cu K α (which has a wavelength of 1.54051 nm) radiation operated at 40 kV and 40 mA with a beam mask of 10 mm and divergent slit of 2°. Scans were made from 5° to 80° with a scan rate of 0.020°/sec and the scan type used was continuous. To calculate the L_c (crystallite stacking height), L_a (crystallite size), and d-spacing (height between adjacent layers in the z direction), the JADE+ Version 7.1 was used. The database used to analyze the data is the PDF4, 2005 edition. The same software was used to determine the identity of other peaks in the samples, thought to be minerals and mixtures of carbon and oxygen with minerals (carbides and oxides).

Proximate analysis was done on a Thermogravimetric Analyzer LECO MAC 400, and was used to determine the ash and volatile content of the coal and products. The moisture temperature was set at 105°C, the temperature for measurement of volatiles was set at 950 °C, and the ash temperature was set at 750 °C.

Neutron activation analysis (NAA) was done using the following procedure. The sample was placed near the reactor core so that could be bombarded by a beam of neutrons. After a predetermined amount of time, the sample was removed and taken to the counting laboratory. Measurements were taken using a multi-channel analyzer HPGe detector system and the unknown elements were determined using the gamma ray energies detected. A comparative method was used to convert the output of the analyzer, which is in gamma ray energies, to parts per million (ppm) or weight percent. The coal samples were transferred from the sealed packaging to clean Pyrex evaporating bowls and dried in an oven for approximately 2 hours; the samples were then placed into clean, pre-weighed polyethylene vials and the weight of each sample determined. Depending on the sample, the irradiation time used was 30 seconds or 1 h, the reactor power was set at 25, 50, or 200 kW, and the reactor flux was set at 1.7×10^{12} - 8.5×10^{11} n/cm²-sec. The decay time was 10 minutes or 7 days and the count time was 2, 4, or 167 minutes.

Maire and Mering defined a degree of graphitization (DOG) based on the d_[002] by comparing a thermally annealed sample to “ideal” graphite and non-graphitic carbon; however, according to the literature, this equation is only useful for thermal treatments above 1800°C.¹⁸ For samples that have been thermally treated to 1200-1500°C, Feret developed a method using a curve-fitting program to deconvolute the graphitic and non-graphitic carbon portions of the [002] peak to calculate the areas of each for inclusion in Equation A.¹⁹

$$g = (A_{\text{graphite}} / A_{\text{coke+graphite}}) \times 100\% \quad (\text{A})$$

For BMT-HT, BMT-dry-HT, and BMT-wet-HT, the [002] peaks were curve-fitted and areas for each deconvoluted peak calculated using the ThermoGalatic GRAMS program. The R^2 for the curves generated using this program ranged from 0.96-1.03, and areas of the peaks and g have been included in Table 2.

RESULTS AND DISCUSSION

The discussion will focus on examining the products of the coal before and after thermal annealing, by separating the discussion into the different milling parameters, i.e., before milling (BMT and BMT-HT), after milling 80 h (BMT-dry and BMT-dry-HT), and after milling 80 h in cyclohexene (BMT-wet and BMT-wet-HT).

Examination of BMT and BMT-HT. The nominal particle size of BMT as received is -60 mesh, or 250 μm and smaller. SEM (Figure 1a and b) of the surface of the particles indicates that after thermal annealing, the surface is rougher, a possible indication of volatile evolution.

The XRD parameters of BMT and BMT-HT are in Figure 2a, and parameters for the XRD are shown in Table 2. For BMT, the spectrum is fairly typical for an anthracite coal, with broad peaks at 26, 40-45, 53, and 78° representing carbon. The mineral peaks have been preliminarily identified as SiO_2 , SiC, Fe_xO_y , Fe_xSi_y , Fe_xC_y and other minerals that could be composites of the elements associated in the sample. The carbon peaks are broad, an indication of the sample containing amorphous carbon, with a d_{002} of 3.42 Å, L_c of 12 Å, and a L_a of 38 Å. When BMT is heated to 1400 °C, the d_{002} does not change significantly (3.41 Å). L_c and L_a increase slightly to 20 Å and 40 Å, respectively. The slight increase is expected with heating, but the d_{002} of BMT-HT indicates the sample is not graphitic. The DOG for BMT-HT was 13.6%, suggesting a small portion of the sample graphitized.

The TPO of BMT and BMT-HT are in Figure 3a. For BMT, the sample oxidizes over a relatively broad temperature range of 500-750 °C. The major peak occurs at ~575 °C, but there are numerous peaks in this sample as expected for the relatively heterogeneous coal. Thermal annealing shifts the oxidation temperature of BMT-HT to 600-1000 °C, with the major peak at ~900 °C. The high temperature of oxidation is even greater than that observed for a graphite powder, which oxidized at ~850 °C.

Examination of BMT-dry and BMT-dry-HT. SEM micrographs indicated the particle size of BMT-dry was ~5 μm (Figure 1c). Heat treatment (BMT-dry-HT, Figure 1d) led to some agglomeration of small particles to form large particles on the order of 100 μm . Rod-like spikes were observed in SEM in certain areas of BMT-80-1400.

XRD of BMT-dry is similar to its BMT precursor, with broad carbon peaks at 26, 40-45, 53, and 78° (Figure 2b, Table 2). Mineral peaks are not observed in BMT-dry, suggesting amorphitization of the minerals by milling. Ball milling has not significantly altered the d_{002} (3.40 Å), L_c (18 Å), and L_a (36 Å) of BMT-80 compared to BMT. Thermal annealing (BMT-dry-HT) leads to mineral peaks in XRD, and the d_{002} has increased slightly to 3.45 Å (from 3.40 Å), suggesting annealing actually decreases the graphitic order of BMT-dry. However, the DOG of BMT-dry-HT has increased slightly to 21.4% compared to 13.6% for BMT-HT, suggesting a slightly higher proportion of the carbon in the sample is graphitic.

Ball milling decreases the range of oxidation temperature in TPO; BMT-dry oxidizes from 450-600 °C, a narrower temperature range than the BMT precursor (Figure 3b). The major peak occurs at ~540 °C. The narrower temperature range is likely due to homogenization of the

sample during milling and the temperature shift is likely due to a decrease particle size. Thermal annealing shifts the oxidation profile to 500-900 °C, with two major peaks at ~650 and 825 °C (Figure 5X). TPO of BMT-dry-HT suggests two types of carbon, including a portion that is oxidation resistant and a more reactive portion that oxidizes at 650 °C. BMT-dry has a slightly higher metal content, ~0.8% which is iron. BMT-dry-HT has a higher metal content at 13.10 wt%, due to the loss of carbon during thermal annealing. The introduction of metals via milling may shift the TPO profile due to catalytic oxidation. Thus, the shift of BMT-dry-HT compared to BMT-HT is consistent with metal introduction.

Examination of BMT-wet and BMT-wet-HT. SEM indicated that the particle size of BMT-wet was on the order of 100-200 μm (data not shown).¹²⁻¹³ As the particle size of BMT-wet is much larger than BMT-dry, the introduction of cyclohexene into the mill has increased the particle size. The SEM shows increased particle size (100-200 μm); however, while large particles were observed in BMT, upon higher magnification, the surface of BMT-wet is quite different from BMT. The surface of BMT-wet (Figure 1e) appears to have several 1-5 μm particles that appear to have agglomerated or accreted. Upon thermal annealing (BMT-wet-HT), unusual structures are observed in SEM, including amorphous, round particles (Figure 1f, denoted on micrograph as *1), and tubular particles (*2, *3). The tubular particles appear to be attached to the round particles, and vary in size from ~50-500 nm. EDS (data not shown) of the sample indicated the round particles are iron, the tubes are carbon, and background particle is silicon.

The d_{002} spacing of BMT-wet, at 3.49 Å, is greater than the BMT precursor, again suggesting that milling decreases the graphitic order of the carbon (Figure 2c, Table 2). However, the L_c (12 Å), and L_a (40 Å) are not significantly altered. Once again, the mineral peaks are not present in the XRD of the milled material. Thermal annealing (BMT-wet-HT) shows an increased in order of minerals and a reduction in the d_{002} to 3.39 Å. The d_{002} of BMT-wet-HT is less than the other two annealed samples, and the DOG has increased to 74.3% compared to the other thermally annealed samples, suggesting this sample is most graphitic of the three. The mineral peaks have been identified as a mixture of iron and silicon oxides, iron and silicon carbides, and possibly iron silicides, and are much more predominant in BMT-wet-HT than the other annealed samples. Milling in cyclohexene significantly increased the ash content of the material; the ash content of BMT-wet is 10.82 wt% (Table 3) and NAA indicates the iron content has increased to 3.84 wt% relative to the 0.5 wt% content in the BMT precursor. It is evident that significantly more attrition of the milling container occurred in BMT-wet than with BMT-dry. The introduced iron likely plays a role in the graphitizability of BMT-wet.

BMT-wet oxidizes in two major regions, from 150-400 °C and from 450-700 °C (Figure 3c). The secondary oxidation range has two maxima, suggesting there is a third types of carbon in this second range. The major peaks occur at ~275, 550, and 650 °C. Parallel studies suggest this sample desorbs significant cyclohexene and benzene as well as evolves hydrogen,¹⁴⁻¹⁵ thus the low temperature peaks are likely associated with some combination of desorption and oxidation of the desorbed species. Thermal annealing at 1400 °C shifts the TPO to 450-775 °C. The low temperature peak is gone, likely due to removal of this material during the thermal anneal. The TPO again appears bimodal with peaks at ~550 and 700 °C. The ash content of BMT-wet-HT is 22.20 wt% and the metals in this sample may affect the TPO. The oxidation temperature of BMT-wet-HT is typical of a graphitic nanocarbon, but not of graphite. This apparent discrepancy is explained in the subsequent paragraph, based on the structure of the graphitic carbons observed in TEM of BMT-wet-HT.

TEM analysis of BMT-wet-HT was performed due to the unusual structures seen in SEM of this sample. TEM of BMT-wet-HT (Figure 4) has confirmed many types of structures, including nanographene ribbons,²⁰ multiwalled nanopolyhedral particles (a common byproduct in nanotube formation²¹), and curved graphitic regions (Figure 4a, c, d). In many of the TEM images, it was impossible to distinguish between the different types of graphitic carbon due to sample overlap (Figure 3c). Silicon carbide (identified with EELS, data not shown) tubes with a diameter of ~100 nm were also observed in the sample via TEM (Figure 4e). These silicon carbide tubes were highly irregular with variable diameter along the tube length. Nanocrystalline diamond was also found in the samples after thermal treatment and purification (Figure 4b), and is discussed in greater detail in other publications.¹⁴⁻¹⁵

Graphitizing versus non-graphitizing behavior of milled anthracite. Franklin suggested that with thermal annealing, some non-graphitic carbons will graphitize and others are non-graphitizing.¹⁻² She suggested that the hard, non-graphitic carbon can only graphitize and turn into a soft carbon if the crystallites have cross-links that will break upon thermal anneal at 1700-2500°C; others suggest that there must be a catalyst available to promote crystallite growth through carbide formation and decomposition.^{6-8, 10} Graphitization is much less likely to occur if the cross-links are numerous and between layers, even with available catalyst. We will examine our data in comparison with this work.

When coal was thermally annealed without any milling, there is evidence that while the material may be losing volatile matter and becoming more difficult to oxidize, it is a non-graphitizing material, probably due to cross-links inherent in the coal.

When milling the coal without solvent (BMT-dry), the particle size of the coal is reduced. Upon thermal annealing at 1400°C (BMT-dry-HT), it is clearly evident from XRD and TPO that the carbon is beginning to crystallize, although the carbon is non-graphitic carbon.

However, when milling the coal in cyclohexene (BMT-wet), the particle size is significantly larger, the result of agglomeration and possibly reaction of cyclohexene with the coal. Upon thermal annealing at 1400°C (BMT-wet-HT), it is evident from XRD that carbon is more crystalline and approaching graphite. Silicon carbides and iron silicides are clearly observed in XRD in BMT-wet-HT, materials known to catalyze graphite formation and even overcome barriers to graphite formation.⁶⁻¹⁰ However, TPO indicates a less crystalline material. Clearly there are structural differences in the three thermally annealed samples. And as shown in SEM and TEM, other types of graphitic carbons are forming in BMT-wet-HT, such as nanographene ribbons, multiwalled nanopolyhedral particles, curved graphitic regions, silicon carbide tubes, and nanocrystalline diamond.¹²⁻¹³ These types of carbons will oxidize at a lower temperature than graphite. We also believe the high metal content in BMT-wet-HT that may be catalyzing graphite formation (XRD) can also be catalyzing oxidation as seen in TPO and why the results appear contradictory. As discussed elsewhere, another side product of the reaction is the production of hydrogen.¹⁴

CONCLUSIONS

Thermal annealing of anthracite coal that has been ball-milled in cyclohexene leads to a variety of nanocarbons, including non-graphitic carbon and nanographene ribbons. Minerals present in the coal and introduced during milling form metal complexes that crystallize during thermal annealing, as noted by XRD. These crystalline metals appear to catalyze graphitic carbon formation and nanographene ribbon formation in BMT-wet-HT. Milling BMT without

solvent reduced the particle size of the coal (SEM, TPO) and led to a decrease in graphitic carbon upon thermal annealing. Milling in cyclohexene modified the products after thermal annealing. The carbons in BMT-HT and BMT-dry-HT are non-graphitic when compared to BMT-wet-HT according to XRD, and while TPO indicates BMT-wet-HT may be less crystalline than the other heat treated samples, the sample contains graphitic nanocarbons and metals that can decrease the oxidation temperature. Milling in cyclohexene appears to cause an increase in quasi-graphitic carbon upon thermal annealing. This appears to be due increased attrition of metals into the sample when the anthracite was milled with cyclohexene, metals that have been shown to catalyze graphitization.

ACKNOWLEDGEMENTS

The authors wish to acknowledge Dr. Joe Kulik of the Penn State Materials Research Institute for assistance in obtaining TEM micrographs. The authors would like to acknowledge the help of Dr. John W. Larsen and Dr. Harold H. Schobert, who participated in useful discussions about how cyclohexene might interact with coal.

The work has been funded by the Consortium for Premium Carbon Products From Coal, a DOE consortium in collaboration with PSU, WVU, and the carbon and coal industry.

REFERENCES

1. Franklin, R., *Acta Cryst.*, **4**, 253, 1951.
2. Franklin, R., *Proc. Roy. Soc. Ser. A.*, **209**, 196, 1951.
3. Oberlin, A., Terriere, G., *Carbon*, **13** 367, 1975.
4. Bustin, R., Rouzaud, J.N., Ross, J., *Carbon*, **33**, 679, 1995.
5. Couhaut, N., Blanche, C., Dumas, D., Guet, J.M., Rouzaud, J.N., *Carbon*, **38**, 1391, 2000.
6. Pappano, P.J., Mathews, J.P., Schobert, H.H., *Preprints, Amer. Chem. Soc. Div. Fuel Chem.* **44** (1999) 567.
7. Pappano, P.J., M.S. Thesis, The Pennsylvania State University, University Park, PA, 2000.
8. Pappano, P.J., PhD. Thesis, The Pennsylvania State University, University Park, PA, 2003.
9. Andréseñ, J.M., Burgess, C.E., Pappano, P.J., Schobert, H.H., *Fuel Proc. Tech.*, **85** (12), 1373-1392, 2004.
10. González, D., Montes-Morán, M.A., Garcia, A.B., *Energy Fuels*, **19**, 263, 2005.
11. Evans, E., Jenkins, J., Thomas, J., *Carbon*, **10**, 637, 1972.
12. Lueking, A.D., Principal Investigator, Final and Quarterly Reports for "Nanostructured Anthracite-Metal Composites for Hydrogen Storage," Internal Agreement No. 2670-TPSU-DOE-1874, for US DOE Prime Award No.: DE-FC26-03nt41874, (a) 1st Quarterly Report, June 15, 2004 (b) 2nd Quarterly Report, Sept. 15, 2004, (c) 3rd Quarterly Report, Dec. 15, 2004, (d) 4th Quarterly Report, March 31, 2005, and (e) Final Report.
13. Burgess-Clifford, C.E., Lueking, A.D., Naranayan, D., 1st Quarterly Report, "Nanocarbons from Anthracite Coal," Internal Agreement No. 2875-TPSU-DOE-1874, for Award No.: DE-FC26-03NT4187, June 15, 2005.

14. Lueking, A.D., Gutierrez, H.R., Fonseca, D.A., Narayanan, D.L., Van Essendelft, D.T., Jain, P., Clifford, C.E.B., *J. Amer. Chem. Soc.*, **128** (24), 7758-7760, 2006.
15. Lueking, A.D., Gutierrez, H.R., Jain, P., Van Essendelft, D., Clifford, C.E.B., "Structural transformations in a ball-milled anthracite coal after thermal and chemical processing: Role of HCl and NaOH purification treatment," *Carbon*, accepted for publication, 2007.
16. Chen, Y., Conway, M.J., and Fitzgerald, J.D., *Appl. Phys. A*, **76**, 633-636, 2003.
17. Chen, Y., Conway, M.J., Fitzgerald, J.D., Williams, J.S., and Chadderton, L.T., *Carbon*, **42**, 1543-1548, 2004.
18. Maire, J. and Mering, J., *Chemistry and Physics of Carbon*, Marcel Dekker, New York, 1970, vol. **6**, p 125.
19. Feret, F.R., *Analyst*, 1998, **123**, 595-600.
20. Li, Y., Xie, S., Zhou, W., Tang, D., Zou, X., Liu, Wang, G., *Carbon*, **39**, 615-628, 2001.
21. Subramoney, S. *Adv. Mater.*, **10**, 1157, 1998.

TABLES AND FIGURES

Table 1: Ultimate and proximate analyses of BMT coal.

Analytical Method	Value
Moisture, as received	6.53
Ash, wt %, dry	6.83
Volatile Matter, wt %, dry	3.65
Fixed Carbon, wt%, dry	89.52
Carbon, wt %, dmmf	88.85
Hydrogen, wt %, dmmf	1.29
Nitrogen, wt %, dmmf	0.78
Sulfur, wt %, dmmf	0.49
Oxygen (by difference), wt %, dmmf	1.76
Vitrinite reflectance, %	5.45
Inertinite reflectance, %	14.1

Table 2: XRD parameters of coal before and after thermal annealing.

Processing Method	XRD Parameters			Measurement of DOG ^a		
	d_{002} (Å)	L_c (Å)	L_a (Å)	A_{graphite}	A_{coke}	g (%)
BMT	3.42	12	38	n.d.	n.d.	n.d.
BMT-HT	3.41	20	40	1369.63	8698.42	13.6
BMT-dry	3.40	18	36	n.d.	n.d.	n.d.
BMT-dry-HT	3.45	29	40	1829.00	6718.34	21.4
BMT-wet	3.49	12	44	n.d.	n.d.	n.d.
BMT-wet-HT	3.39	50	44	968.40	605.68	74.3

a Degree of graphitization, determined by Feret's method.¹⁹

Table 3: Ash content of coal before and after thermal annealing.

Processing of PSOC 1468	Total Ash (wt%)	Iron ^c (wt%)	Magnesium ^c (wt %)	Aluminum ^c (wt%)
BMT	6.60 ^a	0.494	0.060	1.337
BMT-HT	8.23	n.d.	n.d.	n.d.
BMT-dry	6.80 ^a	0.78	0.027	1.200
BMT-dry-HT	13.10	n.d.	n.d.	n.d.
BMT-wet	10.82 ^a	3.84	0.041	0.982
BMT-wet-HT	22.20	n.d.	n.d.	n.d.

a Ash content measured by Proximate Analysis on different sample than earlier PSU characterization

b Ash content measured by TGA

c Individual metal content measured by Neutron Activation Analysis

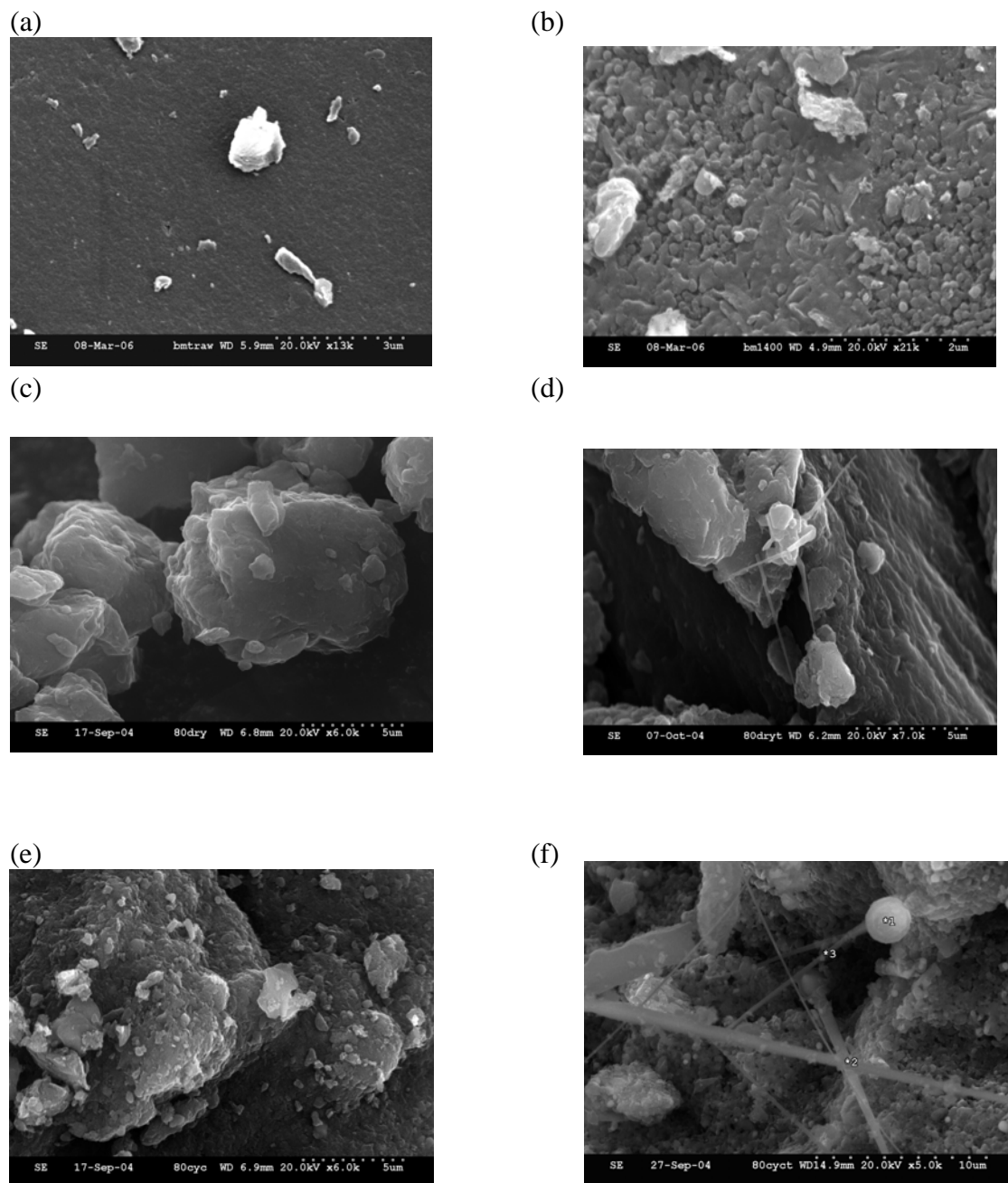


Figure 1: SEM micrographs of sample with no milling (a) before (BMT) and (b) after heat treatment at 1400 °C (BMT-HT), sample ball milled without solvent for 80 h (c) before (BMT-dry) and (d) after heat treatment at 1400 °C (BMT-dry-HT), sample ball milled with solvent for 80 h (e) before (BMT-wet) and (f) after heat treatment at 1400 °C (BMT-wet-HT).

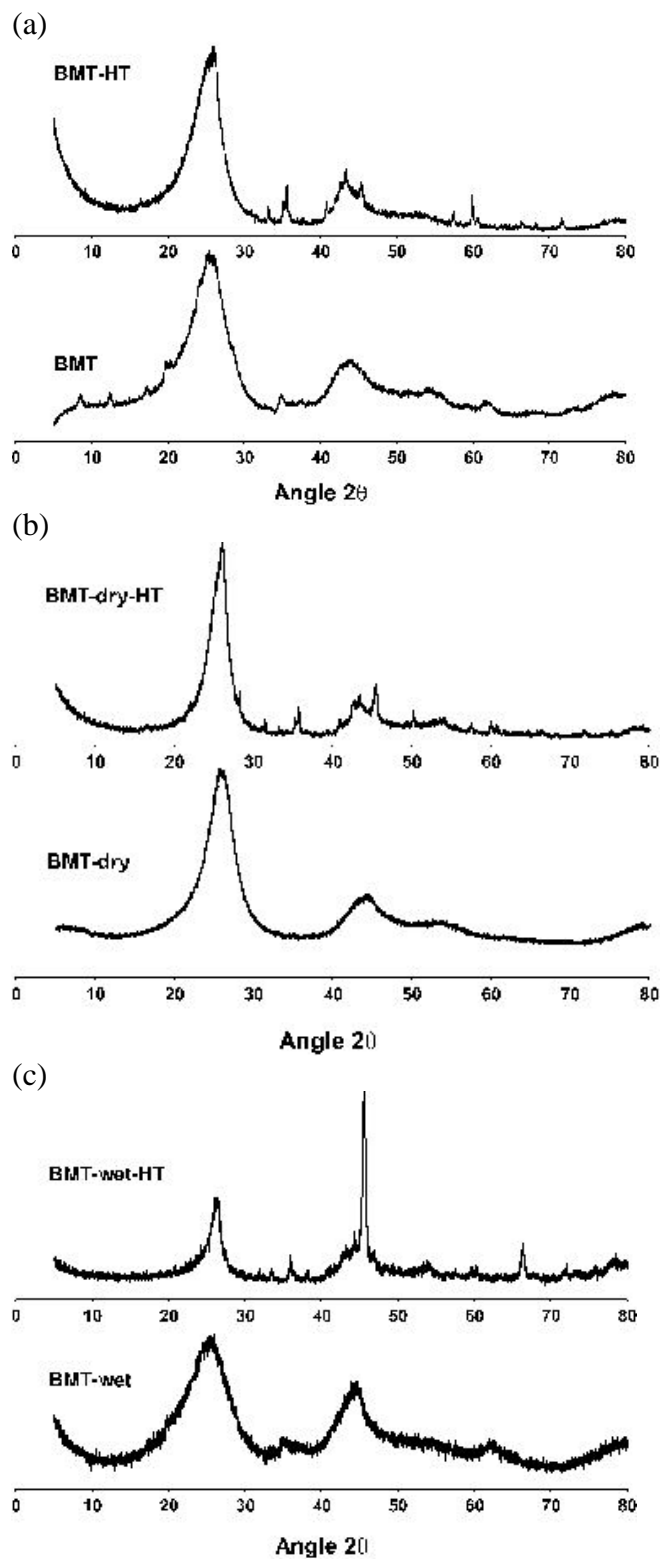


Figure 2: XRD spectra of (a) BMT and BMT-HT, (b) BMT-dry and BMT-dry-HT, and (c) BMT-wet and BMT-wet-HT.

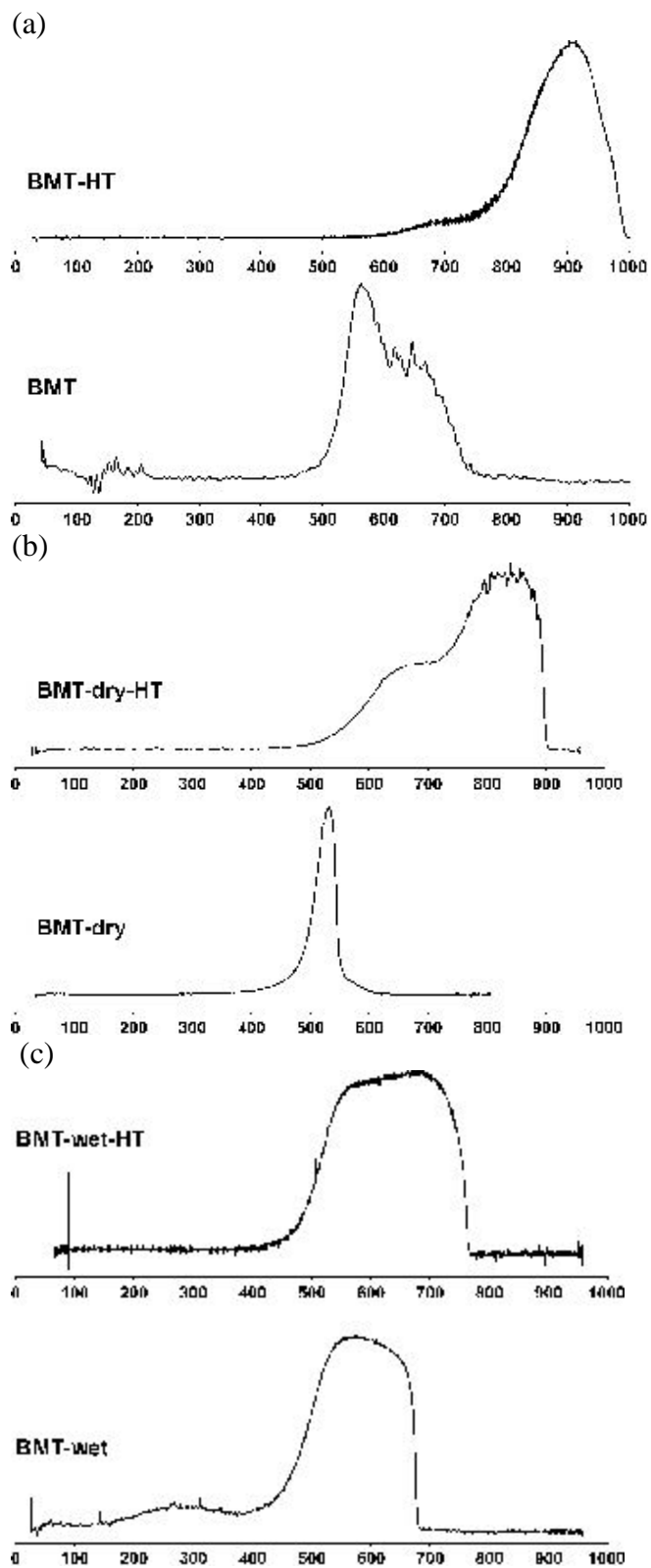
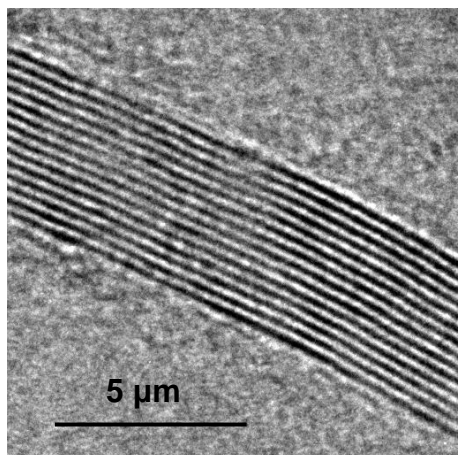


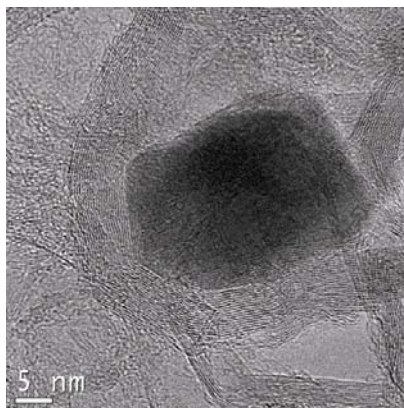
Figure 3: TPO, the derivative of the mass loss for (a) BMT and BMT-HT, (b) BMT-dry and BMT-dry-HT, and (c) BMT-wet and BMT-wet-HT.

Figure 4: TEM of coal samples after milling in solvent and thermal annealing. Includes TEM micrographs of several different structures observed in BMT-wet-HT (a) nanographene ribbon, (b) nanocrystalline diamond, (c) carbon overlap (d) curved graphitic regions (e) silicon tubes.

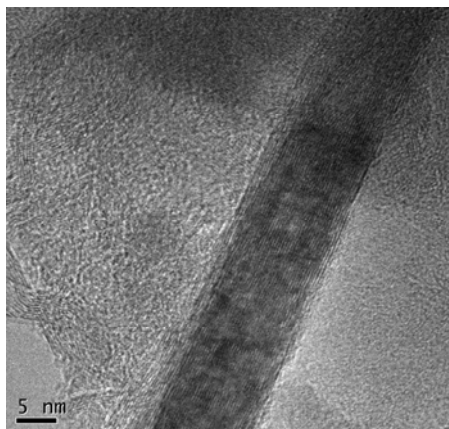
(a)



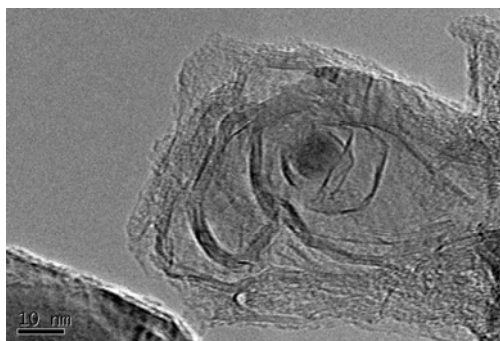
(b)



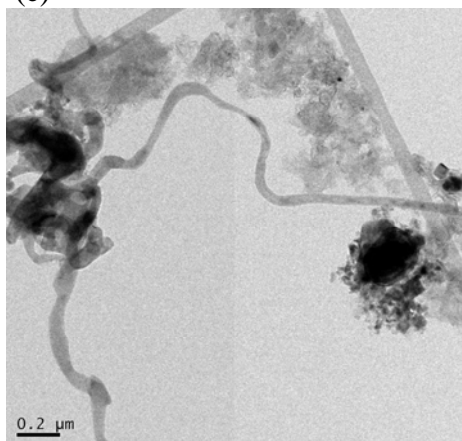
(c)



(d)



(e)



CENTRIFUGATION OF COAL LIQUEFACTION PRODUCTS

Charles W. Kling, Elliot B. Kennel, J. Joshua Maybury, Alfred. H. Stiller,
and Robert C. Svensson*

West Virginia University
Department of Chemical Engineering
PO Box 6102 Morgantown, WV 26506-6102
304-293-2111 x2423
Elliot.Kennel@mail.wvu.edu

*Permanent address:

Chalmers Lindholmen University College
Department of Physics and Engineering Physics
Kemigård 1, Fysikgränd 3
SE-412 96 Göteborg
SWEDEN

ABSTRACT

The production of synthetic tar or synthetic crude from coal via direct liquefaction process results in the creation of slurries of hydrocarbon tar with solid matter, necessitating separation of the two phases. This paper describes the use of a commercially available, reaction-turbine style centrifuge to reduce the ash level in the synthetic tar product. The synthetic tar can then be converted to carbon products such as binder pitch or anode grade coke. Alternatively, synthetic tar can be refined to produce fuels products including gasoline, diesel, aviation fuel, etc. The ash-containing component has significant fuel value and is suggested as a possible fuel for coal gasification systems such as FutureGen.

For this study, a synthetic tar was created by dissolving powdered coal at about - 50 mesh in a hydrogenated commodity solvent similar to naphthalene. Approximately 85% of the dry-ash free material was dissolved. The remainder is a solid phase material consisting primarily of mineral matter (ash) and fixed carbon. Hence centrifugation is required to separate the solid and liquid phases. Accordingly, a pressure vessel and return system were designed to allow continuous flow through the centrifuge. The return system operates using pressure differentials, enabling the system to be self-regulating. This return system allows the centrifuge to run continuously at a constant flow rate until acceptable ash levels are obtained in the product. Proximate Analysis was performed to determine ash levels of the product (centrate) and cake.

The centrifuged product can then be further processed and used for a variety of applications. Carbon Products at West Virginia University is currently researching ways to make electrode binder pitch from the centrifuged product and is also investigating liquid automotive fuels from coal. The centrifugation process is a necessary step for the production of carbon products from coal.

INTRODUCTION

Separation of solid materials from coal liquefaction-derived crude is problematic due to the tendency of heavy aromatic liquids to form viscous tarry phases. Solid particles, mainly consisting of mineral matter and fixed carbon, are often found suspended in the tarry phase. This makes conventional filtration problematic. For activities at the pilot scale and beyond, it is important to identify credible means for handling this problem.

A low cost solution was considered, based on the use of a centrifuge mass produced for use in large diesel engines to filter engine oil. For this research, a Spinner II Centrifuge (C. F. Hudgins, Houston TX 77292) was selected as a representative unit. The centrifuge is normally powered by the pressure differential between the high pressure oil line and the low pressure oil pan, so that oil flows through hollow spindle into rotating bowl (see Figure 1). As oil passes through the rotating bowl, centrifugal force separates the working fluid into two phases. The solid phase is deposited as a solid cake on the surface the cleanable bowl. Clean oil exits through opposing, twin nozzles that power the turbine, and returns to the crankcase from the level control base. Flows of up to 16 gpm can be accommodated by large units of this type, although for the experiments described herein, a smaller Model 60 unit rated at 0.8 gpm was used.



Figure 1. Centrifuge Diagram (courtesy T. F. Hudgins Inc).

The operation of the centrifuge separates the slurry into two components. The first component, referred to as the centrate, contains a reduced level of solids. The second component, referred to as the residue, contains an enhanced level of solids. Continuity requires that

$$m_{\text{tot}} = m_c + m_t \quad , \quad (1)$$

Where m_{tot} is the total initial mass of the slurry, m_c is the mass of the liquid phase or “centrate,” and m_t is the mass of the solid phase or “tails”. The ash content in the centrate is described by

$$m_{\text{ash},c} = m_c C_{\text{ash},c} \quad , \quad (2)$$

where the ash concentration in the centrate $C_{\text{ash},c}$ is determined by proximate analysis or some other appropriate technique. Likewise, the mass of ash in the tails is given by

$$m_{\text{ash},t} = m_t C_{\text{ash},t} \quad . \quad (3)$$

The centrifuge separation ratio ξ is given by

$$\xi = \frac{C_{\text{ash},t}}{C_{\text{ash},c}} \quad . \quad (4)$$

Thus a perfect centrifuge would be one in which ξ tends toward infinity. The centrifuge separation ratio ξ is likely not constant for most centrifuges but would likely vary according to the particle size distribution present in the centrifuge medium, the concentration, fluid viscosity and other parameters.

In the case of a direct liquefaction slurry, it is intended to create two main products. The centrate, i.e., a low-ash heavy liquid, would be used as a synthetic crude. The centrifuge tails would be coked to drive off volatile gas and nominated as a gasification fuel (e.g., for a coal gasifier such as FutureGen).

Because the tails are of much lower economic value than the centrate, it is desirable to maximize the relative yield of the centrate. A slurry made up of one part Lower Kittanning bituminous coal with a nominal ash content of 6%, when dissolved in three parts coal tar distillate would exhibit an ash content of about 1.5%. The required maximum ash content is 0.5% in order to create a precursor for a binder pitch extender (i.e., binder pitch would be produced by distilling the precursor and combining the distillation residue with other pitches in order to meet binder pitch specifications. Thus the problem can then be reduced to that of removing a quantity of ash equal to 1.0% of the total working fluid mass.

For example, a 55 gallon drum with 10% head space (total quantity of slurried working fluid 49.5 gallons), and an average density of 1.1 kg/liter would have a mass given by

$$m_{\text{tot}} = 55 \text{ gal} * 8.3 \frac{\text{lb}}{\text{gal}} * 1.1 * 0.90 \quad (5)$$

$$= 452 \text{ lbs} = 205 \text{ kg} \quad (6)$$

An initial ash content of 1.5% by mass implies that the total mass of ash would be 6.77 pounds or 3.07 kg. Approximately two thirds of this total will be rejected in the tails, or about 2 kg.

For a given centrifuge separation ratio ξ , and assuming a value of 0.5 mass percent for the maximum ash content in the centrate, the value of ash concentration in the tails would be

$$C_{\text{ash,t}} = 0.005\xi \quad (7)$$

The total quantity of tails can then be determined from Equation 3, or

$$m_t = \frac{m_{\text{ash,t}}}{C_{\text{ash,t}}} = \frac{2 \text{ kg}}{0.005\xi} = \frac{400 \text{ kg}}{\xi} \quad (8)$$

A plot of total quantity of tails versus centrifuge ratio ξ is shown below.

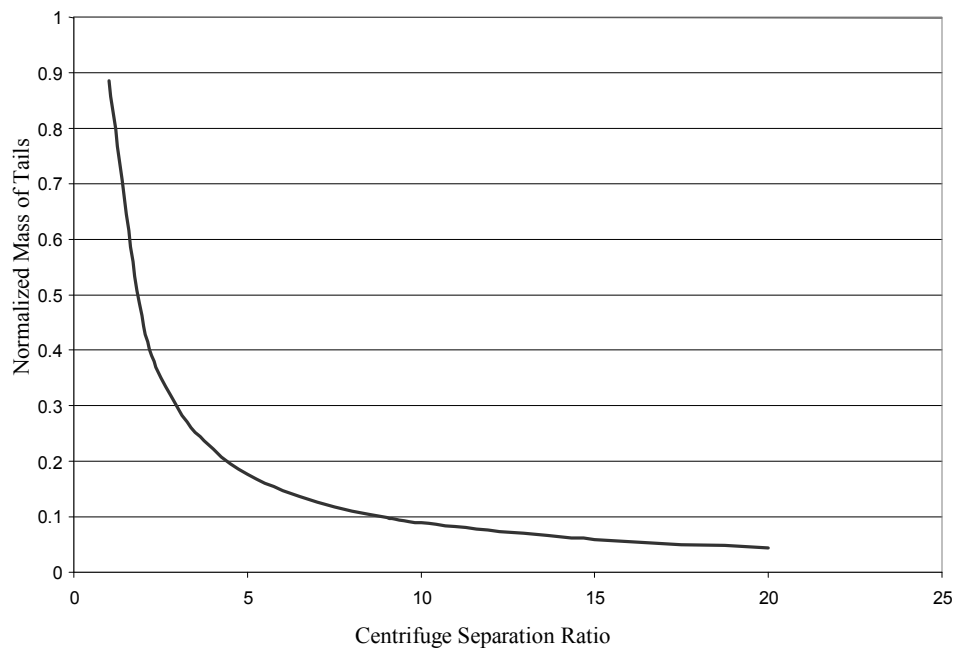


Figure 2. Normalized Mass of Centrifuge Tails Produced as a Function of Centrifuge Separation Ratio.

EXPERIMENTAL

A synthetic crude was extracted using bituminous coal (Lower Kittanning seam, with an ash level of about 6% by mass as measured by proximate analysis).¹ The solvent was a coal tar distillate obtained from Koppers Inc. and modified via a mild hydrogenation such that the hydrogen concentration was enhanced by about 0.5% by mass. The coal was dissolved in the solvent at a ratio of 1:3. Total solubility is estimated at 90% by mass, with the result being a slurry with about 2.5% solids (1.5% ash and 1.0% fixed carbon) and the balance being a high viscosity hydrocarbon liquid.

Because the centrifuge was designed for operation with motor oil rather than the higher viscosity coal slurry, tests were conducted to determine the effectiveness of the centrifuge. Figures 3 and 4 show that the centrifuge rotational velocity is considerably slower as a function of air pressure when a coal liquid slurry is utilized, but still within the effective operating performance of the device. That is, to obtain equivalent performance with the coal slurry compared to engine oil, it would be necessary to increase the air pressure to the unit by some 40 to 60 psig.

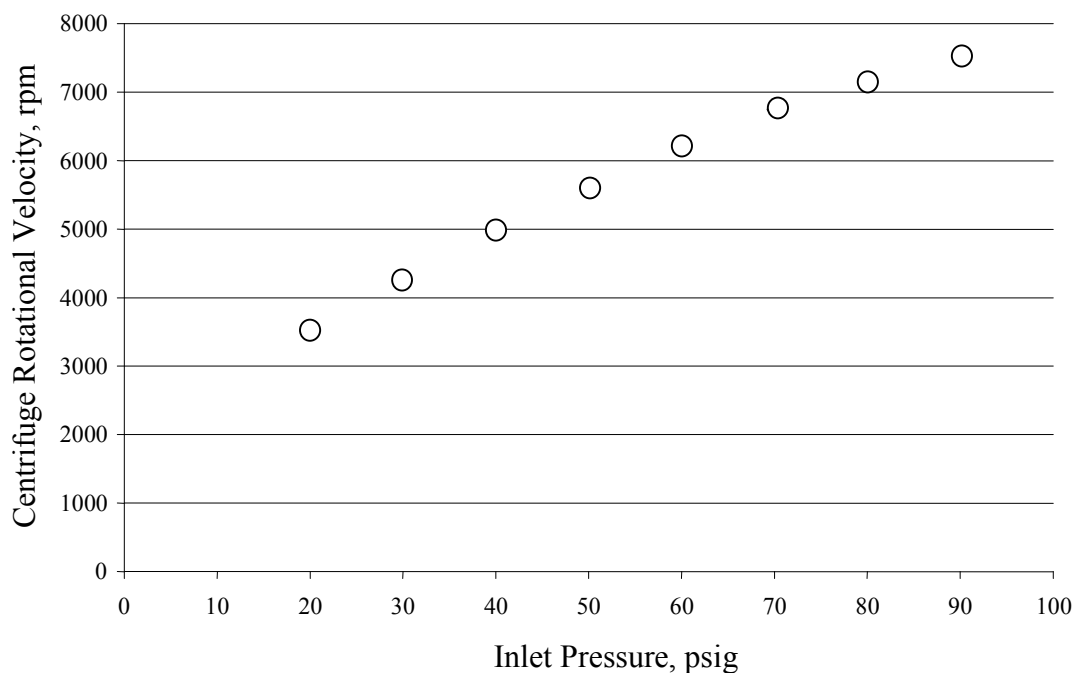


Figure 3. Centrifuge Rotational Velocity with SAE 30 Motor Oil Working Fluid at 75°C.

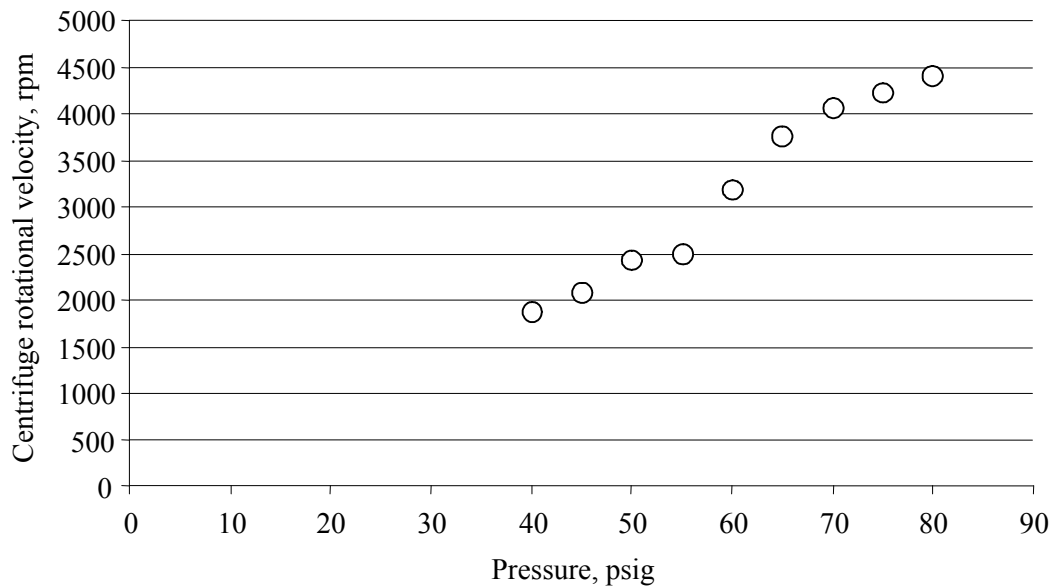


Figure 4. Centrifuge Rotational Velocity with Coal Slurry Working Fluid at 49°C.

A pressure vessel and return system were designed to allow the continuous operation of the centrifuge. A twenty gallon pressure vessel was outfitted with a bottom outlet valve, a side return valve with internal mixing arm, a top return valve, a top gas inlet for pressurizing, a top gas bleed valve and a top pressure relief valve. During operation, the pressure vessel was maintained at a pressure of 60 psig and a temperature of 50°C. From the tank, the working fluid travels out the bottom valve into the centrifuge. From the centrifuge, the filtered tar is then directed to a reservoir which is open to atmospheric pressure. The 60 psig pressure differential powers the centrifuge. Using a pneumatic pump, the centrate is then pumped back into the pressure vessel (see Figures 5 and 6).

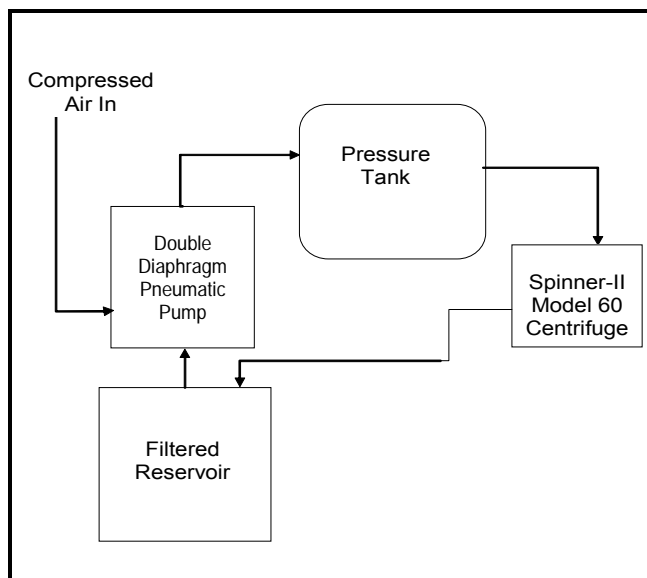


Figure 5. Spinner II Model 60 System Schematic.



Figure 6. Spinner II Model 60 Centrifuge Experimental Setup.

Heating bands are used to regulate the temperature of the tank at 50°C. Compressed nitrogen or air is used to bring the pressure vessel to an initial pressure of 65 psig. Upon initiation of the centrifugation process, a pressure of 60 psig is maintained in the tank by returning the product under pressure. Through the use of a pneumatic powered return pump, the pressure in the pressure vessel is self regulating and remains fairly constant.

The centrifugation process was timed to determine the effectiveness of the centrifugation over time. Periodically the centrifugation process was stopped to take measurements and to empty the cake from the centrifuge. To stop the process, the bottom feed valve was closed to stop flow to the centrifuge. Any product in the

centrifuge was removed with compressed air. The centrate in the reservoir was pumped back into the pressure vessel. The centrifuge was disassembled and the bowl was weighed to determine the mass of the removed solids. Samples were taken of the tails and of the centrate. The bowl was then cleaned and the centrifuge was reassembled. The centrifugation process was then resumed.

The samples were analyzed by proximate analysis according to ASTM D-3172 to determine ash concentrations. The results indicate that the centrifuge significantly reduced the ash levels in the centrate, especially in the first few hours of operation (see Figure 7). The goal of less than 0.5% ash concentration was met after about seven hours of centrifugation. Somewhat disappointingly, however, the ash levels were no lower than about 0.4% even after 20 hours of treatment. The ability to produce centrate with 0.5% ash level would be adequate for the purpose of producing a binder pitch extender, but would not be acceptable if the synthetic pitch thus produced were the majority constituent.

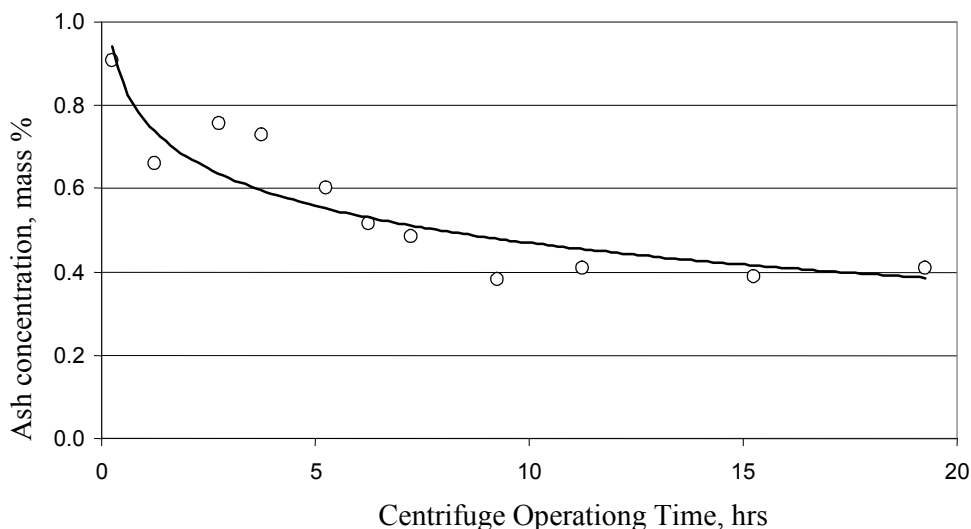


Figure 7. Percent Ash in Coal Derived Tar over Centrifuge Time.

The centrifuge tails were also tested according to ASTM D-3172 to determine the amount of ash present in the tails. Results of these tests correlate with the tests on the centrate. Results show that the amount of ash in the centrifuge cake was high initially but diminished within several hours of operating time (See Figure 8).

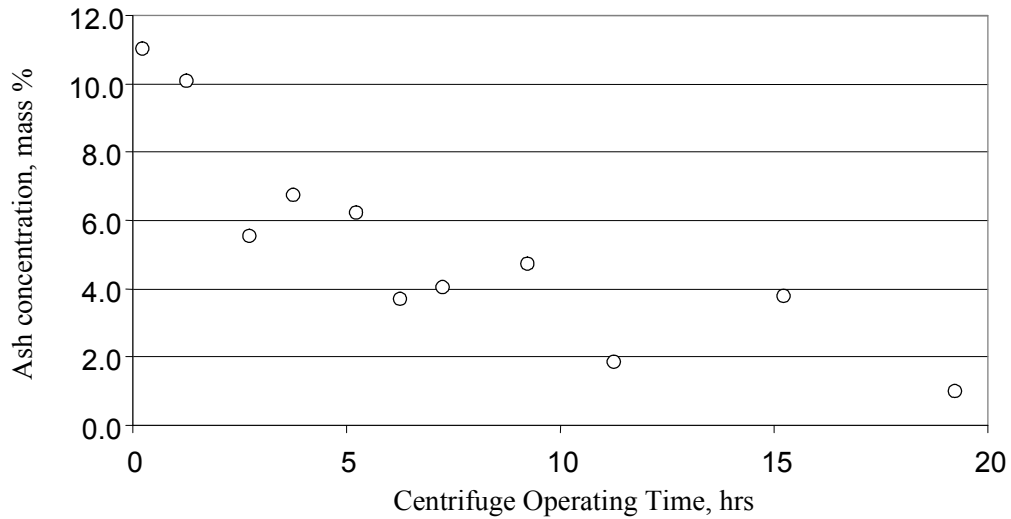


Figure 8. Ash Content in Centrifuge Tails as a Function of Operating Time.

Figure 8 confirms that the centrifugation process was less effective as a function of operating time. This is not unexpected, as the larger, more-easily-removed particles are captured early on, leaving behind smaller particles in the centrate that are more difficult to remove. Figure 9 confirms that after 20 hours, a point of diminishing returns was probably reached.

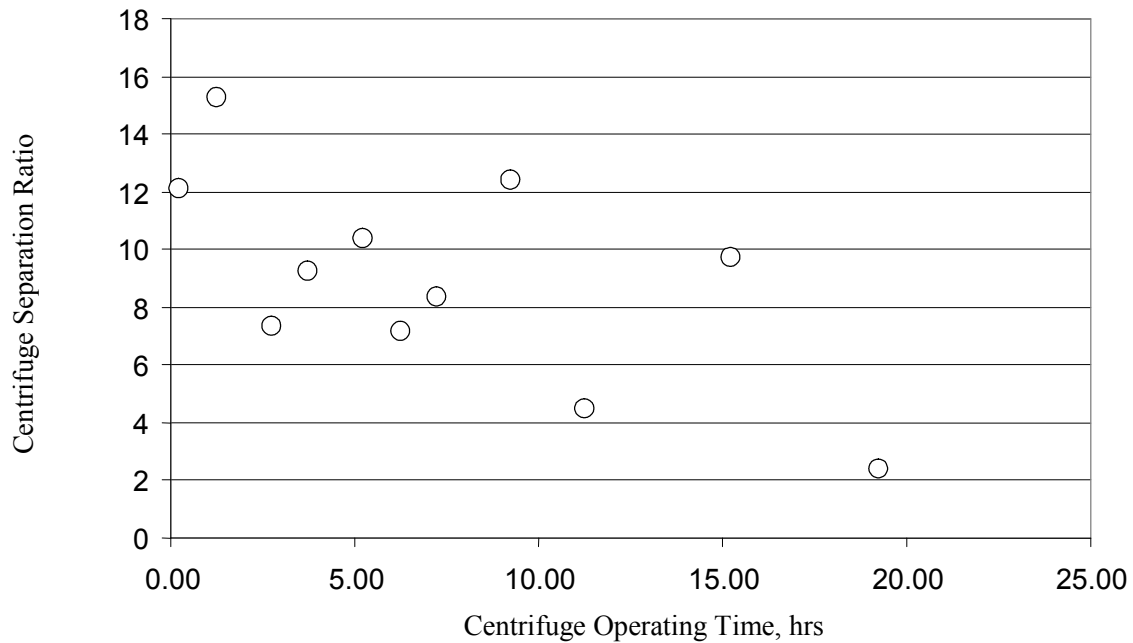


Figure 9. Centrifuge Separation Ratio ξ as a Function of Operating Time.

CONCLUSION

The centrifuge tested, although primarily used for removing particulates from engine oil, can be used successfully to remove particulates from coal liquids. A 55 gallon drum would contain about five gallons of centrifuge tails, based on the achieved values of centrifuge separation ratio in Figure 9. Acceptable ash levels were observed in the centrate after several hours of centrifugation, although it proved difficult to achieve ash levels in the centrate below about 0.4% by mass. Slightly higher temperature might produce better results if the viscosity of the coal liquids is enhanced sufficiently, although the polymer seals used in the device currently limit working fluid temperatures to about 70 °C. Higher pressure would also presumably improve performance, especially the centrifuge separation ratio. Limitations on the in-house air supply prevented the use of higher pressure that might have been able to improve the centrifuge separation ratio.

An additional factor may have been the use of carbon steel pressure vessels and storage drums, which could present an avenue for the generation of metal oxide corrosion products, which would appear as ash during proximate analysis.

ACKNOWLEDGMENT

The support of the US Department of Energy, National Energy Technology Laboratory, Contract DE-FC26-03NT41873, is gratefully acknowledged.

REFERENCES.

-
- ¹ E. B. Kennel et al., "Carbon-Rich Product Suites from Direct Liquefaction," *The 32nd International Technical Conference on Coal Utilization & Fuel Systems*, June 10 – 15, 2007, Sheraton Sand Key, Clearwater, Florida.

Fabrication of electrochemical double layer capacitors using carbon derived from coal tar pitch/polyethylene glycol diacid blends

Ramakrishnan Rajagopalan¹, Keith Perez² and Henry C. Foley²

*¹Materials Research Institute and ²Department of Chemical Engineering
The Pennsylvania State University, University Park, PA 16802*

ABSTRACT

Nanoporous carbon materials with high surface area (1500 – 2000 m²/g) and narrow pore size distribution ranging from 1 – 3 nm were synthesized using coal tar pitch/polymer blends. Coal tar pitch was dissolved in tetrahydrofuran and the insoluble fraction of coal tar pitch was extracted and mixed with an oxidizing agent such as sulfuric acid. The resultant mixture was pyrolyzed and activated using CO₂ at 900°C. Electrical double layer capacitor was fabricated using the synthesized carbons and specific capacitances was measured using cyclic voltammetry (CV), constant current charge/discharge measurements (CC) and electrochemical impedance spectroscopy (EIS). Carbon derived from the modified coal tar pitch alone showed specific capacitances as high as 100 F/g using sulfuric acid as electrolyte. When a pore former like polyethylene glycol diacid was added to the modified pitch, the gravimetric capacitances as high as 130 F/g was achieved.

INTRODUCTION

Porous carbon research has fueled interest in some recent applications like electrochemical capacitors and batteries. Microporous carbon materials possess huge surface area in the order of 600 – 3000 m²/g. This property makes them excellent candidates for electrode materials for double layer electrochemical capacitors. In order to use high surface area carbons for this application, it is important to create optimum porosity in the material. Typically, pores less than 1 – 2 nm are not accessible by the electrolyte ions while pores greater than 5 nm lead to loss of surface area and density [1]. In addition to this, capacitance of carbon-based capacitor are also affected by conductivity of carbon-binder composite, blockage of carbon pores by the binder, thickness of the composite, electrolyte characteristics and their properties. As a result, charge accumulated in a practical capacitor varies widely from one activated carbon to another. The proper selection of carbonaceous material is thus very important for further electric double layer capacitors (EDLC) development.

Several different forms of carbon such as carbon black, carbon aerogels, glassy carbon and carbon fibers have been investigated as potential electrodes for ultracapacitors [2]. Specific capacitances as high as 100 – 250 F/g can be achieved when these carbons are activated thermally using carbon dioxide or chemically using sodium or potassium hydroxide. However, the volumetric capacitances of most of these carbons are low. In terms of high volumetric capacitances, pitch based carbons seems to be a promising material [3]. In this investigation, we report the synthesis of high surface area carbons derived from modified coal tar pitch/polymer blends for ultracapacitor applications.

EXPERIMENT

Synthesis of NPC derived from Coal tar pitch/polyethylene glycol diacid blends

5g of coal tar pitch was dissolved in 50 ml of tetrahydrofuran (THF) and allowed to stir for 2 hours. The dissolved mixture was then filtered using suction filtration and the residue (THF insoluble) and the filtrate (THF soluble) were collected separately. After the extraction, 3g of THF insoluble were mixed with 10g of PEG600 diacid and 2ml of H₂SO₄. The solution was stirred overnight and the mixture was carbonized at 800°C.

The pyrolyzed carbon was then placed in a quartz boat and placed in a tube furnace. The sample was heated under argon atmosphere to 900°C in one hour and soaked for another hour. This was followed by activating under CO₂ atmosphere at 900°C. After activation, the sample was cooled down to room temperature under argon atmosphere.

Pore size distribution

The pore size distribution of the carbon was calculated using methyl chloride adsorption tests. The pore size was calculated using H-K model described elsewhere [4].

Electrode preparation

0.2g of carbon was mixed with polyvinylidene powder (0.02g) and grinded using a mortar and pestle. The resultant powder was dispersed in 1 ml of N-methylpyrrolidone. The solution was ultrasonicated for half hour and the resultant paste was applied onto a gold foil (1 cm²) and blow dried to form a thin carbon film. The weight of the carbon film was ~ 20 mg for every experiment.

Fabrication of double layer electrochemical capacitor

Two-electrode electrochemical capacitor was fabricated by sandwiching a Celgard 5400 membrane between two identical carbon electrodes. The carbon electrodes were prepared by mixing 90wt% carbon with 5wt% Teflon solution and 5wt% acetylene black. The resultant mixture was kneaded into dough and pressed into a 50 μ thick carbon film. Two stainless steel meshes were used as the current collector. The assembly was then immersed in 1M H₂SO₄ for 2 hours before beginning any testing. One of the carbon electrodes acted as both the counter electrode and as well as the reference electrode. The capacitor was then tested using both galvanostatic charge-discharge experiments, cyclic voltammetry and electrochemical impedance spectroscopy.

RESULTS AND DISCUSSION

Coal tar pitch was dissolved in THF and the insoluble fractions of the pitch were extracted. The insoluble fraction was then mixed with sulfuric acid, carbonized and activated using CO₂ at 900°C for 2 hours. We used sulfuric acid, as it is known to accelerate polycondensation reactions of lighter volatile fractions in the pitch and create more insoluble fractions, which in turn, induces more disorder in the carbonized pitch [5,6]. Our investigation showed that addition of sulfuric acid to the insoluble fraction aids in creating significant amount of microporosity (5 – 6 Å) in the pyrolyzed carbons. These carbons upon CO₂ activation has surface area of about 1000 - 1500 m²/g with significant of micropores ranging from 1 – 2 nm. When a pore former like PEG was mixed with the modified pitch, pyrolyzed and activated using similar conditions, the surface area increased to 1500 - 2000 m²/g while maintaining narrow pore size distribution of 1 – 2 nm. Similar treatments with the soluble fraction of the pitch yielded a carbon with surface area as high as 1000 m²/g but with a narrow pore size distribution of 5 - 6Å.

Demonstration of double layer electrochemical capacitor

The fabricated capacitor was tested using Galvanostatic charge/discharge experiments, cyclic voltammetry and Electrochemical Impedance Spectroscopy. Carbon derived from the mixture of insoluble fraction and H_2SO_4 showed a gravimetric specific capacitance of 100 F/g and had a time constant of 43 seconds. The bulk density of this carbon was about 0.72 g/cc. The high bulk density with controlled pore size distribution makes it a promising candidate for making high volumetric capacitor applications. When PEG600 was added in the precursor, the gravimetric specific capacitance increased to 120 F/g and the time constant was 25s. However, the bulk density also reduced to 0.62 g/cc. When the soluble fraction was used as the precursor, we saw that the gravimetric capacitance was lower (85 F/g) and the time constant increased to 125s. In this case, the bulk density of the sample was about 0.78 g/cc.

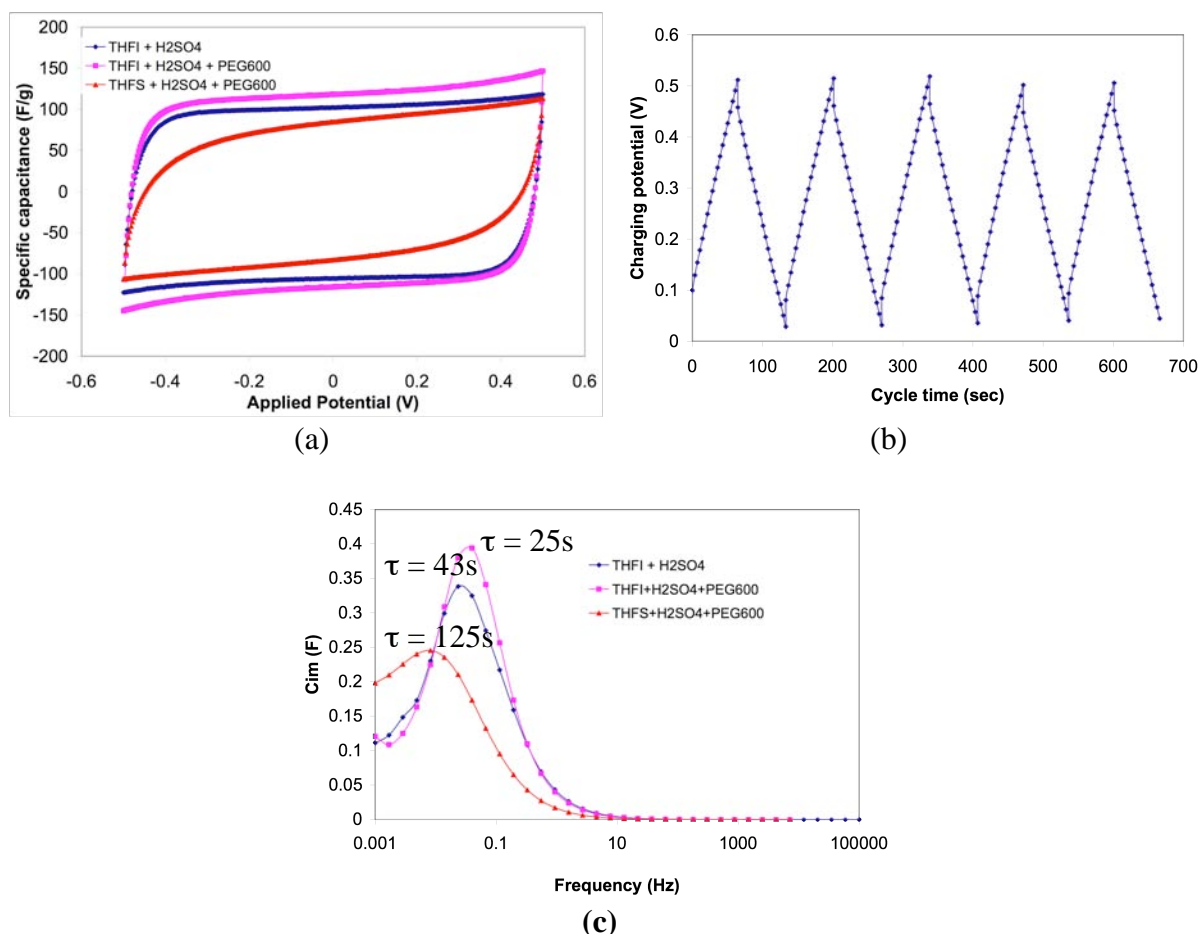


Figure 1. Cyclic voltammogram of two-electrode ultracapacitor fabricated using nanoporous carbon derived from coal tar pitch/PEG600 blends, (b) Charge/discharge galvanostatic measurements under a constant current load of 1 A/g and (c) Plot of imaginary capacitance versus frequency as a function of composition of precursors

CONCLUSIONS

CTP when modified with H_2SO_4 can be used as a suitable precursor to yield high surface area carbon with controlled porosity. We believe that this carbon can be used to make high energy density capacitors as the bulk density of these carbons can be as high as 0.5 – 0.8 g/cc. The

developed carbons were systematically studied using cyclic voltammetry and electrochemical impedance spectroscopy. We have also fabricated a two-electrode electrochemical double layer capacitor using these carbons as electrodes. Using sulfuric acid as electrolyte, we were able to make capacitors with capacitances as high as 100 -130 F/g. These are very promising and we believe that there is potential to extend the use of these capacitors in organic electrolyte system to achieve higher energy densities.

ACKNOWLEDGMENTS

The authors would like to acknowledge Consortium of Premium Carbon Products from Coal (Subcontract no. 2872-TPSU-DOE-1874) for funding this project.

REFERENCES

1. "Ultracapacitors: Why, how and where is the technology" A. Burke, *J. Power Sources*, **91** (2000) 37-50.
2. "Carbon properties and their role in supercapacitors" A.G. Pandolfo and A. F. Hollenkamp, *J. Power Sources*, **157** (2006) 11-27.
3. "Activated carbon produced from Sasol-Lurgi pitch and its application as electrodes in supercapacitors" A. Alonso, V. Ruiz, C. Blanco, R. Santamaria, M. Granda, R. Menendez and S.G.E. de Jager, *Carbon* **44** (2006) 441-446.
4. R.K. Mariwala and H.C. Foley, *Ind.Eng.Chem.Res.*, **33** (1994) 2314.
5. B. Petrova, T. Budinova, N. Petrov, F.Yardim, E. Ekinci and M. Razvigorova, *Carbon* **43** (2005) 261-267.
6. B. Petrova, T. Budinova, E. Ekinci, N. Petrov and F. Yardim, *Carbon*, **45** (2007) 704-709.

Mild Coal Extraction for the Production of Anode Coke

Rodney Andrews*, David Jacques, Terry Rantell and James C Hower.
University of Kentucky Center for Applied Energy Research
2540 Research Park Dr, Lexington, KY 40511

ABSTRACT

The quality and availability of petroleum coke used in the manufacture of carbon anodes for aluminum production is becoming of increasing concern to the industry. Coke quality and yields have progressively declined as changes in refinery practice and the move towards processing an increasing proportion of heavier sour crudes have affected coke properties, resulting in an increase in the metal impurities and sulfur content of the coke. An alternative supply of anode coke is required to supplement or eventually replace calcined petroleum coke. The significant domestic reserves of coal could represent a viable carbon resource for anode production, provided defined coke specifications can be met and at a cost that is economically viable.

The principal objective of this study was to examine the feasibility of producing anode grade coke by the UKCAER process for the mild solvent extraction of coal. Selected coals were dissolved in a high boiling solvent, the mineral matter and unreacted products removed by filtration and the clean coal liquids converted to coke. A range of feedstocks and process conditions were examined that offered the most likely route to producing the required result. A simple solvent extraction screening test was established to assess potential candidate materials and process variables without the need for prolonged and complex routines. The most promising materials in both performance and economic viability were assessed in more detail by conducting larger scale extraction tests to yield sufficient material for conversion to coke. The clean coal solutions were coked in a series of tests to assess the optimum process conditions. The green cokes were calcined and the product characterized. The composition and structure of the calcined cokes were compared to typical petroleum coke and assessed for their use in the fabrication of carbon anodes.

[*andrews@caer.uky.edu](mailto:andrews@caer.uky.edu); 859-257-0265

INTRODUCTION

The carbon anodes used in the production of aluminum are manufactured by carbonization of a blend of petroleum coke with a small proportion of coal tar binder pitch. Impregnation with more pitch is commonly used to produce the dense anodes needed to meet the required performance standards. Consumption rates of the anodes in the molten fluoride salt electrolysis cell are high, approaching 0.5t of carbon for each tonne of aluminum produced. Hence, large quantities of coke are required for carbon anode manufacture to satisfy the demands of the indigenous aluminum industry in the USA, amounting to ~1.6m tonnes/annum of calcined petroleum coke.

Unfortunately, the supply of petroleum coke of the required quality is becoming more uncertain. Impurity levels in petroleum cokes have been progressively increasing in recent years as the refineries have been obliged to accept a higher proportion of heavy sour crudes. This trend and changes in refinery practice, dictated by the economics of the petroleum market aimed at maximizing the yield of lighter high value products, have resulted in an increase in the sulfur content of the petroleum coke. Impurities in the crude oil become concentrated in the coke and can have undesirable effects on aluminum production. Metal impurities such as vanadium and nickel catalyze carbon oxidation reactions and lead to higher carbon consumption in the electrolysis cell. Other impurities collect in the refined aluminum and can lower its value. An alternative supply of anode coke is required to supplement or eventually replace calcined petroleum coke supplies. The principal objective of this project was to demonstrate that the significant domestic reserves of coal could be converted into coke suitable for anode fabrication by a mild solvent extraction process⁽¹⁾.

Component	Value	Method
Ash	≤ 0.1 %	ASTM D2415
S	≤ 1.0 %	Leco or XRF
Fe	≤ 300 ppm	ICP, AA or XRF
Si, V & Ni	≤ 200 ppm	ICP, AA or XRF
Na	≤ 100 ppm	ICP, AA or XRF
Ca	≤ 50 ppm	ICP, AA or XRF
P	≤ 5 ppm	ICP, AA or XRF
Pb, Be, As, Cd, Cr & Hg	≤ 1 ppm	ICP, AA or XRF

Table 1 Generic Coke Specification for Anode Production

The process developed by UKCAER has previously used anthracene oil (a coal tar distillate) as the solvent without the need for a hydrogen atmosphere or the use of high pressures, expensive catalysts or exotic solvents that make alternative processes economically unattractive. Dissolution of the coal in the digestion reactor allows the mineral matter and undissolved coal fraction to be removed from the coal solution by a solids separation step. Filtration is generally used for this purpose as the ill-defined separation between the dissolved coal and the boiling point distribution of the heavy process solvent make the use of alternative anti-solvent de-ashing techniques impractical. Virtually all of the mineral matter present in the coal is removed during the filtration stage and the clean coal solution can then be fed directly to a coking drum, from which the solvent can be recovered and recycled. Green coke would be discharged from the coker and calcined by heating to ~1300°C. As a proof of concept study this project was initiated

in order to examine the feasibility of producing anode grade coke of the required specification, Table 1 by the solvent extraction of coal.

EXPERIMENTAL

A simple, rapid and effective screening test was established to determine the optimum process conditions and identify possible coals and solvents as feedstocks for conversion to anode grade coke. The test can be completed in a short period of time and does not require investment in significant resources or infrastructure. A set of micro-reactors were constructed consisting of 200mm lengths of 12.7mm diameter stainless steel tubing (1.25mm wall) closed at one end with a cap and at the other with a valve via a reducing union.

Coals		WKy#6	WKy#9	Blue Gem	Pittsburgh	
Proximate	H ₂ O	(%)	2.5	5.2	3.4	1.4
	Ash	(%)	7.4	19.0	1.2	8.1
	VM	(%)	38.4	34.6	37.0	38.5
	FC	(%)	51.7	41.2	58.4	51.9
Ultimate (daf basis)	C	(%)	83.1	78.0	84.8	83.9
	H	(%)	5.8	5.2	5.5	5.0
	O (by diff)	(%)	6.5	10.1	7.0	6.8
	N	(%)	1.8	1.7	2.0	1.6
	S total	(%)	2.9	5.0	0.7	2.7

Table 2 Coal Analysis

In the test procedure, the reactor was loaded with a slurry of coal and solvent and heated by immersion in a fluidized sand bath controlled at the required temperature. The reactor, mounted in a cradle was oscillated at ~120cycles/min to provide agitation for the slurry. At completion, the reactor was quenched in water and allowed to dry. The gas evolved during the reaction was determined by weighing the reactor before and after venting the gas through the valve. The amount of undissolved solids in the coal digest was determined from the filter cake yield following filtration of the reaction products through a GFA glass fiber filter. Quinoline, used as a diluent, was displaced by THF before vacuum drying. The dry filter cake contains mineral matter and insoluble organic matter (IOM). Calculation of the IOM from the weight of dry cake and the known ash content of the coal allowed determination of the amount coal converted to soluble products on a dry ash-free basis. The tests were performed in duplicate.

Two Kentucky coals, WKy#6 from Western Kentucky and Blue Gem from Eastern Kentucky were targeted as the primary feed materials. In addition, a Western Kentucky coal (WKy#9) used in previous coal dissolution studies was employed to provide reference data since some information on its performance in solvent extraction was available⁽²⁾ and a Pittsburgh coal (Bailey mine) was used to prepare bulk coal solutions for testing the coking procedures. The coals were crushed to the required specification, 80% <75 μ m and analyzed, Table 2. All tests were conducted at a solvent/coal ratio of 2:1 and for residence times of 60minutes. In the first series of tests the reactivity of WKy#6 was determined over a range of reaction temperatures by extraction with the reference process solvent, anthracene oil (AOil#2) supplied by Reilly Industries to give a benchmark in the assessment of alternative solvents. Anthracene oil, a coke

oven by-product has commonly been used as the process solvent in the solvent extraction of coal. However, if the process were to be adopted as a viable means of producing even a small proportion of the ~1.6mt of anode grade coke consumed by the aluminum industry in the US each year, an alternative process solvent would be required, as there is only a limited supply of anthracene oil. A range of petroleum derived solvents have been assessed. These were mostly the lower value by-products from a refinery fluid catalytic cracker (FCC) and would be available in the quantities required for a large scale industrial application.

Decant Oil, the heaviest fraction from an FCC unit was considered to be the most likely candidate to make an acceptable solvent for the extraction of coal and, therefore, separate samples were obtained from two different refineries, (A & B). In addition, other lighter oil refinery fractions were investigated for this purpose. These included a heavy coker gas oil and a vacuum gas oil from refinery 'A'. The solvents were sampled and analyzed, Table 3. The petroleum derived solvents contain significantly more hydrogen than the coal derived anthracene oils reflecting their aliphatic character which may inhibit their performance in the solvent extraction of coal. The heavier oils, FCC Decant Oils are the most likely to make suitable process solvents.

Solvent	Source	Ultimate Analysis, (%)				
		C	H	O (by diff)	N	S
Anthracene oil #2	Reilly Industries	90.7	6.31	2.5	0.23	0.25
Coker heavy gas oil	Refinery 'A'	91.8	7.52	0.6	0.07	0.08
Vacuum gas oil		84.6	11.90	<0.1	0.15	3.35
FCC Decant Oil		89.5	8.95	0.9	0.11	0.60
FCC Decant Oil	Refinery 'B'	91.0	8.22	0.5	0.08	0.16

Table 3 Solvent Analysis

Larger scale tests were required in order to prepare coal extract solutions for assessment as feedstocks for the production of anode grade coke. A series of coal extraction tests were conducted using a 2liter stirred autoclave. The Pittsburgh coal and WKy#9 reference coal were used in the commissioning tests to produce clean coal solutions that were used to determine the best operating conditions for the coking reactor. The low ash Blue Gem and reactive WKy#6 were then used to generate the coal solutions and subsequent calcined cokes for the study. After charging the reactor and purging with nitrogen, it was rapidly brought to the operating temperature to commence the digestion stage. The pressure was maintained at 1.4MPa (200psi) by venting gas and light distillate evolved through a manual control valve and into the condensate traps and gas collection bags. At completion (60minutes residence time) the reactor was allowed to cool to ~280°C and residual gas vented through the collection train to depressurize the reactor. The digest was drained from the reactor, sampled for analysis and filtered at 250°C through glass fiber membrane using ~70kPa (10psi) nitrogen pressure differential. Filtration rate decreases with time as the thickness of the cake progressively increases by the deposition of solids and hence increases the pressure drop across the cake. The rate was recorded and the filtrate viscosity measured using a Brookfield viscometer. Determination of the specific

cake resistance, α and the fluid viscosity, μ effectively define filtration characteristics of the slurry⁽³⁾.

Coking tests were conducted by heating samples of coal solution batch-wise in a steel reactor. The samples were heated to $\sim 450^{\circ}\text{C}$ and held at this temperature to allow growth of mesophase while retaining some solvent to enhance mobility. Turbulence and shear were promoted by sparging with nitrogen to induce coalescence of the mesophase. To prevent premature loss of solvent and hence give time for growth of the mesophase domains, a reflux column was fitted to the reactor. The reactor was controlled under these conditions for ~ 3 hours in the initial tests and for longer periods in the later tests, before the temperature was raised to $\sim 550^{\circ}\text{C}$ to complete the coking process. Although far removed from the conditions found in an authentic delayed coker, it was considered that the coke produced by this route could be characterized and its structure compared to a typical coker feed treated in the same way. An additional test was conducted under the same conditions but using Decant Oil alone as the feedstock in order to make this comparison. Low boiling material generated by the thermal cracking of the feed was carried from the reactor to collection traps downstream.

Coking tests CK23, 24 & 26 were conducted using sub-samples of the coal solution prepared from WKy#6 coal and Decant Oil. The first test followed the procedure established above while in the following tests mesophase growth was encouraged by a slow heating regime, whereby the coal solution was held under quiescent conditions at 450°C for an extended period (5 to 20h). The temperature was then increased to 550°C to produce a green coke. Similar conditions were used in the last test CK28 using the coal solution derived from Blue Gem coal. Samples were calcined at 1350°C and the structure and properties of the cokes characterized by measurement of the proximate and ultimate analyses and by determination of the metals content by x-ray fluorescence (XRF). Samples were also set in epoxy resin, sectioned and polished to observe coke structure by polarized light optical microscopy.

RESULTS AND DISCUSSION

(i) Micro-Reactor Tests. Extraction of the reference coal (WKy#9) with anthracene oil was impractical at 400°C . The reaction temperature was too low producing some partially digested residual coal particles with sticky deformable surface properties which rapidly blinded the pores in the filter cake or membrane, making filtration virtually impossible. Increasing the reaction temperature by 10°C had a marked affect upon coal dissolution, producing residual solids that collectively formed a porous filter cake. The conversion, 68 to 70%daf coal, Table 4 are typical of values for the conversion of bituminous coals in a non-hydrogen donor aromatic solvent like anthracene oil⁽⁴⁾. The data are in good agreement with the results from the previous 2liter reactor tests under the same conditions⁽²⁾, giving confidence to this simple but effective test and at much less expenditure of time and effort. The ability to filter the quinoline diluted digest likewise gives valuable information on the filtration performance of the digest on a larger scale.

Very high conversions, approaching 90% on a dry ash-free basis were obtained for the solvent extraction of the targeted coal sample, WKy#6 in anthracene oil, Figure 1. This compares with 68 to 70% obtained for WKy#9. A reaction temperature of 400°C was likewise too low for this coal when using anthracene oil as the solvent. Increasing the reaction temperature by 10°C to 410°C again had a marked affect upon coal dissolution. Conversion was very high ($\sim 90\%$) and

filtration accomplished without difficulty. However, when the reaction temperature was further increased to 420°C, the conversion fell to ~80%, resulting from polymerization reactions of the dissolved coal in the non-donor solvent. There was also a small increase in gas yield at the expense of the more valuable liquid product, effectively allowing more side chains to be lopped from the large parent coal molecules.

Experiment MR#	1	3	5	6
Coal	WKy #9*			
Solvent	Anthracene Oil #2			
Solvent/Coal ratio	2 : 1	2 : 1	2 : 1	2 : 1
Temperature °C	400	410	410	410
Time min	60	60	60	60
Coal Conversion % daf coal	†	69.9	69.0	67.9

† Could not be filtered

Table 4 Extraction of WKy#9 with Anthracene Oil

With the petroleum-derived Decant Oils, the coal extraction behavior was quite different. In contrast to the digests made using anthracene oil those made with the Decant Oil surprisingly presented no filtration problems over the whole range tested, 390 to 420°C, a significant processing benefit compared with anthracene oil. With the Decant Oil from refinery 'B' a very high coal conversion was again achieved with this reactive coal, 88 to 91% (Figure 2), at reaction temperatures of 400 and 410°C. The conversion fell off significantly outside this range. A similar trend was observed for the refinery 'A' Decant Oil but at a lower level of conversion, 76 to 78%.

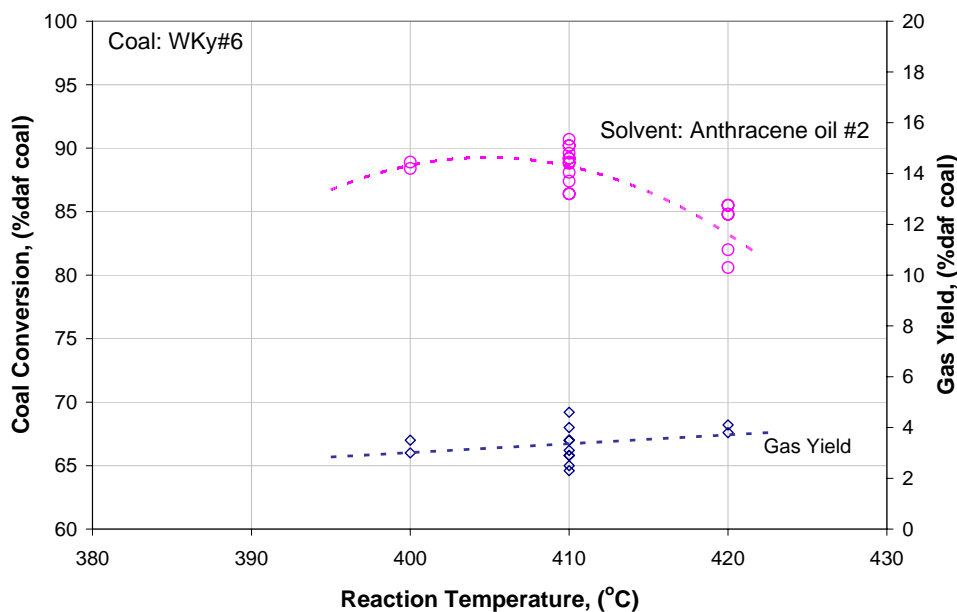


Figure 1 Extraction of WKy#6 with Anthracene Oil

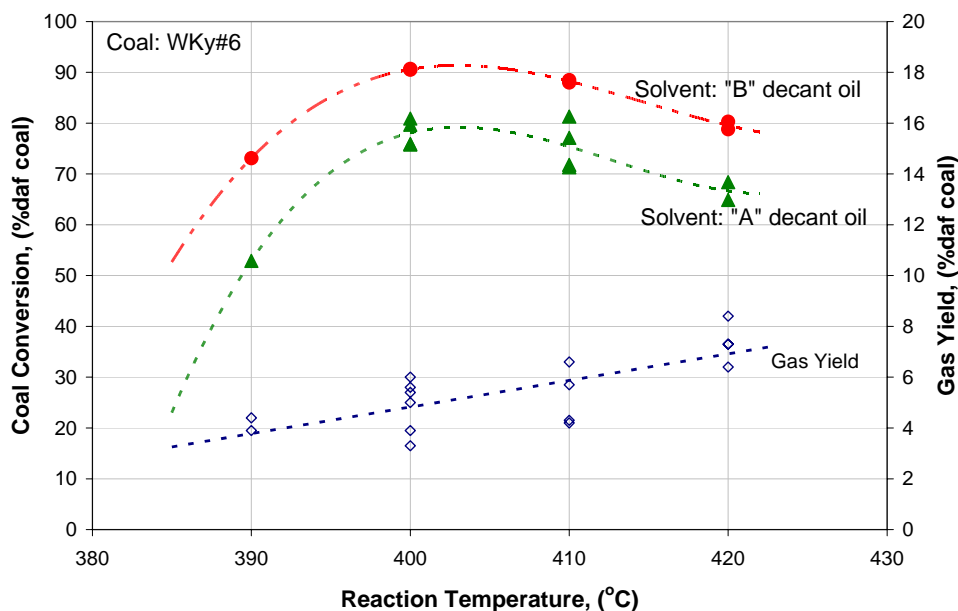


Figure 2 Extraction of WKy#6 with Decant Oil

Gas yields increased progressively with reaction temperature for both solvents at higher levels than obtained with anthracene oil coal extraction. The other two solvents, heavy coker gas oil and vacuum gas oil were tested over the most promising temperature range, 400 to 410°C. Coal conversion with the coker gas oil was again high, 81 to 86%, while the results for the vacuum gas oil were much lower, 30 to 50% with significantly more gas evolution, Table 5.

Coal	Western Kentucky #6			
Solvent	Heavy coker gas oil		Vacuum gas oil	
No of tests	2	2	2	2
Solvent/Coal ratio	2 : 1	2 : 1	2 : 1	2 : 1
Temperature °C	400	410	400	410
Time Min	60	60	60	60
Gas yield % daf coal	2.7	4.1	4.9	9.7
Coal conversion % daf coal	86	81	47	32

Table 5 Extraction of WKy#6 with the Lighter Petroleum Fractions

(ii) 2l Reactor Tests. A 2liter reactor was used to prepare larger samples of coal solution for the coking tests. The conditions selected were based upon the results from the screening tests using the micro-reactors and with similar results. The definitive test using the primary coal WKy#6 and Decant Oil 'B' produced a very encouraging set of results. The micro-reactor tests had shown that filtration of coal digests made using the Decant Oils was insensitive to the conditions used to prepare the digest (over the range tested). Thus, to maximize liquid yield the digestion temperature was reduced to 405°C in order to reduce the predicted higher gas yield with this solvent. Filtration was fast, with rates of ~90kg/m²/h.

The conversion of the targeted coal WKy#6 to liquid products during solvent extraction with Decant Oil was high, yielding a conversion of around 83%daf, a slightly lower conversion than achieved in the micro-reactor screening tests (~90%daf). The low ash Blue Gem coal was extracted under the same conditions with a conversion of ~75%daf and filtration rate of ~60kg/m²/h. Coal conversions in the tests using the reference coal WKy#9 and Anthracene Oil were also similar to the results from the micro-reactor tests, 65 to 70%daf coal. Mass balance closures were in the range 96 to 100%. Losses can be largely attributed to uncontained vapor emissions during transfer of the digest from the reactor to the filter and during filter cake blowing, performed to recover the coal solution from the cake.

(iii) Coking Tests. The yield of green coke from the clean coal solutions was in the range 28 to 33%, depending on source. Calcining yields were in the range 90 to 95% of the green coke as a result of the loss of a small amount of residual volatile material. However, when the soak time at 450°C was increased from 3 to 7 or 20h there was a marked increase in the yield of coke from the coal solutions, by over 50%. This implies that a proportion of the Decant Oil was converted to coke in the later tests, since the amount of dissolved coal in the feed coal solution was approximately 30%.

The amount of ash, generally around 0.2 to 0.5%, was above the target specification for anode coke, <0.1%, Table 6. However, the sulfur contents of 0.1 to 0.35% were well within the specified limit, <1wt%. Metal contents were somewhat variable although the concentrations naturally follow the trend set by the ash content. Nickel and vanadium, the metals of concern in relation to carbon consumption and hence increased cost to the process were very low, well below the specified value of <200ppm. Sodium was present at equally low concentrations while the phosphorus content, <10ppm, appeared to meet the specification (<5ppm) to within the sensitivity limits of the method of analysis. The same is true for the chromium content, <10ppm for the WKy#6 cokes (compared to the spec. of <1ppm). However, for the Blue Gem coke Cr was much higher. The high silicon, calcium and iron contents of this same sample suggest that contamination of the sample may have occurred. For the other coke samples the silicon and iron contents were within the target values (<200 & <300ppm respectively). However, some of the ash and hence metals in the coke can be attributed to contamination from the coking vessel. This was apparent from analysis of pitches made by vacuum distillation in glassware of sub-samples of the same coal solutions. Here, the ash contents were significantly lower, 0.1 to 0.3%, about half of the coke ash values, although still above the target of <0.1%, while the yields were not dissimilar. The likely ash content in the coke can be calculated from the pitch ash contents and their relative yields derived from the same coal solution. All of the predicted ash values were well below the measured values, generally by factors of between 50 and 100%. The implications are that the samples are contaminated during coking, presumably from the walls of the coking vessel. On an industrial scale the increase in volume to surface area ratio of several orders of magnitude, renders wall effects insignificant for the coke from a delayed coker.

Run No	CCK23	CCK24	CCK26	CCK28	Anode Grade Specification
Coal	WKy#6	WKy#6	WKy#6	Blue Gem	
Ash %	0.36	0.18	0.50	0.24	≤ 0.1
VM %	0.62	0.52	0.72	0.45	
FC %	99.0	99.0	98.7	99.3	
C %daf	98.5	97.0	93.5	99.0	
H %daf	0.03	0.02	0.04	<0.01	
O* %daf	0.3	1.4	5.1	0.03	
N %daf	0.41	0.57	0.57	0.42	
S %daf	0.12	0.34	0.35	0.33	≤ 1.0
Na ppm	<1	7	9	<1	≤ 100
Mg ppm	10	4	3	23	
Al ppm	17	7	20	100	
Si ppm	55	3	105	75	≤ 200
P ppm	<1	2	3	<10	≤ 5
K ppm	<1	<1	2	<1	
Ca ppm	48	13	7	210	≤ 50
Ti ppm	166	43	125	<1	
V ppm	<1	<1	<1	<1	≤ 200
Cr ppm	10	5	2	78	≤ 1
Mn ppm	<1	5	<1	6	
Fe ppm	115	5	11	475	≤ 300
Ni ppm	<1	4	1	35	≤ 200

Table 6 Analysis of Calcined Cokes from the Dissolution of Coals in Decant Oil

Comparing the microstructure of cokes from a typical coker feed, FCC decant oil, (a) prepared in the laboratory reactor to that (b) produced in a delayed coker shows that while the former has well-developed anisotropic domains, it does not exhibit the needle like structure of typical anode cokes produced in a delayed coker, Figure 3. It can therefore be argued that, provided some evidence of mesophase growth and coalescence can be demonstrated in coal extract cokes, cokes suitable for anode fabrication could be produced by this method when generated under the optimum conditions found in a true delayed coker. In practice, the structure of cokes derived through coal extraction in anthracene oil, although essentially anisotropic, is predominantly composed of small mosaics. However, there was some evidence of larger mesophase domains in infrequent isolated zones in the coke, Figure 4 that offers the prospect for developing cokes with the required properties. In contrast, it is the microstructure of the cokes derived from the Decant Oil coal extracts that are most interesting. The cokes display an extensive array of anisotropic domains with particularly well-defined large areas of well-aligned mesophase that should be ideal for the fabrication of carbon anodes. The structure became progressively more pronounced and impressive with increasing soak time in the laboratory reactor, Figure 5.

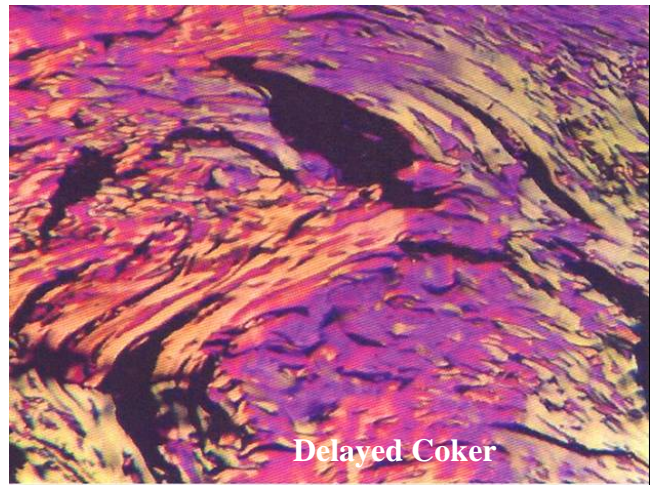


Figure 3 FCC Calcined Coke from Laboratory & Delayed Coker

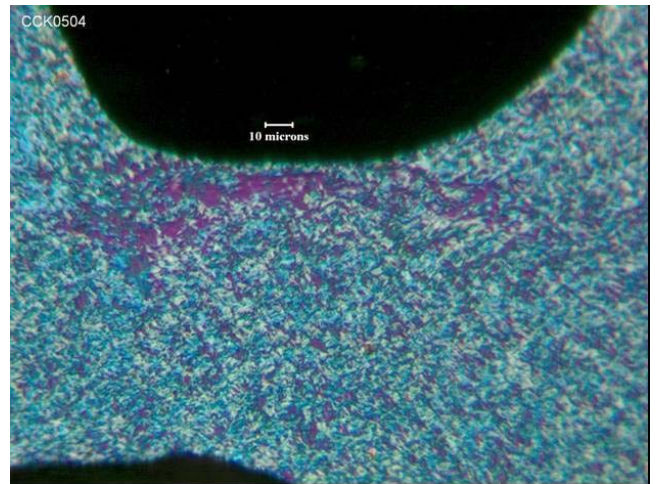
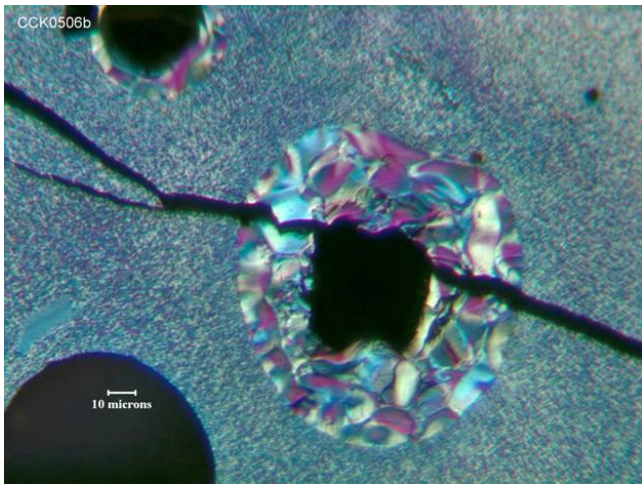


Figure 4 Small Mozaic Anisotropy of Anthracene Oil derived Coal Extract Cokes

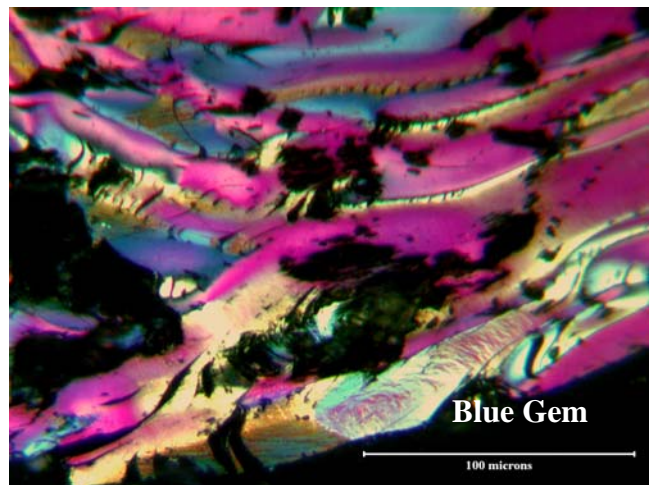


Figure 5 Large Anisotropic Domains of Decant Oil derived Coal Extract Cokes

(iv) Material Balance Based on data from the solvent extraction of WKy#6 with Decant Oil and the coking data from CK23, a material balance was constructed, Figure 6. A plant built for a coal throughput of 100t/h would produce calcined coke suitable for the fabrication of carbon anodes at a rate of 79t/h. The reject stream of dry filter cake residue would amount to 24t/h with a high value gas/light distillate yield of ~10t/h. However, a make-up supply of process solvent (Decant Oil) of 35t/h would be required to maintain the solvent inventory.

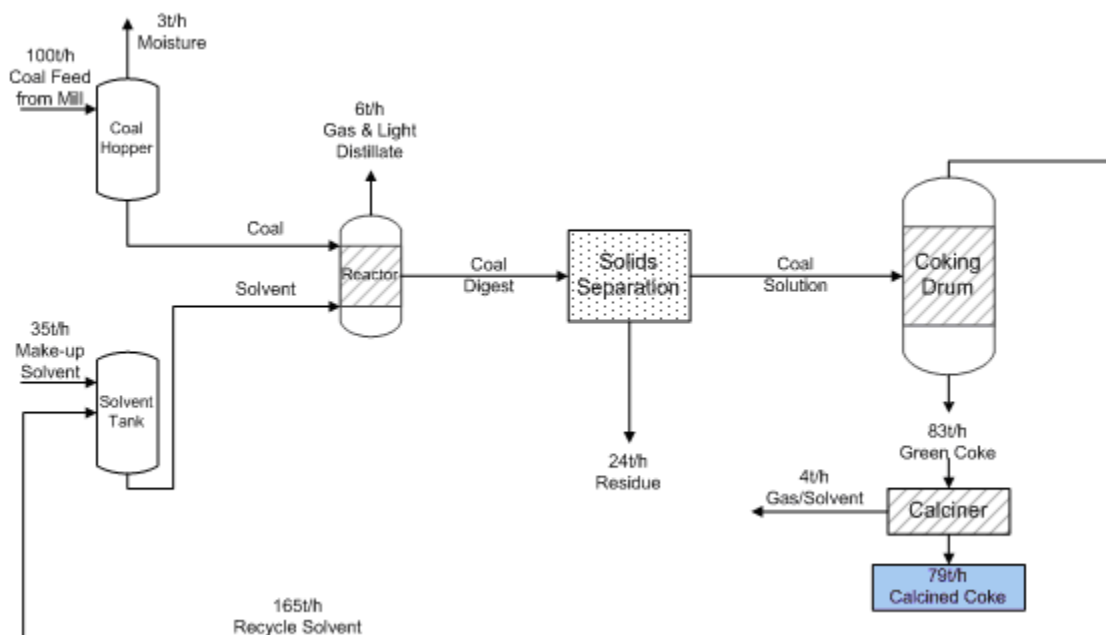


Figure 6 Conceptual Plant Material Balance

CONCLUSIONS

- A simple micro-reactor test to assess the dissolution of coals in process solvents has been established and validated. A feature of the test is the fast response time giving reliable results on the performance of coals and solvents in the conversion to soluble products.
- A Western Kentucky coal (WKy#6) was very reactive with conversions of ~90%daf coal at 410°C with either anthracene oil or decant oil 'B' as the solvent. A lower conversion (~80%) was achieved with a decant oil from refinery 'A', but well above the typical values for bituminous coals (~70%) in non-donor solvents. Gas yields were slightly higher with decant oil as solvent.
- Filtration of the decant oil digests was fast under all conditions tested. In contrast, it was critical that the reaction temperature was $\geq 410^\circ\text{C}$ for viable filtration of anthracene oil digests.
- Bulk samples of clean coal solution were prepared using a 2l reactor. The conversion achieved for the extraction of WKy#6 in decant oil was slightly lower (83%daf) than achieved in the micro-reactors while filtration was fast, $\sim 90\text{kg/m}^2/\text{h}$. This feature of Decant Oil coal digests offers the prospect for facile process control in an area that can be problematic for anthracene oil extracts. The conversion achieved with Blue Gem coal was 75%daf with a

filtration rate of $\sim 60 \text{ kg/m}^2/\text{h}$, while the conversion of WKy#9 was more typical of bituminous coals at 65 to 70% daf and filtration rate of $\sim 70 \text{ kg/m}^2/\text{h}$.

- Coke yields were increased by heat soaking at 450°C . Growth and coalescence of mesophase were also promoted by this action.
- Ash contents of the cokes exceeded the anode coke specification but some of this can be attributed to contamination from the laboratory coker. The effect of scale in an industrial process should eliminate this problem.
- Metals concentrations were mostly within the required limits defined for anode cokes while sulfur was well within the defined limit.
- The microstructure of the anthracene oil / coal extract cokes was a predominantly small anisotropic mosaic with a few isolated larger anisotropic domains.
- The microstructure of the decant oil / coal extract cokes showed extensive arrays of coalesced anisotropic domains, ideal for the fabrication of carbon anodes.
- Determination of the process mass balance showed that for coal feed rate of 100t/h the calcined coke yield would be 79t/h with a gas and light distillate make of $\sim 10\text{t/h}$. However, $\sim 35\text{t/h}$ of decant oil make-up solvent would be required to maintain solvent inventory.

REFERENCES

- (1) CPCPC Report No 2865-UK-DOE-1874, October 2006.
- (2) "Technical and Economic Assessment of Mild Coal Extraction", CPCPC Report No 2691-UK-DOE-1874, May 2005.
- (3) Purchase DB, "Industrial Filtration of Liquids", 2nd edition, CRC Press, 1971.
- (4) "Reactivity of British Coals in Solvent Extraction", Clarke JW, Kimber GM, Rantell T & Shipley DE, ACS Symposium Series #139, 1980.

PREMIUM CARBON PRODUCTS FROM COAL: A SULFUR-BASED APPROACH

Maria Sobkowiak, Harold Schobert and Paul Painter
The Energy Institute
Penn State University
University Park
PA 16802

Abstract

The goal of this research is to develop methods for producing marketable forms of carbon from coals using a sulfur dehydrogenation process. If successful, this work could have considerable impact, allowing the development of a new, environmentally cleaner process for coke and carbon production, expanding the number of coals that can be used to make these products and allowing the development of a CO₂ free, carbon neutral, source of H₂. Initial work has focused on fundamental research to establish feasibility and an understanding of the relationships between processing conditions, coal structure, the mechanism of dehydrogenation, and the nature of the carbon being produced. The results presented in this communication demonstrate that the extent of dehydrogenation by sulfur at 500°C appears comparable to that obtained in the absence of sulfur, only at much higher temperatures. This is broadly consistent with the findings of Jusino and Schobert (2006) who produced a product much like metallurgical coke but at much lower temperatures than in a conventional coke oven. Flow-reactor tests at 700°C also produced coke cenospheres, which may have interesting potential applications.

Introduction

The focus of the research described here is the production of premium carbon products from coal through the development of a dehydrogenation process that uses vapor-phase sulfur. This builds on the recently reported work of Jusino and Schobert (2005). These authors used vapor-phase sulfur to dehydrogenate a medium volatile bituminous coal through the formation of H₂S. Yields of 70–75% of the hydrogen in a medium volatile bituminous coal were obtained in this way. CO₂ was not produced in this process. Furthermore, the carbon so produced met or exceeded the specifications for fixed carbon, ash, low sulfur content and friability of conventional metallurgical coke, even though it was produced at lower temperatures than those used in typical by-product coke ovens. Jusino and Schobert (2005) proposed a process in which the H₂S is subsequently converted to hydrogen and sulfur and the sulfur is recycled through the reactor. With the present intense interest in developing a “hydrogen economy”, the production of hydrogen as a by-product in this process would obviously be extremely attractive.

The work of Jusino and Schobert (2005) demonstrated that sulfur vapor reacts rapidly with coals at temperatures above the normal boiling point of sulfur (445°C), producing a carbon with intriguing properties. Our goal is to study the relationships between processing conditions, coal structure, the mechanism of dehydrogenation, and the nature of the carbon being produced. A fundamental understanding of the chemistry of the reaction and its relationship to the properties of the final products is a prerequisite for the rational design of processes that can produce high-value carbon materials. Here we will present some of our initial results.

Experimental

The coal used in the work was a medium-volatile bituminous coking coal, DECS-30, from Virginia, USA. On an as-received basis, this coal has an ash content of 3.81 %, with 29.51% volatile matter, 64.62% fixed carbon and a sulfur content of 0.77%. The coal was selected in part for its low ash yield and sulfur content, so that the effect of coal minerals and initial sulfur content on the results would be minimized.

The flow reactor was similar to that described by Jusino and Schobert. Essentially, a Pyrex glass tube (about 1 m long, 5 cm diameter) was heated in an electric furnace. The ends of the reactor were closed with stoppers that have provisions for an inert gas sweep inlet tube and an exist tube. The inert gas sweeps the sulfur vapor, as it is formed in a separate “boat”, through a bed of coal, and prevents the vapor from diffusing away from the coal. This procedure also allowed the hydrogen sulfide produced to be swept out of the reactor into gas washing bottles that contained a solution of cadmium chloride. These solutions were used to determine the amount of hydrogen sulfide generated.

Weighed quantities of coal and sulfur were placed in the reactor. The ratio of sulfur to coal was varied according to the requirements of the experiment. The reactor was heated to the desired test temperature and allowed to run for the desired test duration (usually 1 hour, but in one case the reaction time was prolonged to 2 hours). At the end of the reaction, nitrogen flow through the reactor was continued for several additional minutes, to insure that all the hydrogen sulfide in the reactor was swept through the wash bottles. The contents of the wash bottles were filtered to remove precipitated cadmium sulfide. The amount of cadmium remaining in solution was determined by atomic absorption spectroscopic analysis of the filtrate. Given the known amount of cadmium in solution at the start of a test and that remaining in solution at the end, the amount of cadmium sulfide formed, and hence the amount of hydrogen sulfide generated, was determined by straightforward stoichiometric calculations.

Proximate analysis of the samples (volatile matter, VM; ash; and fixed carbon, FC) was performed using a LECO MAC-400 Proximate Analyzer. Sulfur content was determined using a Leco SC-32 analyzer. Fourier-transform infrared (FTIR) spectra were obtained using a Digilab FTS 45 spectrometer and a diffuse reflectance attachment. A Hitachi S-35000N scanning electron microscope (SEM) with a Princeton Gamma-Tech (PCT) energy dispersive X-ray spectrometer (EDS) was used for analysis of selected samples.

Results and Discussion

In initial work two sets of reactions were performed. First, the coal was heated under a flow of nitrogen alone at temperatures of 500°C, 600°C and 700°C, for one hour. The experiments were then repeated with sulfur in the reaction vessel (in a separate vessel to the coal), so that dehydrogenation by sulfur vapor could occur and the changes in coal structure compared.

There are distinct differences in the visual appearance of the products. The coal heated to 500°C in the absence of sulfur and held at that temperature for one hour passed through the anticipated fluid stage and reformed into a very, brittle, porous, carbonaceous mass that broke into smaller particles on being removed from the reaction vessel. At 600°C, the product consisted of two phases. One phase consisted of large lumps of material that had a coke-like appearance, while the second phase was similar to that formed at 500°C. As an example, a picture of these products is shown in figure 1. At 700°C only large lumps of material that had a coke like appearance were formed.



Figure 1. Products formed at 600°C. The product consisted of two phases. One phase consisted of large lumps of material that had a coke-like appearance, while the second phase was a powder similar to that formed at 500°C

FTIR spectra of these samples were obtained. It is important to note that infrared spectra cannot be obtained from a highly carbonaceous material like coke; all one obtains is a sharply sloping baseline and noise. Accordingly, we could not obtain spectra from the coke-like lumps formed at 700°C, but did manage to obtain spectra from the smaller, broken-up particles formed at lower temperatures and one of the coke-like lumps formed at 600°C. The spectra of the products formed at this latter temperature are shown in Figure 2, where they are compared to the spectrum of the original coal.

The spectra show that dehydrogenation occurs primary through the loss of aliphatic CH groups. In the broken-up smaller particles, the aliphatic CH content (as measured by the stretching modes near 2900 cm^{-1}) is less than half that of the original coal. In the coke-like product, the aliphatic stretching modes have essentially been eliminated. The aromatic CH groups appear to be only slightly affected by heating to this temperature, however. In addition, a band near 1670 cm^{-1} , possibly due to quinone or semiquinone-like structures, becomes more prominent in the spectra of the products. (This latter mode may also be an overtone or combination mode of the out-of-plane aromatic CH bending vibrations between 700 cm^{-1} and 900 cm^{-1} .) Finally, if the spectra are carefully examined in the 700 cm^{-1} to 900 cm^{-1} region of the spectrum, it can be seen that the band at 815 cm^{-1} , assigned to out-of-plane motions of two

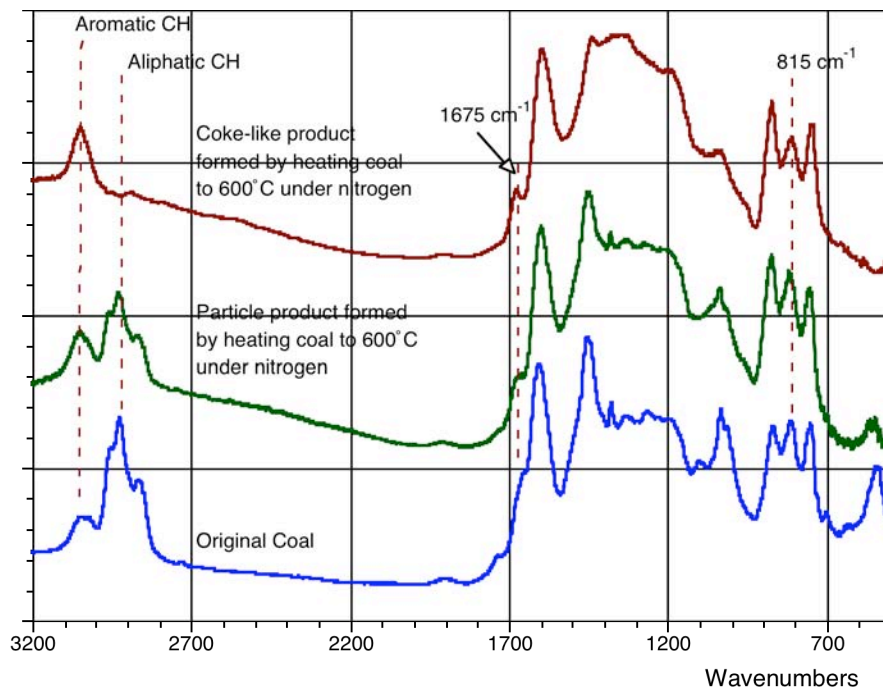


Figure 2. FTIR spectra of the original coal, DECS 30 (bottom); broken-up particulate material produced at 600°C (middle); and the coke-like material also formed at 600°C (top).

adjacent aromatic CH₂ groups has a lower relative intensity than its two immediate neighbors, near 975 cm⁻¹ and 775 cm⁻¹, assigned to isolated CH vibrations and vibrations of three adjacent CH groups, respectively. This suggests that such groups, presumably on the edge of aromatic clusters, are involved in the formation of the larger molecules that, in turn, lead to mesophase formation.

The samples dehydrogenated by sulfur at these temperatures had a different character. At 500°C, a two-phase system consisting of larger lumps of a product with a coke-like appearance were formed, together with what appeared to be small particles formed by a degree of “melting” and fusing of the even smaller coal particles originally present. Visually, these have the appearance of a roughly ground coal. At 600°C a similar two-phase system was occasionally observed, although in some experiments the smaller particles were obtained with some larger lumps. These larger lumps are extremely brittle, unlike the lumps formed in the absence of sulfur at the same temperature, and often fell apart upon simply being touched. They look like an agglomeration of bigger particles that are only weakly attached to one another. Similar results were obtained for samples heated to 700°C.

Only the FTIR spectra of samples obtained at 500°C could be obtained. These demonstrated that in the presence of sulfur, the extent of dehydrogenation at 500°C appeared comparable to that obtained at higher temperatures in the absence of sulfur. The fact that spectra of samples obtained by heating to higher temperature could not be obtained at all also implies that there is a greater degree of dehydrogenation. This conclusion is supported by the results of proximate analysis, where it was seen that the amount of fixed carbon is higher in the samples dehydrogenated in the presence of sulfur.

SEM micrographs of the samples heated both in the presence and absence of sulfur were obtained. Continuous structures appeared in the micrographs of the coke-like lumps formed by heating in the absence of sulfur. These are presumably what one would expect if the coal forms a mesophase through the condensation of aromatic molecules. Such large, continuous structures are not formed by sulfur dehydrogenation under these conditions. However, what is really interesting are the particles that are formed by sulfur dehydrogenation. SEM micrographs of these samples are shown in figure 3.

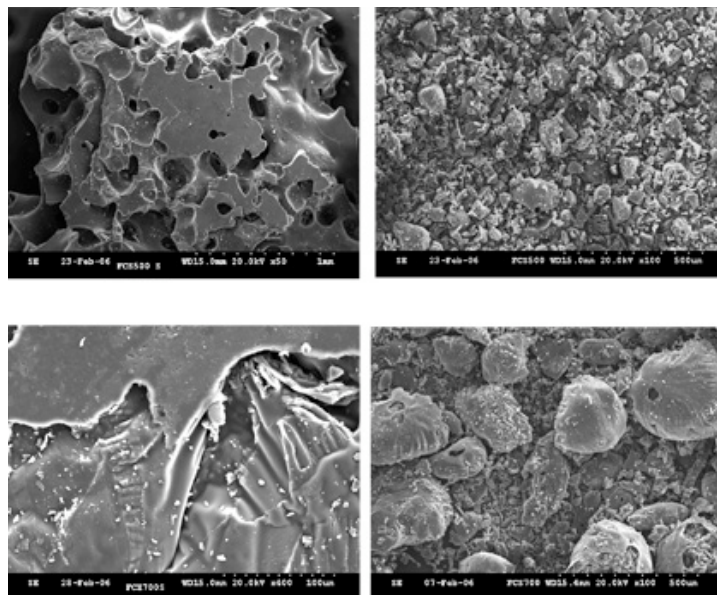


Figure 3. The SEM of carbon products formed at 500°C (top two micrographs) and 700°C (bottom two micrographs) by sulfur dehydrogenation. On the left side are the micrographs of the coke like lumps cokes, on the right side are micrographs of the powder or particle fractions.

The particles formed at 500°C are smaller and “more solid” than those formed at 700°C. The latter appear to be hollow. Gray has discussed the formation of such coke cenospheres (1989). Their formation is attributed to swelling of plasticized particles of coal by gases trapped inside the particle. This is particularly the case when the heating of the coal is relatively rapid and the coal particles are unconfined (Gray and Krupinski, 1997). Hollow carbon spheres might prove to be useful products and we are proposing to investigate their properties in future work. Preliminary work in this laboratory has indicated that these cenospheres might make a good catalyst support, while preliminary work by a colleague at Penn State (Ramakrishnan Rajagopalan) has shown that these carbons could form electrodes with very high volumetric capacitance.

Acknowledgements

The authors gratefully acknowledge the support of DOE under subcontract # 3152-TPSU-DOE-1874, DOE Prime DE-FC26-03NT4187

References

Gray, R.J., 1989. Coal to coke conversion. In: Introduction to Carbon Science (Marsh, H., Ed.) Butterworths: London; pp. 286-321.

Gray, R.J., Krupinski, K.C., 1997. Pitch production: Supply, coking, microscopy and applications. In: Introduction to Carbon Technologies (Marsh, H., Heintz, E.A., Rodríguez-Reinoso, F., Eds.). University of Alicante: Alicante; Chapter 7.

Jusino, A.; Schobert, H. H. 2006. Hydrogen from coal: A sulfur based approach. *International Journal of Coal Geology*. 65, 223-234.